Evaluation of dynamic models for refrigeration system components

A thesis presented in partial fulfilment of the requirements for the Degree of Doctor of Philosophy in Process and Environmental Technology at Massey University

Silvia Estrada Flores
B.Sc. (I.A.) (FESC-UNAM)

1996

ABSTRACT

There is a paucity of proven models for predicting the energy transients of walls used in low temperature applications and pressure vessels commonly used in refrigeration plants. The aim of this work was to investigate how the accuracy of feasible models for these situations was affected by changing model complexity.

Wall models were developed by assuming each wall layer could be represented by one of five possible thermal behaviours: null, resistance only, capacity only, alternating resistance and capacity (lumped) or fully distributed resistance and capacity. A range of feasible models for each of four common low temperature wall types was investigated by comparison of simulated behaviour to predictions by a finite element model (which was itself validated by comparison to experimental data for wall systems). Several model evaluation measures are presented to aid engineering judgement in selecting appropriate wall models for particular applications.

Only resistance needs be considered for accurate prediction of mean heat flux entering a room. It is recommended that metal layers be represented by capacity only models, thin insulation layers by resistance only models, thicker insulation layers by lumped or fully distributed models, and concrete layers by lumped or fully distributed models. The recommended number of zones within a lumped or distributed model for a layer rises as the amplitude of the expected repeating temperature cycle for that layer increases.

Four models of different complexity were derived to represent a typical industrial intercooler (pressure vessel). These models were tested by comparison of predictions to the measured time-temperature response of two pilot plant calorimeters containing R134a, when subjected to changing heat inputs. The measured response rate was most strongly influenced by sensible heat storage in the calorimeter shells and liquid refrigerant. Little difference in predictions by the four models was obtained in spite of the less complex models neglecting many known physical phenomena. A model considering only the thermal capacity in the shell and liquid refrigerant predicted rates of temperature change within 10% of predictions by all other models, and also close to the experimental data. An industrial case study suggested that the conclusions from the calorimeter study may be valid over much wider ranges. Suggestions are made on ways to improve the simplest model accuracy, and to gain greater benefit from the more complex models.

ACKNOWLEDGEMENTS

To my supervisors, Prof. Andrew C. Cleland and Prof. Donald, J. Cleland, for their commitment and for all those spirited debates that helped to shape my vision of this project and my whole research philosophy from now on. I have learned a lot from you.

To my supervisor, Prof. Ron W. James (South Bank University, London, UK), whose wisdom and friendship has been truly inspiring. I am also grateful to Dr. John Missenden for his generous help while in South Bank University and whose input to my experimental work in the South Bank calorimeter was always valued.

I acknowledge the useful comments and advice of Dr. Simon Lovatt during the development of the wall chapters. Your PhD thesis set the grounds for developing key features of this work. Thank you.

To Dr. Forbes Pearson and Star Refrigeration, Ltd (Glasgow, Scotland), for generously allowing me to conduct a part of my experimental research in the Star calorimeter. To Mr. Paul Shepperd, Mrs. Lynn Sharp and all the Star staff that contributed with technical help, ideas, logistics and good old Scottish friendship, God Bless.

To Mr. Ben Phillip, Mr. Ashtar Gupta and Mr. Raymond Mills, for their technical assistance during the construction of the South Bank calorimeter. To Dr. Jaffar Khaled, for taking the calorimeter photographs. To Mr. Issa Chaer and Mr. Graeme Maidement, for their technical advice and for illustrating me in the Soho lifestyle. I am grateful.

To Mr. John Elger and Mr. Bruce Collins, for their technical assistance during the construction of the testing facility for wall structures at Massey University.

To the Dept. of Process and Environmental Technology, for the assistance given during the development of the present work.

To Ms. Sirichom Luangon, for the many cups of coffee, bread slices and kind talks that kept me awake and fed during the long nights of thesis writing. To Ms. Delwyn Cook, for proof-reading and for putting up with a messy living room.

To the Merts family, whose unconditional help and friendship pulled me through many bumpy roads. Thank you.

To the postgraduate students that have shared with me good and bad times. Your friendship is a privilege. Your support throughout these years was fundamental to keep me going.

To my family and friends in México, all my love. You are my life force.

To the National Autonomous University of Mexico (UNAM) for the scholarship from Dirección General de Asuntos del Personal Académico. May the investment you made on me be rewarded. To Dr. Sara E. Valdés, I.A. Laura Viloria and Dr. Roberto A. Cervantes, for their incredible support and help with the many documents needed to keep my studies afloat.

This thesis is dedicated to the past, present and future generations of women in my Estrada-Flores family. *Esta va por nosotras.*

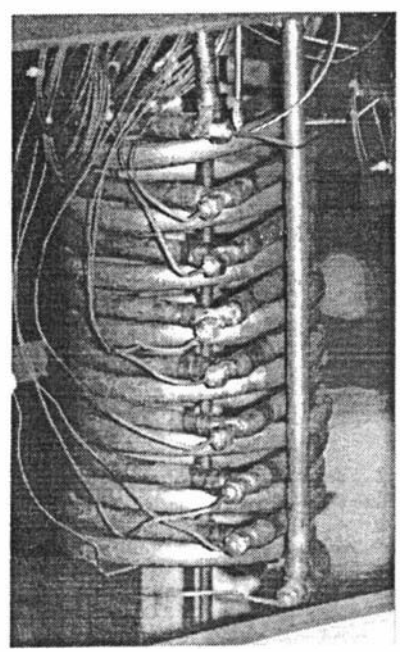

Coil of the Star calorimeter.
Picture by Paul Shepperd (1995)

"The important thing is not to stop questioning. Curiosity has its own reason for existing. One cannot help but to be in awe when he contemplates the mysteries of eternity, of life, of the marvellous structure of reality. It is enough if one tries merely to comprehend a little of this mystery every day. Never loose a holy curiosity".

-With apologies to Albert Einstein

TABLE OF CONTENTS

LIST OF FIGURES

LIST OF TABLES

CHAPTER 1: INTRODUCTION

A model is "a simplified representation of a system, intended to enhance our ability to understand, predict and possibly control the behaviour of the system" (Neelamkavil, 1987). The adaptation of such models into a programming code or language to execute simulations of physical phenomena under a variety of scenarios has been performed in a wide range of fields.

The dynamic modelling of the behaviour of refrigeration systems has been a research objective for the last 20 years. However, dynamic models have probably been developed to a lesser extent than in many other engineering-based applications. One of the factors that may have contributed is the complex nature of the refrigeration systems. Very detailed and accurate dynamic models considering all the factors affecting refrigeration plants might result in prohibitive development costs, long computation times and/or considerable amounts of data required from the user. Though the aim of the modelling process is to achieve an accurate representation of a real process or entity, the modeller has to balance the contradictory demands of accuracy and the working efficiency of the software. Simple yet accurate refrigeration models with modest data requirements could find wide application.

In order to enable a fair, objective comparison of models of different complexity for specific refrigeration plant components, a structured analysis of the loss of accuracy versus model simplicity would be helpful. The present research was therefore directed towards improvement of knowledge in the area of model complexity/accuracy trade-offs.

CHAPTER 2: LITERATURE REVIEW ON DYNAMIC MATHEMATICAL MODELLING OF REFRIGERATION SYSTEMS.

In the present research, a refrigeration system is defined as the entity arising from the integration of the components involved in the energetic exchange between the refrigerant circuit, the application and the environment. The application is defined as a mass to be maintained at low temperatures. Such a mass can be product, a secondary refrigerant, air or the combination of these. Implicitly, an application is defined as the final user of the cold effect.

Several extensive and critical reviews of dynamic models for refrigeration systems have been published (Cunniffe *et al.*, 1985; James *et al.*, 1986; Cleland, 1990; Lovatt, 1992). Hence, in the present survey, only a short review of models used for complete plants and individual components that have been developed in the last 20 years is given, to illustrate the spectrum of mathematical models that has been used. The survey also aims to illustrate the heterogeneity of modelling approaches used for some particular systems.

The complete refrigeration system models are reviewed first and particular models and assumptions for the component models within a system are covered in the second part.

2.1. Classification of refrigeration system models.

Whilst various authors have outlined general bases for classifying the different models of complete systems and components, consensus for classification has not been successfully agreed. Possibilities include:

a) **According to the model subject.** Nowotny (1983) classified mathematical models into five groups: thermodynamic properties, capacity, process, data and logical/mathematical executive operation models. Even though this classification can be applied to some component models, it would be difficult to use when a model combines, for example, thermodynamic process data as well as heat capacity.

b) **According to applied steady or unsteady state assumptions.** James *et al.* (1986) classified models according to the approach used for dealing with the refrigeration components; two groups were considered: the simpler steady state approach and the more detailed dynamic approach in which the transient performance of the component is

examined. However, this classification is only valid for component models rather than refrigeration system models, since complete simulations can contain a number of steady and unsteady state component models.

c) **According to the numerical solution.** Another set of criteria were adopted by Touber (1984), for establishing three categories:

1) Fully dynamical mathematical modelling using time-and-space dependent variables. In this case, partial derivatives equations (PDE) are needed for solving the model.

2) Fully dynamical mathematical modelling using only time-dependent variables. Only ordinary derivatives equations (ODE) are used.

3) Input/Output or "black box" type, using time constants and gain factors as empirical or calculated constants.

This general classification can be applied for component models as well as for complete models, but a more specific grouping for studying refrigeration system models is desirable.

Under this same criteria, Wang and Touber (1990) made a distinction between lumped models and distributed models. The lumped models dealt with spatial dependence by separating the object into one or several zones and calculating energy and mass balances for each zone. In this way, only ODEs are needed. Distributed models add more detail to the mathematical model since partial differential equations (PDEs) are used for time- and space-dependent variables.

d) **According to the level of complexity.** An alternative general basis of classification for refrigeration system models has been proposed by Cleland (1990), considering the level of detail and balance between the mechanical refrigeration and the applications. Three groups were defined:

1) Type I models: The emphasis was focused on the refrigeration circuit more than the application; that is, the interaction between the refrigeration circuit parameters and the application dynamics was ignored. Hydrodynamics were modelled in detail for the refrigerant circuit, but the application was modelled very simply. Most of the papers

published in the dynamic simulation of refrigeration plants are classified under this category. It can be described as a "mechanical" model.

2) Type II models: A balance between the dynamics of mechanical refrigeration plant and the application was achieved, since the main objective of such models was to simulate the real dynamics of the application as well as the refrigeration circuit. Although this type of models could be considered as the ideal approach, the mathematical treatment of the variables involved becomes large and the computation time increases as the number and complexity of the models are increased. Such models are also defined as mechanical models.

3) Type III models: Detailed modelling of the dynamics of applications was achieved, but less detail for the refrigeration circuit was considered. The thermodynamics have priority over the hydrodynamics of the system, and thus the start-ups were not modelled as accurately as the normal operating time of a plant. The simplicity of the models avoided larger computation times and less inputs were needed when a program was designed. These models are defined as thermal models.

In general, the balance of mathematical detail in modelling the refrigerant circuit flows and the thermal storage dynamics is not important in this classification. An overall view of the strategy used in model design can be discerned, allowing a better understanding of the current research trends in dynamic modelling of refrigeration systems. Using this latter classification system, some of the papers published from 1975 to 1992 are summarized here.

2.1.1. Models of Type I.

Hargreaves and James (1979) produced a model for simulating a marine chiller water plant. The plant included a screw compressor and a seawater condenser. A lumped single zone model was used for simulating the water chiller, neglecting the superheating of the vapour and two-phase flow phenomena occurring during the evaporation. Despite these assumptions, good agreement between experimental and simulated responses was found.

Chi and Didion (1982) modelled a heat pump system using ordinary differential equations (ODEs). Short time steps were required for the numerical solutions, leading to large computing times. The model used first order differential equations for describing single and

two phase flow equations. The dynamic responses of compressor, motor, fans, pressure vessels, heat exchangers and a thermostatic expansion valve were predicted. Single and two-phase fluid heat, mass and momentum transfer were considered.

Nowotny (1983) reported a number of computer programs used for simulating refrigeration plants, cold stores and heat pump installations using absorption principles. Subprograms simulated the freezing phenomena in the product and a complete system model could probably be achieved. Gauss-Jordan algorithms, Gauss-Newton processes, integrations by the trapezium rule and Runge-Kutta methods for the numerical solution were reported. Detailed description of the problem must be provided by the user. No testing of simulated results against experimental data was reported.

Yasuda *et al.* (1983) simulated a vapour compression system, using a laboratory scale refrigeration plant to verify the accuracy of the model. The finite difference technique was applied for evaporator modelling. The compressor was modelled considering two time-dependent variables (pressures and refrigerant mass flow rate). The thermostatic expansion valve model used a steady-state model for the refrigerant expansion phenomena and lumped parameter assumptions for the sensor bulb section. The condenser model was a lumped parameter type. Good agreement between the experimental and simulated values was achieved.

A mathematical model for simulating the transient behaviour of a heat pump was developed by MacArthur (1984). Both time-and space-dependence of the refrigerant thermodynamic properties in the condenser and evaporator were considered. Two-phase flow equations were used for describing the evaporator transients. Three ODEs were used to model the compressor (see Section 2.2.2.3). Thermostatic and fixed orifice expansion valves were modelled using a time constant. An accumulator vessel was represented by a lumped-parameter model to model the energy and mass transients. Although no experimental validation was reported in this paper, numerical treatment of the simulated data did not present inconsistencies with the conservation of mass and energy and the author concluded that a sound model based on first principles had been achieved.

Tree and Weiss (1986) simulated the start up of a heat pump using a two time constant assumption. Both time constants were related to the mass flow of refrigerant. The experimental results showed that the model was valid for this purpose.

James and James (1986a) modelled a heat pump with a solar collector using ODEs solved by Euler's method. The compressor was modelled using six zones and assuming a perfect mixing of fluids (oil, water and refrigerant) within each zone. The condenser was divided into three boundary layer zones. The liquid receiver was separated in 3 zones and 2 boundary layers. The dry expansion evaporator was modelled using two zones and two phase flow assumptions. The model was verified with experimental data and good agreement was found.

A model for a liquid chilling plant comprising a compressor, condenser, heat exchanger and a dry expansion evaporator was developed by Wong and James (1988). Thermodynamic approaches were used to derive 11 ODEs and 53 algebraic equations. The evaporator and condenser were represented as a single zone, using the assumptions of Cleland (1983) to define such zones. Even though this model included the application, no modelling of surface heat infiltration or the use of chilled water was carried and the paper focused on the refrigerant cycle simulation. Thus it is better described as a Type I model.

MacArthur and Grald (1989) produced a dynamic model for a heat pump in unsteady state conditions, following the work of MacArthur (1984). The model included two heat exchangers and PDEs were derived to describe the energy and mass transients. The evaporator model included single and two phase flow equations. The predictions showed good agreement with experimental results.

Zhijiu and Weihan (1990) modelled a small scale refrigeration system using a lumped parameter model for the hermetic compressor, PDEs for the evaporator and condenser and two ODEs for the capillary tube; a comparison with experimental data showed that the compressor was not modelled as accurately as the rest of the models and the authors attributed this fact to model weakness in the representation of the heat transfer phenomena.

Deng (1990) proposed a model for a direct expansion air plant with a condensing unit, two expansion valves and an evaporator. The model consisted on a set of 11 ODEs, 57 algebraic equations and 11 state equations for the refrigerant properties. The Euler method was used for solving the differential equations and a program in QuickBasic was developed. In a latter paper (Deng and Missenden, 1990) the equations for representing the refrigeration piping and the air ducting were added and the experimental validation of the model was achieved.

A dynamic model for a refrigeration system using air cooled condensers was developed by Colding *et al.* (1991); 9 ODEs and 16 algebraic equations were used and a program was implemented in the Pascal language. The experimental validation for a commercial single stage compression system showed some inaccuracies in the evaporator temperature.

Chen and Ling (1991) carried out a dynamic simulation of a small scale refrigeration system, using a fully space-distributed scheme for modelling the refrigerant mass flow rate, the compressor power and the temperatures across the system. This model was later extended (Chen *et al.*, 1995) to incorporate product and infiltration heat loads, using a thermal response method described by Stephenson and Mitalas (1967). The validation of the model was carried out using R22, R152a and R134a as refrigerants and the experimental results showed good agreement with the simulated response.

Yasuda *et al.* (1995) presented a dynamic model of a vapour compression cycle consisting of a scroll compressor, a cross-fin-tube condenser, a cross-fin-tube evaporator, an electrically driven expansion valve and an accumulator. The model considered unsteady-state behaviour in the evaporator and condenser, but the compressor, the accumulator and the expansion valve were modelled using steady-state assumptions. The experimental results showed excellent agreement with simulations during plant start-up.

The use of different levels of complexity to simulate different plant components was considered by Shen *et al.* (1995). The plant modelled consisted of an hermetic compressor, a condenser, a subcooler tank, a manual expansion valve and an evaporator. Whereas the compressor, expansion valve, the condenser and the secondary refrigerant in the subcooler plant were modelled in a simple manner, the mathematical description of the primary refrigerant in the condenser, subcooler and evaporator used PDEs. Comparisons with experimental data showed significant disagreement with the temperatures and pressures registered in the real system, possibly due to the assumptions needed to link the most complex component models with the simple ones.

2.1.2. Models of Type II.

The best example of a Type II model is that of Marshall and James (1975). The model simulated a quick freezing refrigeration system, employing a two stage ammonia cycle with a pump feed to the evaporators and a coiled intercooler. The dynamics of the freezing tunnel considered time and space dependence, but PDEs were avoided using the lumped parameter

"stirred tank" approximation. Eight zones for the cold air, eight zones for the produce and three zones for the metal and refrigerant in the evaporators were considered. The refrigerant circuit components were modelled using time-dependant variables. As the main objective of the research was to show the advantages of better control strategies, some of the conclusions derived were related to feed control, temperature measuring devices and the control of liquid level in the pressure vessels. However, the mathematical model was a very important contribution in the field of the dynamic simulation of refrigerated systems.

Yu *et al.* (1995) modelled the behaviour of a domestic refrigerator during start-ups and off situations. The mathematical model comprised a number of 3-dimensional PDEs to describe the product heat load and the refrigerated space, and ODEs to model the evaporator, condenser and capillary tube. The predictions agreed with the trend of the experimental data, but the timing of the responses did not accurately match the real response.

2.1.3. Models of Type III.

An early model of Type III reported is that of Cleland *et al.* (1982), simulating the dynamics of a fish freezing process and the storage on a fishing vessel. The thermal modelling concept (ignoring refrigeration circuit hydrodynamics) was adopted, representing the evaporator and condenser with lumped models. The expansion valve was modelled as a component of the evaporator and the compressor was represented algebraically. Seven variables were considered time-dependent: the air temperature in the refrigerated hold, the freezing front position in partially frozen fish, the temperature of stored frozen fish, the temperature of the metal fittings in the hold, the ice thickness on the evaporator and the evaporator and condenser temperatures. The overall results broadly agreed with measured data, but some discrepancies were found during loading times and start-ups.

Cleland (1983) proposed a model for a large meat processing plant refrigeration system, following some of the assumptions of Marshall and James (1975) and Cleland *et al.* (1982), but added simplifications related to the refrigerant distribution and introduced new models for the product heat load and air interchanges due to door openings, among others. A single ODE was used for describing the dynamics of each of the mechanical components and to minimize the number of differential and algebraic equations required. The experimental testing of the model (Cleland, 1985) showed good prediction for normal operation, although some transients of the system (e.g. start-up of evaporators, defrosting) were not modelled accurately.

From this work, a computer programme for calculating the time-variable and averaged heat loads of complex plants was created under the name RADS. Complete descriptions of versions 2.0 and 3.0 of this package have been reported by Cornelius (1991) and Lovatt (1992). The main functions of RADS were focused on design, equipment selection, energy efficiency and simulation of the plant performance.

Glockner and Findeisen (1984) developed a programme for simulating the dynamic behaviour of cold stores. The software, designated LF74, was used for calculating the heat transfer in a fruit cold store and computer simulations obtained using this package were later published (Glockner *et al.*, 1990). No details of the mathematical models used were reported.

Colding (1987) reported a dynamic simulation of a refrigeration plant with two storage rooms, six freezing tunnels and an air conditioned area cooled by a two-stage ammonia plant with pump circulation. A programme called SPADE was used to solve the algebraic and differential equations by a second order numerical solution method. Experimental validation of the model was not reported.

Pham (1991) reported a computer program for calculating meat plant refrigeration heat loads. The author assumed dynamic behaviour for the product heat load and steady state operation for the other elements of the refrigeration system. Computation times were shorter than those achieved with the RADS package, but predictions of the heat load versus time were less accurate. The software was applied to six plants with good results for predicting the impact of new equipment on the behaviour of the system. The program was considered more "user friendly" than other packages.

A major development of models for complete refrigeration systems was accomplished by the REFSIM package (Lovatt, 1992). Even though some models were based on those from the RADS package, 16 new models were developed. The product heat load model is described in Section 2.2. Most of the models were ODEs solved using Runge-Kutta procedures. Lovatt compared various component models within REFSIM with a dynamic simulation package (ISIM) and the complete model against RADS versions 2.2 and 3.1. Two complex refrigeration plants were studied in order to obtain experimental data for model validation. The results showed good agreement with these and an improvement in flexibility of model implementation was found.

Lopez *et al.* (1995) presented a dynamic analysis of a centralised refrigeration system in

a food plant. The thermal modelling approach of Finer *et al.* (1993), which is similar to that of Cleland (1983), was applied. Several ODEs were used to simulate the product heat load. The plant consisted of a compressor, a condenser, an evaporator and a water chiller. No experimental validation was presented.

2.2. Modelling of system components.

Component models have been more extensively studied than complete models. This reflects that experimental measurements are usually difficult for complex plants and there are difficulties in detecting the factors that have led to inaccuracies in the response.

The factors that contribute to the transient behaviour of a refrigerant circuit have been extensively investigated (James *et al.*, 1986) but less is known about the room thermal behaviour and the interactions between application components.

2.2.1. Modelling of application components (objects).

A number of approaches for modelling components considering their thermal capacity (thermal objects) have been used. Broadly, these include the components physical properties in an energy balance across all or part of the components (Cleland, 1989; Wang, 1991; Lovatt, 1992). The approaches have been classified according to the number of zones used to define the components. Some of these models are described below.

2.2.1.1. Room space models.

The modelling of air distribution and temperature in refrigerated vehicles has been extensively studied (Van der Ree *et al.*, 1974; Meffert and Van Beek, 1983, 1987; Stera, 1996). The air dynamics inside coolstores have been less extensively investigated, perhaps due to the complexity in modelling coupled mass and energy transfer phenomena during larger time scales than those expected during transportation.

Wang (1991) defined a refrigerated room as a "confined space with air flowing inside, with objects producing heat and moisture, with cooling units refrigerating, with heat or mass transferred through walls or doorways". This concept implies that the room air space model considers only the room air mass, energy and moisture contents. Examples of interactions with room air include the opening of a door creating an inflow of air at different temperature

and relative humidity, respiration producing a net flow of both moisture and heat from product to the air, and the migration of vapour water from the air to the refrigeration evaporator coil (where it may condense or freeze). All effects such as these must be taken into account in the energy and mass balances.

This room air definition has been commonly accepted for modelling the application part of a refrigeration system and is used in the present survey. The room air takes the shape of the room other than where air is displaced by product or structures present in the room. Thus there is no easy mathematical description of the air, but a variety of models of different complexity have been proposed, depending on the extent to which position variability in the room is considered.

The governing partial differential equations are often solved using rectangular grid methods such as finite difference or control volume formulations in Computational Fluid Dynamics (CFD) packages. Though such models have been tested in design applications (Amraie *et al.*, 1988, 1989; Amraie, 1993; Chan and Scott, 1991; Missenden *et al.*, 1995), the simulation of transient behaviour of refrigerated rooms has seldom been investigated. The basis and purposes of most CFD models are quite different to those in food refrigeration so it may not be possible to apply them without substantial modification. Therefore, the present discussion is limited to models that have been applied to refrigerated rooms used in food processing.

a) Single Zone Models

Cleland *et al.* (1982), Cleland (1983,1985) and Lovatt (1992) used a single fully-mixed zone for representing the air conditions in a room. This assumes that any interaction with any other component model instantaneously affects the full room air volume. ODEs were derived for both air temperature and air absolute humidity by mass and energy balance. Cleland (1983) concluded that single zone models were sufficiently accurate for overall heat load predictions. Dynamic simulation of air flow and temperature patterns within a room is not possible with this model.

Lovatt (1992) attempted to overcome one potential weakness of the single zone. When the absolute humidity is sufficiently high moisture may condense from the air, thus leading to condensation and/or freezing of water vapour either as a fog within the room or as a deposit on surfaces such as walls, floors and ceilings. These processes were modelled

separate to the deposition of water on the evaporator coil which is taken into account in the evaporator model. Lovatt's model considered the size of the condensate "pool" that would arise if a relative humidity above 100% would otherwise be achieved, but did not specify where this would be located in the room. Some arbitrary assumptions about the evaporation of this "pool" to rejoin the bulk air when the air was not saturated were made. However, in practice the location of the condensed water is important to predict the evaporator efficiency, defrost frequency and the surface conditions of any other surface exposed to the air (*e.g.* walls, product, packaging). The use of an enthalpy-based approach in the energy balances taking into account the changes of densities with respect to the air temperature was considered. However, the models would have become too complex, requiring a set of simultaneous equations to be solved at every time step of the simulation. Therefore, the latter refinement was not implemented and no testing to demonstrate benefits was reported.

b) Multi-zone Models

As was mentioned in Section 2.1.3, Marshall and James (1975) used 8 air zones to model the quick freezing tunnel air. The air in each zone was modelled with an ODE for temperature instead of a PDE. There was no consideration of water vapour in the air.

Amos (1995) followed a similar approach, zoning a coolstore and assuming a "stirred tank" behaviour in each zone, thus enabling predictions of both time and positional variations of the air temperature and humidity. Each air zone was able to interact with external surfaces, heat generators, inert materials, evaporators, fans, doors and products. Amos concluded that the use of 5 to 8 air zones yielded the best balance between accuracy and complexity in the application in which the model was tested.

c) Distributed Models

Van der Ree *et al.* (1974) predicted the transients of the air temperature distribution in a refrigerated container, using a computer program called BERTREM. The finite difference technique was applied to solve PDEs derived by energy balance. Fixed air flows were considered. The main disadvantages of this program were the time consuming and detailed work required to define input data. The authors found that the rate of air circulation significantly affected the dynamic behaviour. A weakness of their work was that air pressure losses due to the stack pattern and humidity changes were neglected. No experimental verification of the model was reported.

Meffert and Van Beek (1987) presented a simpler computer program for modelling the air flow distribution in a container, based on hydrodynamic principles and neglecting most of the heat transfer phenomena. The thermal and physical properties of the product were not taken into account and as a consequence the model was not capable of simulating the cooling or heating of product. Due to these limitations, the air temperature profile was not accurately predicted. The authors suggested that the program could be used for design and operational decisions associated with refrigerated containers.

In both papers, hydrodynamics (air mixing) was assumed to be more important than the effects of surface heat transfer in determining the air temperature profile. This assumption may be justified because of the relatively low volume of the containers and the relatively fast response of air temperature to door openings. The assumption may not be valid when the refrigerated air volume is increased (as in a coolstore) and hydrodynamics and surface heat transfer may both be important.

A major study of the mass, momentum and energy changes in the air of refrigerated rooms was carried out by Wang and Touber (1988, 1990, 1991). In their first approach (1988) the authors used the definitions of macro- and micro-climate for establishing boundaries between the air outside the product package and the air in direct contact with the product. The momentum equation was decoupled from the mass and energy equations, allowing solution of the air flow equations through a CFD package (PHOENICS) and use of these results as input data in a finite difference scheme implemented by the authors to solve the mass and energy PDEs. Using this technique, the air temperature simulation compared well with experimental results.

In the later work (1990, 1991) a number of restrictions related to the interaction of the room model with objects immersed on the air body were identified: air pressure drops across the product pallets can be important, the assumption of a constant convective heat transfer coefficient to the wall surfaces may be limiting, and experimental data collection for complete model validation (with respect to the air humidity and velocity distribution) was difficult.

2.2.1.2. Objects.

a) Doors.

A door allows air exchange between a room and the external environment. The modelling of a door requires knowledge of the opening frequency and duration as well as airflow through the door. Any variation of the external temperature affects the extent of the net air mass and energy exchange with other environments. The most common assumption has been to set constant external conditions (temperature and humidity, for example). Irrespective of the door model used, the impact on the inner conditions is determined by the room space model and the door is treated as an interface between the environment and the room.

The RADS package, as described by Cornelius (1991), assumed a constant air temperature outside the room. Sensible and latent heat flow variations were considered. During any door opening the air mass flow rate was considered constant and equal in each direction and a pseudo-random model was used to determine the frequency of door openings. Each door opening was assumed to be one time step long during the integration. A separate ventilation model, basically a continuously open door, represented the interchange of two air flows at different conditions of humidity and temperature for cases where such ventilation occurred deliberately.

Wang (1991) used a modification of the model developed by Gosney and Olama (1975) to determine flow rate through a door. The air entering the room was assumed to affect the regions near the door only. The inflow and outflow air volumes were assumed equal. The final implementation included appropriate terms in the boundary condition equations for the regions near the walls. No information about time and frequency of door openings was reported.

Lovatt (1992) modelled doors assuming an equal mass flow in each direction. An exponentially distributed random model was used to simulate the time variability of door openings and their duration.

Moreno (1987) modelled the mass flow component due to air interchanges through an open doors. The aim of the paper was to improve the precision of Tamm's equation (Tamm, 1963). However, the solution involved matrix elements and the author could not achieve a simple solution.

b) Structures.

This term refers to objects such as those needed for the palletization of the product during cooling/freezing/storage processes or to building supports. The intrinsic properties of a structure are its thermal capacity and being totally internal to the room space. During room start-up the cooling of structures (usually made of metal) increases the total load. Once they have reached the operating room temperature, structures act as buffering thermal masses interacting with the room air. Some examples of this interaction are intermediate start-ups, new product loads or air exchange. The overall effect is a smoothing of the variations of room air temperature.

Marshall and James (1975) considered temperature dependence of the metal fittings, but not the initial cooling. No specific results and discussion were reported.

In the models of Cleland (1985) and Lovatt (1992), time-dependence of the fittings temperature was considered by using an energy balance which included the buffering effect. No specific test results were reported.

c) Walls, ceilings and floors.

The walls, ceiling and floor of a room represent the physical limits of the room space model and the separation between the room and the external environment. These structures incorporate significant thermal resistance, but they can also act as thermal capacity objects with a strong influence on the application dynamics (Lovatt, 1992). In a sense, the walls and floor could be defined as dual components.

Under continuous operation conditions, the heat transfer between low temperature spaces and the environment is dominated by the conduction and convection components through the room surfaces and to/from the walls. It has been stated that the floor thermal capacity often contributes more than other objects to the cooling load from structures (Cleland and Cleland, 1995). In air conditioning applications, the concrete floor has been classified as the largest component of the building precooling load (Ruud *et al.*, 1990). Both the external environment-to-wall and the wall internal thermal resistance are the major contributors to the heat transfer.

Some of the mathematical methods used for solving the energy transients of walls have been

Laplace transfer functions (Athienitis *et al.*, 1990), finite differences and recursive estimation models (MacArthur *et al.*, 1990). The practical value of such models for refrigeration applications has not been investigated; this survey considers those models identified as interesting approaches for modelling walls commonly used in low temperature applications.

Van der Ree (1974) reported a finite element method for solving the heat transfer between a wall and a flowing medium. The computer programme BERTREM was used to implement the model. The model was not experimentally validated and the mathematical treatment was not presented in the paper.

Cleland *et al.* (1982) and Cleland (1983,1985) assumed a constant external temperature on the wall structure. In the simulation of a whole meat plant (Cleland, 1983) the overall heat transfer coefficient was calculated considering the conduction through the wall layers with significant thermal resistance. The walls were modelled twice, once as a buffering object within the room and separately as a surface to give heat infiltration by conduction/convection. The six walls were thus considered to interact with the external environment as static thermal resistance only objects and their thermal capacity was considered in the interaction with the internal environment (cold air). Lovatt (1992) used these same assumptions for the model implemented in REFSIM. Even in rooms for which the model as a whole performed well, some disagreements between experimental room temperatures and simulated values were found. Lovatt (1992) suggested that the buffering capacity of structures (especially the floor) could have been underestimated. He concluded that a floor model integrating both conductivity and heat capacity properties would probably perform better.

Wang and Touber (1987) modelled a cold store with heat transfer through the six walls using a finite difference scheme. The authors followed this approach in other papers (1988, 1990). The wall model was used to establish the boundary conditions needed to determine the transients of the room air (see Section 2.2.1.1.), and the treatment of the external phenomena was simplified by assuming steady state conditions in the external environment. Hence, the dynamics of the wall temperature were mainly determined by the room air conditions.

The following models which have not formed part of a complete refrigeration simulation package may include important applicable concepts.

Sunden (1987) proposed a numerical solution for the transient heat conduction of a composite slab, considering time-variable surface conditions. A perfectly insulated external surface was considered, and the temperature profile for the internal surface and internal layers was predicted. Coupled convection-radiation-conduction heat transfer mechanisms were considered. A finite difference scheme was implemented and the results showed good agreement with the experimental data.

The problem of thermal bridges in the coolstore walls and floor was analyzed by Delsante *et al.* (1983). It was concluded that for thermal bridges or structures near the ground, accurate modelling for a coolstore panel would require a 3 dimensional model.

Ding *et al.* (1995) presented a model based on z-transfer functions to model unsteady heat transfer through composite slabs. The method was accurate when compared to responses obtained from a Laplace transform method and is suitable for non-linear situations. This method was based on the model of Stephenson and Mitalas (1978).

d) Product.

There is a broad spectrum of literature associated with the prediction of freezing and chilling times, most of which was reviewed by Cleland (1990). Only those relevant to the approaches used to model product heat load are discussed here.

A product is usually modelled as a thermal object that possesses a significant heat capacity, but in some cases has a dual behaviour due to internally generated heat and water vapour as well.

Marshall and James (1975) modelled the product heat load with an ODE for product temperature in each of the eight zones of the tunnel. The product thermal capacity was changed between zones to model latent heat release. The experimental data showed that overall the model was sufficiently accurate for control purposes, but the model did not represent the actual freezing phenomena.

Cleland *et al.* (1982) modelled the time-variable heat load on a fishing vessel assuming a thermal model with a single ODE, solved by a Runge-Kutta method of 4th order for non-freezing product and the first model for freezing that accounted for movement of a freezing front. In later works the model was improved to take into account irregular product

geometries (Cleland, 1983, 1985). Reynoso and De Michelis (1988) applied a simpler technique for cryogenic freezing, assuming low values for the heat transfer coefficient and considering the surface heat transfer as the dominating heat transfer mechanism.

Wade (1984) presented a model for the estimation of the heat load in the cooling of vegetables, using an ODE similar to that presented by Cleland (1983) and using an empirical factor for representing the product shape. An underestimation of the cooling rates was observed when compared to the experimental data.

Lovatt (1992) presented an improved model for the product heat load prediction, using 3 separate equations for the cooling, freezing and subcooling stages. For the subcooling heat load, a similar equation to that for cooling was used, by applying the frozen thermal properties. The final model reported comparable results to those obtained with the finite difference method and a good agreement with the experimental data. This work was later extended in order to model refrigeration process indicators (Lovatt, 1995).

In addition to the product heat load there is usually a heat load caused from the respiration rates of products and the product packaging. Generally, the later has been modelled by lumping its effect with the product heat load. Respiration rates were modelled as an algebraic function of the average product temperature by Cleland (1985) and Lovatt (1992). Packaging heat load was included in the sensible heat load from the product by Cleland (1985), Pala and Devres (1988) and Lovatt (1992). This modelling strategy did not take into account the possible heat transfer buffering effect of the package or its interaction with the water vapour transfer.

Radford *et al.* (1976) reported a mathematical model that considered the simultaneous diffusion of water through slab-shaped meat products and heat conduction. Ten zones were used for representing the moisture and temperature gradients. A good agreement between simulated and experimental data was found.

Ansari *et al.* (1984) proposed a model for the simultaneous heat and mass transfer during the air cooling of spherical products. The finite difference technique was applied for solving the time and spatial dependence of both parameters. The cooling times were overestimated when only the heat transfer was considered and closer predictions to the experimental values were obtained by considering both mass and heat transfer.

Gaffney *et al.* (1985) studied the influence of the air exchange factors on the weight loss of fruit in packed beds. A finite difference scheme was applied, using a five node grid and considering the radiation and convective terms in the energy heat balance. Although the objectives of this paper were not related to heat load modelling, some temperature calculations at different positions in the product were made.

Wang and Touber (1990) used a finite difference technique to model heat and mass transfer during the cooling of a box of apples, treating this object as a porous solid. Heat generation and product weight loss were both considered. The main objective of this paper was the simulation of temperature fluctuations in the air surrounding the product (see Section 2.2.1.1) and no specific comparison between the measured and simulated data were reported.

Van der Sluis (1993) developed a model to predict the cooling and freezing of bakery products, emphasizing the migration of moisture to the surrounding environment. The PDE model was solved using a finite element technique. This model was later applied to chilling of turkey carcasses (van der Sluis, 1995). Whereas the cooling times showed disagreements of ±20% with the experimental data, the weight losses were calculated within less than ±10%.

f) Electro - mechanical devices.

Under this subject three main items are considered: lights, the cooling fluid motion devices (usually fans) and the product handling systems.

The head load from the fans has been usually considered as a stable heat load and the value is calculated using the volumetric flowrate, the pressure drop and the efficiency of the fan and fan motor (Cleland, 1985; Cleland and Cleland, 1995). The heat generating capability was thus modelled but not the object thermal capacity.

-

The use of dynamic refrigeration models for controlling air fan systems has been studied (Wee *et al*, 1991). In this case, the dynamic response of the fan heat load was set as a consequence of both the air temperature and the remaining need for cooling or freezing within a certain time.

In some refrigerated rooms a mechanical, electrical or electromechanical system for transporting and palletizing product is installed inside the store/equipment. Such devices increase the heat load due to the transfer of electricity through mechanical work to heat. This

can be an important part of the total heat load, depending on the frequency of use. An algebraic model is often used (Cornelius, 1991). No specific dynamic modelling of this type of component has been detected.

2.2.1.3. Miscellaneous.

The group of heat loads comprising defrost, hot water use and people have been modelled algebraically, since their contribution to the total load is usually relatively small. Defrosting systems and people are both water vapour and dry heat generators. Except in densely populated work-rooms, the heat load and water vapour generation due to people is generally negligible in food refrigeration systems (Cleland, 1990). Wet floors and walls are sources of water vapour and heat as well, but they are a special case that only applies to certain applications and conditions. Simple models for such loads are used in RADS (Cleland, 1985) and REFSIM (Lovatt, 1992).

2.2.2. Modelling of refrigerant circuit components.

The importance of transients on refrigeration circuit modelling has been discussed by Wong and James (1986) and James *et al.* (1986). Two types of approaches have been used for developing models. The first of these is detailed models that use time and spatial dependence, involving PDE schemes. Some examples were presented in the discussion of Type I models. The second type, usually found in models of Type III, visualizes the refrigeration equipment as an object with lumped thermal mass and hence uses ODE schemes. This survey discusses both approaches, including the papers that were not analyzed previously in the complete models section.

2.2.2.1. Evaporators and expansion valves.

Similar categories to those used for room models have been used for describing the complexity of the evaporators. The most simple models assumed a lumped thermal capacity for representing the evaporator by ODEs, avoiding hydrodynamic considerations and minimising the computation time. An intermediate complexity model might use a grid for zoning the evaporator, but still lumping the thermal capacity of each zone to achieve ODEs. Fully distributed models assume a time and spatial dependence of the refrigerant flow and require PDEs.

In all the categories the possible governing equations for the flow of the refrigerant could be defined under single and/or two phase flow conditions. The selection of one regime or another depends on the type of evaporator and the complexity of the approach taken. If a lumped parameter model is to be developed, single phase flow equations might describe the feeding of the evaporator as pure liquid and the exit conditions as pure superheated gas. Intermediate and distributed models cannot avoid consideration of two co-existent phases. The expansion valve (*e.g.* thermostatic expansion valve, TEV) is often included in the evaporator model, so the models considering this device are reviewed here as well.

a) Single zone models.

Hargreaves and James (1979) modelled the evaporator with a lumped parameter model, assuming one zone for the refrigerant and one for the application (chilled water). For the TEV the authors used a similar model to that of James and Marshall (1976) which was discussed earlier, but represented the sensor dynamics by a first order lag.

Higuchi and Hayano (1982) studied the dynamic response of a TEV in relation to the detection of superheating in the evaporator, using empirical correction factors. A time constant was applied and no differential equations were used.

Cleland *et al.* (1982) used a single refrigerant zone for the evaporator of a fishing vessel. The expansion valve was modelled using an algebraic expression. They showed that changes in the thermal capacity of the evaporator barely affected the predictions. The simulated values had a good match with the experimental data. Cleland (1983,1985) also used a single zone for representing the dynamics of the evaporator. He concluded that in radical transient situations such as start-up, the model had significant inaccuracy in predicting room air temperature, but for slower changes the prediction were accurate.

Bonte and Vedhoven (1983) used a lumped thermal capacity approach for dealing with the dynamics of the evaporator, but empirically calculated factors were added to improve the accuracy of the model. The evaporator was separated into an evaporating region and a superheating region. The model for the latter region was related to an algebraic model for the TEV, calculating the superheat enthalpy and mass flow through the TEV. The results showed satisfactory agreement with measured temperatures, except for the superheating temperature.

Wong and James (1988) used the same approach as Cleland (1983) for simulating the evaporator in a liquid chilling plant model. The chiller water outlet temperature was modelled with an algebraic equation. The experimental data was in good agreement with the model in the simulation of the chilled water outlet temperature in response to compressor speed, but poorer agreement was found in the comparison of predicted and experimental chilled water outlet temperature versus time profiles.

b) Multi-zone Models

Marshall and James (1975) modelled a quick-freezing installation with three evaporators fed by refrigerant pump circulation. Three zones were considered for the metal structures and the refrigerant (each zone representing one of the three evaporators). The metal temperature was defined as time variable and simultaneous mass and energy balances were stated for the refrigerant flow. In a later report (James and Marshall, 1976) the authors described a model with a single ODE, where the mass flow was a time-dependent variable. A TEV was modelled with an ODE for evaluating the mass flow rate as a function of the superheating temperature gradient.

A direct expansion evaporator and a liquid sensing expansion valve were modelled by van der Meer *et al.* (1984). The expansion valve consisted of a measuring device, the expansion valve and a calculation/control module. A PID controller was considered for controlling the valve. The equations derived were not presented. A comparison with a TEV model showed that this expansion device could control the mass flow with a lower superheat than a TEV.

James and James (1986a) used the evaporator model presented by James and Marshall (1973). This involved two zones to represent the refrigerant and metal components respectively. The energy and mass balances described the refrigerant volumetric enthalpy, density and metal temperature as a function of time. A TEV was modelled in conjunction with the evaporator model, using a first order lag. The pressure drop was modelled using single and two phase flow equations. In a latter paper (James and James, 1986b) a detailed comparison of four models of different levels of complexity for the TEV was presented. It was concluded that the models with a larger number of zones for the phial and suction tube metal could be used for design and integration with system models when the dynamic of the TEV are found of special interest. The simpler model which assumed a thermal equilibrium between the metal and the phial, or a first order lag for representing the phial with a single zone for the evaporators outlet tube, could be suitable for system models where a simpler

TEV representation is required or where there is significant heat transfer between the phial and surroundings but this heat transfer is not to be modelled.

Deng (1990) simulated a direct expansion air cooling plant with two types of expansion valves: a TEV and a thermal electrical expansion valve (TEEV). For the TEV isenthalpic behaviour was assumed and an ODE to describe the time-dependence of mass flow was proposed. The TEEV was modelled with similar equations to those for the TEV, but no superheat section was considered. The validation of the model (Deng and Missenden, 1990) showed excellent accuracy in the simulation of a laboratory-scale plant. A latter paper (James and Eftekhari, 1990) used this same model with some modifications for developing a flow regulation system.

A mathematical model for simulating an evaporator using a step exciting method was developed by Wenxue and Kraft (1991). Laplace transformed equations were used for modelling the superheat and mass flow rate at the outlet of the refrigerant. The results obtained responded to a 1st order system with delay.

c) Distributed models.

Yasuda *et al.* (1983) applied evaporator zoning with a different mathematical approach to the models previously discussed. For the evaporative side, the refrigerant and pipe wall temperature were considered time-dependent. A source of heating water representing the application part of the evaporator was modelled with the finite difference technique. In the superheat region the refrigerant, pipe wall and the heating water temperatures were considered as time and spatially dependent with respect to the evaporator length. The TEV was modelled separating the expansion effect as a static model and the sensor bulb as a dynamic one by applying 4 ODEs and 1 algebraic equation. The results showed good agreement with the experimental measurements, but some problems were detected in obtaining accurate experimental data in the vicinity of the interface between the evaporating and the superheat regions.

In a mathematical simulation of an air conditioning evaporator described by Murphy and Goldschmidt (1984), energy balances considering convection and radiation were used to derive PDEs. These were discretised using 6 nodes. The temperature of the metal was assumed to be a time-dependent variable and a finite difference procedure was used to simulate the transients of the refrigerant. The results showed good agreement between the

experimental and simulated data. Due to the application type (air conditioning), steady-state was reached in only six minutes.

MacArthur (1984) modelled the evaporator of a heat pump system using PDEs and considering the enthalpy changes in the two-phase and single phase regions (see Section 2.1.1). No experimental validation was presented.

Wang and Touber (1991) modelled an air cooler assuming two phase flow equations with phase change for the evaporation region and single phase flow for the superheating region. A set of PDEs for time-and space-dependent variables were solved for the refrigerant side and wall. Even though the experimental validation was positive, large computation times were required.

2.2.2.2. Condensers.

This equipment has generally been modelled using ODE schemes, due to the relative simplicity of its function. The majority of models differ from each other only in the number of zones used for describing the condensing effect and whether single and/or two phase flow equations were derived.

a) Single zone models.

Cleland *et al.* (1982) and Cleland (1983, 1985) modelled a condenser as a single zone with similar equations to those used for evaporators. Lovatt (1992) followed the assumptions made by Cleland (1985). Good agreement with experimental data for condensing temperatures was obtained.

Wong and James (1988) used a single zone with an ODE derived by energy balance. Variations in the refrigerant mass flowrate through the circuit were not accounted for. The condensing water outlet temperature was calculated algebraically.

Zalewski (1993) proposed a mathematical model for an evaporative condenser, assuming a steady state ambient condition and including spatial dependence of the temperature of the refrigerant and walls. The experimental results showed a disparity of about 20% from the simulated values.

b) Multi-zone Models.

The condenser modelled by Marshall and James (1975) was separated in three zones: the vapour, the condensed refrigerant and the metal wall. The enthalpy and mass changes were modelled as time-dependent variables.

Yasuda *et al.* (1983) represented the condenser using 4 ODEs (for the mass and energy content of the refrigerant, the condenser wall temperature and the cooling water temperatures). The results showed that the assumption of constant refrigerant subcooling at the condenser outlet was generally valid. However, for transient behaviour like start-up, defrosting or radical changes in the applications heat load, liquid subcooling did vary significantly.

Vidmar (1987) developed a model for simulating the transient response of condensers used in household applications during start-up. The equations involved two phase flow assumptions. The temperatures and densities of the cooling air, refrigerant and the tube wall were considered as time-dependent. After discretisation the resulting ODEs were solved using the Runge-Kutta 4th order numerical solution method. No experimental validation was reported, but the predictions were comparable to those from earlier models.

In the model of James (1988) the equations derived for the condenser considered 4 zones: vapour, liquid refrigerant, metal wall and water zones. For each zone an energy and mass balance was considered. Another simplified model similar to that presented by Cleland (1983) was reported in the same paper. The simplified model used a single ODE for the mean refrigerant temperature in the condenser and an algebraic equation for the condenser water outlet temperature. No specific results on the performance of the two models were reported.

c) Distributed models.

MacArthur (1984) modelled a condenser taking into account the energy and pressure transients of the system. The energy and mass balances assumed a space-and time-dependence of the enthalpy and refrigerant flow. The pressure transients were determined by calculation of refrigerant flow rates and pressure drops in response to energy flows within the system.

Zhijiu and Weihan (1990) represented the condenser with two PDEs derived from the

momentum and energy balances. The numerical solution method proposed were to either divide the tube in a number of sections, or to apply the finite difference technique. Both solution methods led to results which agreed with the measured data. The models were considered valid.

2.2.2.3. Compressors.

With few exceptions, the compressor has not been considered as a dynamic element in the refrigerant circuit and algebraic equations have been used for determining the related thermodynamic parameters. In the majority of the models reviewed, refrigerant flow rates, pressures and temperatures are calculated as consequential values from the dynamics of the condenser or evaporator models. In a few cases, parameters related to the efficiency of the compression process have been simulated dynamically, for example, oil or housing temperatures.

Yasuda *et al.* (1983) modelled an open type reciprocating compressor, using zoning for representing the four-phase compression cycle (suction, compression, expansion and discharge). Nine algebraic and differential equations were used, switching from one to another in order to simulate the four steps of compression. The dynamic behaviour of the valve plates was not considered. The experimental results showed that the model was accurate during a period of 400 seconds.

MacArthur (1984) modelled a compressor using five parameters (clearance factor, piston displacement, compression efficiency, heat transfer coefficient and thermal mass). The enthalpy of the compressed refrigerant and the thermal masses of the compressor cylinder and shell were modelled with 3 ODEs.

In the hermetic compressor model of James and James (1986) the modelled components were the compressor, refrigerant vapour, cooling water, oil and the metal structures for the oil and vapour enclosures. Seven ODEs based on energy and mass balances plus algebraic expressions were used in the model.

Zhijiu and Weihan (1990) presented a lumped model for an hermetic compressor, describing the suction, compression, discharge and expansion phases. In a similar approach to the model of MacArthur (1984), the refrigerant volume and mass, the heat transfer and cylinder temperature were considered as time-dependent variables. The experimental data

collected showed disagreement for the compressor discharge temperature, attributed to uncertainty in knowledge of the heat transfer phenomena in the compressor.

Bartolini and Caressana (1991) modelled the compression process in a screw compressor using ODEs to model the energy and mass contents of the volume enclosed by the screws as they turned. Ideal gas theory was used for calculating the pressure change and the variation in mass and volume was considered. No experimental results were reported.

2.2.2.4. Vessels.

Pressure vessels and their interaction with the performance of a whole refrigerant circuit has been less investigated than the rest of the system components. The modelling approaches for this element vary in complexity between lumping the thermal capacity with the evaporator (when a flooded evaporator was modelled, as described by Cleland (1990) and Lovatt (1992)) to multiple zoning of the vessel. In this latter technique, the zones are normally selected according to the refrigerant physical states coexisting in the vessel.

Marshall and James (1975) modelled a receiver vessel (high pressure), a liquid separator (low pressure) and an intercooler with a subcooling coil (intermediate pressure) for a pump flooded evaporator system. For the first vessel, an algebraic model was used. For the second vessel, energy and mass balances were used to derive two ODEs. The feed dryness fraction was modelled with an algebraic equation. In the case of the intercooler, 4 sections were assumed to exist: vapour, liquid, vapour bubbles temporarily in the liquid and the subcooling coil. The equations for the refrigerant layers were based on energy and mass balances, calculating the dry fraction as in the liquid separator. The subcooling effect in the coil was calculated using the coil area, temperature difference between the refrigerant outside and inside the coil and the overall heat transfer coefficient.

MacArthur (1984) represented an accumulator vessel with a two-zone lumped parameter model, considering the mass and energy changes with respect to time. The model detailed the internal mass transients, including evaporation from the liquid phase to the vapour phase. The solution of the 4 resulting ODEs is achieved by an iterative line-by-line search (Patankar, 1980) of the temperatures and enthalpies at each time step. No experimental validation was presented in this paper.

James and James (1986a) modelled a liquid receiver by separating zones at the vapour-

metal interface, the liquid-metal interface and having two boundary layers representing the vapour-liquid mixture and the vapour/metal interface. The vapour, liquid and metal zones were represented using ODEs derived by mass and energy balances. The boundary layer behaviour was described with algebraic equations. Experimental results of James (1988) for the liquid separator pressure as a function of time were used to test the model. Some disagreement between predicted and experimental values was found during plant start-ups and shut-down.

The model used by Cleland (1985) and described by Cornelius (1991) assumed that the liquid mass present in a vessel was constant and that the liquid phase thermal capacity was significantly larger than that of the vapour phase. In that way, the vessel dynamics could be determined by the liquid refrigerant properties and the net inflow of energy to the vessel. Lovatt (1992) followed this model for the REFSIM simulation package. Although the simulation performed well for the general behaviour of plants with low, intermediate and high pressure vessels, the specific performance of the vessels models was not investigated.

Wang (1991) simulated vessel dynamics using a similar approach, describing the mass and pressure changes with ODEs. No specific comparisons of predicted and measured data were presented.

2.2.2.5. Pipe lines and other devices.

Pipe lines thermal capacity and variations in mass of refrigerant present have been neglected in the majority of the models. However, James (1988) stated that this could be an erroneous approach since most of the refrigerant mass is usually found in the vessels and pipes, not in the main equipment.

Marshall and James (1975) simulated the suction and discharge lines between the liquid separator/compressor and the compressor/condenser of an industrial refrigeration system by considering a constant volume, infiltration of heat through the insulation and known fluid flow parameters.

Cleland (1985) and Lovatt (1992) assumed a fixed pressure drop and no time delay in pipes. Therefore the outlet conditions of flowrate and temperature equalled the inlet conditions at the same time, but the pressure was lower. In some cases, the pipe was considered as a part of the main equipment and its capacity lumped, *e.g.* the liquid distribution pipe from the condenser to the receiver was considered a part of the condenser.

CHAPTER 3. PRELIMINARY CONSIDERATIONS AND OBJECTIVES.

3.1. Summary of literature review.

The literature reviewed highlighted a number of shortcomings in existing refrigeration system models, and areas in which little research has been carried out. It is convenient to summarise the present state of model development:

- There exists a lack of systematic procedures for evaluating the validity of a model. A statement such as "good agreement with the data" usually mean deviations range from between 5 and 20% of measured data. Even though the nature of refrigeration systems models differ to some extent, there is a need for establishing unified methodologies for the purposes of comparison between models. This point of view reinforces the conclusion of James (1988), who stated that "some component models are integrated into experimentally validated system models but there is no record of a comparison between models for a particular component being undertaken". Advantages and disadvantages of most published models have been discussed, but the comparisons have been limited to qualitative (and often subjective) judgements.

- It has been pointed out that complex models are not always justified in terms of the accuracy obtained relative to the cost of collecting data to use the models, the accuracy with which these data can be obtained and the computation costs (Cleland, 1990; Darrow *et al.*, 1991; Lovatt, 1992; Finer *et al.*, 1993). A cost/benefit analysis should consider these 3 factors in seeking to establish guidelines for appropriate model complexity.

- The imbalance in model complexity and accuracy for different components detected by Lovatt (1992) is still apparent. Even when an adequate development has been achieved for some components like product models, other components still have inaccurate mathematical representations (such as doors, room surfaces and structures) or not considered at all.

- The various models of the main equipment items on the refrigerant side have wide ranging degrees of complexity. No consensus about an appropriate level of complexity for specific applications has been achieved.

- The apparent lack of development of models for some linking elements in systems

(*e.g.* pipes, valves and pressure vessels) may be attributed to their assumed low thermal mass. Other components which have larger thermal masses have been assumed to be more important. Most published models ignored the linking elements or their thermal capacities were lumped with main equipment. An example of this later approach is the lumping of the thermal capacity of liquid/vapour separator vessels with flooded evaporators.

The simulation of heat transfer through the walls, ceiling and floor of refrigerated rooms has been less extensively studied than other application heat loads. Most of the proposed models were algebraic, the transient heat flow resulting from thermal storage in the wall were neglected and/or variations in the external environment conditions were not taken into account. In the simulation of complete refrigeration systems both surfaces and structures have an important effect on the predicted heat load profile. Component models with different degree of complexity might be justified in order to obtain appropriate levels of accuracy in simulations for different purposes. There is a lack of published data for validation of heat infiltration models in low temperature applications.

3.2. Modelling Overview.

The process of selecting a level of complexity for a model is generally based on 3 issues:

1) Definition of the type of balances needed: Energy, mass and/or momentum balances according to the component type and use of the model have to be established. Often the nature of the components allows the simplification of the governing equations so that only one type of balance is required, but sometimes the accuracy of the model can be limited if only one type of balance is used.

2) Selection of domains to be considered in the model: Even when the physical reality of a component is that it exhibits both time-and space-dependent behaviour, modelling all the simultaneous changes with respect to time and space in every component of the plant would be costly and probably ineffective in practical terms. Therefore, the system is usually represented by a part of it in which most of the variations are expected to occur. An analysis has to be made in order to decide which terms should be treated as constant values, time-dependent, space-dependent or both.

3) Discretization of selected domains. The number of model equations is directly related to the discretization used to represent the domain(s) of the component modelled. Although a better approximation to reality is generally achieved when the number of zones is increased, the error remaining can still be significant. The mathematical technique will depend on the selection of domains and the number of zones selected. For example, when a space domain is divided into a number of zones, each zone can be treated with a single ODE equation for the time-dependent terms. When a more precise approximation is needed, the use of PDEs may be required.

Unfortunately, consideration of these issues alone does not guarantee that the most appropriate selection of the complexity level will have been achieved.

3.3. Objectives.

The present work was centred on two areas in which the present "best" models either still exhibit apparent lack of fit with experimental data or their accuracy has not been thoroughly tested: the thermal behaviour of walls surrounding the refrigerated space and the pressure vessels used for storing, distributing and controlling the refrigerant in a mechanical vapour compression plant. Testing of wall and vessel models was limited by the availability of experimental facilities and resources, but the selections proved to be well suited to the task of investigating the impact of decision-making processes during the early stages of model development. Both walls and vessels have a significant dynamic influence, so unsteady-state energy transfer phenomena were the primary interest in the research.

The specific objectives were to:

I. Develop new dynamic models for simulating the thermal behaviour of a variety of walls commonly used for low temperature applications, considering both the thermal capacity and transmission properties of the wall materials.

II. Theoretically validate the models across a range of conditions of operation and assess the effect of different levels of complexity on the accuracy of the simulations.

III. Design and implement an experimental apparatus for collection of time-variable temperature-data in different types of walls, so that model validation was experimentally based.

IV. Develop new dynamic models for pressure vessels (such as intercoolers and low pressure receivers) of varying levels of complexity.

V. Design and implement an experimental apparatus for collection of refrigerant pressure and temperature data during time-variable pressure vessel behaviour, in order to validate new and existing vessel models.

VI. Established the extent to which increasing the complexity of the pressure vessel model increased the accuracy of the model predictions

CHAPTER 4. WALL STRUCTURES: CONCEPTUAL AND MATHEMATICAL MODELLING.

A wall, ceiling or floor is a composite barrier between the refrigerated and external environments. Besides its obvious structural function, its main feature is to act as a resistive layer to the heat transfer that occurs due to the temperature gradient between the refrigerated space and the ambient environment surrounding the room.

The dynamics of the room enclosures have been previously modelled dissociating the thermal resistance and capacity of the wall into a number of zones (Korsgaard, 1969; Grossmann *et al.*, 1969; Ding *et al.*, 1995). Analytical and response variable (*e.g.* z transform) solutions have been used, but numerical integration has been less investigated. In the present chapter, the goal set was the development of a modelling philosophy to generate models using different mathematical approaches, including algebraic equations, ODEs and PDEs.

To achieve a consistent modelling philosophy, a general hierarchy of models was required. Lovatt (1992) classified existing dynamic refrigeration models into 4 types: item, interface, environment and instrument models. The latter is not relevant to this work. Lovatt stated that an item model contains one or more dynamic or variable properties. It may or may not be linked to other models and can be referred to as a central model since it contains the variables of direct interest to the modeller. The room enclosures and structures models can be classified under this type, due to their so-called "thermal object" nature.

An interface model serves as a link between two other models. It is structured of properties derived from the two models involved, but it does not have properties by itself. In a sense, an interface model has an intangible nature, but it is necessary for specifying the relation between two models. Boundary conditions are typical examples of interface models. In the present work, because the boundary conditions must be stated for an object model, the term "interface" will be used in the context of "sub-model" and not as a model itself.

An environment model represents the external ambient conditions or acts as a convenient vehicle for representing components that are under steady-state conditions or for which the rate of change is known before the simulation. The "external environment" model is an example of this type.

Fig. 4.1 presents a classification of the models of interest to the first stage of this

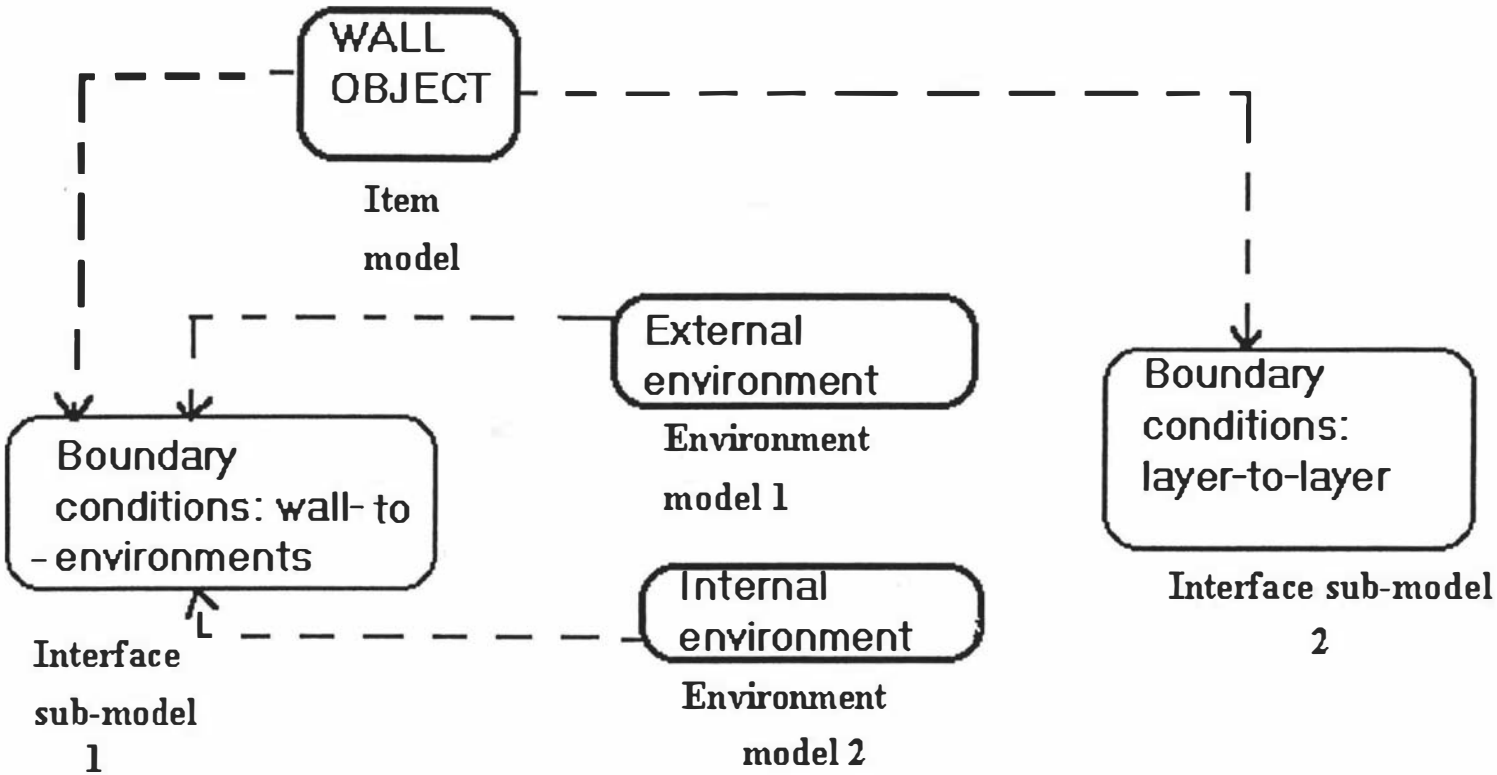

Figure 4.1. Classification of the models used in the mathematical modelling of walls.

project. Using the models presented, a variety of walls can be simulated. The flow chart of Fig. 4.2 presents the methodology used to develop mathematical models for various wall types.

4.1. Physical models.

In climate control applications such as commercial buildings, the thermal mass of the furniture inside the room, the heat flow from the room users and the solar radiation and convective flows entering through the fenestration are much more significant than the dynamics of the other components. Generally, the wall has a heavy structure combined with low levels of insulation and models have been constructed accordingly.

Low temperature rooms, particularly those used in the food industry, exhibit quite different behaviour. Radiation between walls and both the external environment and the enclosed objects might be present, but the heavily insulated walls used in refrigerated rooms markedly reduce the internal room response to the external environment. The control required for the room air temperature is usually more demanding than in air-conditioning applications and there is less structural mass in the building. Condensed water might freeze on or evaporate from a wall surface, depending on the temperature and humidity transients of the volume of air inside the room. Therefore the approaches used for developing wall models in climate control applications may not be appropriate in low temperature rooms.

In the scope of the present work, a number of assumptions were made in order to simplify the analysis of energy transients for wall structures found in low temperature applications.

4.1.1. Wall models.

A one-dimensional model was considered an adequate description for the aims pursued in this project. Because the boundary conditions on either side of the wall are different, there was no possibility of symmetry conditions across the wall. A variety of materials are used in the construction of walls for low temperature applications, including glass fibre and foam insulations, steel and aluminium lining materials, and structural components made from concrete, wood and plastic. The models must be flexible to deal with these.

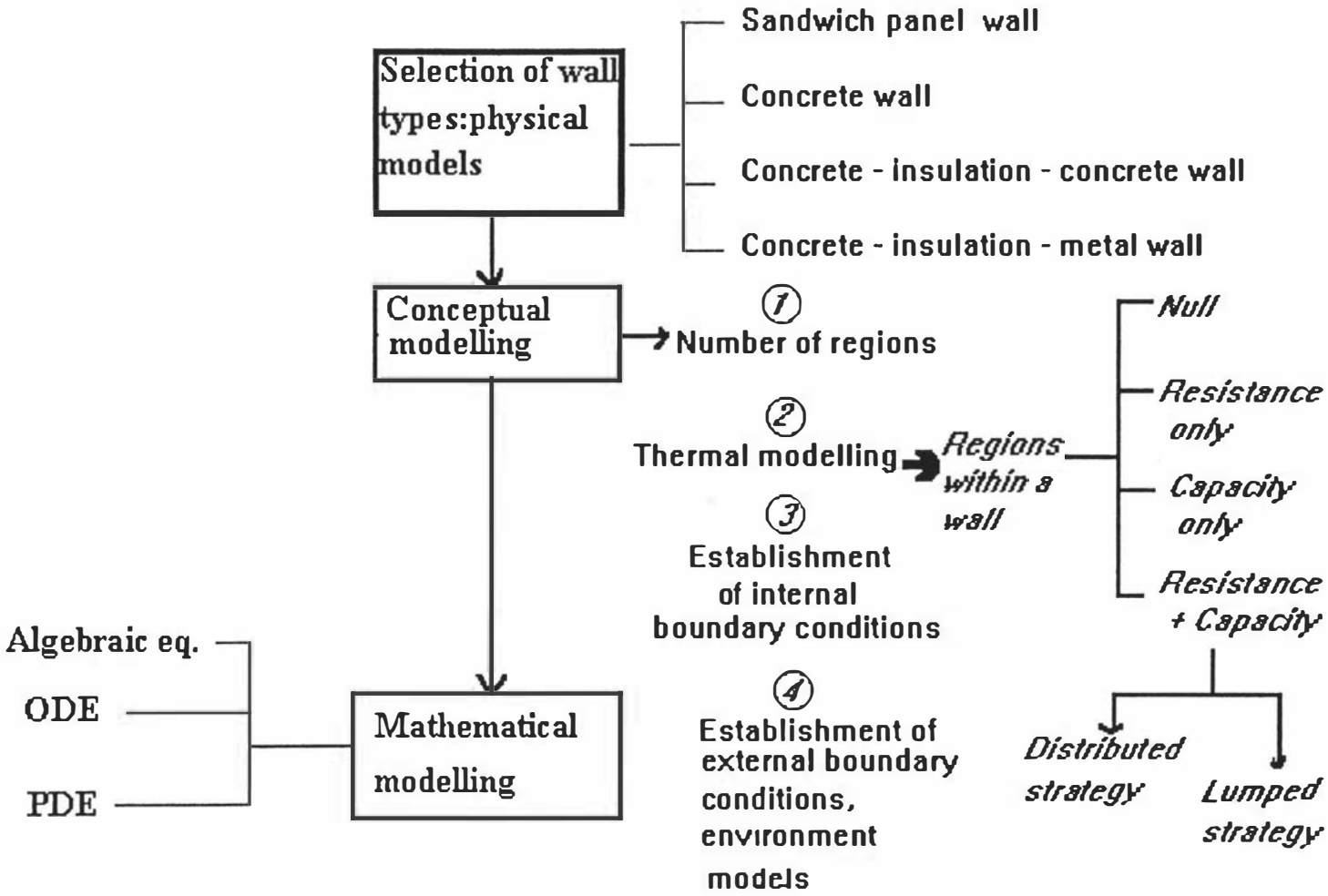

Fig.4.2. Methodology followed for the modelling of walls as thermal objects

4.1.2. Environment models.

The following assumptions were used for the modelling of the external environment:

1) Only convection and radiation were included in the external boundary conditions for walls and ceilings.

2) The external ambient temperature was represented as a time-variable condition. A semi-sinusoidal signal with a peak equalling the highest temperature recorded during the day was assumed.

3) The external heat transfer coefficient was considered constant and uniform across the wall surface, for reasons of simplicity.

4) External radiation was separated into two effects: solar and emitted radiation. The incident solar radiation was modelled as a semi-sinusoidal signal and the emitted radiation was dependent on the difference between the surface temperature and the sky temperature.

The modelling of the internal environment assumed that:

1) The room internal environment interacted with the wall by convection only. Thus, condensation, freezing and evaporation effects were not modelled. The later inclusion of these effects in the boundary conditions would not demand radical changes in the mathematical models.

2) The air temperature inside the room was constant.

Floors interact differently with the external environment. Conduction is the primary mechanism of heat exchange, but convection is also possible if an air duct is installed below the room to allow heat transfer between warm flows of air or water and the floor external layer. Another alternative is concrete wearing layer on top of insulation which itself sits on a concrete slab with an electrical heating system to avoid under floor freezing beneath the insulation. This latter specific situation can be modelled if the heating effect is considered as a heat generation term in the concrete slab.

Floors contacting the ground are usually subjected to less drastic changes in the external environment than those changes occurring in walls and a typical temperature profile is expected to be more or less constant during a day. Hence, the models were only tested in the more demanding situation of a vertical wall or roof.

4.2. Thermal object conceptual models.

The conceptual "thermal object" of Lovatt (1992) was defined as "a solid component of a refrigeration application which may change in temperature during the simulation". In the present context, the most important characteristic of a wall thermal object is the heat flow provided to the room environment.

A thermal object has 3 main characteristics:

1) Thermal resistance or resistance to heat transmission by conduction ($\mathbf{R}$, m^2 K/W). For a one-dimensional slab, this is:

$$\mathbf{R} = \frac{X}{\lambda} \tag{4.1}$$

where:

X = Thickness (m)

λ = Thermal conductivity of the object (W/m K)

2) Thermal capacity ($\mathbf{C}$, J/m^2 K), which is the potential for energy storage (resistance to change in temperature with time or "thermal inertia") within the object.

$$\mathbf{C} = \frac{V \rho c}{A} = X \rho c \tag{4.2}$$

where:

V = Volume (m^3)

ρ = Density (kg/m^3)

c = Specific heat capacity (J/kg K)

A = Surface area (m^2)

3) Heat generation (Hg, W/m^2), which is the conversion of other forms of energy into heat within the object.

$$Hg = H X \tag{4.3}$$

where:

H = heat generation rate within the object (W/m^3)

In Chapter 2 it was stated that room structures could act as buffering thermal masses, as objects to be cooled or both. Hence, the modelling strategy must contemplate both the wall resistance to the heat transfer and its capacity to accumulate energy. In practice, heat generation within structures or walls is not common.

The relative importance of resistance and capacity within an object varies. For example, a so-called sandwich panel wall could be visualised with only thermal resistance, since the insulation layer combines a low thermal conductivity and low density. Both the resistance and thermal capacity of the metal sheets on the sides of the insulation could be assumed negligible. However, when the metal sheets are substituted by concrete layers, neglecting the thermal capacity might lead to inaccurate simulation of the transients of the wall. The differences between specific heat capacities for different building materials used is relatively small, but thermal conductivities and density vary over wider ranges.

4.2.1. Number of regions and shape associated to an object.

One of the early issues addressed was whether to treat an object as a single entity or as a composite body comprising several layers.

It was assumed that an homogeneous wall constructed from a single material should be visualised as one region, whereas composite walls were represented by multiple regions, the number of regions equalling the number of different materials (up to a maximum of 3 regions).

4.2.2. Modelling of thermal characteristics of regions.

According to Fig. 4.2, regions can be defined using resistance only, capacity only, resistance plus capacity (lumped and distributed models) or null characteristics. A brief description of each of these is given below. In all models it was assumed that the thermal properties were not temperature dependent and that each wall layer is internally homogeneous.

As a convention, the external boundary is conceptually always placed on the left, so that heat flows entering the wall follow the left-to-right direction.

1) Thermal resistance only (*R*).

Figure 4.3. illustrates this case. An ***R*** region has no thermal capacity. Thus the general heat conduction equation is:

$$\lambda\left(\frac{\partial^2 T}{\partial x^2}\right) = \frac{V \rho c}{A X}\left(\frac{\partial T}{\partial t}\right) = \frac{\mathbf{C}}{X}\left(\frac{\partial T}{\partial t}\right) = 0 \qquad 0 \le x \le X \tag{4.4}$$

which is further simplified to a linear temperature profile with respect to space:

$$Q_{cond} = \frac{q_{cond}}{A} = \lambda\left(\frac{\Delta T}{X}\right)_{region} = \left(\frac{\Delta T}{\mathbf{R}}\right) \tag{4.5}$$

where:

T	=	Temperature at x (°C)
Q_{cond}	=	Heat flux conducted across the slab (W/m^2)
q_{cond}	=	Heat flow conducted across the slab (W)
t	=	time (s)

2) Thermal capacity only (*C*).

According to Fig 4.4, ***C*** regions have no thermal resistance and thus no temperature change with position. The governing equation can only be defined when the boundary conditions are specified. A single ordinary differential equation (ODE) defines the energy balance for the region: If Q_{in} denotes the heat flow entering the region from the left and Q_{out} denotes the heat flow leaving the region to the right, the ODE can be expressed as:

$$\Sigma Q_{in} - \Sigma Q_{out} = \frac{V \rho c}{A}\left(\frac{dT}{dt}\right) = \mathbf{C}\left(\frac{dT}{dt}\right) \tag{4.6}$$

It is noted that within the region:

$$\frac{dT}{dx} = 0 \tag{4.7}$$

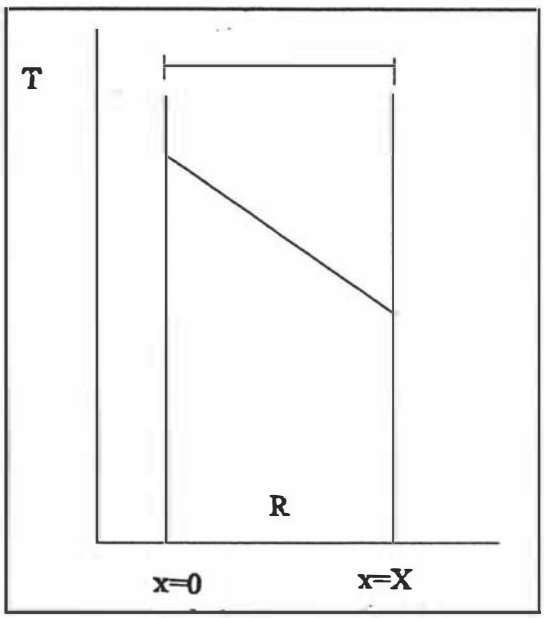

Figure 4.3. Distribution of temperatures through the thickness of a "resistance only" region.

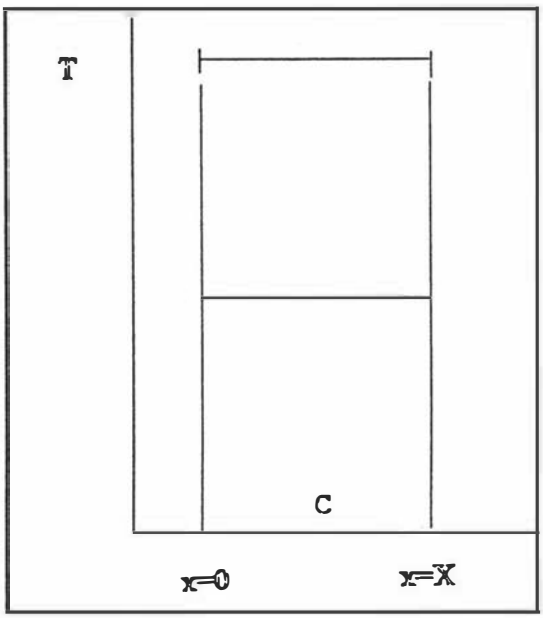

Figure 4.4. Distribution of temperatures through the thickness of a capacitive region.

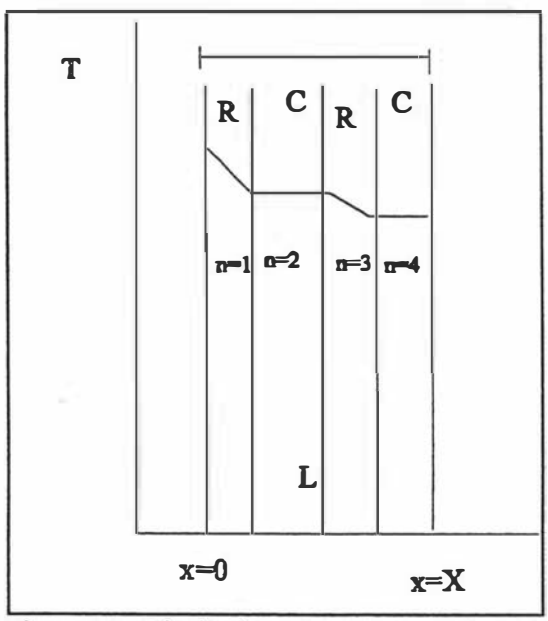

Figure 4.5. Distribution of temperatures through the thickness of "lumped thermal resistance + thermal capacity" regions.

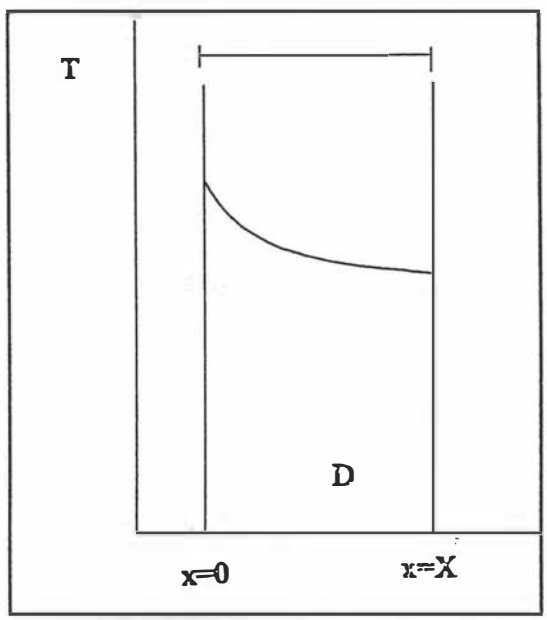

Figure 4.6. Distribution of temperatures through the thickness in "fully distributed thermal resistance + thermal capacity" regions.

3) Thermal resistance plus thermal capacity.

The two options for modelling the combined effect of these thermal properties are the lumped and fully distributed models:

*3a) Lumped model (**L**)*

The lumped or multi-zone type (Fig. 4.5) sub-divides the region into alternating resistive zones (*r*) and capacitive zones (*c*). Thus, resistance and capacity were not considered as fully distributed properties.

The equation describing the behaviour of a *c* zone located between two resistive zones is defined by:

$$\rho \, \Delta x_n \, c \left(\frac{dT}{dt}\right)_n = \lambda \left(\frac{\Delta T}{\Delta x}\right)_{n-1} - \lambda \left(\frac{\Delta T}{\Delta x}\right)_{n+1} \tag{4.8}$$

where n is the code number of the capacity zone and Δx is the thickness of the 3 zones involved.

*3b) Distributed model (**D**).*

The fully distributed model for both thermal resistance and thermal capacity (Fig. 4.6) is the most general and physically correct conceptual representation of a wall region. At any point in the region, the capacity and resistance properties are both significant. The general one-dimensional equation is:

$$\frac{\mathbf{C}}{X} \frac{\partial T}{\partial t} = \frac{\partial}{\partial x}\left(\lambda \frac{\partial T}{\partial x}\right) \qquad 0 \le x \le X \tag{4.9}$$

4) "Null" region (*N*).

The *N* model assumes that a region does not have a significant role in the thermal transients of a wall by neglecting its thermal resistance and capacity, thus only continuity equations at the region boundaries describe its behaviour, implying

$$\frac{\partial T}{\partial x} = 0 \tag{4.10}$$

and

$$T_{x-0} = T_{x-X} \tag{4.11}$$

4.2.3. Theoretical possibilities for walls.

Using the 5 types of models for wall regions, the possible mathematical combinations of model types are:

a) For 1 region walls: $5^1 = 5$;
b) For 2 region walls: $5^2 = 25$;
c) For 3 region walls: $5^3 = 125$.

The implementation of all the possible models for a 3-layered wall object is impractical. Furthermore, not all models match the characteristics of common wall systems. Therefore, a reduction of possibilities was carried out for each type of wall. This process is discussed further in Section 4.4. The conceptual models applicable to a single layer are listed in Table 4.1 as a function of the total number of zones (*nz*) found within the layer. An ***L*** model may decrease the computation times compared to a ***D*** model, since only algebraic equations and ODE's are used. However, this advantage might only be achieved when *nz* is less than the number of nodes required for an accurate finite difference approximation to the partial differential equation (PDE).

4.2.4. Distribution of thermal resistance and capacity in mathematical schemes.

The visualisation of spatial distribution of ***R***, ***C***, ***L*** and ***D*** models is presented in Figs. 4.3 to 4.7 and the mathematical interpretation was as follows:

*4.2.4.1 Resistance distribution in **R** models.*

An ***R*** region is effectively a one-zone special case of a multi-zone model and it is defined as in Eq. (4.5), using the total thickness of the region to calculate the resistance term. The explicit mathematical scheme for ***R*** models is:

$$Q_{cond,nr} = \left(\frac{T_{nr,1} - T_{nr+1,1}}{\mathbf{R}_{nr}} \right) \tag{4.12}$$

where:

nr	=	Number of the region (1,2 or 3)
$Q_{cond,nr}$	=	Conductive heat flux across region nr (W/m^2)
$T_{nr,1}$	=	Temperature at the boundary defining the start of the region nr (°C)
$T_{nr+1,1}$	=	Temperature at the boundary defining the end of the region nr (°C), also defined as $T_{nr,2}$
$\mathbf{R}_{nr}$	=	Thermal resistance for region nr, as defined in Eq. (4.1) (m^2 K/W)

The subscripts used to define the temperatures in the models are further explained in Section 4.2.4.3 and Fig. 4.7. In the present project, the number of the region nr can vary between 1 and NR, where the later is the total number of regions in a wall. In this project, a maximum of $NR = 3$ has been established, but it is conceptually possible to increase this number for other purposes.

NUMBER OF ZONES (nz)	POSSIBLE CONCEPTUAL MODELS	EQUATION FORM
1	1) ***R*** 2) ***C*** 3) ***N***	1) Algebraic 2) ODE 3) None
>1	1) ***L*** 2) ***D***	1) Algebraic + ODE 2) PDE

TABLE 4.1. CONCEPTUAL AND MATHEMATICAL SCHEMES FOR A WALL LAYER.

4.2.4.2 Capacity distribution in C models.

The mass and volume considered for calculating the thermal capacity term are those of the whole region and the mathematical representation of this model is:

$$\mathbf{C}_{nr}\left(\frac{dT_{nr,1}}{dt}\right) = Q_{in,nr} - Q_{out,nr} \tag{4.13}$$

where:

$T_{nr,1} = T_{nr+1,1}$	=	Temperatures at boundaries defining the start and the end of the capacitive region (°C)

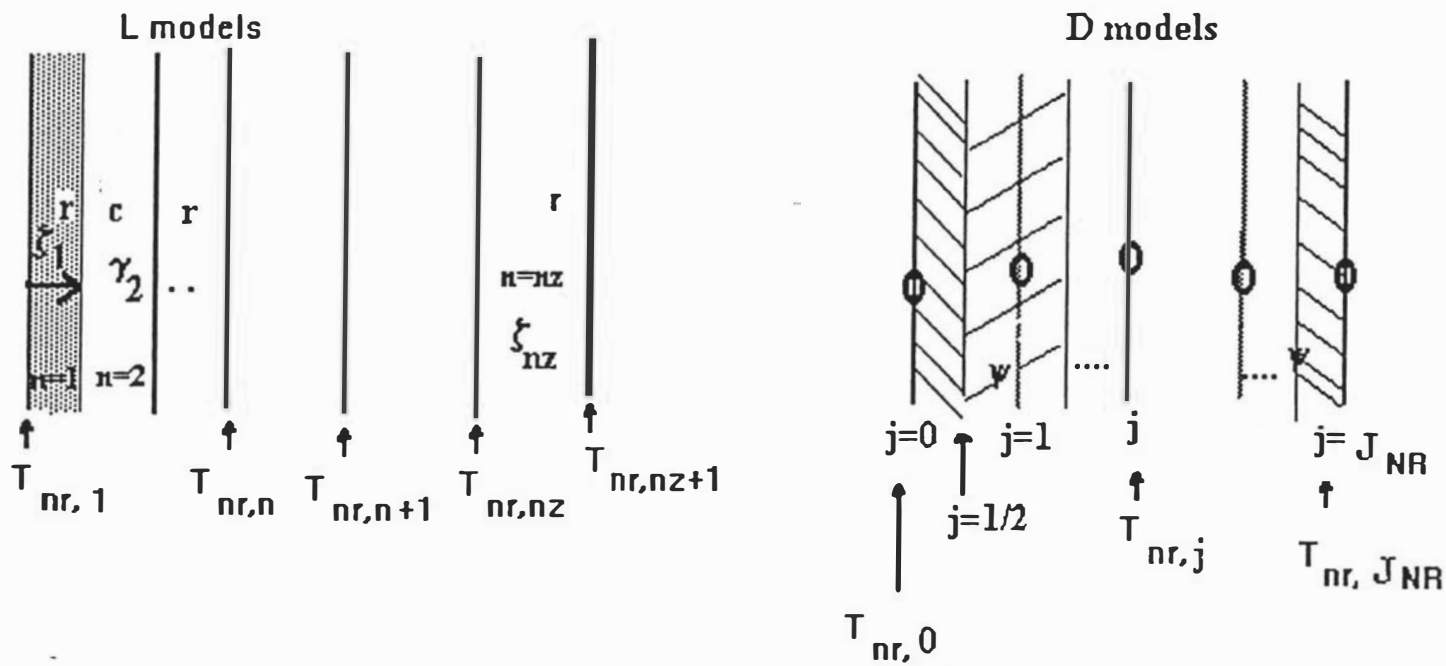

Fig. 4.7. Zone and element definitions in lumped *(L)* and distributed *(D)* models

$Q_{in,nr}$, $Q_{out,nr}$ = Conductive, convective and/or radiative heat fluxes entering and leaving the region, respectively (W/m^2).

Because the ***C*** region is represented by a single temperature, it follows that the temperatures on the boundaries with adjacent regions must be the same.

*4.2.4.3 Resistance and capacity distribution in **L** models.*

In an ***L*** model (Fig. 4.7), the overall thermal resistance and thermal capacity can in theory be placed anywhere throughout the zones, provided that the total resistance and capacity are conserved. There are *nz* zones (*nz*+1 interzone boundaries) in total within the region.

A fraction ζ of the total resistance was assigned to each of the *r* zones and γ fraction was similarly used for the *c* zones. The total sum of the fractions across a region must equal 1 for the total resistance and total capacity to be conserved. Therefore:

$$\sum_{n=1}^{nz} \zeta_n \, \mathbf{R} = \mathbf{R} \tag{4.14}$$

$$\sum_{n=1}^{nz} \gamma_n \, \mathbf{C} = \mathbf{C} \tag{4.15}$$

A large number of combinations of *r* and *c* fractions is possible without violating these limits. Note that within a region, *r* and *c* zones must alternate. In *r* zones, γ_n=0 and in *c* zones, ζ_n=0. This is further discussed in Section 4.2.6.

When referring to ***L*** models two subscripts were used in order to account for: 1) the region and 2) the zone number (*n*). Densities ρ, thermal capacities $\mathbf{C}$ and specific heat capacities ***c*** can be defined using a single subscript, since the thermal properties remain constant in a specific region of the wall.

Thus, the heat flux over an *r* zone in a region was defined as:

$$Q_{cond,nr,n} = \left(\frac{T_{nr,n} - T_{nr,n+1}}{\mathbf{R}_{nr} \, \zeta_{nr,n}} \right) \tag{4.16}$$

where:

nr = number of region (1,2 or 3)

n = number (position) of zone, proved that $2 \leq n \leq nz$ where nz = total number of zones

$Q_{cond,nr,n}$ = conductive heat flux through zone n of region nr (W/m^2)

$T_{nr,n}$ = Temperature at the boundary defining the start of the zone n in region nr (°C)

$T_{nr,n+1}$ = Temperature at the boundary defining the end of the zone n in region nr (°C)

$\mathbf{R}_{nr}$ = Thermal resistance of region nr, as defined in Eq. (4.1) (m^2 K/W)

$\zeta_{nr,n}$ = fraction of total thermal resistance of region nr occurring in zone n (non-dimensional)

This definition could also be applied to a single zone in a region by setting:

- $\zeta_{nr,n} = 1$
- $T_{nr,n+1} = T_{nr+1,1}$

when the total number of zones is 1 ($n = nz = 1$). Thus, equation (4.16) might be used for both r and $\boldsymbol{R}$ thermal models. The equivalent capacitive zone definition for zone n in region nr becomes:

$$\mathbf{C}_{nr}\,\gamma_{nr,n}\left(\frac{d\,T_{nr,n}}{d\,t}\right) = \frac{1}{\mathbf{R}_{nr}}\left[\left(\frac{T_{nr,n-1} - T_{nr,n}}{\zeta_{nr,n-1}}\right) - \left(\frac{T_{nr,n} - T_{nr,n+1}}{\zeta_{nr,n+1}}\right)\right] \qquad (4.17)$$

where:

$\gamma_{nr,n}$ = Fraction of the total capacity for region nr occurring in zone n (non-dimensional)

The simplification of this equation for a one-zone region (nz = 1) so that Eq. (4.17) can be used for both c and $\boldsymbol{C}$ thermal models is achieved by setting:

- $\gamma_{nr,n} = 1$
- $T_{nr,n-1} = T_{nr-1,nz}$
- $T_{nr,n+1} = T_{nr+1,1}$

For ***L*** models Eq. (4.16) and (4.17) apply to n between 2 and nz, where nz = total number of zones. A region with nz zones has nz+1 boundaries, including the boundaries with external and internal environments and all interzone boundaries.

*4.2.4.4 Distribution of resistance and capacity in **D** models.*

A finite difference approximation to implement the fully distributed model implies the use of nodal temperatures defined in space (j) and time (i) coordinates. The thermal properties are defined according to the region number nr. Two subscripts for defining the position within the wall and one superscript for defining the time coordinate were used in the notation of temperatures. According to Figure 4.7, the definitions of j and i are the following:

- j = 0 defines the node at the left boundary, which may be the external environment → wall (outer most boundary of the region) boundary or an inter-region boundary
- $j=J_{nr}$ defines the node at the right boundary, which may be an interregion boundary or the wall → internal environment boundary, where J_{nr}= total number of space divisions (elements) in region nr
- $0 < j < J_{nr}$ defines any node between the boundaries of region nr.

For simplicity, an explicit finite difference (FD) scheme with an equal spatial distribution for all the general elements of a ***D*** region was used. The distribution was given according to the equation:

$$\Delta x_{nr} = \frac{X_{nr}}{J_{nr}} \tag{4.18}$$

where:

Δx_{nr}	=	Space step in the x dimension in region nr (m)
J_{nr}	=	Total number of space divisions (elements) in region nr
X_{nr}	=	Thickness of region nr (m)

It follows that:

$$\frac{\lambda_{nr}}{X_{nr}} = \frac{\lambda_{nr}}{J_{nr}\,\Delta x_{nr}} = \frac{1}{\mathbf{R}_{nr}} \tag{4.19}$$

and:

$$\mathbf{R}_{nr}\left(\frac{1}{J_{nr}}\right) = \mathbf{R}\,\psi_{nr} = \left(\frac{\Delta x}{\lambda}\right)_{nr} \tag{4.20}$$

The definition of the thermal resistance still follows Eq. (4.1) and the fraction of the total resistance occurring in any element is J_{nr}^{-1} for explicit FD schemes. This can be defined as ψ_{nr}. Since the factor ψ is the same for all elements within a region, only one subscript is required to identify the ***D*** region.

In a similar manner, the thermal capacity $\mathbf{C}$ associated with the general nodes is defined as:

$$\mathbf{C}_{nr}\left(\frac{1}{J_{nr}}\right) = \mathbf{C}_{nr}\,\psi_{nr} = (\Delta x\ \rho\ c)_{nr} \tag{4.21}$$

The fractional factor ψ is the same as that for resistance. The ***D*** model fixes the placement of the resistance and capacity, contrasting with the flexibility of the ***L*** model.

In the case of nodes placed at the boundaries with external and internal environments or adjacent regions, the thermal capacity is halved. Thus, the left hand side of Eq. (4.21) is replaced by:

$$0.5\ \mathbf{C}\psi_{nr} \qquad \text{for } j=0 \text{ and } j = J_{nr} \tag{4.22}$$

In an explicit FD scheme, the general element equation is:

$$\mathbf{C}_{nr}\,\psi_{nr}\left(\frac{T^{i+1}_{nr,j} - T^{i}_{nr,j}}{\Delta t}\right) = \left(\frac{T^{i}_{nr,j-1} - 2\,T^{i}_{nr,j} + T^{i}_{nr,j+1}}{\mathbf{R}_{nr}\,\psi_{nr}}\right) \tag{4.23}$$

4.2.5 Modelling of thermal contact between regions.

In all types of walls investigated, perfect thermal contact and continuous heat transfer between layers were assumed, even though a "perfect contact" assumption may not accurately represent the physical reality of some surface-to-surface contacts, *e.g.* a concrete surface against an insulation layer made of preformed slabs of polystyrene might allow air voids between the two surfaces. However, because of the substantial thermal resistance in the insulation, extra resistance caused by non-perfect contact can be neglected without introducing a significant error in the model. Consideration of non-perfect contact would probably lead to unnecessary complexity in the conceptual and mathematical models.

The continuity equation at the boundary between two regions (or zones) is described as:

$$\begin{pmatrix} \textit{Heat flux entering} \\ \textit{boundary} \end{pmatrix} = \begin{pmatrix} \textit{Heat flux leaving} \\ \textit{boundary} \end{pmatrix} \tag{4.24}$$

The various cases of contact between two regions or zones are summarised in Table 4.2. The boundary conditions for *r* or ***R*** zones or regions can be visualised straightforwardly, but the boundary equations between two consecutive capacitive zones or regions have to be visualised in terms of the heat flows entering and leaving the zone, represented by environment models or adjacent resistance zones or regions.

4.2.6 Modelling of two consecutive regions/zones with the same thermal characteristic.

The ***L*** models comprise a number of alternative *r* and *c* zones which means that the case of two consecutive zones within a region with the same thermal definition cannot occur. However, some models present contact between 2 different regions with the same thermal characteristic, *e.g.* an ***LL*** model setting the last zone of region 1 as *c* and the first zone of region 2 as *c*. The sequence of zone properties across the region boundary would be $r \rightarrow c \rightarrow c \rightarrow r$ and the mathematical treatment of such case demands the lumping of the central thermal masses between the 2 resistance zones to create an $r \rightarrow \Sigma c \rightarrow r$ model.

There are other models that require the contact of an ***L*** model with an ***R*** or ***C*** model. In the ***LR*** case, if 3 zones are defined for the ***L*** region in the sequence $r \rightarrow c \rightarrow r$, the complete model would be: $r \rightarrow c \rightarrow r \rightarrow \boldsymbol{R}$. Conceptually, the case could be simplified to an $r \rightarrow c \rightarrow \Sigma \boldsymbol{R}$ (3 region) model, but the thermal resistance used for *r* and ***R*** are different.

For two consecutive fully distributed regions (***DD***), the solution places a node in the boundary of two regions, thus requiring it to account for the thermal capacity of parts of the two regions. The case of a ***D*** region in contact with an ***L***, ***C*** or ***R*** model also has to consider the lumping of capacity and possibly resistance in the boundary element and zone.

TABLE 4.2. CONTINUITY EQUATIONS FOR PERFECT CONTACT BETWEEN 2 REGIONS/ZONES.

The region *nr* is placed at the left of the boundary and the region *nr+1* is at the right of the boundary.

The left hand side (LHS) of the equations represent the heat flux entering the boundary and the right hand side (RHS) represents the heat flux leaving the boundary.

To obtain the boundary condition for an specific contact case, select the region or zone placed at the LHS and follow the same row to find the required region or zone at the RHS.

		REGION $nr+1$			
	n	r	R	D	c/C
REGION nr	c/C	$Q_{out,nr} = \left(\frac{T_{nr+1,1} - T_{nr+1,2}}{\mathbf{R}_{nr+1}\, \zeta_{nr+1,1}} \right)$ (4.25)	$Q_{out,nr} = \left(\frac{T_{nr+1,1} - T_{nr+2,1}}{\mathbf{R}_{nr+1}} \right)$ (4.26)	$Q_{out,nr} = \left(\frac{T_{nr+1,j=0} - T_{nr+1,j=1}}{\mathbf{R}_{nr+1}\, \Psi_{nr+1}} \right)$ (4.27)	$Q_{out,nr} = Q_{in,nr+1}$ (4.28)
	r	$\left(\frac{T_{nr,nz} - T_{nr,nz+1}}{\mathbf{R}_{nr}\, \zeta_{nr,nz}} \right) = \left(\frac{T_{nr+1,1} - T_{nr+1,2}}{\mathbf{R}_{nr+1}\, \zeta_{nr+1,1}} \right)$ (4.29)	$\left(\frac{T_{nr,nz} - T_{nr,nz+1}}{\mathbf{R}_{nr}\, \zeta_{nr,nz}} \right) = \left(\frac{T_{nr+1,1} - T_{nr+2,1}}{\mathbf{R}_{nr+1}} \right)$ (4.30)	$\left(\frac{T_{nr,nz} - T_{nr,nz+1}}{\mathbf{R}_{nr}\, \zeta_{nr,nz}} \right) = \left(\frac{T_{nr+1,j=0} - T_{nr+1,j=1}}{\mathbf{R}_{nr+1}\, \Psi_{nr+1}} \right)$ (4.31)	$\left(\frac{T_{nr,nz} - T_{nr,nz+1}}{\mathbf{R}_{nr}\, \zeta_{nr,nz}} \right) = Q_{in,nr+1}$ (4.32)

continued...

Table 4.2 continued...

REGION $nr+1$					
REGION nr	n	r	R	D	c/C
	R	$\left(\frac{T_{nr,1} - T_{nr+1,1}}{\mathbf{R}_{nr}}\right) - \left(\frac{T_{nr+1,1} - T_{nr+1,2}}{\mathbf{R}_{nr+1}\,\zeta_{nr+1,1}}\right)$ (4.33)	$\left(\frac{T_{nr,1} - T_{nr+1,1}}{\mathbf{R}_{nr}}\right) - \left(\frac{T_{nr+1,1} - T_{nr+2,1}}{\mathbf{R}_{nr+1}}\right)$ (4.34)	$\left(\frac{T_{nr,1} - T_{nr+1,j=0}}{\mathbf{R}_{nr}}\right) - \left(\frac{T_{nr+1,j=0} - T_{nr+1,j=1}}{\mathbf{R}_{nr+1}\,\Psi_{nr+1}}\right)$ (4.35)	$\left(\frac{T_{nr,1} - T_{nr+1,1}}{\mathbf{R}_{nr}}\right) = Q_{in,nr+1}$ (4.36)
	D	$\left(\frac{T_{nr,j=J-1} - T_{nr,j=J}}{\mathbf{R}_{nr}\,\Psi_{nr}}\right) - \left(\frac{T_{nr+1,1} - T_{nr+1,2}}{\mathbf{R}_{nr+1}\,\zeta_{nr+1,1}}\right)$ (4.37)	$\left(\frac{T_{nr,j=J-1} - T_{nr,j=J}}{\mathbf{R}_{nr}\,\Psi_{nr}}\right) - \left(\frac{T_{nr+1,1} - T_{nr+2,1}}{\mathbf{R}_{nr+1}}\right)$ (4.38)	$\left(\frac{T_{nr,j=J-1} - T_{nr,j=J}}{\mathbf{R}_{nr}\,\Psi_{nr}}\right) - \left(\frac{T_{nr+1,j=0} - T_{nr+1,j=1}}{\mathbf{R}_{nr+1}\,\Psi_{nr+1}}\right)$ (4.39)	$\left(\frac{T_{nr,j=J-1} - T_{nr,j=J}}{\mathbf{R}_{nr}\,\Psi_{nr}}\right) = Q_{in,nr+1}$ (4.40)

The mathematical treatment of these cases and the lumping techniques for consecutive regions/zones with the same thermal characteristic are described in Section 4.4.2.

4.3. Environment boundary conditions.

4.3.1. External environment model.

a) **Convection**. This component of the boundary condition followed the well-known expression:

$$Q_c = h_1 \left(T_a - T_{1,1}\right) \tag{4.41}$$

where:

Q_c = Convective heat flux (W/m^2)
h_1 = External heat transfer convective coefficient W/m^2 K)
T_a = Ambient temperature (°C)
$T_{1,1}$ = $T_{1\,j=0}$ in ***D*** models

The ambient temperature T_a was modelled using the equations of Kimball and Bellamy (1986), whereas h_1 was considered constant. During the day, the ambient temperature was calculated as:

$$T_a = T_{\min} + \left(T_{\max} - T_{\min}\right) \sin\left[\frac{\pi \left(t_d - t_{\min}\right)}{\left(D_a + 3.72\right)}\right] \tag{4.42}$$

During the nights, an exponential decay was assumed:

$$T_a = \left(T_{\min} - y\right) + \left[T_{set} - \left(T_{\min} - y\right)\right] \exp\left[\frac{-b\left(t_d - t_{set}\right)}{\left(24 - D_a + z\right)}\right] \tag{4.43}$$

where:

$$y = \frac{T_{set} - T_{\min}}{\exp(b) - 1} \tag{4.44}$$

and:

T_{min}, T_{max} = Minimum and maximum temperatures in a 24 hr cycle (°C)
t_d = Solar time in a 24 hr cycle (hrs)

t_{min}	=	time of minimum ambient temperature in a daily cycle (hrs)
D_a	=	Astronomical day length (hrs)
T_{set}	=	Temperature at sunset time (°C)
t_{set}	=	Sunset time (hrs)
z	=	constant = -0.17 for New Zealand conditions
b	=	constant = 2.2 for New Zealand conditions

b) **Radiation.** The incident solar radiation was defined (Gray and Mueller, 1974) as:

$$Q_{inc} = W \alpha \theta \tag{4.45}$$

where:

Q_{inc}	=	Incident radiative heat flux (W/m^2)
W	=	Solar constant = 1,390 W/m^2
α	=	Absorptivity (dimensionless) = 0.2 (assumed)
θ	=	Cosine of the angle of incidence measured between the solar beam and the normal to the surface (dimensionless) A, page 55

The emitted radiation was a function of the absolute surface and ambient temperatures (Gray and Mueller, 1974):

$$Q_{em} = \varepsilon \sigma \left(T_{1,1}^4 - T_{sky}^4\right) \tag{4.46}$$

where:

Q_{em}	=	Emitted radiative heat flux (W/m2)
ε	=	Emissivity (dimensionless)
σ	=	Stefan-Boltzmann constant = 5.66 x 10^{-8} W/m^2 K^4
$T_{1,1}$ and T_{sky}	=	absolute surface and sky temperatures (K)

The sky temperature in Celsius was calculated as a power law function of the ambient temperature:

$$T_{sky} = 0.0552\ T_a^{1.5} \tag{4.47}$$

The net radiative heat flux Q_{rad} (W/m^2) was described as:

$$Q_{rad} = Q_{inc} - Q_{em} \tag{4.48}$$

c) **Convection + radiation external environment model.**[B] The sum of convection and radiation entering the wall from the external environment ($Q_{a\rightarrow w}$, W/m^2) was defined as:

$$Q_{a\rightarrow w} = Q_c + Q_{rad} = h_1 \left(T_a - T_{1,1}\right) + W \alpha \theta - \varepsilon_1 \sigma \left(T_{1,1}^4 - T_{sky}^4\right) \qquad (4.49)$$

4.3.2. Internal environment model.

The convective heat flux entering the room was expressed as:

$$Q_{w\rightarrow room} = h_2 \left(T_{NR,nz+1} - T_{room}\right) \qquad (4.50)$$

where:

NR	=	total number of regions in a wall.
$T_{NR,nz+1}$	=	$T_{NR\,j=J}$ in ***D*** models

4.3.3. Boundaries "External environment" → "Wall" → "Internal environment".

Table 4.3 presents the boundary equations that can arise for these situations. Again, the cases of capacitive regions / zones in the boundaries were defined in terms of the parameters in the adjacent region.

[A] The appropriate equations for time dependency of θ were:

$$\theta = \sin(-40.4)\sin(\delta) + \cos(-40.4)\cos(\delta)\sin\left(15\,\pi\,(t - 12)/180\right) \qquad (4.45a)$$

$$\delta = 23.45\,\sin\left(360\,(284 + day)/365\right) \qquad (4.45b)$$

where -40.4 is the latitude for Palmerston North and *day* is the Julian day (the day selected was 160). Some of these symbols are not defined in the Nomenclature.

[B] This model was used to generate tabular data for Q_{inc}, T_a and T_{sky} vs time. These data are presented in Section 5.1, Fig. 5.1.

CONTACT INTERFACE MODEL → OBJECT MODEL/SUB-MODEL→ INTERFACE MODEL			
External environment → Wall (nr=1)		Wall → Internal environment (nr=NR)	
C	c	***C***	c
$Q_{a\to w} = Q_{in,1}$ (4.51)		$Q_{out,NR} = Q_{w\to room}$ (4.52)	
R	r	***R***	r
$Q_{a\to w} = \left(\frac{T_{1,1} - T_{2,1}}{\mathbf{R}_1}\right)$ (4.53)	$Q_{a\to w} = \left(\frac{T_{1,1} - T_{1,2}}{\mathbf{R}_1\ \zeta_{1,1}}\right)$ (4.54)	$\left(\frac{T_{NR,1} - T_{NR,2}}{\mathbf{R}_{NR}}\right) = Q_{w\to room}$ (4.55)	$\left(\frac{T_{NR,nz} - T_{NR,nz+1}}{\mathbf{R}_{NR}\ \zeta_{NR,nz}}\right) = Q_{w\to room}$ (4.56)
D		**D**	
$Q_{a\to w} = -\lambda_1 \left(\frac{\partial T}{\partial x}\right)_{1,j=0}$ (4.57)		$\lambda_{NR}\left(\frac{\partial T}{\partial x}\right)_{NR,j=J} = -Q_{w\to room}$ (4.58)	

TABLE 4.3. BOUNDARY CONDITION EQUATIONS FOR EXTERNAL AND INTERNAL ENVIRONMENT MODELS.

Note: Q_{in} is the heat flow entering the first region and Q_{out} is the heat flow leaving the last region of wall. $Q_{a\to w}$ is calculated through Eq. (4.49) and $Q_{w\to room}$ is similarly defined in Eq. (4.50).

4.4. Construction of mathematical models.

4.4.1. Heat fluxes entering and leaving a region/zone.

Table 4.4 presents the mathematical expressions for conductive heat flows that could appear when constructing a thermal model for a wall object. In some cases, a (+) or (-) has been used to define whether the heat flux is entering or leaving the wall. The equations of Table 4.4 account for cases of 2 and 3 consecutive resistive regions and zones, discussed in Section 4.2.6. Recalling Section 4.2.4.1, when an ***R*** region is described the total number of zones *nz* must be equal to 1. In cases involving an *r* zone, *nz* must be greater than 1.

4.4.2. Heat accumulation in a wall.

Table 4.5 presents the expressions for Q_{acc}, the rate of heat accumulation that could appear in 1, 2 and 3 regions and/or zones represented by thermal capacity, or in a full distributed scheme. Similarly to the conductive heat flows, when a ***C*** region is described *nz* must be equal 1. For a *c* zone, *nz* must be greater than 1.

TABLE 4.4. CONCEPTUAL AND MATHEMATICAL REPRESENTATIONS OF CONDUCTIVE HEAT FLOWS ENTERING AND LEAVING A WALL/REGION/ZONE (Note: Q_{cond} may be either Q_{in} or Q_{out}).

CASE	EQUATION (Q_{in} or Q_{out})	APPLICATION REMARKS
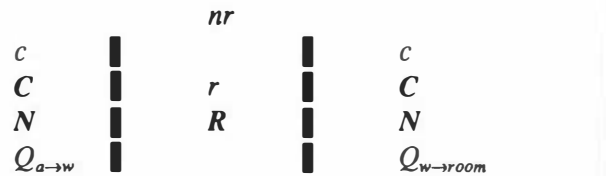 Resistive region/zone between *c*, ***C***, ***N*** or external/internal environment models	$Q_{cond} = \left(\frac{T_{nr,n} - T_{nr,n+1}}{\mathbf{R}_{nr}\ \zeta_{nr,n}} \right)$ (4.59)	$1 \le nr \le NR$ Case *r*: $\zeta_{nr,n}<1$ Case ***R***: $\zeta_{nr,n}=1$ and $n=1$
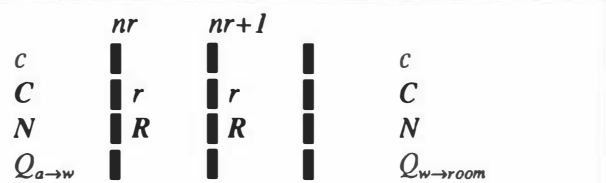 Two adjacent resistive regions/zones between *c*, ***C***, ***N*** or external/internal environment models	$Q_{cond} = \left(\frac{T_{nr,nz} - T_{nr+1,2}}{\mathbf{R}_{nr}\ \zeta_{nr,nz} + \mathbf{R}_{nr+1}\ \zeta_{nr+1,1}} \right)$ (4.60)	$1 \le nr \le NR$ Cases *rr* and *rR*: $\zeta_{nr,nz}<1$ Cases *rr* and ***Rr***: $\zeta_{nr+1,1}<1$ Cases ***RR*** and ***Rr***: $\zeta_{nr,nz}=1$ and $nz=1$ Cases ***RR*** and *rR*: $\zeta_{nr+1,1}=1$

continued....

Table 4.4 continued...

CASE	EQUATION (Q_{in} or Q_{out})	APPLICATION REMARKS
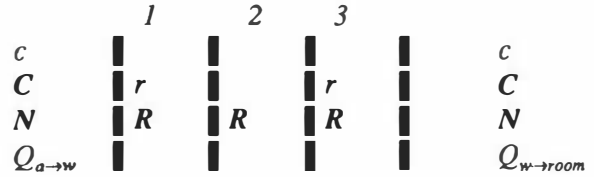 Three adjacent resistive regions/zones between *c* or external/internal environment models	$Q_{cond} = \left(\frac{T_{1,nz} - T_{3,2}}{\mathbf{R}_1 \zeta_{1,nz} + \mathbf{R}_2 + \mathbf{R}_3 \zeta_{3,1}} \right)$ (4.61)	Cases *rRr* and *rRR*: $\zeta_{1,nz}<1$ Case *rRr* and *RRr*: $\zeta_{3,1}<1$ Case *RRr* and *RRR*: $\zeta_{1,nz} = 1$ and $nz=1$ Case *RRR* and *rRR*: $\zeta_{3,1} = 1$ In all cases: $\zeta_{2,1}=1$
 One distributed region between *c* , *C* or *N* models (conduction to nodes placed within the region boundaries)	$Q_{cond} = \pm \left(\frac{T^{i}_{nr,j\pm1} - T^{i}_{nr,j}}{\mathbf{R}_{nr}\ \Psi_{nr}} \right)$ (4.62)	$1 \le nr \le NR$ $0 < j < J_{nr}$ (+) heat flux from the node (-) heat flux to the node

continued...

Table 4.4 continued...

CASE	EQUATION (Q_{in} or Q_{out})	APPLICATION REMARKS
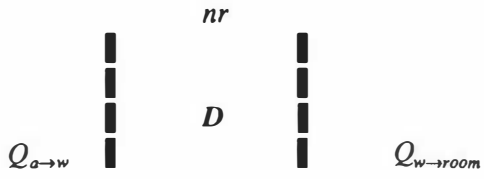 One distributed region between environment models (conduction to nodes placed in the wall boundaries)	See Table 4.3, Eqs.(4.57) and (4.58)	See boundary conditions, Section 4.3
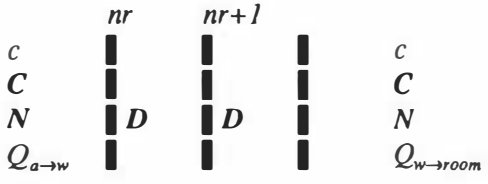 Two adjacent distributed regions between *c*, ***C***, ***N*** or External/internal environment models (conduction to nodes placed in the boundary between regions)	See Table 4.2, Eq.(4.39)	See continuity equation conditions, Section 4.2.6

continued...

Table 4.4 continued...

CASE	EQUATION (Q_{in} or Q_{out})	APPLICATION REMARKS
Case a) 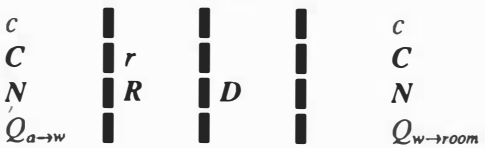 *Case b)* 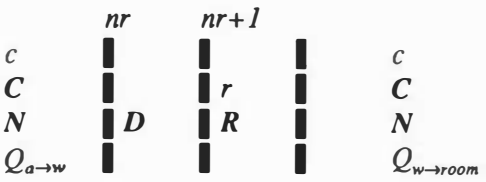 One distributed region adjacent to one resistive region/zone, both between *c*,*C*, *N* or External/internal environment models (conduction to nodes placed in the boundary between regions)	*Case a*) : $Q_{cond} = \left(\frac{T_{nr,nz} - T^{i}_{nr+1,j=0}}{\mathbf{R}_{nr}\ \zeta_{nr,nz}} \right)$ (4.63) *Case b*) : $Q_{cond} = \left(\frac{T^{i}_{nr,j=J} - T_{nr+1,2}}{\mathbf{R}_{nr+1}\ \zeta_{nr+1,1}} \right)$ (4.64)	$1 \leq nr \leq NR$ Case *rD*: $\zeta_{nr,nz}<1$ Case *RD*: $\zeta_{nr,nz}=1$ Case *DR*: $\zeta_{nr+1,1}=1$ Case *Dr*: $\zeta_{nr+1,1}<1$

continued....

Table 4.4 continued...

CASE	EQUATION (Q_{in} or Q_{out})	APPLICATION REMARKS
Case a) 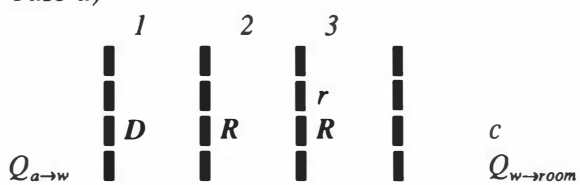 *Case b)* 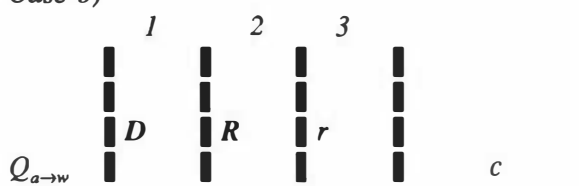 One distributed region 1 adjacent to two resistive regions/zones, between external/internal environment models (conduction to nodes placed in the boundary between regions)	$Q_{cond} = \left(\frac{T^{i}_{1,j=J} - T_{3,2}}{R_2 + R_3 \zeta_{3,1}} \right)$ (4.65)	Case ***DRr***: $\zeta_{3,1} < 1$ Case ***DRR***: $\zeta_{3,1} = 1$

continued....

Table 4.4 continued...

CASE	EQUATION (Q_{in} or Q_{out})	APPLICATION REMARKS
Case a) 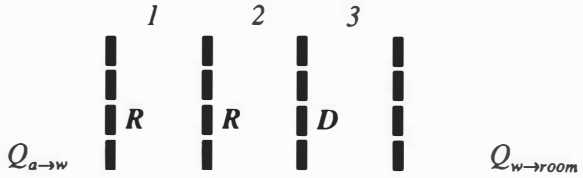 *Case b)* 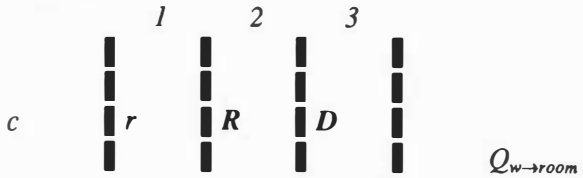 One distributed region 3 adjacent to two resistive regions/zones, between external environment, internal environment or capacitive models (conduction to nodes placed in the boundary between regions)	$$Q_{cond} = \left(\frac{T_{1,nz} - T^{i}_{3,j=0}}{\mathbf{R}_2 + \mathbf{R}_1 \zeta_{1,nz}} \right)$$ (4.66)	Case ***RRD***: $\zeta_{1,1} = 1$ Case ***rRD***: $\zeta_{1,1} < 1$

TABLE 4.5. CONCEPTUAL AND MATHEMATICAL REPRESENTATIONS OF HEAT ACCUMULATION IN A WALL/REGION/ZONE Q_{acc}.

CASE	EQUATION (Q_{acc})	APPLICATION REMARKS
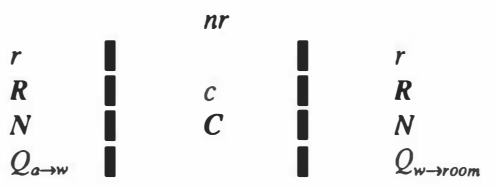 One capacitive region/zone between *r*,***R***, *N* or external/internal environment models	$Q_{acc} = \mathbf{C}_{nr}\,\gamma_{nr,n}\left(\frac{d\,T_{nr,n}}{d\,t}\right)$ (4.67)	$1 \le nr \le NR$ Case *c*: $1 \le n \le nz$ and $\gamma_{nr,n}<1$ Case ***C***: $n=nz=1$ and $\gamma_{nr,n}=1$
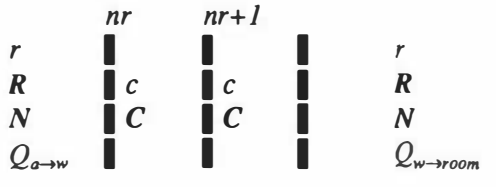 Two adjacent capacitive regions/zones between *r*,***R***, *N* or External/internal environment models	$Q_{acc} = \left(\mathbf{C}_{nr}\,\gamma_{nr,nz} + \mathbf{C}_{nr+1}\,\gamma_{nr+1,1}\right)\left(\frac{d\,T_{nr,nz}}{d\,t}\right)$ (4.68)	$1 \le nr \le NR\text{-}1$ Case *cc* and *c**C***: $\gamma_{nr,nz}<1$ Case *cc* and ***C**c*: $\gamma_{nr+1,1}<1$ Case ***CC*** and ***C**c*: $\gamma_{nr,nz}=1$ and $nz=1$ Case ***CC*** and *c**C***: $\gamma_{nr+1,1}=1$
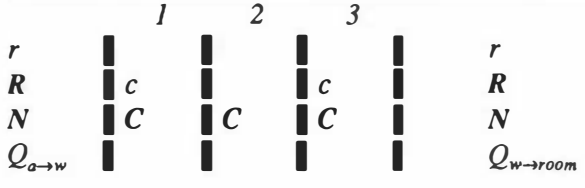 Three adjacent capacitive regions/zones between *r* or external/internal environment models	$Q_{acc} = \left(\mathbf{C}_1\,\gamma_{1,nz} + \mathbf{C}_2 + \mathbf{C}_3\,\gamma_{3,1}\right)\left(\frac{d\,T_{2,1}}{d\,t}\right)$ (4.69)	Case *cCc* and *cCC*: $\gamma_{1,nz}<1$ Case *cCc* and ***CC**c*: $\gamma_{3,1}<1$ Case ***CCc*** and ***CCC***: $\gamma_{1,nz}=1$ Case *cCC* and ***CCC***: $\gamma_{3,1}=1$

continued....

Table 4.5 continued...

CASE	EQUATION (Q_{acc})	APPLICATION REMARKS
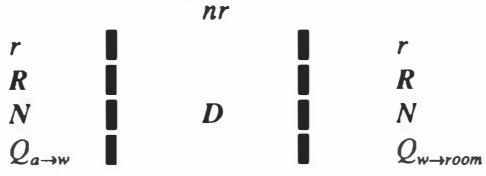 One distributed region between any models (thermal mass of elements placed within the region boundaries)	$Q_{acc} = \mathbf{C}_{nr}\ \Psi_{nr} \left(\frac{T^{i+1}_{nr,j} - T^{i}_{nr,j}}{\Delta t} \right)$ (4.70)	$1 \le nr \le NR$ $1 \le j \le J_{nr}\text{-}1$
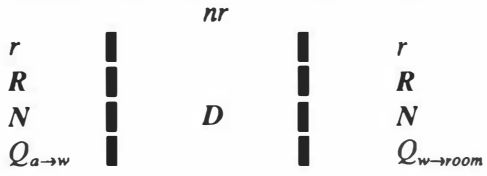 One distributed region between any models (thermal mass of elements placed on the wall boundaries)	$Q_{acc} = 0.5\ \mathbf{C}_{nr}\ \Psi_{nr} \left(\frac{T^{i+1}_{nr,j} - T^{i}_{nr,j}}{\Delta t} \right)$ (4.71)	$1 \le nr \le NR$ $j = 0$ *or* $j = J_{nr}$

continued...

Table 4.5 continued...

CASE	EQUATION (Q_{acc})	APPLICATION REMARKS
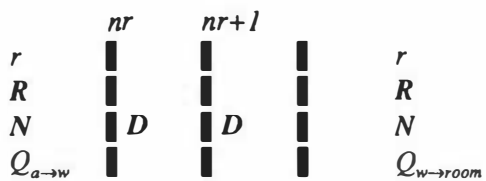 Two adjacent distributed regions between *r*, ***R***, *N* or external/internal environment models (thermal mass of elements placed in the boundary between regions)	$Q_{acc} = 0.5\,(\mathbf{C}_{nr}\,\Psi_{nr} + \mathbf{C}_{nr+1}\,\Psi_{nr+1})\left(\frac{T^{i+1}_{nr,j} - T^{i}_{nr,j}}{\Delta t}\right)$ (4.72)	$1 \le nr \le NR\text{-}1$ $T^{i}_{nr,j=J} = T^{i}_{nr+1,j=0}$ at any i

continued...

Table 4.5 continued...

CASE	EQUATION (Q_{acc})	APPLICATION REMARKS
Case a) 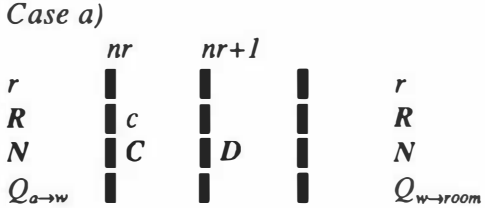 *Case b)* 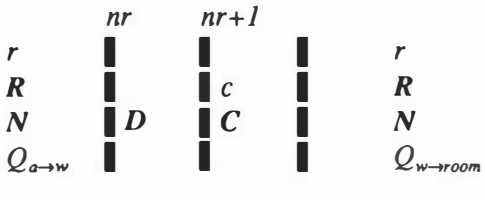 One distributed region adjacent to one capacitive region/zone, both between *r*,***R***, ***N*** or external/internal environment models (thermal mass of elements placed in the boundary between regions)	*Case a)* $Q_{acc} = \left(\mathbf{C}_{nr}\,\gamma_{nr,nz} + 0.5\,\mathbf{C}_{nr+1}\,\psi_{nr+1}\right)\left(\frac{T^{i+1}_{nr+1,j=0} - T^{i}_{nr+1,j=0}}{\Delta t}\right)$ (4.73) *Case b)* $Q_{acc} = \left(0.5\,\mathbf{C}_{nr}\,\psi_{nr} + \mathbf{C}_{nr+1}\,\gamma_{nr+1,1}\right)\left(\frac{T^{i+1}_{nr,j=J} - T^{i}_{nr,j=J}}{\Delta t}\right)$ (4.74)	$1 \le nr \le NR\text{-}1$ Case a): ***CD*** model: $\gamma_{nr,nz}=1$ and $T_{nr,1} = T_{nr,2}=T^{i}_{nr+1,j=0}$ and $nz=1$ at any i *cD* model: $\gamma_{nr,nz}<1$ and $T_{nr,nz} = T_{nr,nz+1} = T^{i}_{nr+1,j=0}$ at any i Case b): ***DC*** model: $\gamma_{nr+1,1}=1$ and $T_{nr+1,1}=T^{i}_{nr,j=J} = T_{nr+1,2}$ at any i *Dc* model: $\gamma_{nr+1,1}<1$ and $T_{nr+1,1}=T^{i}_{nr,j=J} = T_{nr+1,2}$ at any i

continued...

Table 4.5 continued...

CASE	EQUATION (Q_{acc})	APPLICATION REMARKS
Case a) 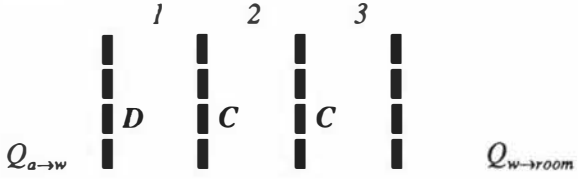 *Case b)* 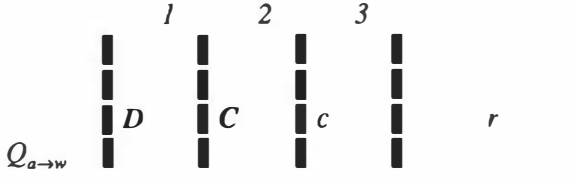 One distributed region 1 adjacent to two capacitive regions/zones between an external environment, internal environment or a resistance model (thermal mass of elements placed in the boundary between regions)	$$Q_{acc} = \left(0.5\ \mathbf{C}_1\ \psi_1 + \mathbf{C}_2 + \mathbf{C}_3\ \gamma_{3,1}\right) \left(\frac{T^{i+1}_{1,j=J} - T^{i}_{1,j=J}}{\Delta t}\right)$$ (4.75)	Case ***DCC***: $\gamma_{3,1} = 1$ and $T_{2,1}=T_{3,1}=T_{3,2}= T^{i}_{1,j=J}$ at any i Case ***DCc***: $\gamma_{3,1} < 1$ and $T_{2,1}=T_{3,1}= T_{3,2}= T^{i}_{1,j=J}$ at any i

continue...

Table 4.5 continued...

CASE	EQUATION (Q_{acc})	APPLICATION REMARKS
Case a) 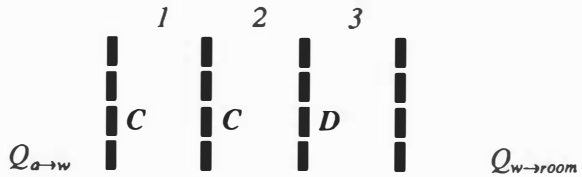 *Case b)* 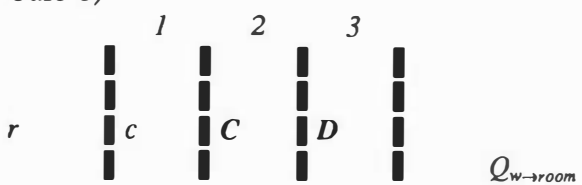 One distributed region 3 adjacent to two capacitive regions/zones between external environment, internal environment or a resistance model (thermal mass of elements placed in the boundary between regions)	$$Q_{acc} = \left(0.5\ \mathbf{C}_3\ \psi_3 + \mathbf{C}_1\ \gamma_{1,nz} + \mathbf{C}_2\right) \left(\frac{T^{i+1}_{3,j=0} - T^{i}_{3,j=0}}{\Delta t}\right)$$ (4.76)	Case a): $\gamma_{1,nz} = 1$ and $T_{1,1}=T_{2,1}= T_{2,2}= T^{i}_{3,j=0}$ at any i Case b): $\gamma_{1,nz} < 1$ and $T_{1,nz}= T_{1,nz+1}=T_{2,1}= T_{2,2}= T^{i}_{3,j=0}$ at any i

4.5 Specific cases investigated.

The methodology described in the previous sections was applied to 4 specific types of walls: sandwich panel (SPT), concrete (CT), concrete-insulation-concrete (CIC) and concrete-insulation-metal (CIM) types (Fig.4.9). The most appropriate conceptual models were selected according to the thermal properties of the wall materials and these are summarised in Table 4.6, categorized according to their degree of mathematical complexity from the most simple to the most complex scheme.

The equations used are given in Tables 4.7 to 4.10 which use Tables 4.4 and 4.5, since the equations described in those apply directly in all cases. The degree of complexity, the implementation and the solution of the equations can be derived from these tables: for regions and zones in which the Q_{acc} term is non-zero, thermal capacity is considered and an ODE or an explicit FD scheme is needed to solve this region/zone. If Q_{acc} is equal to 0, an algebraic solution is obtained.

The fully distributed model ***DDD*** was implemented using an explicit FD approach exclusively in the concrete-insulation-concrete wall. Hence, the derivation of the model is presented only in Section 4.5.3.5. For all other cases, a well established finite element method developed by Cleland (1985) was applied, so the equations are not given in Tables 4.7 to 4.10.

The rationale applied to obtain the models for each case is outlined below.

4.5.1. Sandwich panel type (SPT) wall.

Fig. 4.8a illustrates the physical system, consisting of a thick insulation layer surrounded by two metal sheets (often aluminium or steel layers). The conceptual models considered that the metal sheets had a low or negligible thermal resistance, but significant resistance and negligible thermal capacity was assumed for the central insulation layer. A key issue was whether the energy stored in the external and internal regions was significant or not.

Table 4.7 presents the equations of the mathematical model for the two selected schemes for the STP wall. An explanation of the assumptions for each model is given below.

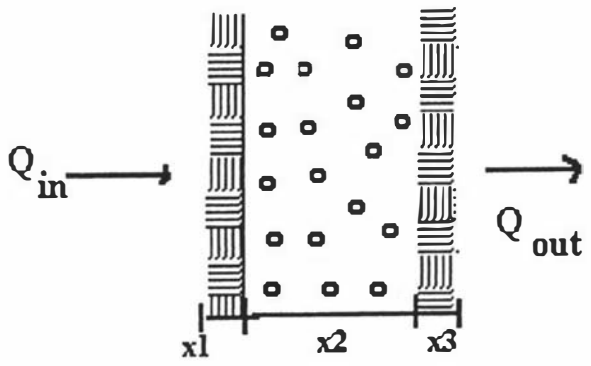

a) Sandwich panel type wall
(STP)

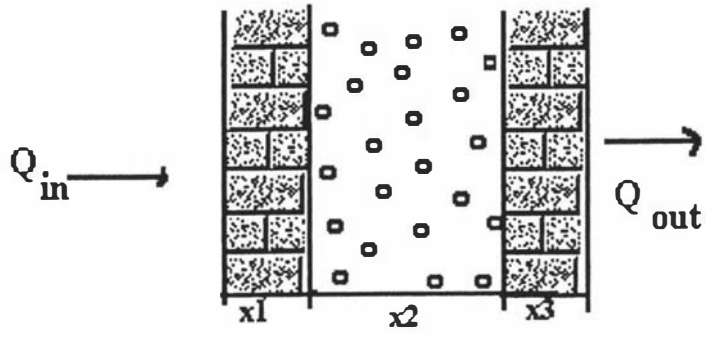

b) Concrete - insulation - concrete wall
(CIC)

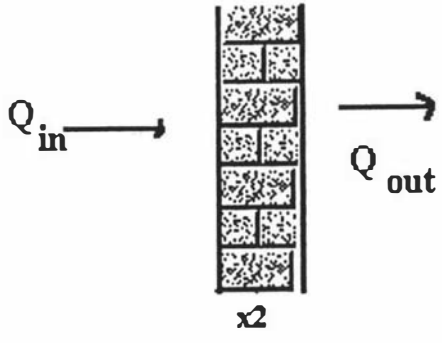

c) Concrete type wall
(CT)

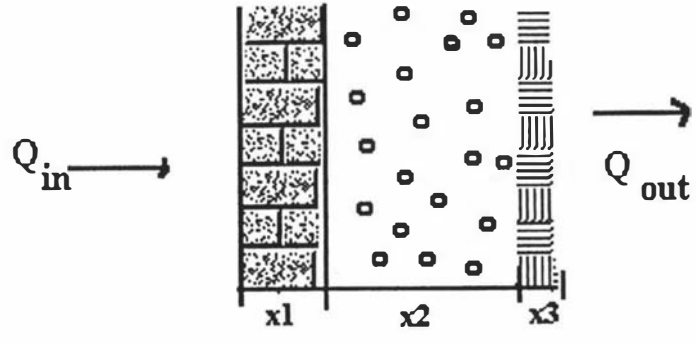

d) Concrete - insulation - metal wall
(CIM)

Fig.4.8. Thermal modelling of walls: systems investigated.

PHYSICAL SYSTEM	*MODELS TESTED*
1) Sandwich panel type wall	*1) **N R N*** *2) **C R C*** *3) **D D D***
2) Concrete only	*1) **N L N*** *2) **N D N*** *3) **D D D***
3) Concrete - insulation - concrete	*1) **R R R*** *2) **R R L*** *3) **L R L*** *4) **D R D*** *5) **D D D***
4) Concrete - insulation - metal	*1) **R R C*** *2) **L R C*** *3) **L L C*** *4) **R D C*** *5) **D D D***

TABLE 4.6 WALLS THERMAL MODELLING: PHYSICAL AND CONCEPTUAL MODELS SELECTED.

4.5.1.1. ***NRN** (Null → Resistance → Null) model.*

This model is commonly used in design applications. The insulation layer is represented as thermal resistance only. The resistance and the heat capacity of the metal sheets were assumed negligible (*N* regions).

4.5.1.2. ***CRC** (Capacity → Resistance → Capacity) model.*

The model assumed a negligible resistance in the metal layers combined with a high thermal capacity. The insulation remained represented as an ***R*** region as for ***NRN***.

The use of a more complex model than ***CRC*** was difficult to justify on grounds of complexity. Hence, models such as ***CLC*** or ***LLL*** were not tested, though they are theoretically possible.

STP MODEL	REGION (*nr*)	Q_{acc} = (W/m²)	Q_{in} - (W/m²)	Q_{out} (W/m²)
NRN	*1*	0	Eq. (4.53)	
	2	0	Eq.(4.53) = Eq.(4.59)	Eq.(4.59) = Eq.(4.55)
	3	0	Eq.(4.55)	
CRC	*1*	Eq.(4.67)	Eq.(4.51)	Eq.(4.59)
	2	0	Eq.(4.59)	Eq.(4.59)
	3	Eq.(4.67)	Eq.(4.59) *for nr=2*	Eq.(4.52)

TABLE 4.7. MATHEMATICAL MODELS USED FOR THE SANDWICH PANEL TYPE WALL.

4.5.2. Concrete type wall (CT).

Fig. 4.8c illustrates this system. The concrete only wall is not commonly used in low temperature practical situations, except in some air conditioned applications. However, the investigation of this wall allowed determination of the effect of the concrete slab separately from the effect of insulation layers. Two conceptual models for representing the concrete thermal mass were investigated.

*4.5.2.1. **NLN** (Null → Lumped → Null) model.*

For concrete structures both thermal capacity and resistance are significant and simpler representations than ***L*** models are unlikely to be useful. To keep computation times lower than for to an ***NDN*** model, a minimum and maximum of one and four *c* zones respectively were used in this scheme. The alternative models for the ***L*** case were:

L1: The ***L*** model has an *r* zone in both external and internal boundaries.

L2: A *c* zone is placed in both external and internal boundaries.

L3: An *r* zone is placed in the external boundary and a *c* zone is placed in the internal boundary.

L4: A *c* zone is placed in the external boundary and an *r* zone is placed in the internal boundary.

The equations used for these alternative mathematical models are presented in Table 4.8.

4.5.2.2. ***NDN*** *(Null → Distributed → Null) model.*

The ***D*** model was selected as the most complex scheme to account for both thermal resistance and capacity. The selection of grids is discussed in Chapter 5.

TABLE 4.8. MATHEMATICAL MODELS USED FOR THE CONCRETE TYPE WALL.

CT MODEL	REG (*nr*)	ZONES (*n*) OR NODES (*j*)	Q_{acc} = (W/m²)	Q_{in} - (W/m²)	Q_{out} (W/m²)
NLN	*1*	*n=nz=1*	0	Eq.(4.51)	
	2	*n=1*	If model is either ***L1*** or ***L3***, Q_{acc}=0	Eq.(4.54)	Eq.(4.59)
			If model is either ***L2*** or ***L4*** , use Eq.(4.67)	Eq.(4.51)	Eq.(4.59) for *n=2*
		c zones, 1<n<nz[1]	Eq.(4.67)	Eq.(4.59) *for n-1*	Eq.(4.59) for *n+1*
		n=nz	If model is either ***L1*** or ***L4***, Q_{acc}= 0	Eq.(4.59)	Eq.(4.56)
			If model is either ***L2*** or ***L3***, use Eq.(4.67)	Eq.(4.59) *for n= nz-1*	Eq.(4.52)
	3	*n=nz=1*	0	Eq.(4.52)	
NDN	*1*	*j=J=0*	0	Eq.(4.57)	
	2	*j=0*	Eq.(4.71)	Eq.(4.57)	Eq.(4.62)
		J>j>0	Eq.(4.70)	Eq.(4.62)	Eq.(4.62)
		j=J	Eq.(4.71)	Eq.(4.62)	Eq.(4.58)
	3	*j=J=0*	0	Eq.(4.58)	

[1] The mathematical model for the non-boundary zones of ***L*** regions requires only the statement of the ODEs for *c* zones between *n*=2 and *n=nz*-1. The algebraic equations for the *r* zones between *n*=2 and *n=nz*-1 are used in the ODEs and their solutions are found simultaneously to the solution of the *c* zones.

4.5.3. Concrete-insulation-concrete type wall (CIC).

The concrete layers (Fig. 4.8b) are the external and internal regions, with a central region of insulation between them. The combined thermal resistances of the concrete and insulation materials provide a significant heat transfer resistance, but the concrete thermal capacity is also important. Therefore, the conceptual models investigated both properties. The models are presented in Table 4.9. Different models for the external and internal concrete slabs were tested.

4.5.3.1. ***RRR*** *(Resistance → Resistance → Resistance) model.*

The model assumes that concrete and insulation layers possess thermal resistance only, neglecting all thermal capacities.

4.5.3.2. ***RRL*** *(Resistance → Resistance → Lumped) model.*

This model uses a detailed model in the internal layer, considering both the thermal capacity and resistance of the internal concrete layer. The insulation was modelled as resistance only. Within the ***L*** region, 4 sub-models outlined in Section 4.5.2.1. were possible.

4.5.3.3. ***LRL*** *(Lumped → Resistance → Lumped) model.*

In the ***LRL*** model both concrete layers were modelled with the same degree of complexity, but the simple representation was used to represent the insulation. Similarly to the ***RRL*** model, the sub-models ***L1, L2, L3*** and ***L4*** were possible.

4.5.3.4. ***DRD*** *(Distributed → Resistance → Distributed) model.*

This model assumed both distributed thermal capacity and resistance in the concrete layers, but the insulation remained represented with an algebraic equation.

4.5.3.5. ***DDD*** *(Distributed → Distributed → Distributed) model.*

This scheme assumed equally distributed resistance and capacity in all layers.

TABLE 4.9. MATHEMATICAL MODELS USED FOR THE CONCRETE - INSULATION - CONCRETE TYPE WALL. *Shaded boxes indicate the lumping of Q_{con} for adjacent conductive regions/zones.*

CIC MODEL	REG (*nr*)	ZONES (*n*)	Q_{acc} = (W/m^2)	Q_{in} - (W/m^2)	Q_{out} (W/m^2)	
RRR	*1*	*n=nz=1*	0	Eq.(4.53)		Eq.(4.61)
	2	*n=nz=1*	0	Eq.(4.61)		Eq.(4.61)
	3	*n=nz=1*	0	Eq.(4.61)		Eq.(4.55)
RRL	*1*	*n=nz=1*	0	Eq.(4.53)		Eq.(4.60)
	2	*n=nz=1*	0	Eq.(4.60)		If model for *nr*=3 is either ***L1*** or ***L3***, use Eq.(4.61)
						If model for *nr*=3 is either ***L2*** or ***L4***, use Eq.(4.60)

continued...

Table 4.9 continued...

CIC MODEL	REG (*nr*)	ZONES (*n*)	Q_{acc} = (W/m²)	Q_{in} - (W/m²)	Q_{out} (W/m²)
RRL	*3*	*n=1*	If model is either ***L1*** or ***L3*** then Q_{acc}=0	Eq. (4.61)	Eq. (4.61)
			If model is either ***L2*** or ***L4*** then use Eq. (4.67)	Eq. (4.60)	Eq.(4.59) for *n*=2
		c zones,	Eq. (4.67)	Eq.(4.59) *for n-1*	Eq.(4.59) for *n*+1
		n=nz	If model is either ***L1*** or ***L4***, Q_{acc}= 0	Eq.(4.59)	Eq.(4.56)
			If model is either ***L2*** or ***L3***, use Eq.(4.67)	Eq.(4.59) with *n= nz-1*	Eq.(4.52)

1 The mathematical model for the non-boundary zones of ***L*** regions requires only the statement of the ODEs for *c* zones between *n*=2 and *n*=*nz*-1. The algebraic equations for the *r* zones between *n*=2 and *n*=*nz*-1 are used in the ODEs and their solutions are found simultaneously to the solution of the *c* zones.

continued....

Table 4.9 continued...

CIC MODEL	REG (*nr*)	ZONES (*n*)	Q_{acc} (W/m²)	= Q_{in} (W/m²)	- Q_{out} (W/m²)
LRL	*1 (2 solved simultaneously)*	*n=1*	If model is either ***L1*** *or* ***L3***, *Qacc*= 0	Eq.(4.54)	Eq.(4.59)
			If model is either ***L2*** or ***L4*** use	Eq.(4.51)	Eq.(4.59) *for n+1*
		c zones,	Eq.(4.67)	Eq.(4.59) *for n-1*	Eq.(4.59) *for n+1*
		n=nz	If model is either ***L1*** or ***L4***, Q_{acc}=0	Eq.(4.60)	If model for *nr*=3 is either ***L1*** or ***L3*** use Eq.(4.61)
					If model for *nr*=3 is either ***L2*** or ***L4*** use Eq.(4.60)
			If model is either ***L2*** or ***L3*** use Eq.(4.67)	Eq.(4.59) with *n=nz-1*	Eq.(4.26)

1 The mathematical model for the non-boundary zones of ***L*** regions requires only the statement of the ODEs for *c* zones between *n*=2 and *n=nz*-1. The algebraic equations for the *r* zones between *n*=2 and *n=nz*-1 are used in the ODEs and their solutions are found simultaneously to the solution of the *c* zones.

continued....

Table 4.9 continued...

CIC MODEL	REG (nr)	ZONES (n)	Q_{acc} (W/m^2)	= Q_{in} (W/m^2)	- Q_{out} (W/m^2)
LRL	*3*	$n=1$	If model is either ***L1*** or ***L3***, $Q_{acc}=0$	Solved simultaneously with $nr=1$, $n=nz$. See box above.	Eq.(4.59)
			See previous box. If model is either ***L2*** or ***L4***, use Eq.(4.67)	Eq. (4.59) with $nr=2$, $n=nz$	Eq. (4.59) for $n=2$
		c zones, $1<n<nz$ [1]	Eq.(4.67)	Eq.(4.59) *for n-1*	Eq.(4.59) *for n+1*
		$n=nz$	If model is either ***L1*** or ***L4*** $Q_{acc}=0$	Eq.(4.59)	Eq.(4.56)
			If model is either ***L2*** or ***L3*** use Eq.(4.67)	Eq.(4.59) with $n=nz-1$	Eq.(4.52)

[1] The mathematical model for the non-boundary zones of ***L*** regions requires only the statement of the ODEs for c zones between $n=2$ and $n=nz-1$. The algebraic equations for the r zones between $n=2$ and $n=nz-1$ are used in the ODEs and their solutions are found simultaneously to the solution of the c zones.

continued....

Table 4.9 continued...

CIC MODEL	REG (*nr*)	NODES (*j*)	Q_{acc} =	Q_{in} -	Q_{out}
DRD **and** ***DDD***	***DRD**:1 (region 2 solved simultaneously)* ***DDD**:1*	*j=0*	Eq.(4.71)	Eq.(4.57)	Eq.(4.62)
		$0<j<J_1$	Eq.(4.70)	Eq.(4.62)	Eq.(4.62)
		$j=J_1$	***DRD*** model:Eq.(4.71)	***DRD*** model:Eq.(4.64)	***DRD*** model:Eq.(4.64)
			DDD model:Eq.(4.72)	***DDD*** model:Eq.(4.62)	***DDD*** model:Eq.(4.62) *for*
	***DDD**:2*	*j=0*	See previous box (*j =0 for region 2 is also* $j=J_1$ for region 1)		
		$0<j<J_2$	Eq.(4.70)	Eq.(4.62)	Eq.(4.62)
		$j=J_2$	Eq.(4.72)	Eq.(4.62)	Eq.(4.62) *for nr=3, j=1*
	3	*j=0*	See box above ($j = J_2$ for region 2 is also $j = 0$ for region 3)		
		$0<j<J_3$	Eq.(4.70)	Eq.(4.62)	Eq.(4.62)
		$j=J_3$	Eq.(4.71)	Eq.(4.62)	Eq.(4.58)

4.5.4. Concrete-insulation-metal type wall (CIM).

This wall (Fig.4.8d) has a special application in the food industry for controlling the condensation on a concrete structure surface. The metal layer is situated inside the cold environment and it is heated to melt and evaporate the ice/water formation formed at its surface. This layer was modelled considering its thermal capacity only. The concrete and the insulation models followed the same assumptions as those used in the concrete-insulation-concrete type walls.

The models were selected to investigate the capacity/resistance balance between the 3 layers so more detailed models for the insulation layer were used. The concrete was modelled both as a resistance only region and using a lumped approach. The metal layer was modelled as a thermal capacitive region, as assumed for the sandwich panel type wall. Table 4.10 describes the mathematical models selected for this wall.

4.5.4.1. ***RRC*** *(Resistance → Resistance → Capacity) model.*

This model assumes thermal resistance in both concrete and insulation layers. The internal metal layer is represented as a ***C*** region.

4.5.4.2. ***LRC*** *(Lumped → Resistance → Capacity) model.*

A more detailed model was set in this case for the concrete layer, but the insulation and metal remain represented as in the previous model.

4.5.4.3. ***LLC*** *(Lumped → Lumped → Capacity) model.*

A detailed model was used for representing the insulation layer, keeping the lumped model for the concrete layer.

4.5.4.4. ***RDC*** *(Resistance → Distributed → Capacity) model.*

The concrete external layer was represented as an ***R*** region, but a detailed model was used for representing the insulation slab. The metal remained represented as capacity only.

TABLE 4.10. MATHEMATICAL MODELS USED FOR THE CONCRETE - INSULATION - METAL TYPE WALL. *Shaded boxes indicate the lumping of Q_{con} for adjacent conductive regions/zones.*

CIM MODEL	REG (*nr*)	ZONES (*n*)	Q_{acc} =	Q_{in} -	Q_{out}
RRC	*1 (region 2 solved simultaneously)*	*n=nz=1*	0	Eq.(4.53)	Eq.(4.60)
	3	*n=nz=1*	Eq.(4.67)	Eq(4.60) with *nr=1*	Eq.(4.52)

continued...

Table 4.10 continues...

CIM MODEL	REG (*nr*)	ZONES (*n*)	Q_{acc} = Q_{in} - Q_{out}		
LRC	*1 (region 2 solved simultaneously*	*n=1*	If model is either ***L1*** or ***L3***, Q_{acc} =0	Eq.(4.54)	Eq.(4.59)
			If model is either ***L2*** or ***L4*** , use Eq.(4.67)	Eq.(4.52)	Eq.(4.59) *for n+1*
		c zones, 1<n<nz [1]	Eq. (4.67)	Eq.(4.59) *for n-1*	Eq.(4.59) with *n+1*
		n=nz	If model is either ***L1*** or ***L4***, Q_{acc} =0	Eq.(4.60)	Eq.(4.60)
			If model is either ***L2*** or ***L3*** use Eq.(4.67)	Eq.(4.59) *for n-1*	Eq.(4.59) with *nr=2*
	3	*n=nz=1*	Eq.(4.67)	Eq.(4.59) with *nr=2*	Eq.(4.52)

[1] The mathematical model for the non-boundary zones of ***L*** regions requires only the statement of the ODEs for *c* zones between *n*=2 and *n=nz*-1. The algebraic equations for the *r* zones between *n*=2 and *n=nz*-1 are used in the ODEs and their solutions are found simultaneously to the solution of the *c* zones.

continued....

Table 4.10 continued...

CIM MODEL	REG (nr)	ZONES (n)	Q_{acc} (W/m²) =	Q_{in} (W/m²) -	Q_{out} (W/m²)
LLC	*1*	*n=1*	If model is either ***L1*** *or* ***L3***, Q_{acc}= 0	Eq.(4.54)	Eq.(4.59)
			If model is either ***L2*** or ***L4***, use Eq.(4.67)	Eq.(4.51)	Eq.(4.59) *for n=2*
		1<n<nz	Eq.(4.67)	Eq.(4.59) *for n-1*	Eq.(4.59) *for n+1*
		n=nz	If model is either ***L2*** or ***L3*** and model for *nr*=2 is either ***L2*** or ***L4*** use Eq. (4.68)	Eq. (4.59) for n-1	Use Eq. (4.59) with *nr=2, n=2*

continued...

Table 4.10 continued...

CIM MODEL	REG (*nr*)	ZONES (*n*)	Q_{acc} (W/m^2) =	Q_{in} (W/m^2) -	Q_{out} (W/m^2)
LLC	*1*	*n=nz*	If model is either ***L2*** or ***L3*** and model for *nr*=2 is either ***L1*** or ***L3*** use Eq. (4.67)	Eq. (4.59) for n-1	Use Eq. (4.59) with *n=1*, *nr=2*
			If model is either ***L1*** or ***L4***, Q_{acc}= 0	Eq.(4.59)	If model with *nr*=2 is either ***L1*** or ***L3***, use Eq.(4.60)
					If model with *nr*= 2 is either ***L2*** or ***L4*** use Eq.(4.59) for *n=2*, *nr=2*

continued....

Table 4.10 continued...

CIM MODEL	REG (*nr*)	ZONES (*n*)	Q_{acc} (W/m²) =	Q_{in} (W/m²) -	Q_{out} (W/m²)
LLC	*2*	*n=1*	The 1st zone of the ***L*** region 2 is solved simultaneously with the solution of n=nz from the previous ***L*** region 1.		
		c zones, 1<n<nz	Eq.(4.67)	Eq.(4.59) for *n*-1	Eq.(4.59) for *n*+1
		n=nz	If model is either ***L1*** or ***L4***, Q_{acc}= 0	Eq.(4.59)	Eq. (4.59)
			If model is either ***L2*** or ***L3***, use Eq.(4.68)	Eq.(4.59) with *n=nz*-1	Eq.(4.59)
	3	*n=nz=1*	See box above. If model for *nr*=2 is either ***L2*** or ***L3***, use Eq.(4.68)	Eq. (4.59) with *nr*=2, *n=nz*-1	Eq. (4.52)
			If model for *nr*=2 is either ***L1*** or ***L4***, use Eq.(4.67)	Eq. (4.59) with *nr*=2, *n=nz*	

continued...

Table 4.10 continued...

CIM MODEL	REG (*nr*)	ZONES (*n*) OR NODES (*j*)	Q_{acc} = (W/m²)	Q_{in} - (W/m²)	Q_{out} (W/m²)
RDC	*1*	*n=nz=1*	0	Eq.(4.53)	Eq.(4.62) with *nr=2, j=1*
	2 (region 3 solved simultaneously)	*j=0*	Eq.(4.71)	Eq.(4.63)	Eq.(4.62)
		$0<j<J_2$	Eq.(4.70)	Eq.(4.62)	Eq.(4.62)
		$j=J_2$	Eq.(4.74)	Eq.(4.62)	Eq.(4.52)

CHAPTER 5. WALL STRUCTURES: THEORETICAL VERIFICATION AND VALIDATION OF MODELS.

Model verification has been defined as "a procedure to ensure that the model is built according to specifications and to eliminate errors in the structure algorithms and computer implementation of the model" (Neelamkavil, 1987). Verification refers to testing the correctness of the model implemented in a computer program. In contrast, validation is "the process of substantiating that the model, within its domain of applicability, is sufficiently accurate for the intended applications" (Schlessinger, 1979). The so-called sensitivity analysis or the testing of different scenarios to assess their effect on the model accuracy is part of the validation procedure. Whereas verification is a routine step executed by the computer programmer, validation is not necessarily always achieved.

Clements (1989) stated that model predictions can be used to produce lower and upper bounds around the true answer. If the model performs within the range of acceptability in the most demanding situation (worst case analysis), there is little point in constructing a more accurate model of the subject under investigation. However, this technique is not the only one that can be used to confront the practical value of models: Kleijnen (1974) recommended that a range of variation in the system parameters, input variables and relationships between parameters should be investigated in order to validate the model. The objectivity of this approach can be increased if a statistical approach is used in order to investigate a meaningful number of variables and combinations. A statistical experimental design reduces the number of trials involved, and thus this approach was followed in the present work.

The fundamental questions to be answered in the present validation were:

- What physical factors affect the performance of the real system?
- Are those the same as the factors affecting the model performance?
- What are the measures by which judgements of accuracy should be based?
- What is the impact of increasing the level of complexity on the accuracy of models?
- Is "accuracy" a fixed value or does it depend on the scenario used for testing the models?
- What are the boundaries within which a model can be defined as accurate?

5.1. Validation methodology.

A Turbopascal computer program was developed for implementing the various models for walls described in Chapter 4. The program was carefully checked and trials were carried out to set time step sizes for each type of wall that assured accurate calculations.

All trials used for model comparison purposes simulated the behaviour of the wall from a uniform initial condition, exposed for several days to a cyclic 24 hour weather pattern in terms of ambient and sky temperatures and incident radiation (Figure 5.1). The predicted heat load entering the internal environment from the wall was used as the key response variable and the simulation was continued until a repeating 24 hour cycle was achieved for this variable.

Accuracy is "the closeness of the agreement between the results of a measurement and the (conventional) true value of the measurand" (ISO Metrology Group, 1994). The accuracy is often given by the absolute error of measurement, defined as "The result of a measurement minus the (conventional) true value of the measurand". The relative error is "The absolute error of measurement divided by the (conventional) true value of the measurand".

In order to establish the "conventional value" against which the accuracy of the models could be assessed a reliable numerical method which assured accurate system simulation was sought. A Finite Element Method (FEM) programme has been developed (Cleland, 1985) and since then its accuracy continuously tested in several simulation situations and improved over the years. A detailed explanation of the model and programme can be found elsewhere (Cleland, 1985). The finite element method has been recognised as one of the most sophisticated tools for numerical heat conduction problems (Myers, 1971) and so it was selected as the base method. In Chapter 6, comparisons with experimental data which verify that the FEM programme closely predicts measured wall performance data are presented, hence justifying this decision.

5.1.1. The finite element programme trials.

The FEM programme implemented a fully distributed scheme, modelling each region by Eq. (4.9), which is the full PDE for heat conduction in a wall layer.

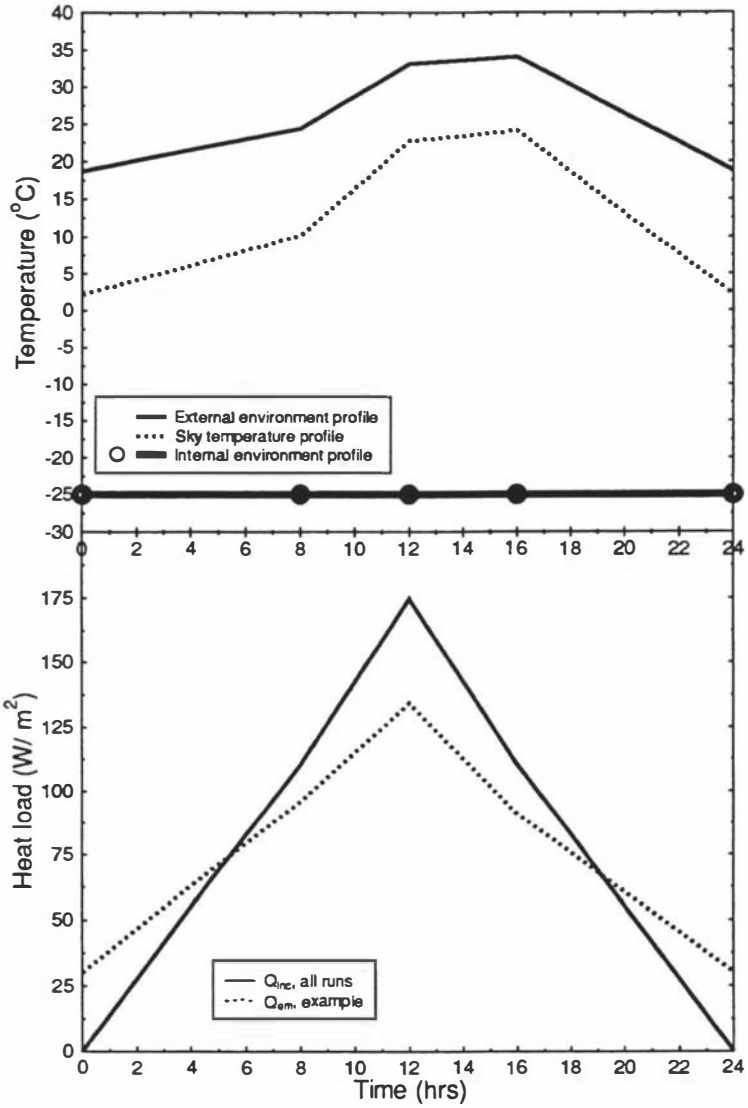

Fig. 5.1. Typical temperature and radiative heat loads profiles used in the testing of the models: a) Daily external (ambient) and sky temperatures and internal (room) temperatures, b) Incident radiation (Q_{inc}) and emmitted radiation (Q_{em})

The trials carried out using the FEM programme used linear, iso-parametric elements and assumed the following:

- 1-dimensional heat transfer
- uniform initial temperature equivalent to the mean ambient temperature in a daily 24 hr cycle
- the incident heat transfer, ambient and sky temperatures were approximated to semi-sinusoidal cycles, using linear interpolation of tabulated data points (Fig.5.1)

The same assumptions were used for the models tested.

The FEM grids and time steps used varied depending on the type of wall to be modelled, but in each run an overall computed internal heat balance across the walls was sought. Cleland (1985) stated the usefulness of such calculation as an indication of numerical errors. The grid selection strategies were set as follows:

a) Sandwich panel type (SPT) wall. A grid comprising one linear element in each metal layer plus 16 linear elements in the insulation and a time step of 1 second gave reliable results. Larger numbers of elements set in the thin metal layers led to appreciable numerical errors, thus suggesting that these might arise due to the combination of very small element sizes in the metal compared to the larger element sizes in the polystyrene. A small temperature gradient across the metal was expected and a single linear element was considered to be sufficiently accurate.

b) Concrete type (CT) wall. A grid of 14 linear elements was selected, using a 5 seconds time step. Since the object had homogeneous thermal properties the restrictions found for the SPT wall were not found for the CT wall.

c) Concrete-insulation-concrete (CIC) wall. The choice of initial temperature and the thermal properties of this type of wall led to slow cooling of the structure and hence the number of days to be simulated for reaching a repeatable cycle was much greater than that needed for the SPT and CT walls. Also, the FEM programme used had a limited data input structure. Therefore for this case the ***DDD*** model implemented by explicit finite differences (FD) was used as the base method. The FEM programme was used as a verification tool by spot checks vs the ***DDD*** model. The FD grid

selected set 10 nodes in each layer of the wall, using a time step of 10 seconds. When the first 3 days of the simulations of FD and FEM schemes were compared, no significant differences were found between the predictions and it was concluded that the performance of the ***DDD*** model was equivalent to the FEM scheme provided an appropriate number of nodes was selected.

d) Concrete-insulation-metal type (CIM) wall. The thin metal layer was again the limiting factor in the selection of the grid and time step. The grid selected comprised 6 elements in the concrete layer plus 8 elements in the insulation and 1 element in the metal layer. The FEM program was used as the basis of comparison, since the existence of only one concrete layer allowed the system to reach a 24 hr repeating cycle in shorter times than those observed in the CIC wall.

5.1.2. Measures used for assessing the performance of the models.

A number of measures derived from the heat flux transferred from the wall to the cold room were used to establish numerical comparisons. Analyses of the variations in the heat load measures were carried out with two distinct focuses:

- factors influencing the heat load response (magnitude and timing of the cycle), and
- factors influencing the accuracy of the model predictions for each response (i.e. how closely the model response matched the FEM response).

Nine measures were used and they were classified in 3 groups as follows:

5.1.2.1. Measures related to the physical behaviour of the system.

The measures directly related to the behaviour of the heat flux across the wall are illustrated in Figure 5.2. The degree of accuracy was defined as the percentage relative error:

$$\% \ accuracy = \left(\frac{model \ response - FEM \ response}{FEM \ response} \right) 100 \qquad (5.1)$$

For all the measures described below, predictions of heat load by both FEM and the models tested during a 24 hr cycle were used. The aim of the conversion of heat load to other

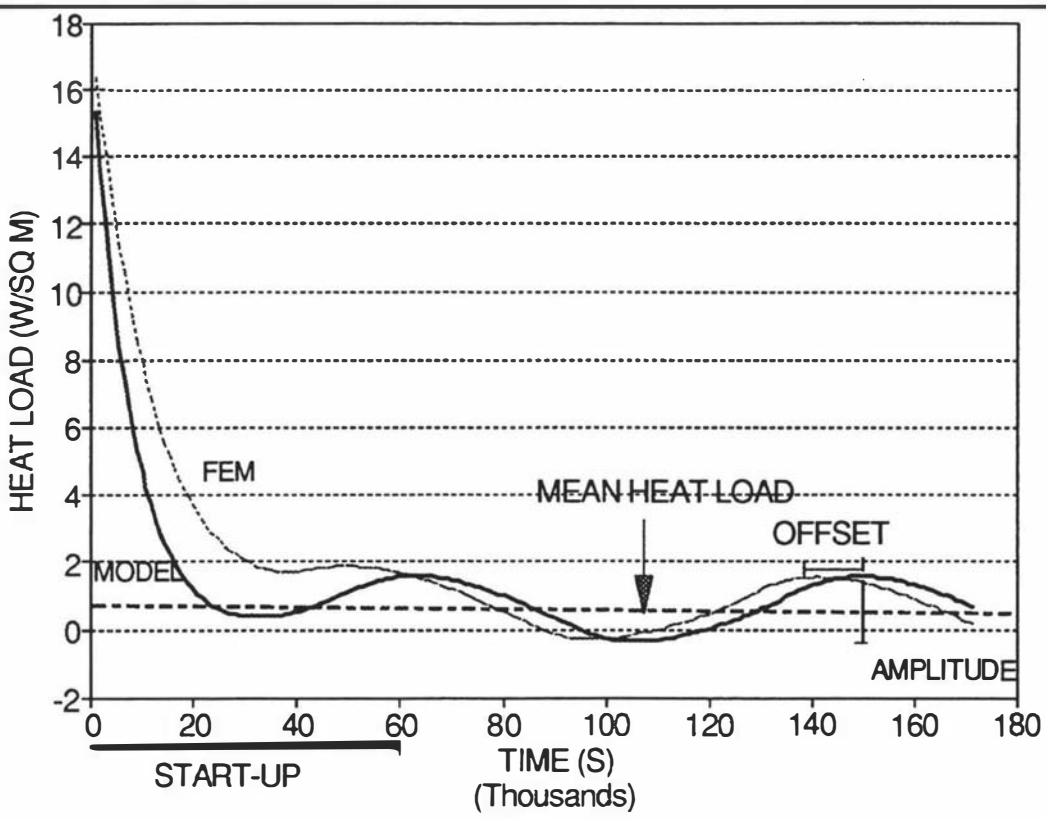

FIG. 5.2. Measures related to the physical behaviour of the system

measures was to obtain more meaningful expressions to compare the models performance.

a) Start-up time. This was defined as the time to achieve a repeating 24 hour cycle pattern in the heat load in response to the 24 hour cycle of the external boundary conditions within a stated tolerance:

$$Band_{upper\ limit} = Heat\ flux_{time\ =\ t,FEM}\left(1 + \frac{\%\ tolerance}{100}\right) \tag{5.2}$$

$$Band_{lower\ limit} = Heat\ flux_{time\ =\ t\ ,FEM}\left(1 - \frac{\%\ tolerance}{100}\right) \tag{5.3}$$

This measure also ensured that in the following analyses, a repeating 24 hour pattern was used. The tolerance used was 5%.

b) Amplitude of the heat load cycle. The amplitude was calculated as the algebraic difference of the maximum (peak) and the minimum heat load simulated in a 24 hour cycle.

c) Offset in time for the model predictions compared to FEM results to reach peak

heat load in a 24 hour cycle. A related concept was the time lag error which was the time elapsed from the moment at which the minimum heat load was achieved to the moment at which the peak load was registered.

d) Mean heat load. The mean heat load entering the room in a 24 hour cycle.

5.1.2.2. Statistical measures.

The interpretation of these measures was based on the definition of the experimental standard deviation (SD): "For a series of n measurements of the same measurand, the parameter 'SD' characterising the dispersion of the results is given by the formula:

$$SD = \sqrt{\frac{\Sigma^{n}_{i=1} (x_i - \bar{x})^2}{n-1}} \tag{5.4}$$

x_i being the results of the ith measurement and $\bar{x}$ being the arithmetic mean of the n results considered" (ISO Metrology Group, 1984). Two measures were derived from this definition:

a) Peak-based standard deviation (SD_{peak}). This measure had a statistical and physical meaning of how the model performance deviated from FEM. The SD_{peak} was defined as a fraction of the FEM peak heat load:

$$SD_{peak} = \frac{\sqrt{\frac{\Sigma (model\ heat\ load - FEM\ heat\ load)^2}{n - 1}}}{FEM\ peak\ heat\ load} \tag{5.5}$$

b) Mean-based standard deviation (SD_{mean}). The SD_{mean} was defined similarly defined to above other than the SD being related to the FEM mean heat load:

$$SD_{mean} = \frac{\sqrt{\frac{\Sigma (model\ heat\ load - FEM\ heat\ load)^2}{n - 1}}}{FEM\ mean\ heat\ load} \tag{5.6}$$

In both measures, the total number of data for a repeatable 24 hr cycle was considered to be a representative sample size. The data processed using these measures was thus obtained from predictions evaluated every 0.25 hrs over the repeatable 24 hr cycle. Hence, 96 data points were obtained from each trial and concerted to peak and mean SDs.

5.1.2.3. Tolerance-related measures.

These established the extent of deviation of predictions beyond a tolerance band around the FEM response. Each of the 96 data points were subjected to an individual test to determine whether they fell within the boundaries of the tolerance band or not. Data falling outside the tolerance envelope around the FEM response were defined as inaccurate. The physical representation of tolerance-related measures is illustrated in Fig. 5.3. Three tolerance bands were calculated as a percentage of the instant heat flux:

a) Variable tolerance band around the instantaneous heat load (raw data). The percentage of data falling within the band was used as a direct measure of accuracy, according to the equations:

$$Band_{upper\ limit} = Heat\,flux_{FEM}\left(1 + \frac{\%\ tolerance}{100}\right)$$
$$Band_{lower\ limit} = Heat\,flux_{FEM}\left(1 - \frac{\%\ tolerance}{100}\right) \qquad (5.7)$$

$$\%\ accuracy = \left(\frac{data\ points\ within\ band}{total\ number\ of\ data\ points}\right)_{24\ hr\ cycle} 100 \qquad (5.8)$$

The tolerance band percentages investigated were 5, 10 and 15%.

b) Fixed tolerance band around the heat load. The fixed tolerance interval was calculated using the FEM peak heat load only, the size of the envelope around the model response being the same for all data:

$$Band_{upper\ limit} = Heat\,flux_{FEM} + \left(\frac{\%\ tolerance}{100}\right) Peak\ heat\ flux, FEM$$
$$Band_{lower\ limit} = Heat\,flux_{FEM} - \left(\frac{\%\ tolerance}{100}\right) Peak\ heat\ fux, FEM \qquad (5.9)$$

Eq. (5.8) was used to state the accuracy of the calculation and the same percentage tolerances were investigated.

c) Variable tolerance band around energy/time rates. A new variable, termed energy/time rate (W/m^2 s) was defined as the rate of change of the incoming heat load with respect to time. It was calculated as the absolute value of the following expression:

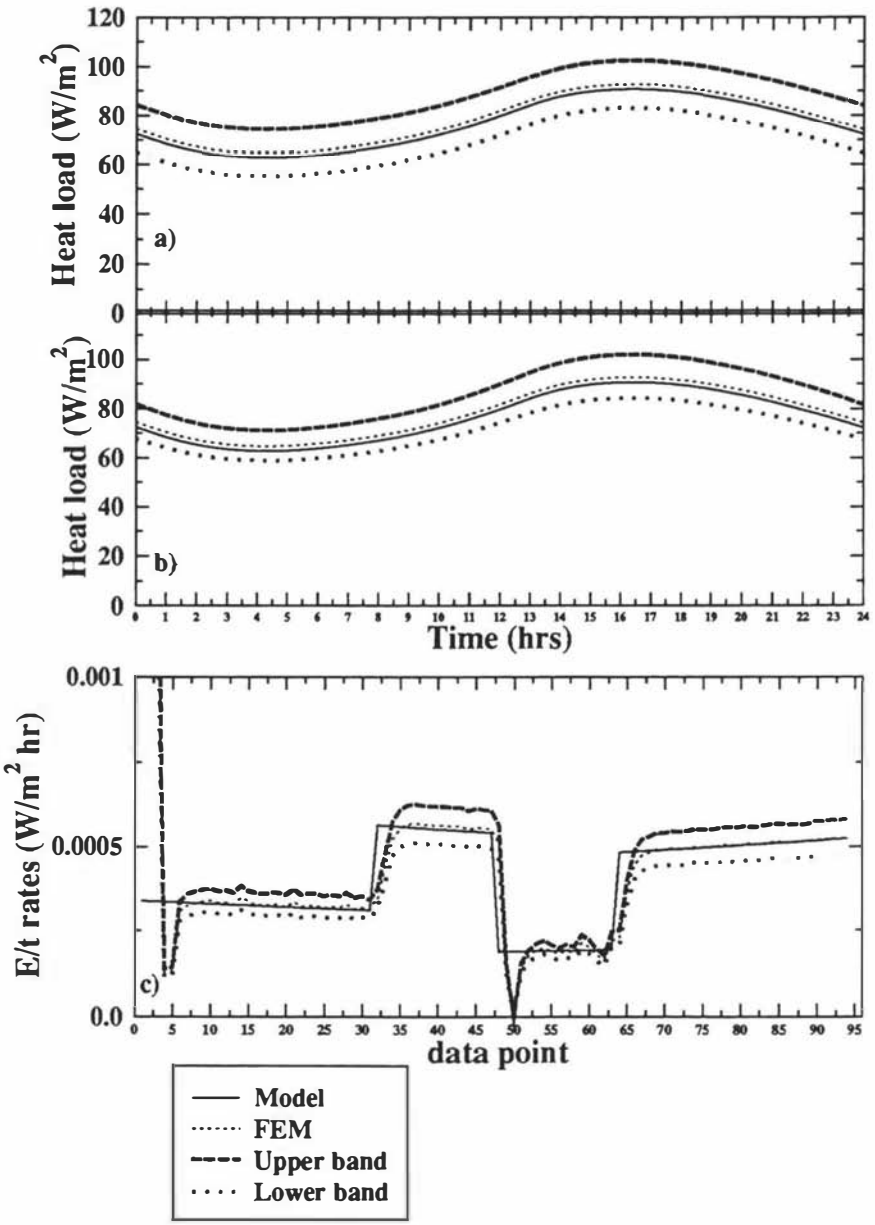

Fig. 5.3. Tolerance - related measures: a) +/-10% tolerance using the instantaneous heat load of the FEM model as the calculation basis, b) +/- 10% tolerance using the peak heat load of the FEM model as the calculation basis and c) +/- 10% tolerance using the heat load transformed to energy/time rates, using the FEM response as the calculation basis

$$\left(\frac{Energy}{time}\right)_{model} = \left(\frac{Heat\,flux_{time = x} - Heat\,flux_{time = x + \Delta t}}{\Delta t}\right) \tag{5.10}$$

and the tolerance bands were defined as:

$$Band_{upper\ limit} = \left(\frac{energy}{time}\right)_{FEM}\left(1 + \frac{\%\ tolerance}{100}\right)$$
$$Band_{lower\ limit} = \left(\frac{energy}{time}\right)_{FEM}\left(1 - \frac{\%\ tolerance}{100}\right) \tag{5.11}$$

A value of Δt = 900 s was used for all cases, so 96 values were available in a 24 hr cycle. Eq. (5.8) was used to predict the accuracy when 5, 10 and 15% tolerances were used.

5.1.3. Application of statistical experimental designs.

To obtain a rigorous testing procedure, the models were tested using a statistically designed sensitivity analysis. The Quality Engineering (QE) methodology proposed by Taguchi (1986, 1991) as described by Ross (1989) was used for developing the experimental design. This approach allowed model performance to be compared under a variety of scenarios, identifying the factors with greatest influence over the accuracy and response of the models. The QE methodology has been used widely as a statistical tool for analyzing experimental results, though fewer applications have been reported for modelling situations (Taguchi, 1986). The experimental design used was a fractional factorial type investigating 4 types of variables:

a) Non-controllable or "noise" variables that could affect wall performance. This group involves ambient environment conditions such as the external heat transfer coefficient (including radiation and convection) and the mean temperature of the external environment. That is, variables that are out of the control of the designer/user.

b) Design variables (factors controlled when designing the room walls). The emissivity of the external surface and the thermal properties of the layers (thermal capacity and thermal resistance) are grouped under this classification.

c) Operational variables (factors under control during the operation of the room). This group includes the internal (room) temperature and the internal heat transfer

coefficient.

d) Model-related variables, such as the coarseness of the grids used in the numerical solution of the models. Grid selection decisions might affect the results and large numerical errors might occur if wrong strategies are used.

Two levels (low and high values chosen to cover a wide range of likely values in industrial practice) were set for each variable under investigation. Table 5.1 presents the summary of the factors and levels tested. Not all the variables were investigated for all types of walls: the relevance of each was assessed and only the most relevant 7 variables were investigated for each type of wall. The QE design (denominated L_8) used to define the conditions of the trials is presented in Table 5.2.

The combination of variables and levels followed a unique sorting of those for each trial, according to the orthogonality[1] rule of the experimental design L_8. In Table 5.2, the number to the left of each row represents the trial or run. The vertical alignments (columns) represent the 7 variables tested. The same L_8 orthogonal array was used for all the models and was replicated using the FEM programme, according to the variables selected.

[1] Orthogonality is a property of an experimental design, consisting of an adequate balance of combinations of factors and levels so that they are equally represented in the same number of combinations.

TABLE 5.1. VARIABLES AND LEVELS TESTED IN MODELS.

VARIABLE	TESTED IN WALLS:	LEVEL 1	LEVEL 2
h_1 (W/m^2 K)	SPT,CT,CIC,CIM	3	10
h_2 (W/m^2 K)	SPT,CT,CIC,CIM	3.5	26.5
T_a (°C)	SPT,CT,CIC,CIM	15	28
Emissivity (ε), layer 1	SPT,CT,CIC	0.12	0.92
T_{room} (°C)	SPT,CT,CIC,CIM	-25	10
$\mathbf{R}_{insulation,layer\ 2}$ (m^2 K/W), fixed λ_2= 0.03 (W/ m K)	SPT,CIC,CIM	2 (x_2= 0.06 m)	8 (x_2= 0.24 m)
$\mathbf{C}_{layer\ 3}$ (kJ/m^{2}K), fixed C_3= 2,376 (kJ/m^3 K)	SPT, CIM	4.8 (x_3= 0.002 m)	23.8 (x_3= 0.01 m)
$\mathbf{R}_{concrete,layer\ 2}$ (m^2 K/W), fixed x_2= 0.2 (m)	CT	0.1 (λ_2= 1.8 W/m K)	2 (λ_2= 0.1 W/m K)

continued...

Table 5.1 continued...

VARIABLE	TESTED IN WALLS:	LEVEL 1	LEVEL 2
$\mathbf{C}_{concrete,layer\ 2}$ (kJ/m^{2}K), fixed x= 0.2 (m)	CT	152 (C=760 kJ/m^3 K)	600 (C= 3,000 kJ/ m^3 K)
$(\mathbf{RC})_{layer\ 1}/(\mathbf{RC})_{layer\ 3}$ (non-dim), fixed λ_1 =0.9(W/m K), fixed λ_3 = 0.9 (W/m K), fixed C_1=1,620 (kJ/m^3 K) and fixed C_3=1,620 (kJ/m^3 K)	CIC	Ratio = 0.027 $\mathbf{R}_{layer\ 1}$=0.056 m^2 K/W $\mathbf{C}_{layer\ 1}$=81 kJ/m^2 K $\mathbf{R}_{layer\ 3}$=0.34 m^2 K/W $\mathbf{C}_{layer\ 3}$=165.24 kJ/m^2 K (x_1=0.05 m,x_3 =0.3 m)	Ratio = 36.4 $\mathbf{R}_{layer\ 1}$=0.34 m^2 K/W $\mathbf{C}_{layer\ 1}$=165.24 kJ/m^2 K $\mathbf{R}_{layer\ 3}$=0.056 m^2 K/W $\mathbf{C}_{layer\ 3}$=81 kJ/m^2 K (x_1 = 0.3 m,x_2 = 0.05 m)
$(\mathbf{RC})_{layer\ 1}$ (s), fixed λ_1=0.9 (W/m K) and C_1=1,620 (kJ/m^3 K)	CIM	$\mathbf{RC}$= 4,536 (x_1=0.05 m) $\mathbf{R}_{layer\ 1}$=0.056 m^2 K/W $\mathbf{C}_{layer\ 1}$=81 kJ/m^2 K	$\mathbf{RC}$=165,240 (x_1 = 0.3 m) $\mathbf{R}_{layer\ 1}$=0.34 m^2 K/W $\mathbf{C}_{layer\ 1}$=165.2 kJ/m^2 K

Note: The representative materials for the layers tested were:

1) Insulation layer: expanded polystyrene (λ = 0.03 W/m^2 C, ρ = 32 kg/m^3, c = 1,190 J/kg K).

2) Metal layer: Aluminium-Magnesium (Hydronalium, λ = 100 W/m^2 C, ρ = 2,652 kg/m^3, c = 896 J/kg K).

3) Concrete layer: Concrete (λ = 0.8 W/m^2 C, ρ = 1,906 kg/m^3, c = 879 J/kg K).

Source: ASHRAE (1995).

The levels were varied to values likely to appear in many industrial situations.

	COLUMNS (VARIABLES)						
TRIAL (RUN)	**A**	**B**	**C**	**D**	**E**	**F**	**G**
1	1	1	1	1	1	1	1
2	1	1	1	2	2	2	2
3	1	2	2	1	1	2	2
4	1	2	2	2	2	1	1
5	2	1	2	1	2	1	2
6	2	1	2	2	1	2	1
7	2	2	1	1	2	2	1
8	2	2	1	2	1	1	2

TABLE 5.2. EXPERIMENTAL DESIGN L_8 . The levels are represented by the numbers 1 and 2 inside the table; the variables are represented by the column letter at the top and the trial number appears in the left column (1 to 8).

*a) Sandwich panel type wall: **NRN** and **CRC** models.* In the SPT case, the effect of the external and internal heat transfer coefficients and the effect of varying the external ambient temperatures in the daily cycle were of interest. It was expected that this last factor and the emissivity of the external layer would significantly affect the results. The temperature of the room, the resistance of the insulation and the thermal capacity of the metal layer were known to affect the results, but the role of these in the final shape of the daily heat load entering the room was not known. The levels were set accordingly to reflect conditions that might arise in a variety of applications (cooling, freezing, etc). Table 5.3 presents the assignment of the factors investigated in both the ***NRN*** and ***CRC*** models.

*b) Concrete wall: **NLN** and **NDN** models.* The lumped model created the possibility of varying the number of zones, of using *c* or *r* zones at the external and internal boundaries (***L1***, ***L2***, ***L3*** and ***L4*** alternative models developed in Chapter 4), and of using different distributions of resistance and capacity represented by γ and ζ.

In order to test the effect of varying these model-related variables on the accuracy of the results obtained, an investigation of the ***L*** model itself was conducted prior to the use of the standard L_8 orthogonal array. The following issues were investigated:

■ **Effect of the number of zones and the thermal characteristic (*r* or *c*) of the boundary zones on accuracy.** A factorial design was used, testing odd and even numbers of zones and setting *c* and *r* in each boundary. Table 5.4 presents the combinations tested.

■ **Effect of the distribution of resistance (ζ) and capacity (γ) on accuracy.** A second factorial design was used, testing 3 types of distribution: Weighting 80% of the variable towards the external boundary, weighting 80% of the variable towards the internal boundary and weighting 40% towards each boundary (Table 5.5). An 8 zones *L4* model was used, investigating 3 strategies:

a) ζ were varied whilst γ were fixed.
b) γ were varied whilst ζ were fixed.
c) Both ζ and γ were varied at the same time.

■ **Effect of the grid coarseness on accuracy.** The complete L_8 design (Table 5.2) was used for each of 3 different grid strategies:

Grid A: 4 zones (***NLN***) or 5 nodes (***NDN***).
Grid B: 8 zones (***NLN***) or 9 nodes (***NDN***).
Grid C: 14 zones (***NLN***) or 13 nodes (***NDN***).

The factors selected for this investigation are presented in Table 5.6. The thermal resistance and capacity of the concrete were specially relevant. The emissivity was varied using the extreme values of polished metals (ε=0.92) and concrete type materials (ε=0.12) to investigate the performance of a radiation shield (for example, a thin layer of aluminium). The radiative heat transfer properties of such an added layer were included, but not the thermal capacity and/or thermal resistance.

*c) Concrete-insulation-concrete: **RRR,RRL, LRL and DRD models**.* The results derived from the CT wall provided guidance which was used to simplify the investigation of the models involving an ***L*** region in the CIC wall. However, the effect of different grids in these models was still investigated. In the ***LRL*** and ***DRD*** models, a fine grid in the external concrete layer was combined with a coarser grid in the internal concrete layer. The opposite case (a coarse grid in layer 1 plus a finer grid in layer 3) was also investigated. The effect of total layer thermal resistance and capacity was assessed using the ratio of $\mathbf{RC}_{\text{layer 1}}/\mathbf{RC}_{\text{layer 3}}$

instead of varying these as separate variables for each layer, thus avoiding a larger number of simulations. The L_8 array of Table 5.2 was used again, with the column assignments presented in Table 5.7. The experimental array was repeated for each of the following grids:

- Grid A (fine grid, layer 3):

  For ***LRL*** model: 3 zones in layer 1 plus 8 zones in layer 3.
  For ***DRD*** model: 3 nodes in layer 1 plus 8 nodes in layer 3.
  For ***RRL*** model: 8 zones in layer 3.

- Grid B (fine grid, layer 1):

  For ***LRL*** model: 8 zones in layer 1 plus 3 zones in layer 3
  For ***DRD*** model: 8 nodes in layer 1 plus 3 nodes in layer 3
  For ***RRL*** model: 3 zones in layer 1.

d) Concrete-insulation-metal: ***RRC, LRC, LLC and RDC.*** For these models, the investigation of the thermal resistance and capacity took priority over other issues. The grid selection strategy was not tested in this type of wall, since previous experimental designs that dealt with the effect of different grid selection strategies were considered to give sufficient guidance. The grids used for the lumped and distributed models tested were:

- ***LRC***: Layer 1 was modelled using an *L2*, 5 zone lumped sub-model
- ***LLC***: Both layers 1 and 2 were modelled using *L2*, 5 zone lumped sub-models
- ***RDC***: Layer 2 was modelled using 6 nodes

The ***RRC*** model did not require grid selection decisions. Table 5.8 presents the variables investigated.

FACTOR	COLUMN NUMBER
h_1 (W/m^2 K)	A
h_2 (W/m^2 K)	B
T_a (°C)	C
ε, layer 1	D
T_{room} (°C)	E
$\mathbf{R}_{insulation,layer\ 2}$ (m^2 K/W)	F
$\mathbf{C}_{metal,layer\ 3}$ (kJ/m^{2}K)	G

TABLE 5.3. FACTORS INVESTIGATED IN *NRN*, *CRC* AND FEM MODELS AND ASSIGNMENT OF COLUMNS IN ORTHOGONAL ARRAY L_8 FOR THE SPT WALL.

TRIAL	SUB - MODEL	*COMPLETE SEQUENCE OF THERMAL CHARACTERISTICS*
1	*L2*, 3 zones	$c \rightarrow r \rightarrow c$
2	*L1*, 3 zones	$r \rightarrow c \rightarrow r$
3	*L4*, 4 zones	$c \rightarrow r \rightarrow c \rightarrow r$
4	*L3*, 4 zones	$r \rightarrow c \rightarrow r \rightarrow c$
5	*L2*, 5 zones	$c \rightarrow r \rightarrow c \rightarrow r \rightarrow c$
6	*L1*, 5 zones	$r \rightarrow c \rightarrow r \rightarrow c \rightarrow r$
7	*L4*, 6 zones	$c \rightarrow r \rightarrow c \rightarrow r \rightarrow c \rightarrow r$
8	*L3*, 6 zones	$r \rightarrow c \rightarrow r \rightarrow c \rightarrow r \rightarrow c$
9	*L2*, 7 zones	$c \rightarrow r \rightarrow c \rightarrow r \rightarrow c \rightarrow r \rightarrow c$
10	*L1*, 7 zones	$r \rightarrow c \rightarrow r \rightarrow c \rightarrow r \rightarrow c \rightarrow r$
11	*L4*, 8 zones	$c \rightarrow r \rightarrow c \rightarrow r \rightarrow c \rightarrow r \rightarrow c \rightarrow r$
12	*L3*, 8 zones	$r \rightarrow c \rightarrow r \rightarrow c \rightarrow r \rightarrow c \rightarrow r \rightarrow c$

TABLE 5.4. LUMPED SUB-MODELS TESTED TO INVESTIGATE THE EFFECT OF THE NUMBER OF ZONES AND THE BOUNDARY THERMAL CHARACTERISTICS.

TRIAL	***SEQUENCE OF THERMAL CHARACTERISTICS AND SPATIAL WEIGHTING γ AND ζ FOR EACH ZONE***
1	*0.25c → 0.8r → 0.25c → 0.067r → 0.25c → 0.067r → 0.25c → 0.066r*
2	*0.8c → 0.25r → 0.067c → 0.25r → 0.067c → 0.25r → 0.066c → 0.25r*
3	*0.8c → 0.8r → 0.067c → 0.067r → 0.067c → 0.067r → 0.066c → 0.066r*
4	*0.25c → 0.066r → 0.25c → 0.067r → 0.25c → 0.067r → 0.25c → 0.8r*
5	*0.066c → 0.25r → 0.067c → 0.25r → 0.067c → 0.25r → 0.8c → 0.25r*
6	*0.066c → 0.066r → 0.067c → 0.067r → 0.067c → 0.067r → 0.8c → 0.8r*
7	*0.25c → 0.4r → 0.25c → 0.1r → 0.25c → 0.1r → 0.25c → 0.4r*
8	*0.4c → 0.25r → 0.1c → 0.25r → 0.1c → 0.25r → 0.4c → 0.25r*
9	*0.4c → 0.4r → 0.1c → 0.1r → 0.1c → 0.1r → 0.4c → 0.4r*

TABLE 5.5. *LA*, 8 ZONE SUB-MODELS TESTED TO INVESTIGATE THE EFFECT OF THE BALANCE OF RESISTANCE AND CAPACITY FRACTIONS.

FACTOR	**COLUMN NUMBER**
h_1 (W/m^2 K)	A
h_2 (W/m^2 K)	B
T_a (°C)	C
ε, layer 1	D
T_{room} (°C)	E
$\mathbf{R}_{\text{concrete, layer 2}}$ (m^2 K/W)	F
$\mathbf{C}_{\text{concrete, layer 2}}$ (kJ/m^{2}K)	G

TABLE 5.6. FACTORS INVESTIGATED IN *NLN*, *NDN* AND FEM MODELS AND ASSIGNMENT OF COLUMNS IN ORTHOGONAL ARRAY L_8 FOR THE CT WALL.

FACTOR	COLUMN NUMBER
h_1 (W/m^2 K)	A
h_2 (W/m^2 K)	B
T_{amb} (°C)	C
ε, layer 1	D
T_{room} (°C)	E
RC ratio$_{layer\ 1}$/**RC** ratio$_{layer\ 3}$	F
R$_{insulation,\ layer\ 2}$ (kJ/m^{2}K)	G

TABLE 5.7. FACTORS INVESTIGATED IN ***RRR***, ***RRL***, ***LRL***, ***DRD*** AND ***DDD*** MODELS AND ASSIGNMENT OF COLUMNS IN ORTHOGONAL ARRAY L_8, CIC WALL.

FACTOR	COLUMN NUMBER
h_1 (W/m^2 K)	A
h_2 (W/m^2 K)	B
T_{amb} (°C)	C
T_{room} (°C)	D
RC$_{concrete,layer\ 1}$ (s)	E
R$_{insulation,\ layer\ 2}$ (kJ/m^{2}K)	F
C$_{metal,layer\ 3}$ (kJ/m^3 C)	G

TABLE 5.8. FACTORS INVESTIGATED IN ***RRC***, ***LRC***, ***LLC***, ***RDC*** AND FEM MODELS AND ASSIGNMENT OF COLUMNS IN ORTHOGONAL ARRAY L_8, CIM WALL.

5.2. Results and analysis.

Figures 5.4a to 5.7b present heat load profiles obtained for the 4 types of walls, in each case indicating the best and worst agreement with FEM results. These illustrate the extent of deviations observed. The variables and levels used for each of these runs can be obtained using Tables 5.1 to 5.3 and Tables 5.6 to 5.8, *i.e.* to determine these parameters for the SPT run 1 presented in Fig. 5.4a, match the number of the run in Table 5.2 with Table 5.3 to

determine the variables (columns) used. Run 1 sets all variables at level 1; use Table 5.1 to determine the conditions that correspond to level 1. The variables and levels for run 1 were set as indicated below:

- Variable A: h_1 = 3 W/m^2 K
- Variable B: h_2 = 3.5 W/m^2 K
- Variable C: $\varepsilon_{\text{layer 1}}$ = 0.12
- Variable D: T_a = 15 °C
- Variable E: T_{room} = -25 °C
- Variable F: $\mathbf{R}_{insulation,\ layer\ 2}$ = 2 m^2 K/W
- Variable G: $\mathbf{C}_{metal,\ layer\ 3}$ = 152 kJ/m^2 K

5.2.1. Variables affecting the physical behaviour of the system.

Tables 5.9 to 5.12 present a summary of the results of analyses of variance (ANOVA) conducted for: 1) the measures, 2) the accuracy of the measures. The first ANOVA defined the factors that most influenced the magnitude of the heat load, whereas the second ANOVA defined the factors that affected the model accuracy. The factors affecting the heat load itself were not necessarily the same as those affecting the accuracy of particular models.

An early observation was that in all models and regardless of the level of mathematical complexity used in each one, the mean heat load was modelled accurately for all the types of walls and its accuracy was not significantly influenced by any factor. The implications of this result will be discussed later.

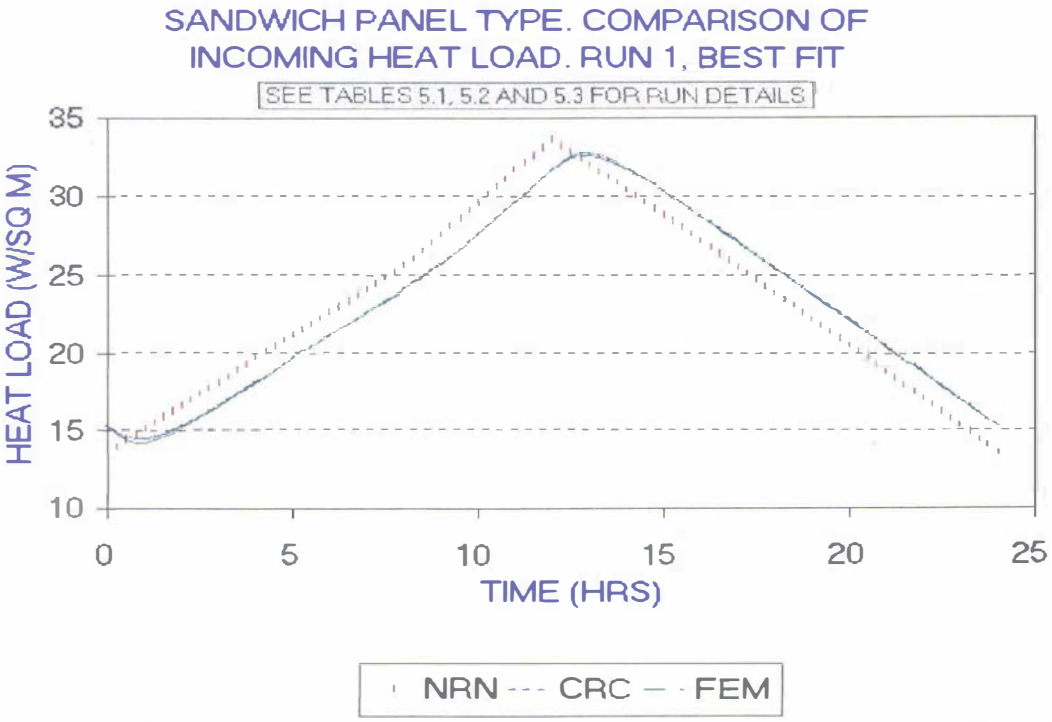

Figure 5.4a. Predictions of incoming heat flux obtained for the SPT wall, Run 1. This run showed the best visual agreement between FEM, ***NRN*** and ***CRC*** responses.

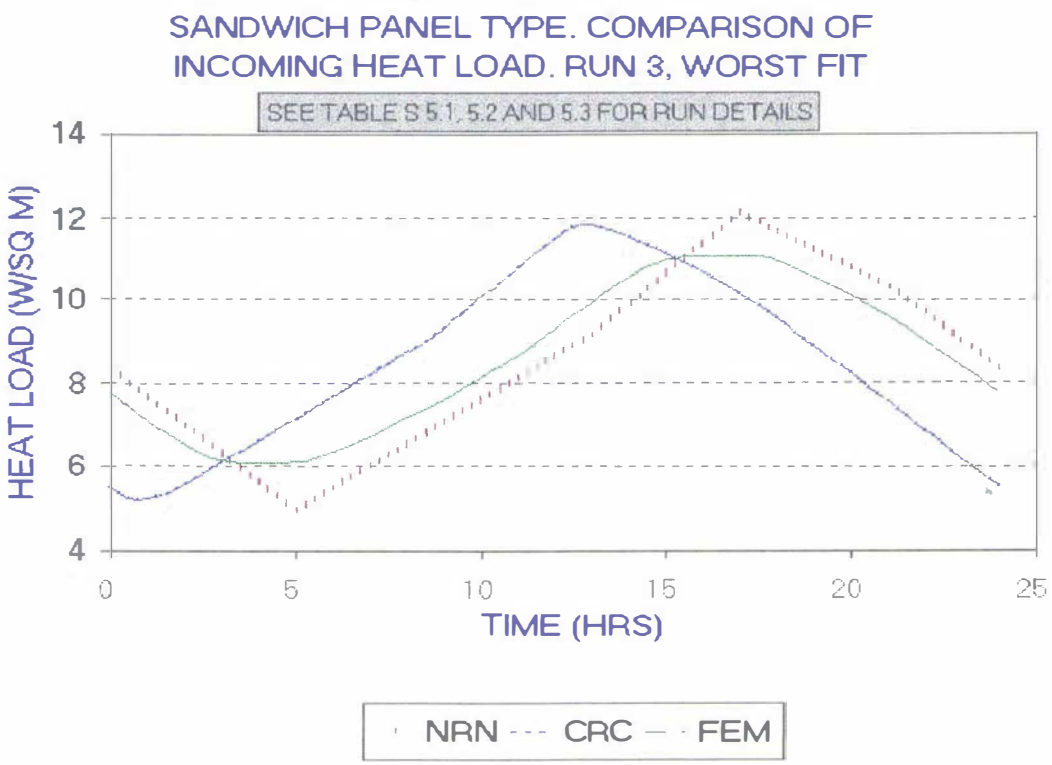

Figure 5.4b. Predictions of incoming heat flux obtained for the SPT wall, Run 3. This run showed the worst visual agreement between FEM, ***NRN*** and ***CRC*** responses.

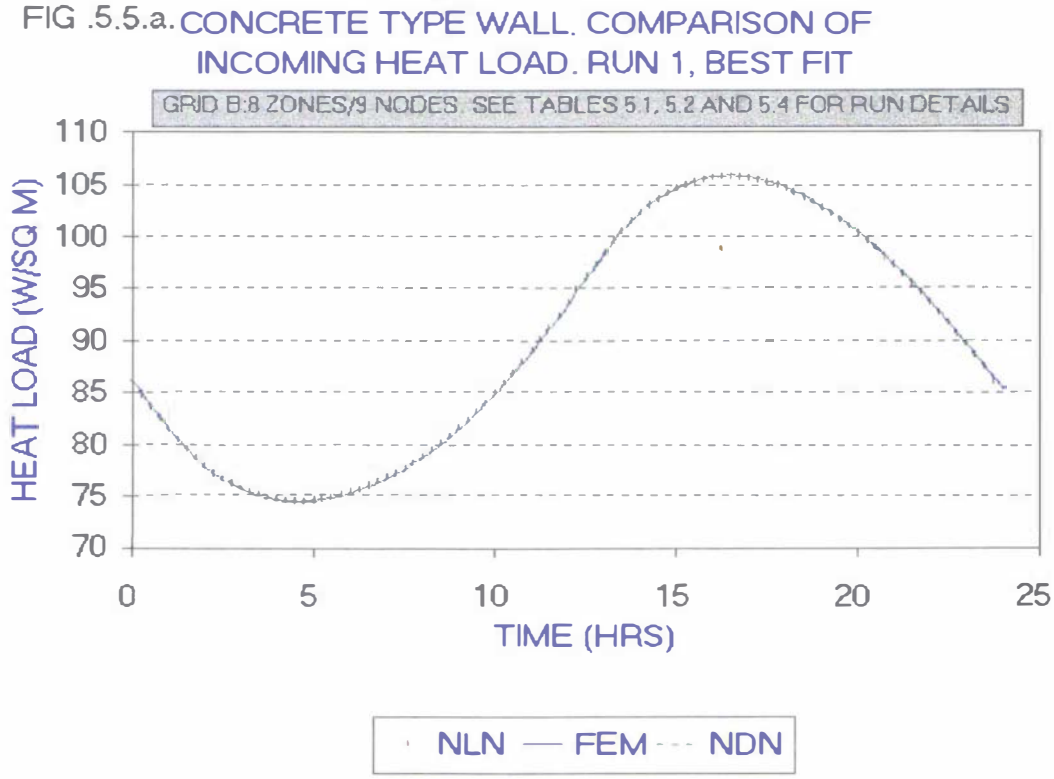

Figure 5.5a. Predictions of incoming heat flux obtained for the CT wall, Run 1. This run showed the best visual agreement between FEM, *NLN* and *NDN* responses.

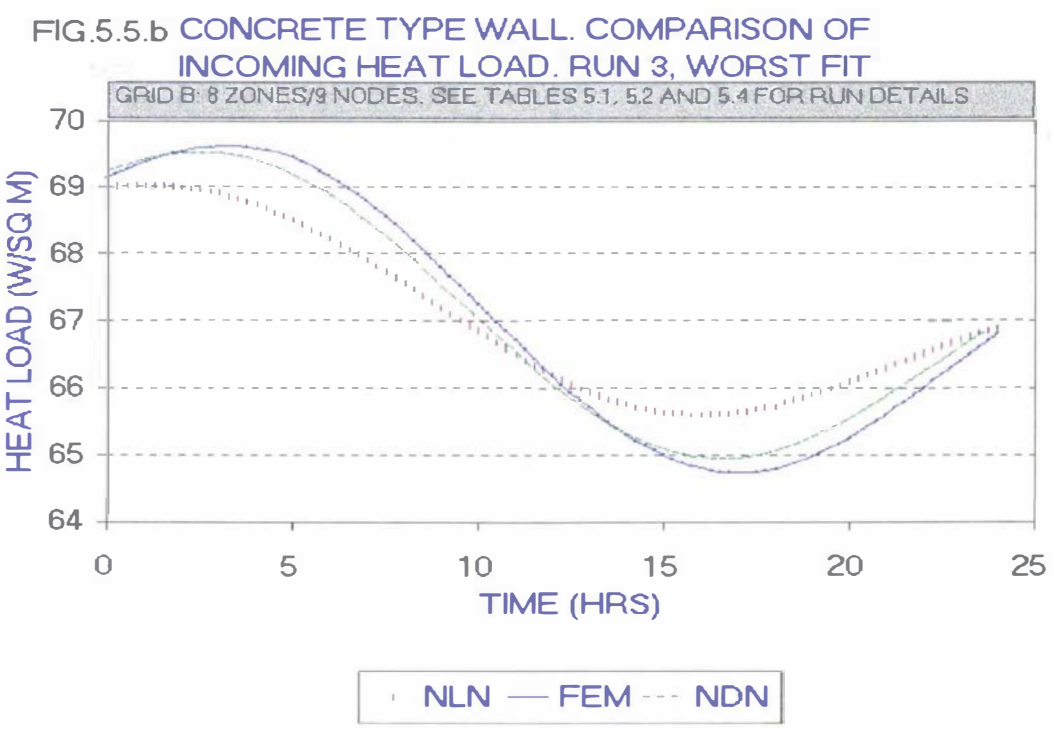

Figure 5.5b. Predictions of incoming heat flux obtained for the CT wall, Run 3. This run showed the worst visual agreement between FEM, *NLN* and *NDN* responses.

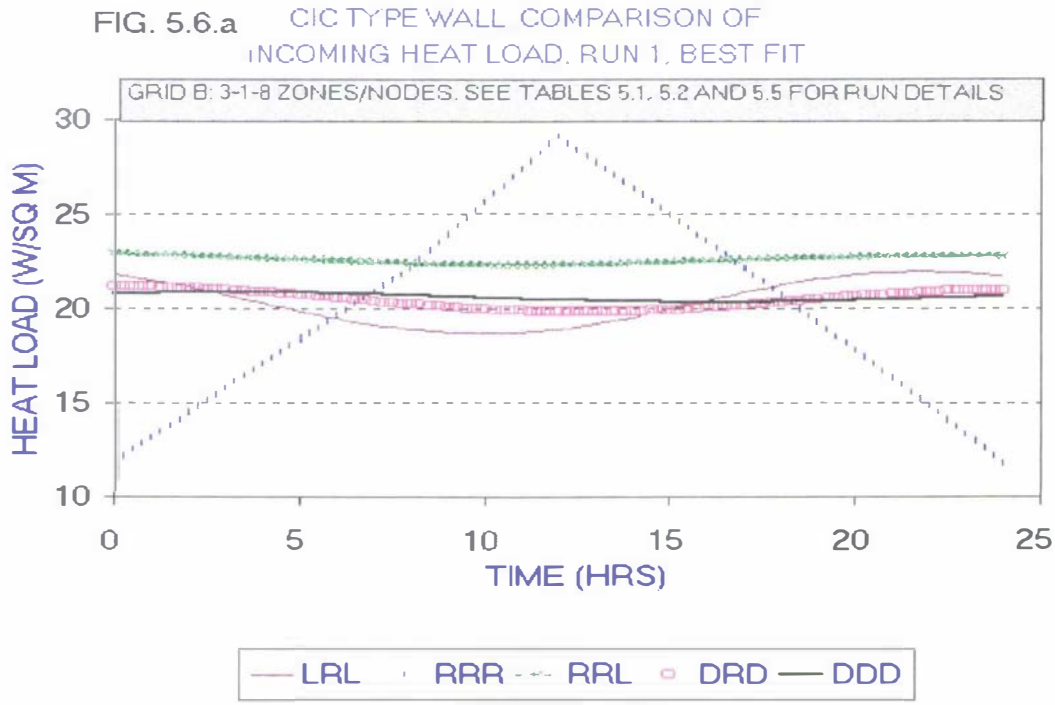

Figure 5.6a. Predictions of incoming heat flux obtained for the CIC wall, Run 1. This run showed the best visual agreement between ***DDD***, ***RRR***, ***RRL***, ***LRL*** and ***DRD*** responses.

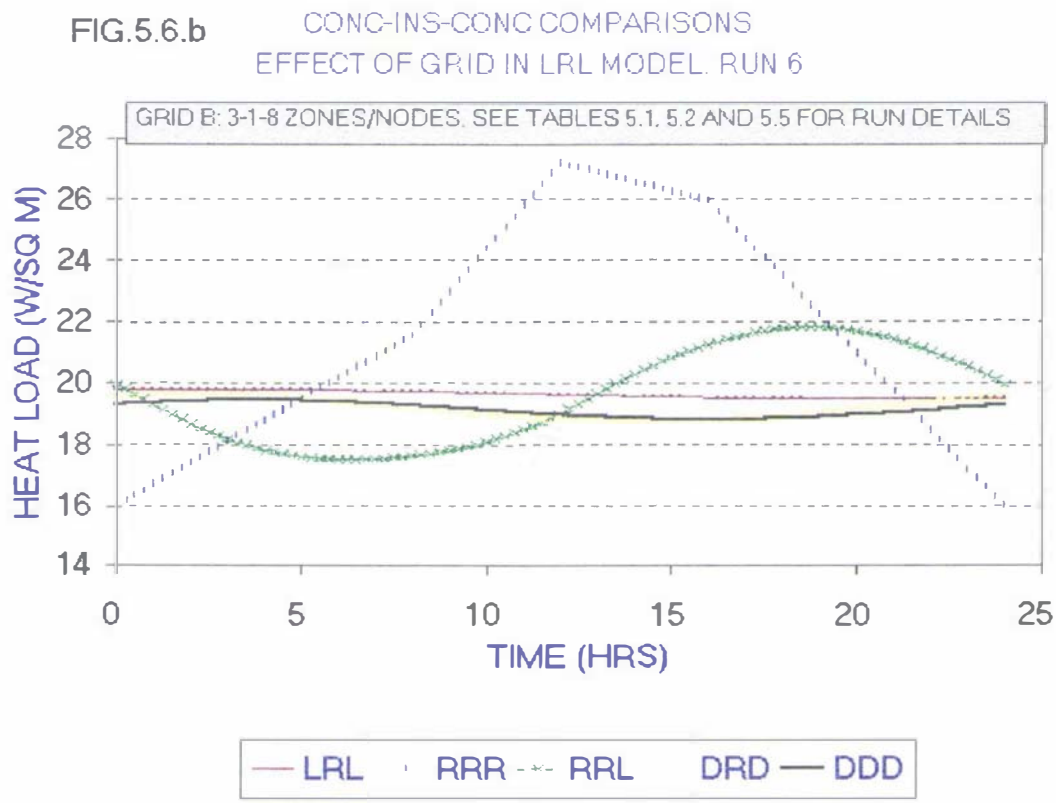

Figure 5.6a. Predictions of incoming heat flux obtained for the CIC wall, **Run 6**. This run showed the **worst** visual agreement between ***DDD***, ***RRR***, ***RRL***, ***LRL*** and ***DRD*** responses.

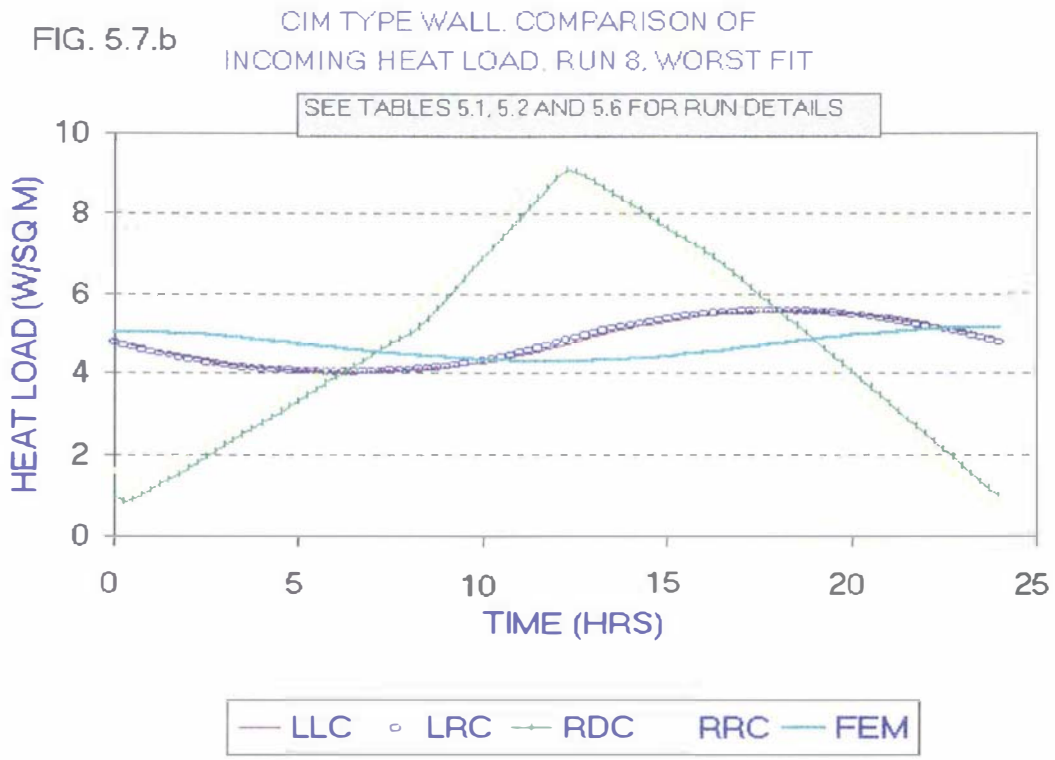

Figures 5.7b. Predictions of incoming heat flux obtained for the CIM wall, **Run 8**. This run showed the **worst** visual agreement between FEM, ***RRC***, ***LRC***, ***RDC*** and ***LLC*** responses.

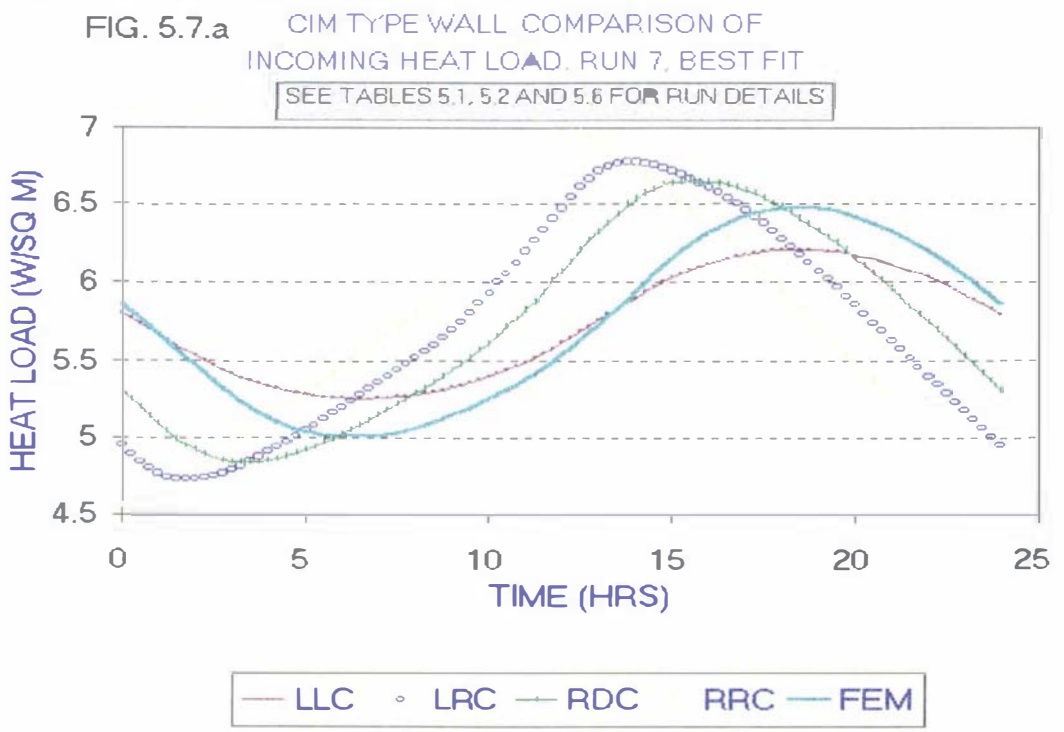

Figure 5.7a. Predictions of incoming heat flux obtained for the CIM wall, **Run 7**. This run showed the **best** visual agreement between FEM, ***RRC***, ***LRC***, ***RDC*** and ***LLC*** responses

TABLE 5.9. SUMMARY OF THE PERCENTAGE CONTRIBUTIONS OF THE VARIABLES INVESTIGATED FOR THE SANDWICH PANEL TYPE WALL TO THE ACCURACY AND MAGNITUDE OF PHYSICAL MEASURES.

S = Start-up time (hrs), A = Amplitude (W/m^2), MHL = Mean heat load (W/m^2), O = Offset (hrs). The % contribution of the factors on the magnitude is given in bold numbers. The % contribution to accuracy in relation to FEM is given in normal font. N/E = No significative effect of this variable on the magnitudes and accuracies was found in the ANOVA analyses.

MODEL	MEASURE	h_1	h_2	T_a	ε	T_{room}	$\mathbf{R}_{insulation,\ layer\ 2}$	$\mathbf{C}_{metal,\ layer3}$
CRC	S	14	15 ▌ **52**	N/E	N/E	**8**	26	40
	A	18 ▌ **21**	N/E	15	N/E	N/E	42 ▌ **58**	12
	M H L	N/E	N/E	N/E	N/E	**38**	**53**	N/E
	O	N/E	N/E	N/E	N/E	N/E	77	N/E
NRN	S	N/E	N/E	N/E	N/E	N/E	N/E	N/E
	A	**15**	N/E	N/E	N/E	N/E	77 ▌ **66**	N/E
	M H L	N/E	N/E	N/E	N/E	**38**	**53**	N/E
	O	N/E	N/E	N/E	N/E	N/E	76	N/E
FEM	S	N/E	**18**	N/E	N/E	N/E	**60**	**11**
	A	**16**	N/E	N/E	N/E	N/E	**70**	**8**
	M H L	N/E	N/E	N/E	N/E	**38**	**53**	N/E
	O	N/E	N/E	N/E	N/E	N/E	N/E	N/E

TABLE 5.10. SUMMARY OF THE PERCENTAGE CONTRIBUTIONS OF THE VARIABLES INVESTIGATED FOR THE CONCRETE TYPE WALL TO THE ACCURACY AND MAGNITUDE OF PHYSICAL MEASURES.

S = Start-up time (hrs), A = Amplitude (W/m^2), MHL = Mean heat load (W/m^2), O = Offset (hrs). The % contribution of the factors on the magnitude is given in bold numbers. The % contribution to accuracy in relation to FEM is given in normal font. N/E = No significative effect of this variable on the magnitudes and accuracies was found in the ANOVA analyses.

MODEL	**MEASURE**	h_1	h_2	T_a	ε	T_{room}	$\mathbf{R}_{concrete,\ layer\ 2}$	$\mathbf{C}_{concrete,\ layer\ 2}$
NLN	S	14 ▌**26**	N/E	N/E	28	24	31 ▌**29**	**33**
	A	9	N/E	N/E	N/E	N/E	30	29
	M H L	N/E	N/E	N/E	N/E	**38**	**53**	N/E
	O	18	N/E	N/E	N/E	N/E	45	30
NDN	S	**23**	N/E	N/E	N/E	N/E	**31**	**37**
	A	23	N/E	N/E	N/E	N/E	45	28
	M H L	N/E	N/E	N/E	N/E	**38**	**53**	N/E
	O	30	N/E	N/E	N/E	N/E	30	30
FEM	S	**25**	N/E	N/E	N/E	N/E	**32**	**37**
	A	N/E	N/E	N/E	N/E	N/E	N/E	N/E
	M H L	N/E	N/E	N/E	N/E	**38**	**53**	N/E
	O	N/E	N/E	N/E	N/E	N/E	N/E	N/E

TABLE 5.11. SUMMARY OF THE PERCENTAGE CONTRIBUTIONS OF THE VARIABLES INVESTIGATED FOR THE CONCRETE -INSULATION -CONCRETE TYPE WALL TO THE ACCURACY AND MAGNITUDE OF PHYSICAL MEASURES.

S = Start-up time (hrs), A = Amplitude (W/m^2), MHL = Mean heat load (W/m^2), O = Offset (hrs)

Note: The % contribution of the factors on the magnitude is given in bold numbers. The % contribution to accuracy in relation to FEM is given in normal font . N/E = No significative effect of this variable on the magnitudes and accuracies was found in the ANOVA analyses.

MODEL	**MEASURE**	h_1	h_2	T_a	ε	T_{room}	$\mathbf{R}_{insulation,\ layer\ 2}$	$(\mathbf{RC})_{layer1/layer3}$
RRR	S	N/E	N/E	N/E	N/E	N/E	N/E	N/E
	A	47 ▌ **11**	6	10	N/E	13	**76** ▌ 21	N/E
	M H L	N/E	**11**	N/E	N/E	**44**	**43**	N/E
	O	N/E	10	23	19	N/E	40	N/E
RRL	S	N/E	**7** ▌ 19	N/E	N/E	11	25	32 ▌ **79**
	A	6	**17**	N/E	**9**	N/E	8▌ 8	56 ▌ **59**
	M H L	N/E	**10**	N/E	N/E	**43**	**40**	N/E
	O	23	20	29	11	N/E	10	N/E

continued....

Table 5.11 continued...

MODEL	**MEASURE**	h_1	h_2	T_a	ε	T_{room}	$\mathbf{R}_{\text{insulation, layer 2}}$	$(\mathbf{RC})_{\text{layer1/layer3}}$
LRL	S	13	**34**	8	N/E	8	13	57 ▌ **46**
	A	**15**	N/E	N/E	N/E	N/E	**20**	**36**
	M H L	N/E	**11**	N/E	N/E	**45**	**39**	N/E
	O	N/E	N/E	N/E	N/E	N/E	N/E	83
DRD	S	N/E	**48**	N/E	**11**	N/E	N/E	**9**
	A	**6**	**4**	**3**	17 ▌ **4**	N/E	**27**	67 ▌ **14**
	M H L	N/E	**10**	N/E	N/E	**44**	**40**	N/E
	O	N/E	30	22	N/E	N/E	21	20
DDD	S	**6**	**8**	N/E	N/E	N/E	**64**	N/E
	A	N/E	**9**	**2**	N/E	**2**	N/E	**55**
	M H L	N/E	**10**	N/E	N/E	**43**	**40**	N/E
	O	N/E	N/E	N/E	N/E	N/E	N/E	N/E

TABLE 5.12. SUMMARY OF THE PERCENTAGE CONTRIBUTIONS OF THE VARIABLES INVESTIGATED FOR THE CONCRETE - INSULATION -METAL TYPE WALL TO THE ACCURACY AND MAGNITUDE OF PHYSICAL MEASURES.

S = Start-up time (hrs), A = Amplitude (W/m^2), MHL = Mean heat load (W/m^2), O = Offset (hrs)

Note: The % contribution of the factors on the magnitude is given in bold numbers. The % contribution to accuracy in relation to FEM is given in normal font. N/E = No significative effect of this variable on the magnitudes and accuracies was found in the ANOVA analyses.

MODEL	MEASURE	h_1	h_2	T_a	T_{room}	$\mathbf{R}_{insulation,\ layer\ 2}$	$\mathbf{C}_{metal,\ layer3}$	$(\mathbf{RC})_{layer1}$
RRC	S	30 ▌ **57**	3 ▌ **4**	**6**	20	**16**	9 ▌ **17**	37
	A	14 ▌ **27**	N/E	**2**	N/E	12 ▌ **59**	65 ▌ **12**	N/E
	M H L	N/E	N/E	N/E	**24**	**48**	N/E	N/E
	O	17	9	15	31	N/E	16	11
LRC	S	26 ▌ **6**	2	**4**	**4**	26 ▌ **7**	41 ▌ **78**	2
	A	20 ▌ **24**	N/E	N/E	13	**33**	52 ▌ **42**	4
	M H L	N/E	N/E	N/E	**24**	**48**	N/E	N/E
	O	N/E	N/E	N/E	N/E	N/E	N/E	N/E

continued...

Table 5.12 continued...

MODEL	**MEASURE**	h_1	h_2	T_a	T_{room}	$\mathbf{R}_{\text{insulation, layer 2}}$	$\mathbf{C}_{\text{layer 3}}$	$(\mathbf{RC})_{\text{layer1}}$
LLC	S	26 ▌ **3**	7 ▌ **20**	N/E	2	43 ▌ **51**	23 ▌ **8**	**2**
	A	4 ▌ **25**	9	2	15	**35**	25 ▌ **39**	21
	M H L	N/E	N/E	N/E	**23**	**49**	N/E	N/E
	O	N/E	N/E	N/E	N/E	N/E	N/E	N/E
RDC	S	**5**	N/E	**7**	**7**	55 ▌ **82**	N/E	N/E
	A	10 ▌ **22**	N/E	N/E	N/E	6 ▌ **62**	83 ▌ **11**	N/E
	M H L	N/E	N/E	N/E	**24**	**48**	N/E	N/E
	O	N/E	N/E	N/E	N/E	N/E	N/E	N/E
FEM	S	N/E	N/E	N/E	N/E	N/E	N/E	N/E
	A	**21**	N/E	N/E	N/E	**30**	**43**	N/E
	M H L	N/E	N/E	N/E	**23**	**49**	N/E	N/E
	O	N/E	N/E	N/E	N/E	N/E	N/E	N/E

5.2.1.1. Sandwich panel type wall.

Table 5.13 summarises the start-up times, amplitudes and mean heat loads found for the ***NRN***, ***CRC*** and FEM models and the discussion below refers to both this table and Table 5.9.

a) Factors affecting the magnitude of heat flux entering the room.

- Start-up times. For the SPT wall, a band of ±1% of the heat load entering the room between time=t and time=t+24 hrs was set as the criteria used for determining the start-up time after which the repeatable cycle was assumed to be occurring.

  For the ***NRN*** case by definition the mathematical model required an equality between the heat flux entering and leaving the wall, and thus the repeatable cycle was immediately established. Variation in insulation resistance had most effect on the start-up times for FEM models. The relatively high importance of variations of the thermal capacity in layer 3 for ***CRC*** but lower importance of this factor for FEM indicates a fundamental difference in model behaviour.

- Amplitudes. The amplitude was most affected by change in $\mathbf{R}_{\text{insulation, layer 2}}$. Further trials, varying $\mathbf{R}_{\text{insulation, layer 2}}$, allowed the construction of Fig. 5.8a, which shows an approximately exponential relationship between amplitude of the heat load cycle and $\mathbf{R}_{\text{insulation, layer 2}}$, amplitude decreasing as $\mathbf{R}$ increases. In physical terms, the extent of damping of the incoming cyclical wave in the heat load increases as the insulation thickness (x) increases and/or thermal conductivity (λ) decreases. Large differences between $\mathbf{R}_{\text{insulation, layer 2}}$ of 2 m^2 K/W to 5 m^2 K/W are observed, but at higher $\mathbf{R}$ values there is little change and further increases in x and/or decreases in λ have a small effect.

- Mean heat load. As expected, for all 3 models changes in $\mathbf{R}_{\text{insulation, layer 2}}$ and T_{room} explained most of the differences between trials. Mean heat load was relatively unaffected by changes in variables such as emitted and incident radiation levels over the wall.

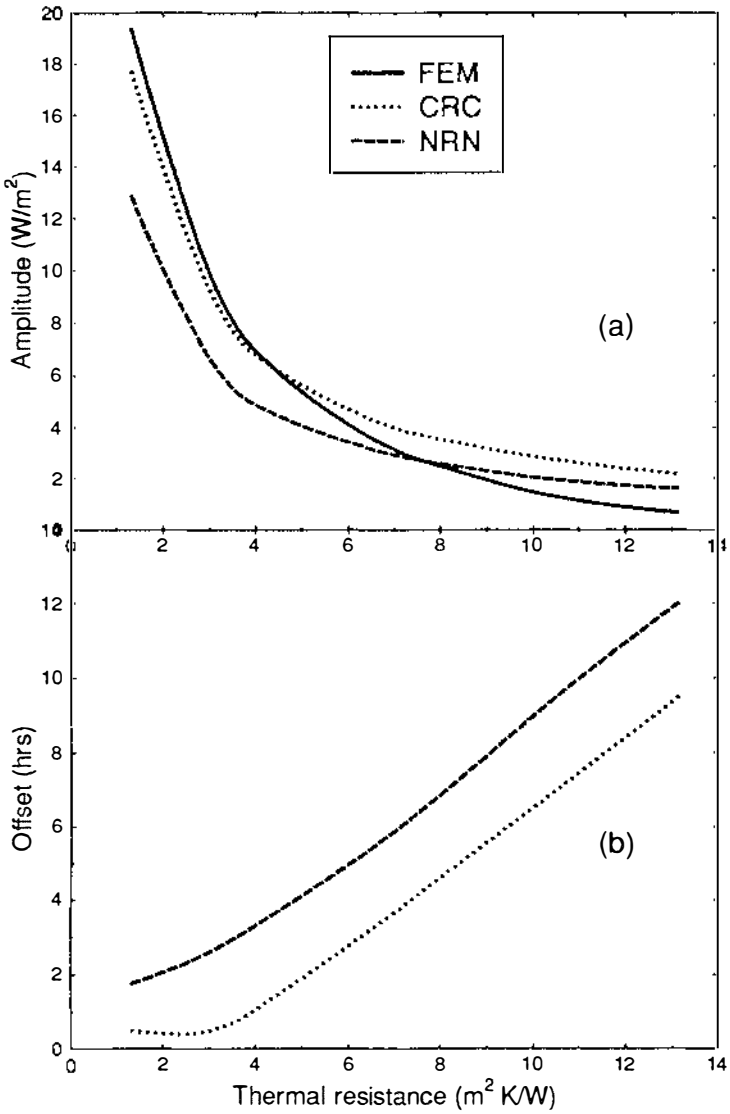

Fig. 5.8. Amplitudes and offsets variations due to the increase of insulation thermal resistance: a) Amplitudes, FEM, CRC and NRN models b) Offsets, CRC and NRN models

b) Factors affecting the accuracy of the models.

- Start-up time. Both the ***NRN*** and ***CRC*** models failed to accurately predict the start-up times predicted by FEM. For ***CRC***, the effects discussed above led to over-prediction of start-up times at low levels of resistance and an under-prediction when using high levels of resistance. ***NRN*** maximised error by failing to predict start-up at all.

- Amplitude. Changes in insulation resistance changed the accuracy of ***NRN***. As $\mathbf{R}_{\text{insulation, layer 2}}$ increased, ***NRN*** was progressively less accurate. Similar behaviour was observed for ***CRC***, though the accuracy of this model was also affected by changes in the external heat transfer coefficient and the mean external ambient temperature.

- Offset. As expected, the time for reaching peak heat loads for ***NRN*** runs remained constant regardless the levels of the factors investigated, due to the immediate algebraic response of ***NRN*** to the external temperatures and incident heat load signal. The ***CRC*** model did model a delay in the response due to the thermal capacity. Both models progressively predicted the timing of the peak heat load less accurately as **R** rose. Figure 5.8b shows the relationship between offset and $\mathbf{R}_{\text{insulation, layer 2}}$. Overall, higher accuracy is expected for low resistances and for the ***CRC*** model.

TRIAL	*NRN*			*CRC*			FEM		
	START-UP (Hrs)	AMPLITUDE (W/m^2)	MEAN HEAT LOAD (W/m^2)	START-UP (Hrs)	AMPLITUDE (W/m^2)	MEAN HEAT LOAD (W/m^2)	START-UP (Hrs)	AMPLITUDE (W/m^2)	MEAN HEAT LOAD (W/m^2)
1	0	20.00	23.25	8.5	18.08	23.27	2.3	18.48	23.23
2	0	3.18	0.58	24.0	1.86	0.59	18.0	1.93	0.59
3	0	7.21	4.29	7.3	6.66	8.51	11.5	4.97	4.33
4	0	17.28	24.45	2.0	16.90	8.21	1.8	16.78	24.39
5	0	13.00	6.94	24.0	8.27	9.81	10.5	10.36	6.95
6	0	3.23	7.29	9.3	3.58	6.26	12.8	2.28	7.32
7	0	2.56	5.50	1.3	2.50	1.44	9.3	1.83	5.53
8	0	7.78	4.93	7.8	7.29	19.00	2.3	7.39	4.91

TABLE 5.13 SANDWICH PANEL TYPE WALL: SUMMARY OF PHYSICAL MEASURES RESULTS, ***NRN***, ***CRC*** AND FEM TRIALS.

5.2.1.2. Concrete wall.

Table 5.14 presents the summary of the results for the physical measures obtained using the ***NLN, NDN*** and FEM models. The summary of measures given in Table 5.10 also gives insight for the interpretation of the following results.

a) Effect of grid selection strategy.

- **Effect of the number of zones and the thermal characteristic of the boundary zones on accuracy.** Fig. 5.9 illustrates the effect on the accuracy of amplitudes and offsets when varying the boundary thermal characteristics and the zoning strategy. These analyses were conducted using the conditions stated in Tables 5.1 to 5.3 and Table 5.7 for run 8. The mean heat load was predicted with negligible errors in all cases.

  The amplitude estimate was affected by the selection of *c* or *r* for the zone in contact with the external environment (Fig.5.9a). The error using a *c* zone in the boundary of layer 1 decreased slowly with increases in the number of zones used in the ***L*** model. In contrast, the error for models using an *r* region at the external boundary was both higher and more sensitive to the number of zones. The amplitude was underestimated when using an *r* zone in the external boundary and slightly overestimated when a *c* zone was selected instead. The best accuracy occurred for 6 or more zones, setting *c* in the external boundary.

  The offsets (Fig.5.9b) were also affected by the selection of *c* or *r* in the layer 3 / low temperature environment boundary. The best accuracy was found when a *c* zone was placed in this boundary - no offset was detected. Offsets ranging from 1800 s to 800 s were observed when an *r* zone was used.

  Overall, the best accuracy was obtained when setting *c* in the external boundary, the condition that applies in lumped models ***L2*** and ***L4***. Beyond 4, the number of zones had little effect on the errors obtained for a fixed set of conditions (run 8). However, this parameter was shown to affect the accuracy in a significant manner when the **C** and **R** levels of the concrete layer were both set at high levels. This point is further discussed in the section related to the effect of the grid coarseness on the accuracy (p.125).

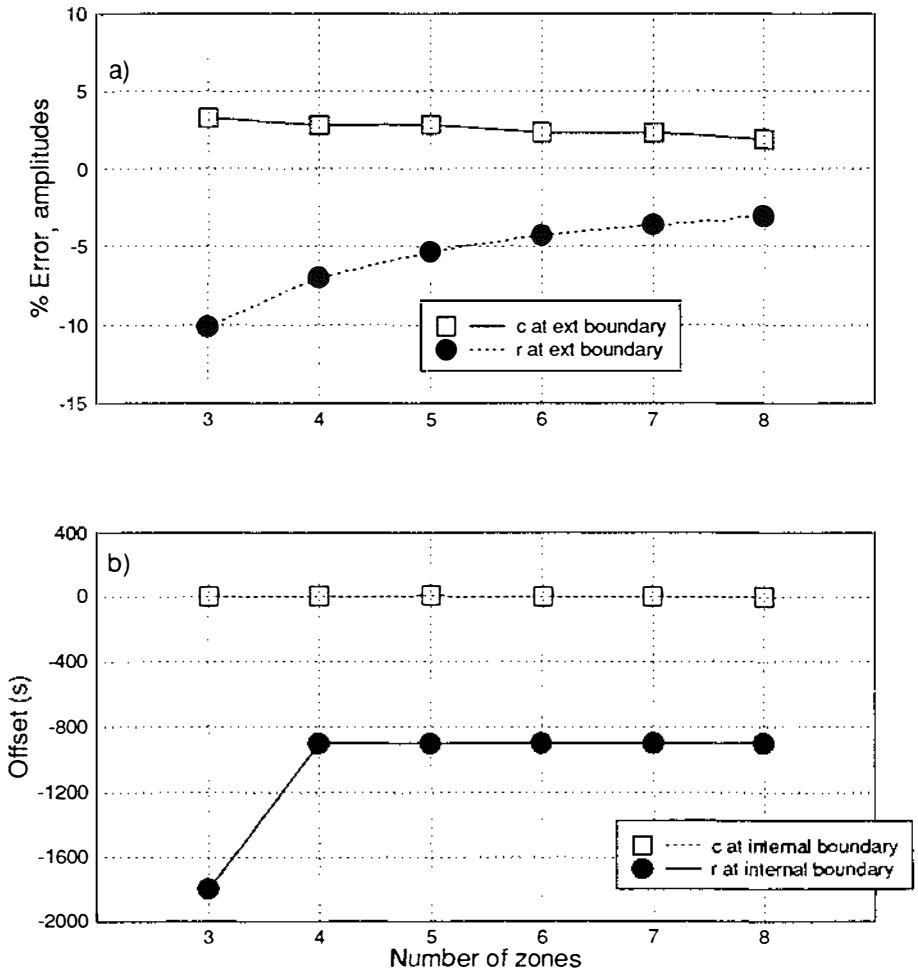

Fig. 5.9. Effect of number of zones and boundary thermal characteristics on the response of a lumped model (conditions of trials given in Table 5.4): Each marker represents one trial. Squares are trials 1,3,5,7,9 and 11. Circles are trials 2,4,6,8,10 and 12. a) Influence of the thermal representation of the external boundary zone on the amplitude error and b) Influence of the thermal representation of the internal boundary zone on the offset in time.

- **Effect of the distribution of resistance (ζ) and capacity (γ) on accuracy.** Figs. 5.10a and 5.10b illustrate the effect of resistance and capacity distribution on the accuracy of the amplitude and offset predictions. Again, run 8 was used to test this variable. The results of the previous experiment suggested that an ***L4***, 8 zones sub-model could be used to test subsequent variables (Table 5.5).

  The accuracy of mean heat load prediction was not affected by the distribution strategy. The amplitude errors were small and only trial 3 which had 80% of the *r* and *c* weighted toward the external boundary (layer 1) showed a large error. The same trial showed the largest offset, and in the rest of the trials an offset of less than 3000 s was observed. The mirror case, that is, setting 80% of *r* and *c* weighted toward the internal environment (layer 3), did not present large errors. This suggests that the variability of temperatures and radiative heat loads in the external environment is best modelled when a physically realistic approach in the first two *c* and *r* zones is used. Thus, the only strategy that should be avoided consists of setting most of both ζ and γ fractions in the boundary zone contacting the external environment. A physically realistic more even distribution of fractions should be preferred.

- **Effect of the grid coarseness on accuracy.** Figs. 5.11 to 5.16 show the percentage error found for ***NLN*** and ***NDN*** models using different grid selection strategies. According to the results in the previous two sub-sections, a model setting *c* in the external boundary with an even distribution of γ and ζ assured good accuracy using the scenario set in run 8. Thus, this combination was used for testing the effect of the noise, design and operation variables for the 4, 8 and 14 zone lumped sub-models tested. The ***NDN*** model followed the grid selection described in Section 5.1.3.

  Finer grids in ***NLN*** models improved the accuracy of the amplitude and offset results in those trials with high **R** and **C** levels. In the case of start-up times, the improvement of accuracy with finer grids was very significant in the trials with high **C** levels. Though the same principle applied to ***NDN*** models, overall accuracy was higher than ***NLN*** models and little accuracy was gained when increasing the number of nodes. This suggests that a structure with high thermal mass and high thermal resistance is more accurately modelled with a fine grid in lumped models. For thin concrete structures, coarse grids might be used with similar results to those observed with finer ones.

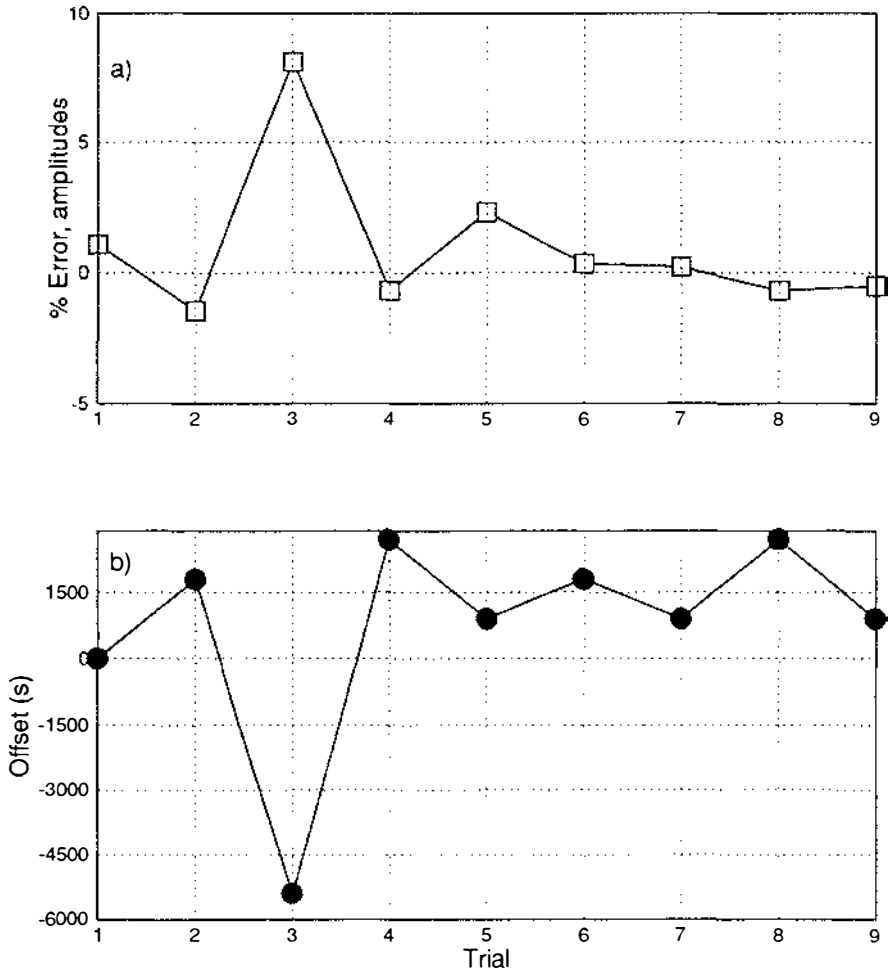

Fig. 5.10. Effect of spatial weighting on the response of a lumped model (conditions for each trial given in Table 5.5): a) Influence of spatial weighting on the amplitude error and b) Influence of spatial weighting on the offset in time

Fig. 5.11.Comparison of start-up errors, grids A, B and C. NLN model

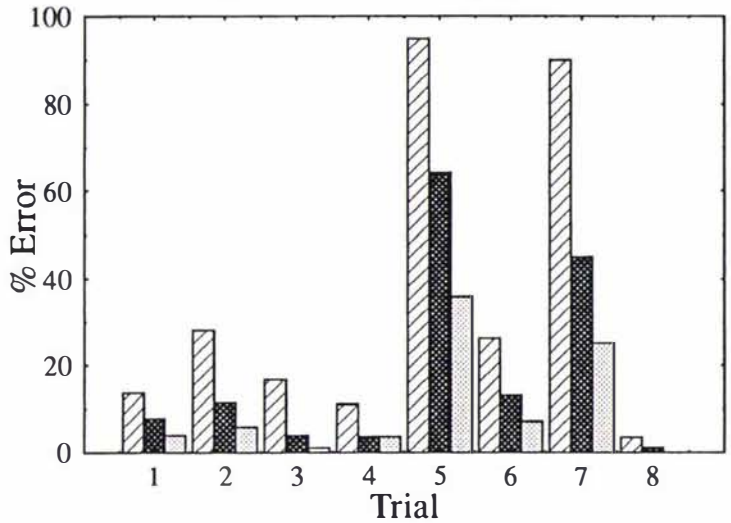

Fig. 5.12.Comparison of start-up errors, grids A, B and C. NDN model

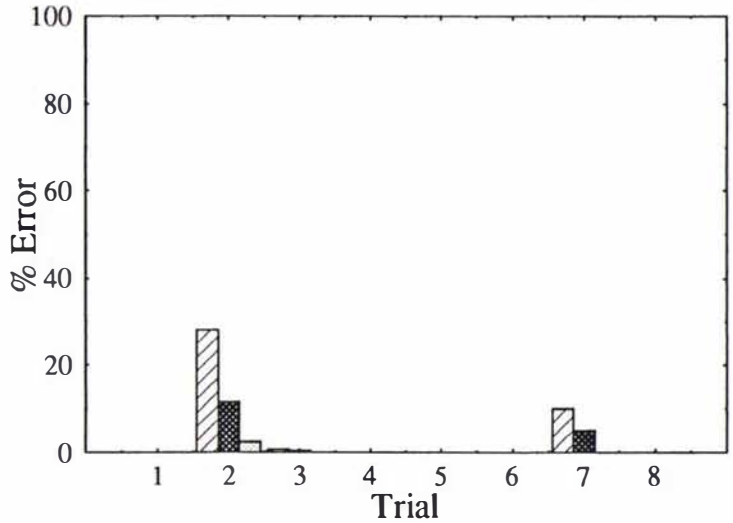

Fig. 5.13.Comparison of amplitude errors, grids A, B and C. NLN model

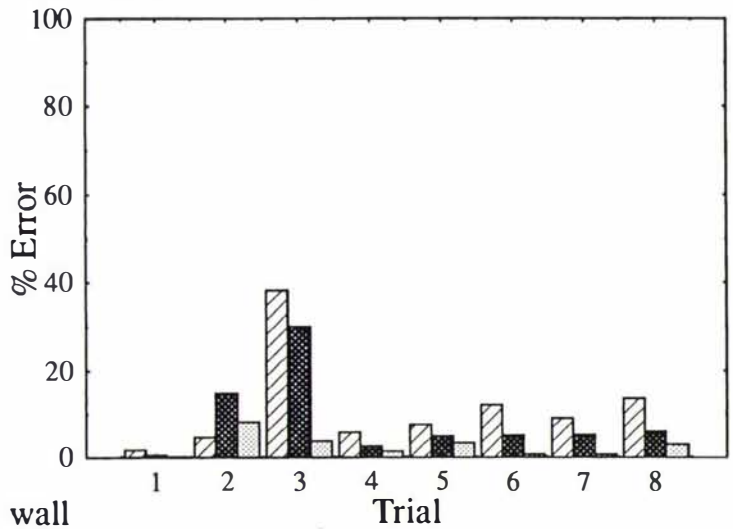

CT wall

Fig. 5.14.Comparison of amplitude errors, grids A, B and C. NDN model

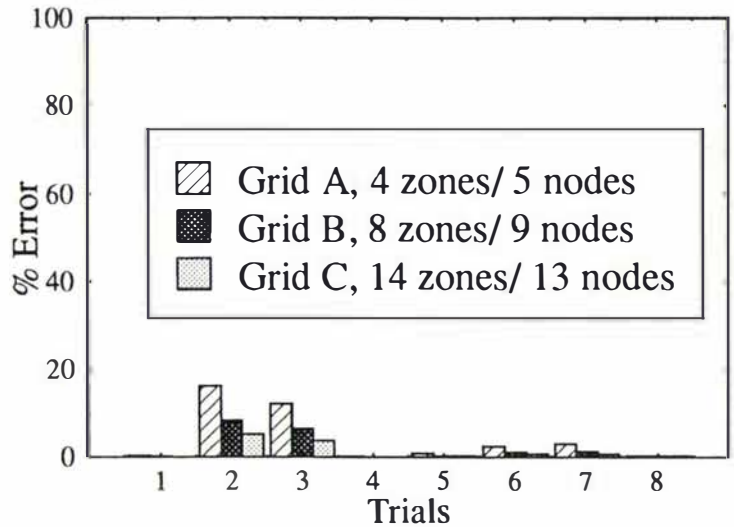

Fig. 5.15. Comparison of offset results, grid A, B and C. NLN model

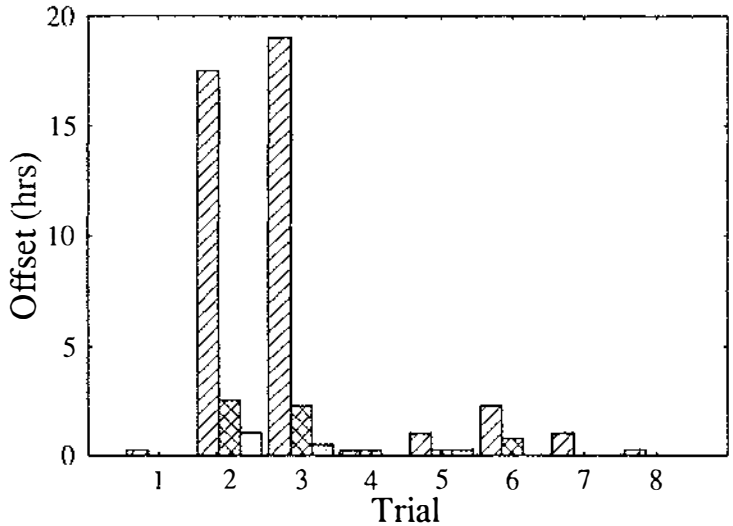

Fig. 5.16. Comparison of offset results, grids A, B and C. NDN model

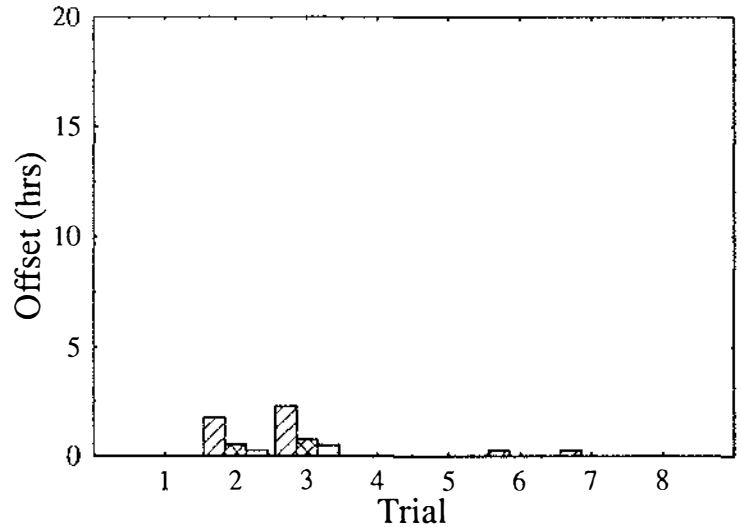

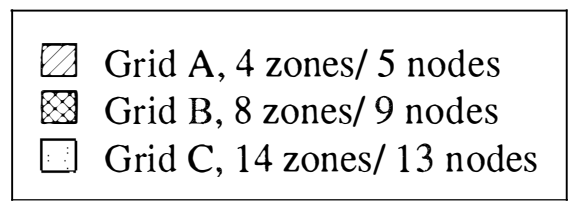

CONCRETE WALL

In terms of accuracy, the use of a 12 zone ***NLN*** model had approximately the same effect as the use of a 9 node ***NDN*** model. A decision as to whether to select a 12 zone ***L*** model or a 9 node ***D*** model could thus be based more on computing time restrictions and less on accuracy grounds. There were no significant differences in computation time between the two schemes. However, it was considered that when simulating a composite structure with sharper changes in the thermal properties of the boundary layers 1 and 3 (*i.e.* a sandwich panel type), the ***L*** models might prove faster.

The analysis of the effect of the grid variables helped to focus later analyses of the ***NLN*** model. All further work used 8 zones which was considered to be representative of the expected behaviour from ***L*** models.

b) Factors affecting the magnitude of heat flux entering the room (Table 5.10).

- Start-up times. The CT wall presents a significant delay in the thermal response compared to the SPT wall. Longer start-up times were found as a consequence and the criteria of repeatability was set as ±5%, instead of the ±1% used for the SPT wall. The computational resources available made longer simulation times impractical and ±5% was considered to be a sufficiently good estimate for the CT wall.

  Variations in h_1, $\mathbf{R}_{\text{concrete, layer 2}}$, and more significantly $\mathbf{C}_{\text{concrete, layer 2}}$ determined the differences in the start-up times found between trials. Long times to establish repeatable cycles arose from the combined effect of high levels of both $\mathbf{C}$ and $\mathbf{R}$.

- Amplitudes. None of the factors investigated proved to be statistically significant in explaining the changes in the magnitude of the amplitudes, but the results suggest that the combined variation of $\mathbf{R}_{\text{concrete, layer 2}}$ and $\mathbf{C}_{\text{concrete, layer 2}}$ was possibly more significant than their isolated effects. Trial 4 - which tested the thermal performance of a thin concrete wall with high ambient temperatures - had a very high amplitude.

- Mean heat loads. As observed in the SPT wall, the factors that most changed this parameter were concrete resistance and room temperature. The use of a radiation shield did not achieve significantly lower mean heat loads, unless combined with a concrete with a high $\mathbf{R}_{\text{concrete, layer 2}}$ value. The highest mean heat load was observed in

trial 8, that used a concrete with a low $\mathbf{R}_{\text{concrete, layer 2}}$ value with a heavy thermal mass and low internal room temperature.

c) Factors affecting the accuracy of the models (Tables 5.10 and 5.14 and Figs. 5.11 to 5.16).

- Start-up times. The prediction of start-ups was excellent for the ***NDN*** model, but less accurate for the ***NLN*** model (Figs. 5.11 and 5.12). The accuracy of the later was particularly affected by changes in h_1, ε, $\mathbf{C}_{\text{concrete, layer 2}}$ and T_{room}.

- Amplitudes. The main factors affecting the accuracy of both ***NDN*** and ***NLN*** models were changes in $\mathbf{C}_{\text{concrete, layer 2}}$, $\mathbf{R}_{\text{concrete, layer 2}}$ and h_1. The accuracy of the ***NLN*** model was good in all trials except those combining high $\mathbf{C}_{\text{concrete, layer 2}}$, $\mathbf{R}_{\text{concrete, layer 2}}$ and h_1. The ***NDN*** model was accurate in all runs.

- Offsets. As observed for the amplitudes, the errors were largest for trials 2 and 3. The accuracy, which was good in most of the trials, was influenced by changes in the values of $\mathbf{C}_{\text{concrete, layer 2}}$, $\mathbf{R}_{\text{concrete, layer 2}}$ and h_1.

TRIAL	*NLN*			*NDN*			FEM		
	START-UP (Hrs)	AMPLITUDE (W/m^2)	MEAN HEAT LOAD (W/m^2)	START-UP (Hrs)	AMPLITUDE (W/m^2)	MEAN HEAT LOAD (W/m^2)	START-UP (Hrs)	AMPLITUDE (W/m^2)	MEAN HEAT LOAD (W/m^2)
1	11.8	31.37	89.73	12.3	31.54	89.77	12.3	31.13	89.73
2	63.8	0.96	4.46	63.8	1.03	4.51	72.0	1.13	4.54
3	60.3	3.41	66.90	62.5	4.55	67.00	62.8	4.86	67.0
4	7.0	109.47	67.71	6.8	112.44	67.90	6.8	112.43	67.51
5	3.5	12.90	48.09	9.8	12.25	48.21	9.8	12.25	48.40
6	18.3	9.59	45.78	21.0	9.12	45.86	21.0	9.02	45.96
7	2.3	10.30	12.70	4.8	10.87	12.71	5.0	10.74	12.72
8	20.8	28.97	186.21	21.1	30.80	186.16	21.0	30.80	186.19

TABLE 5.14. CONCRETE TYPE WALL: SUMMARY OF PHYSICAL MEASURES RESULTS, ***NLN***, ***NDN*** AND FEM TRIALS.

5.2.1.3. Concrete-insulation-concrete wall.

Table 5.15 summarises the magnitudes of the measures found for the ***RRR***, ***RRL***, ***LRL***, ***DRD*** and ***DDD*** models. Table 5.11 summarises the statistical analysis of these measures. As discussed in Section 5.1.3, a ***DDD*** model developed in Chapter 4 was used as the basis to assess the CIC models accuracy.

a) Effect of grid selection strategies.

As stated in Section 5.1.3, two grids were investigated in order to define the effect of fine and coarser grids at the boundaries. Figs. 5.17 to 5.22 present comparisons of the accuracy found for both cases in ***RRL***, ***LRL*** and ***DRD*** models. In most trials, the accuracy of the amplitudes, start-up times and offsets was poor and fundamental differences between the ***DDD*** model and the ***RRL***, ***LRL*** and ***DRD*** models were observed. The mean heat load remained accurate for all models.

These results indicate that the representation of the insulation may be the source of inaccuracy, suggesting that a more elaborate representation than the ***R*** model should be used if better accuracy is needed. The following analyses of magnitude and accuracy are focused on the sub-model using the grid B (fine grid in the external layer with a coarser grid in the internal layer).

b) Factors affecting the magnitude of heat flux entering the room.

- Start-up times. The criteria of repeatability for CIC walls of a 24 hr cycle was set as ±1%.

The start-up times were strongly influenced by change in the thermal mass and resistance of the wall, represented by the $(\mathbf{RC})_{\text{layer 1}}/(\mathbf{RC})_{\text{layer 3}}$ ratio. A CIC wall combining a light layer 1 with a thicker layer 3 generated significantly higher start-up times than the opposite case, a thick layer 1 combined with a lighter layer 3. This is possibly due to the use of the uniform initial temperature calculated as the mean T_a in a daily cycle, which is the most likely situation when most of the external mass is in the external boundary. Start-up times for a CIC wall with high thermal mass in the internal layer ranged from 134 hrs to 327 hrs, in contrast with the times of 11 hrs to 94 hrs required for a wall with a lighter internal layer.

- Amplitude. Change in the $(\mathbf{RC})_{\text{layer 1}}/(\mathbf{RC})_{\text{layer 3}}$ ratio and the insulation resistance mostly affected the amplitudes. However, the effect of these was different from model to model. In models using an ***L*** region in one or both boundaries (***LRL*** and ***RRL***) changes in the insulation resistance showed a higher effect than changes in the $(\mathbf{RC})_{\text{layer 1}}/(\mathbf{RC})_{\text{layer 3}}$ ratio. However, in models using a ***D*** region (***DRD*** and ***DDD***) the situation was reversed. In the simplest model tested (***RRR***) only changes in the insulation resistance and the external heat coefficient showed a significant effect (Table 5.11).
- Mean heat load. Changes in insulation resistance, room temperature and external heat transfer coefficient significantly affected the mean heat load (Table 5.11). The effect of h_i was not observed in previous wall types, which might indicate that change of mean heat loads is more dependent on the ambient conditions (noise factors) when heavy structures are modelled.

c) Factors affecting the accuracy of the models (Table 5.11 and 5.15, Figs 5.17 to 5.22).

- Start-up time. In most of the trials, all models failed to predict the start-up time accurately. The ***RRL*** model gave closer results to the ***DDD*** model in those trials conducted using low levels of $(\mathbf{RC})_{\text{layer 1}}/(\mathbf{RC})_{\text{layer 3}}$ ratios.
- Amplitudes. In the CIC wall, the relative amplitude errors were much greater than for previous types of walls. Whereas the mean heat loads found for the SPT and CT walls were of the order of 10-100 W/m^2, the extent of damping of the semi-sinusoidal signal in CIC walls led to magnitudes that were typically less than 10 W/m^2. Amplitude variations between models and ***DDD*** of less than 2 W/m^2 led to large disagreements between those, whereas the same variations in SPT and CT comparisons did not lead to significant errors.
- Offsets. Figures 5.21 and 5.22 illustrate the magnitude of the offsets for all the models. Differences in model performance were correlated with change in T_a and $(\mathbf{RC})_{\text{layer 1}}/(\mathbf{RC})_{\text{layer 3}}$ ratios. The offsets distribution ranged from 0.2 hrs to 20 hrs, with the lowest values observed for runs 1, 2, 6 and 7. This might indicate that an interaction of the above two variables could be more important than their isolated effects.

Fig. 5.17. Comparison of start-up errors. Grid A. RRR,RRL,LRL and DRD models

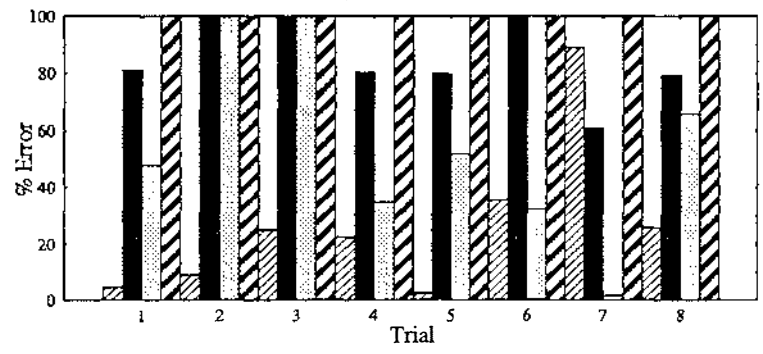

Fig. 5.18. Comparison of start-up errors. Grid B. RRL, LRL and DRD models

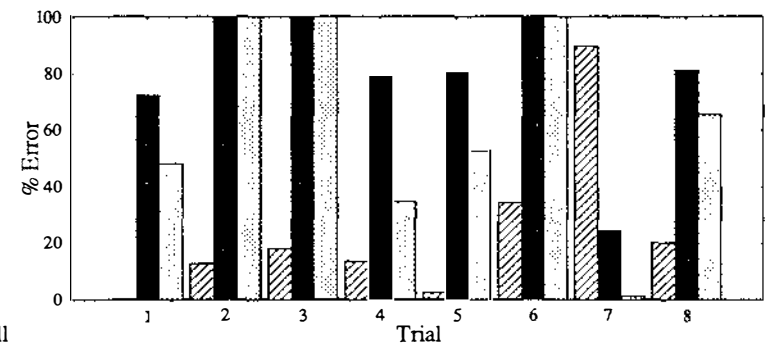

CIC wall

Fig. 5.19. Comparison of amplitude errors. Grid A. RRR,RRL,LRL and DRD models

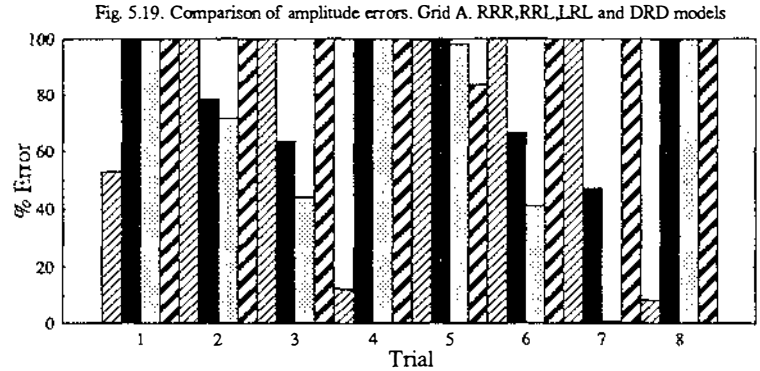

Fig. 5.20. Comparison of amplitude errors. Grid B. RRL, LRL and DRD models

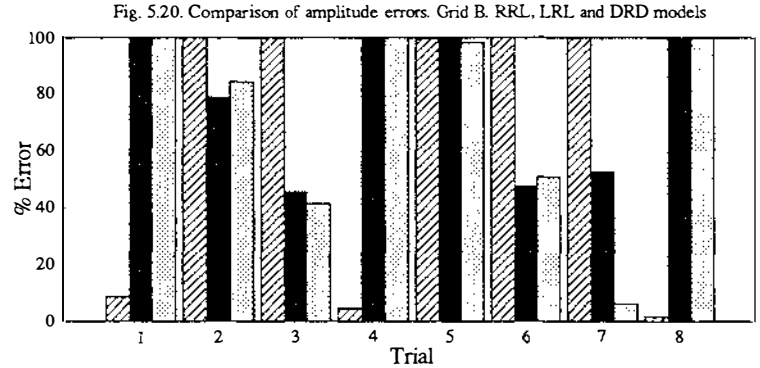

CIC wall

Fig. 5.21. Comparison of offsets. Grid A. RRR,RRL,LRL and DRD models

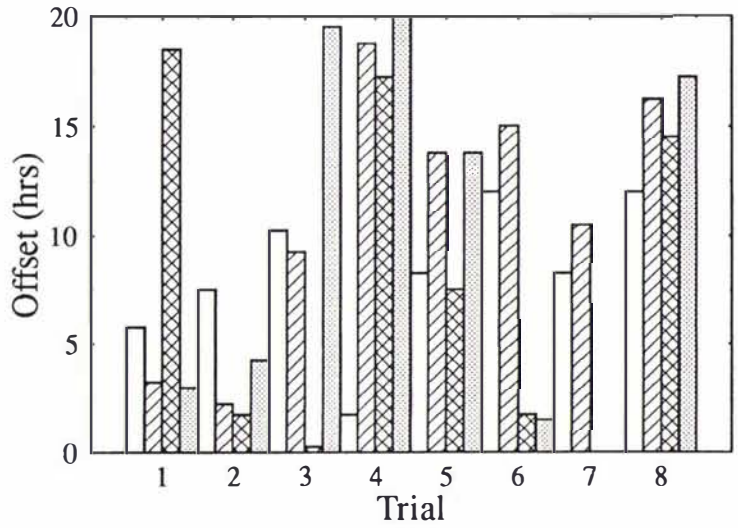

Fig. 5.22. Comparison of offsets. Grid B. RRL,LRL and DRD models

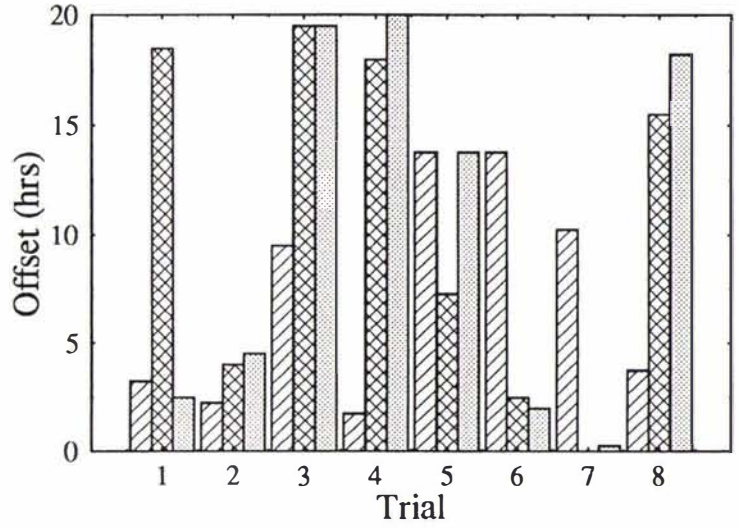

RRR
RRL
LRL
DRD

Grid A, RRL: 3 zones in layer 3
Grid B, RRL: 8 zones in layer 3
Grid A, LRL: 3 zones in layer 1, 8 zones in layer 3
Grid B, LRL: 8 zones in layer 1, 3 zones in layer 3
Grid A, DRD: 3 nodes in layer 1, 8 nodes in layer 3
Grid B, DRD: 8 nodes in layer 1, 3 nodes in layer 3

CIC WALL

TRIAL	*RRR*			*RRL*			*LRL*			*DRD*			*DDD*		
	SU	MHL	A	SU	MHL	A	SU	MHL	A	SU	MHL	A	SU	MHL	A
1	0	20.17	17.32	226.8	22.60	0.57	62.3	20.38	3.26	117.0	20.50	1.35	226.3	20.59	0.53
2	0	0.56	3.04	48.8	0.58	1.15	320.3	0.60	0.02	135.0	0.59	0.16	56.0	0.59	0.09
3	0	8.13	6.90	13.0	8.42	5.82	98.6	8.16	0.12	135.0	8.12	0.31	11.0	8.11	0.22
4	0	7.11	14.95	152.0	7.43	1.60	28.5	7.02	6.92	87.0	7.12	4.36	133.8	7.13	1.53
5	0	2.66	3.54	336.0	2.78	0.10	65.0	2.68	0.94	155.3	2.71	0.40	327.8	2.72	0.11
6	0	20.77	11.27	43.0	19.57	4.30	306.0	19.42	0.32	134.8	19.16	0.91	65.8	19.13	0.60
7	0	5.42	9.51	9.8	4.88	7.03	71.0	4.42	0.34	92.8	4.66	0.76	94.0	4.65	0.71
8	0	4.75	1.94	210.5	4.77	0.18	33.0	4.70	0.95	60.3	4.72	0.61	175.0	4.73	0.18

TABLE 5.15. CONCRETE - INSULATION - CONCRETE TYPE WALL: SUMMARY OF PHYSICAL MEASURES RESULTS FOR ***RRR, RRL, LRL, DRD*** AND ***DDD*** TRIALS.

SU Start-up times (hrs)
A Amplitudes (W/m^2)
MHL Mean heat load (W/m^2)

5.2.1.4. Concrete-insulation-metal wall.

Table 5.16 and 5.12 present a summary of results for the CIM wall. As discussed in Section 5.1.3, grid selection strategy was not investigated in this case. It was expected that the CIM results would show behaviour between that observed for the sandwich panel type wall and the concrete-insulation-concrete wall. Guidance on grid selection could therefore be taken from earlier results. Table 5.16 summarises the start-up times, mean heat loads and amplitudes.

a) Factors affecting the magnitude of heat flux entering the room.

- Start-up times. The criteria for repeatability of the 24 hr cycle of the incoming heat load was set as ±1% for this type of wall. The magnitude of the start-up time was not significantly correlated with change in any specific factor of those tested. However, the unusually high start-up time observed for trial 8 suggests that the magnitude of start-ups might be correlated with an interaction between heat transfer coefficients and the overall resistance and capacity of the wall. The start-up values were of the same order of magnitude that those observed for the CT wall.
- Amplitudes. These were mostly affected by changes in h_1, $\mathbf{R}_{\text{insulation,layer 2}}$ and $\mathbf{C}_{\text{layer 3}}$. For trials 1 and 4 which combined low levels of insulation resistance and metal capacity, the amplitude values were the highest and for trials 2 and 3 - combining high levels of $\mathbf{R}_{\text{insulation, layer 2}}$ and $\mathbf{C}_{\text{layer 3}}$ the lowest values were obtained. The thermal capacity of the metal on the "cold" side of the wall affected the amplitude results, in contrast with the results for the SPT wall. The damping of the heat load entering the room due to the presence of the concrete layer on the "warm" side of the wall led to smaller amplitude values than in the SPT case, thus magnifying the effect of the metal layer to some extent.
- Mean heat loads. Changes in the temperature of the internal environment and the insulation resistance led to significant variation in the average heat load entering the room. Though the mean heat loads were modelled accurately, T_{room} and $\mathbf{R}_{\text{insulation, layer 2}}$ explained about 70% of the variation of the mean heat loads. Unexplained variation was 30% of the total variation in the ANOVA results. An interaction of other variables that did not prove to be significant by themselves (such as h_1 and/or h_2) might explain this uncertainty in the results.

b) Factors affecting the accuracy of the models (Tables 5.12, 5.16 and 5.17).

In general terms, the accuracy found for all models in the prediction of start-ups and amplitudes was low and all models failed to achieve an acceptable relative error for these measures.

- Start-up times. The accuracy of the models for predicting the start-up was highly correlated to h_1, $\mathbf{R}_{\text{insulation, layer 2}}$ and $\mathbf{C}_{\text{layer3}}$. The high errors detected in the start-up analyses might be due to the tight criteria of repeatability between 24 hr cycles (±1%).
- Amplitudes. The factor consistently associated with the accuracy of the amplitudes was the capacity of the metal layer. Those models using a detailed representation for the external layer (***LRC*** and ***LLC*** models) predicted amplitudes closest to those obtained using the FEM model, but the accuracy was poor in general.
- Offsets. Table 5.17 presents the offsets found for the CIM models. No factors were found to affect the offsets in a significant manner. The magnitude of the offsets was similar to that found for the CIC wall. The differences between models indicate that an ***RRC*** model may be a good representation for obtaining accurate offsets results.

TRIAL	*RRC*			*LRC*			*RDC*			*LLC*			**FEM**		
	SU	MHL	A	SU	MHL	A	SU	MHL	A	SU	MHL	A	SU	MHL	A
1	4.0	22.67	18.75	3.00	22.74	13.95	1.75	22.67	18.77	43.00	22.90	13.58	11.25	22.83	8.52
2	6.5	2.74	4.42	96.00	2.74	0.57	7.50	2.74	3.66	253.5	2.63	0.32	6.75	2.27	0.23
3	2.75	8.18	6.87	61.75	8.21	0.83	11.50	8.18	4.82	160.5	8.18	0.8	6.25	7.79	0.26
4	3.75	15.03	24.75	2.00	15.20	16.3	1.25	15.03	24.71	26.25	15.39	14.23	11.50	15.34	11.64
5	40.03	21.43	9.15	34.75	21.52	1.89	6.00	21.43	10.13	65.5	21.60	1.65	15.50	21.56	1.04
6	7.75	2.75	3.5	4.25	2.74	3.11	11.5	2.75	2.63	209.5	2.77	2.81	18.25	2.78	2.17
7	27.00	5.70	2.46	3.25	5.70	2.05	11.00	5.71	1.82	36.75	5.72	0.96	15.50	5.72	1.47
8	55.50	4.72	8.35	55.55	4.79	1.54	1.00	4.72	8.21	36.25	4.79	1.52	79.00	4.71	0.84

TABLE 5.16. CONCRETE - INSULATION - METAL: SUMMARY OF PHYSICAL MEASURES RESULTS FOR ***RRC, LRC, RDC, LLC*** AND FEM TRIALS.

SU Start-up times (hrs)
A Amplitudes (W/m^2)
MHL Mean heat load (W/m^2)

TRIAL	OFFSET (hrs)			
	RRC	*LRC*	*RDC*	*LLC*
1	1.0	13.3	11.5	3.5
2	6.5	18.3	14.3	16.8
3	5.8	15.0	12.8	12.8
4	5.8	11.3	8.5	5.5
5	0.8	15.3	8.5	6.5
6	1.8	8.3	10.5	2.3
7	6.8	6.8	8.5	2.3
8	3.8	9.8	4.3	4.3

TABLE 5.17. CONCRETE - INSULATION - METAL: SUMMARY OF OFFSET RESULTS FOR ***RRC, LRC, RDC*** AND ***LLC*** TRIALS (Note: offsets are meaningful only as a measure of accuracy; the offset for the FEM model is 0).

5.2.2. Statistical measures and tolerance analyses.

Figs. 5.23 and 5.24 illustrate the magnitude of the standard deviations based on the FEM peak and mean heat load for all wall types. As expected, for all models the peak SDs were of lower magnitude than the mean SDs and these measures were highly correlated to the same factors affecting peaks and mean heat loads. For preliminary screening, a maximum deviation from the peaks and means was proposed, so that obviously inaccurate models could be pointed out. The proposed values were deviations of $_{0.25}$ for peak SDs and 0.2 for mean SDs.

Similarly, Figs. 5.25, 5.26 and 5.27 illustrate the energy/time rates, the instantaneous heat load and the peak tolerances obtained for all models.

The band selected for the analyses was a ±10% band around the FEM response. The minimum percentage of data entering the band was set as 80% in order to assess the accuracy of the models.

FIG. 5.23. PEAK STANDARD DEVIATION
ALL MODELS

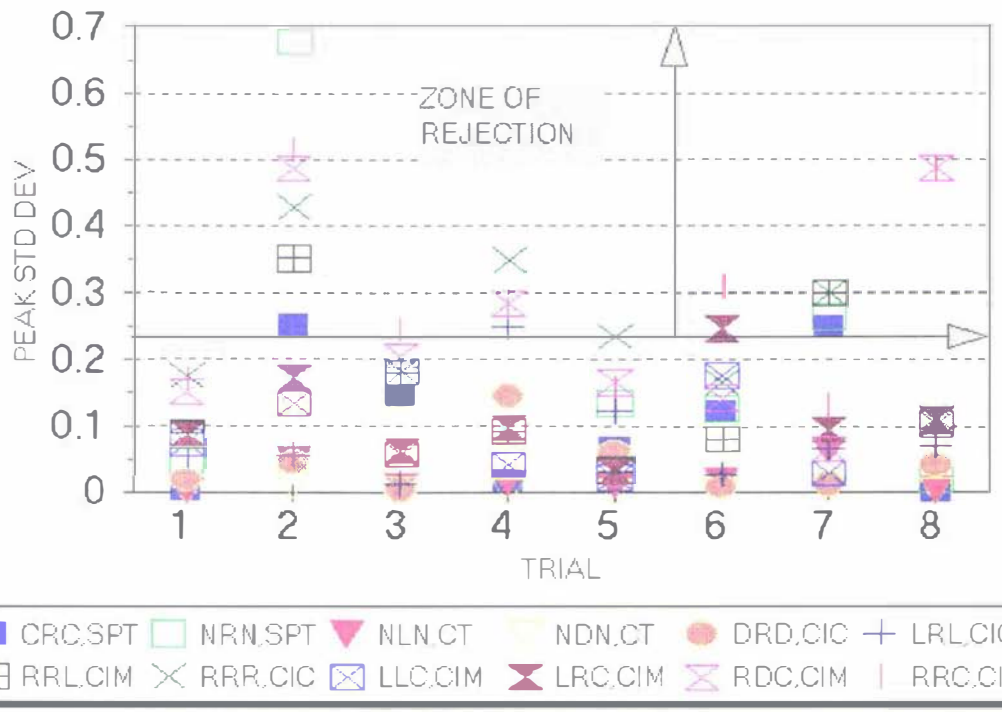

FIG. 5.24. MEAN STANDARD DEVIATION
FOR ALL MODELS

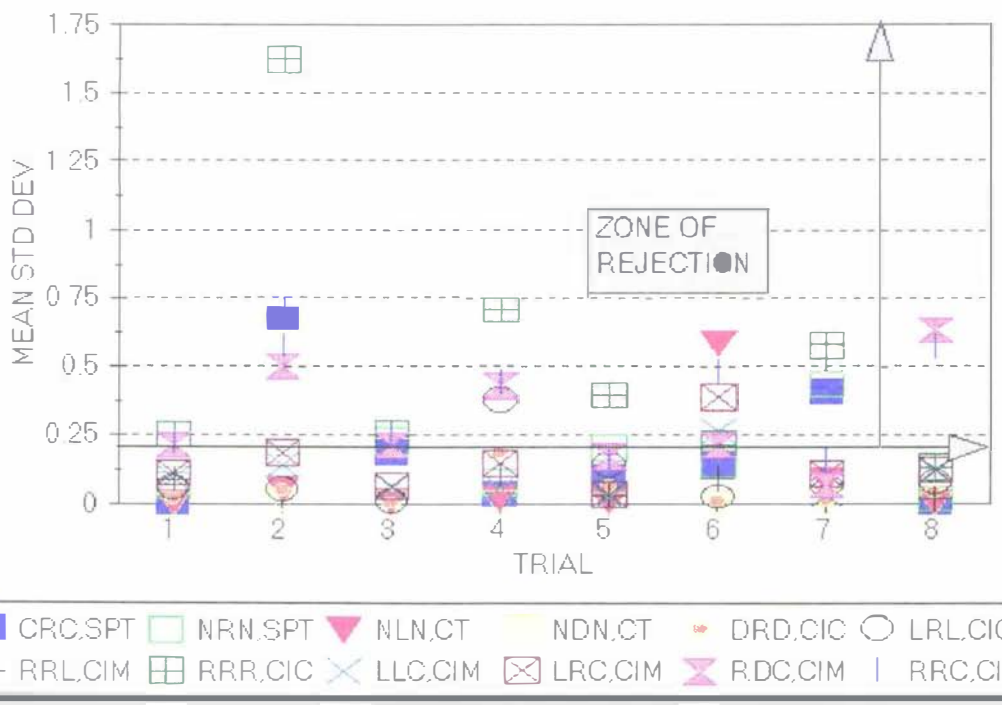

FIG. 5.25 ENERGY/TIME TOLERANCE
CRITERION +10% BAND AROUND FEM

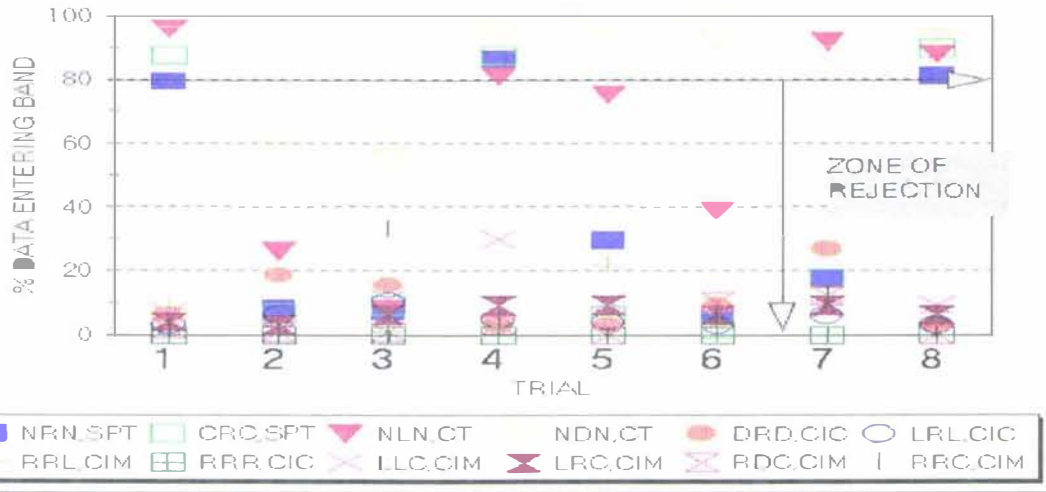

FIG. 5.26. HEAT LOAD TOLERANCES
CRITERION 10% BAND AROUND FEM

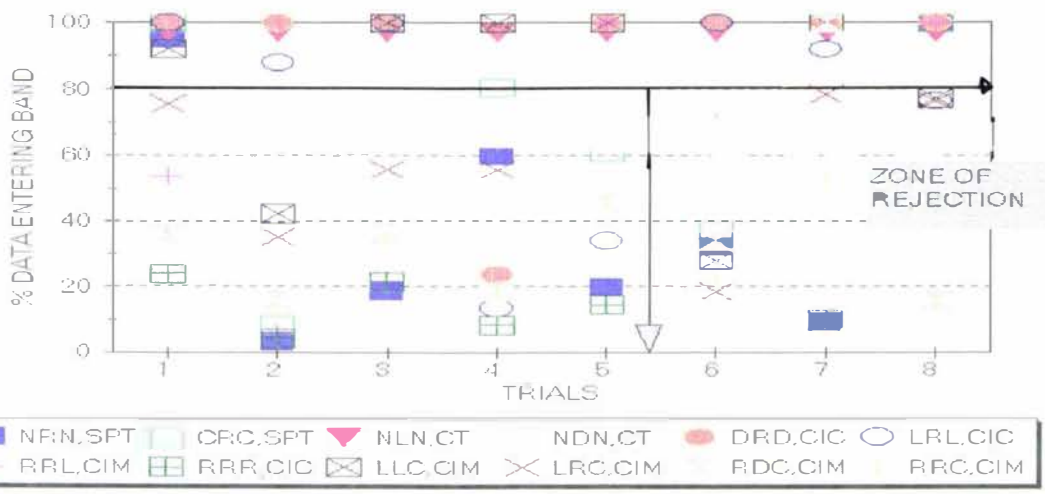

FIG. 5.27 PEAK TOLERANCE
CRITERION 10% BAND AROUND FEM

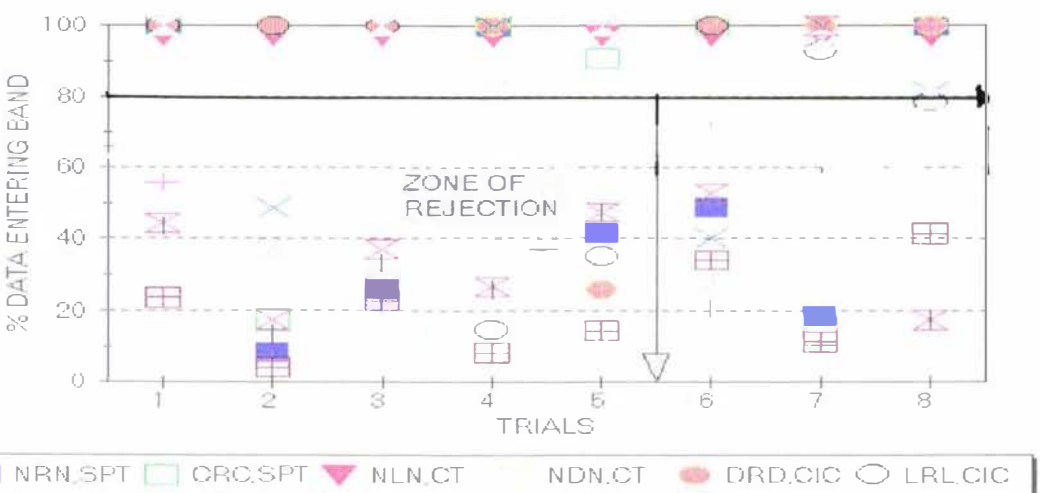

5.2.2.1. Sandwich panel type wall.

- **Peak and mean SDs**: For two trials (2 and 7), both ***NRN*** and ***CRC*** models fell outside the proposed limits for both the peak and mean SDs. In both cases and for both measures, the highest values were observed for those runs conducted at the maximum levels of $\mathbf{R}_{\text{insulation, layer 2}}$ and T_{room}. An ANOVA conducted on the peak and mean SDs showed that changes in these variables account for 73% to 92% of the changes in both SDs for ***CRC*** but they were less influential in the ***NRN*** model, accounting for 47% of the variation. In terms of accuracy, both models reported equivalent results and good accuracy should be expected from both models in scenarios commonly found in coolstores applications (relatively light insulation and high room temperatures), but not for freezers or coldstores, which demand a heavier insulation and lower temperatures. If a linear behaviour of accuracy versus T_{room} is assumed, an acceptable range of use of $\mathbf{R}_{\text{insulation, layer 2}}$ is 2 to 4 m^2 K/W and for T_{room}, 0°C to 10°C could be used. However, these ranges should be further investigated.

- **Tolerance bands**: The ***CRC*** and ***NRN*** models proved to be inaccurate for the same trials pointed out for the SD measures. Again, changes in $\mathbf{R}_{\text{insulation, layer 2}}$ and T_{room} determined the percentage of data falling within the 10% band for the 3 tolerance band types. These measures proved to be more demanding than the SD analyses: In tolerance terms, the use of the ***NRN*** model was slightly more restricted and ***CRC*** should be used instead, possibly within the same ranges mentioned for the peak and mean SDs.

5.2.2.2. Concrete type wall.

- **Peak and mean SDs**: The accuracy of both ***NLN*** and ***NDN*** models was excellent and all trials fell within the limits established for both peak and mean SDs. The results from the ANOVA were consistent with those observed for the SPT wall, with slightly higher SD values for those trials conducted at the maximum levels of $\mathbf{R}_{\text{concrete, layer 2}}$ and T_{room}. Changes in these variables were responsible for 83% to 90% of the SD variations, regardless of the grid selected for the ***L*** and ***D*** regions. Hence, for any concrete wall thickness, room temperature and thermal properties within the boundaries investigated for this wall, good accuracy should be expected from both models.

- **Tolerance bands**: The peak and mean heat load tolerance results for the ***NLN*** model

were significantly different between 4 zone and 8 zone sub-models, but not between 8 zone and 14 zone sub-models. The performance for the 8 zone ***NLN*** model (Figs 5.25 to 5.27) proved to be as accurate as the ***NDN*** model for any grid selection strategy, according to both peak and instantaneous heat load tolerances. However, the results of the energy/time rates tolerances show that only the 9 and 13 node ***NDN*** models are accurate enough to comply with the band selected. Far from suggesting a weakness of the models, these results seem to suggest that the energy/time rates could be a very demanding measure to test the accuracy of models.

5.2.2.3. Concrete-insulation-concrete type wall.

- **Peak and mean SDs**: Whereas most of the results from the physical measures hardly distinguished between models of different levels of complexity for the CIC wall, statistical measures showed a scale that rated the models from the least accurate (most simple) to the most accurate (most complex) scheme. The ***RRR*** model was generally inaccurate for mean SDs and accurate for the peak SDs in half the trials. Both results were highly correlated to T_{room}, which explained 42% and 70% of the variation of mean and peak SDs, respectively. The ***RRL*** model was accurate for most cases except for trials 2 and 7, showing that changes of the SDs were explained in more than 50% of cases by changes in $\mathbf{R}_{\text{insulation, layer 2}}$ and T_{room} alone. Both A and B grids used presented similar results. The ***LRL*** model was accurate except for trial 4, that combined the maximum levels of T_{room}, h_2, $(\mathbf{RC})_{\text{layer 1}}/(\mathbf{RC})_{\text{layer 3}}$ ratio and T_a. Changes in all these variables plus the influence of $\mathbf{R}_{\text{insulation, layer 2}}$ determined more than 70% of the changes in peak and mean SDs. The ***DRD*** model was accurate for both grid selection results and for all trials. The peak and mean SDs variations were largely explained by the same factors affecting the ***LRL*** results, but the percentage contribution of each variable was different.

  Hence, the ***DRD*** model could be safely used in various scenarios. The ***LRL*** and ***RRL*** models should be restricted to the same applications suggested for ***CRC*** and ***NRN*** models in the case of SPT walls, without significant loss of accuracy. The ***RRR*** model would not be a safe choice under most scenarios if peak and mean SD measures are used as the parameter of accuracy.

- **Tolerance bands**: All models failed to meet the 80% of data falling within the ±10% band in the energy/time rates for all trials. In contrast, only the ***RRR*** model failed

completely in achieving these requirements for the instantaneous heat load and peak tolerance bands. A slightly better accuracy was found for the ***RRL*** model, that reached the criteria in two trials (4 and 5 for grid A and 5 and 8 for grid B). The ***LRL*** model was accurate in 5 trials and the ***DRD*** model was accurate in 7 trials (other than trial 4). If these measures are to be used as accuracy criteria, the models that should not be used, even in a restricted manner, are the ***RRR*** and ***RRL*** models. The ***LRL*** and ***DRD*** models could be used across relatively broad ranging circumstances.

5.2.2.4. Concrete-insulation-metal type wall.

- **Peak and mean SDs**: The models applied to the CIM case were difficult to classify in terms of complexity: some models represented layers 1 and 3 using the same model (***LLC*** and ***LRC*** or ***RDC*** and ***RRC***) or layer 2 was represented with approximately the same level of complexity (***LLC*** and ***RDC*** or ***RRC*** and ***LRC***). Hence, the differences between models arose from the conceptual detail for certain layers.

  Similarly to the CIC wall case, the physical measures did not allow a clear classification in terms of accuracy to be established. The statistical analyses, however, showed that the ***LLC*** and ***LRC*** models that represented the external layer in detail were more accurate than the ***RDC*** and ***RRC*** models. Also, the level of detail for representing the insulation (layer 2) highly influenced the degree of accuracy. Overall, the scale of accuracy for the CIM models was (from the most accurate to the less accurate):

  $$\boldsymbol{LLC > LRC > RDC > RRC}$$

  In all these models, the variation of T_{room}, $(\mathbf{RC})_{\text{layer 1}}$ and $\mathbf{R}_{\text{insulation, layer 2}}$ explained the differences found for peak and mean SDs between trials. However, for the models representing layer 1 as an ***R*** region the thermal capacity of the metal (layer 3) became significant, especially for the peak SDs. The ***LLC*** and ***LRC*** models can be used in many situations, but a significant error might appear for heavy insulated walls in temperatures close or below -25 °C. The properties of the concrete layer did not affect the accuracy of the models. The ***RDC*** model could be used for temperatures above 0°C and the ***RRC*** model can be used safely only for walls with light insulation, a thin metal layer, and a light concrete layer in temperatures above 0°C.

- **Tolerance bands**: Similar results to those observed for the CIC wall were found for the CIM wall: none of the models complied with the required level of accuracy for the energy/time rates tolerance band. The instantaneous heat load and peak tolerance analyses showed that the most accurate model was ***LLC***, meeting the accuracy criteria in 5 or 6 trials. The measure that gave most similar results to those observed for the SD measures was the peak tolerance, achieving the same ranking as that obtained in the previous sub-section. If instantaneous heat load tolerances are used, the only accurate model that can be used (other than ***DDD***) is ***LLC***, restricted to walls with light insulation and room temperatures above 0°C

5.2.2.5. Summary.

For the peak SDs:

- the models that totally satisfied the accuracy criteria were ***NLN*** (CT wall), ***NDN*** (CT wall),***LRL*** (CIC wall), ***DRD*** (CIC wall) and ***LLC*** (CIM wall)
- the models that partially satisfied the accuracy criteria, except in 1 or 2 trials, were ***CRC*** (SPT wall), ***NRN*** (SPT wall), ***RRL*** (CIC wall) and ***LRC*** (CIM wall). The reason for failure in these trials was generally a combination of high levels of the parameters affecting the magnitude of the peak heat load.
- the models that failed in 4 of the 8 trials and hence should be restricted to low levels of the critical parameters affecting peak loads magnitudes were ***RRR*** (CIC wall), ***RDC*** (CIM wall) and ***RRC*** (CIM wall).

For the mean SDs:

- the models that totally satisfied the accuracy criteria were ***NDN*** (CT wall), ***DRD*** (CIC wall) and ***LLC*** (CIM wall).
- the models that partially satisfied the accuracy criteria except in 1 or 2 trials were ***CRC*** (SPT wall), ***NRN*** (SPT wall), ***LRL*** (CIC wall), ***LRC*** (CIM wall) and ***RRL*** (CIM wall). The reason for failure in these trials was generally a combination of high levels of the parameters affecting the magnitude of the mean heat load.
- the models that failed in 4 of the 8 trials and hence should be restricted to low levels of the critical parameters affecting mean heat load magnitudes were ***RRR*** (CIC wall), ***RDC*** (CIM wall) and ***RRC*** (CIM wall).

For both SDs:

- the results (accuracies and variables affecting these) were consistent for all grid selection strategies in the relevant models.

For the tolerance measures:

- None of the models succeeded in 100% of cases in meeting the requirements of the energy/time rates tolerances. The ***NDN***, ***NLN***, ***NRN*** and ***CRC*** models partially satisfied this type of tolerance.
- The heat load tolerances showed that only the ***NDN*** model fully complies with the accuracy limits in all trials. However, the ***DRD***, ***NLN***, ***LRL*** and ***LLC*** models proved to be accurate enough in most trials (5 or more).
- The least demanding measure was the peak tolerance. The models ***NLN***, ***NDN***, ***DRD***, ***LRL***, ***CRC***, ***LLC*** and ***LRC*** performed well under the accuracy limit set. The rest of the models can perform well if restricted ranges of the critical variables affecting the accuracy are used.

5.3. Overall model assessment.

The overall assessment of models is discussed in Chapter 7, after the experimental validation of the models. In Chapter 6, the models used to test accuracy (FEM and ***DDD***) were compared against experimental data to test the validity of the initial assumption that these models could be used as a representation of the real behaviour of walls. The conclusions of this part of the project are thus presented in Chapter 7.

CHAPTER 6. WALL STRUCTURES: EXPERIMENTAL VALIDATION.

In Chapter 5, the response predicted using a fully distributed scheme (FEM and ***DDD*** models) was assumed to be equivalent to the real transients of the walls and was thus used as a basis of comparison for assessing the performance of the models derived in Chapter 4. The main goal of the experimental validation was to ensure that this assumption was valid.

The analysis described in Chapter 5 found that the two factors most affecting the thermal response of the walls in terms of the incoming heat load were the thermal resistance and capacity. In the experimental trials different levels of **C** and **R**, accomplished by varying the nature and the thickness of the wall materials, were used.

6.1. Equipment designed for testing the thermal performance of walls.

Figures 6.1 to 6.4 illustrate the experimental system. The equipment consisted of a box constructed of 250 mm thick sandwich panel (Styrolock panel with a core of expanded polystyrene class S, Lanwood Industries, Ltd, Palmerston North), placed inside a small coldstore. A rectangular opening was cut in the top of the box, leaving the inner metallic "skin" of the panel (1 mm thick mild steel) to support the slab-shaped sample of material to be tested. The latter was placed horizontally in the opening with the bottom surface in contact with the metal of the box and the top surface facing the coldstore (low temperature) environment. The sides of the slab were in contact with the insulation of the box. Aluminium foil of negligible thickness was glued to both sides of the panel to minimize radiative effects.

Inside the box, an array of four 100 W light bulbs was used as a heat generator, and a small fan was used to ensure homogeneity in the conditions. The light bulbs were placed out of direct sight of the measurement section and all temperature probes to minimize radiation effects from the bulbs on measured data. A cycle of time-variable air conditions inside the box was achieved by means of a timer which activated automatically at predetermined time intervals, turning on the light bulbs on for 30 minutes and switching them off for 90 minutes. In this manner the environment inside the box varied in a repetitive pattern from 20 °C to 36 °C.

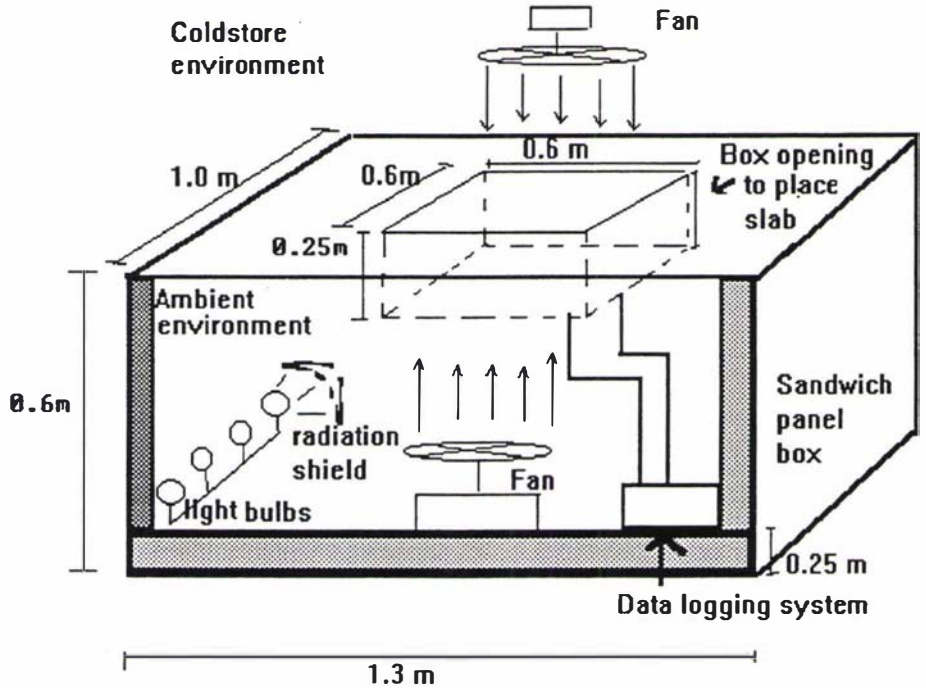

Fig. 6.1. **Schematic diagram of the experimental apparatus used to measure the response of composite slabs to cycling of external conditions.**

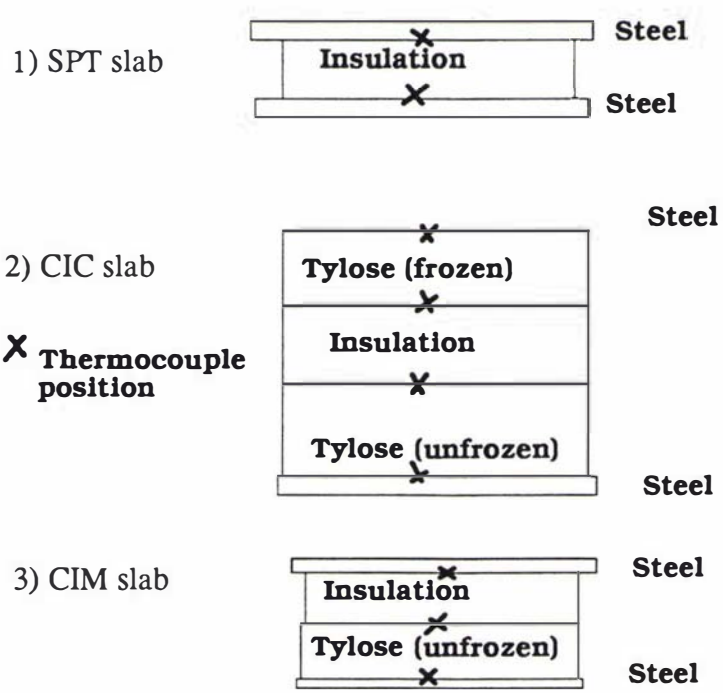

Figure 6.2. Placement of thermocouples in the slabs tested.

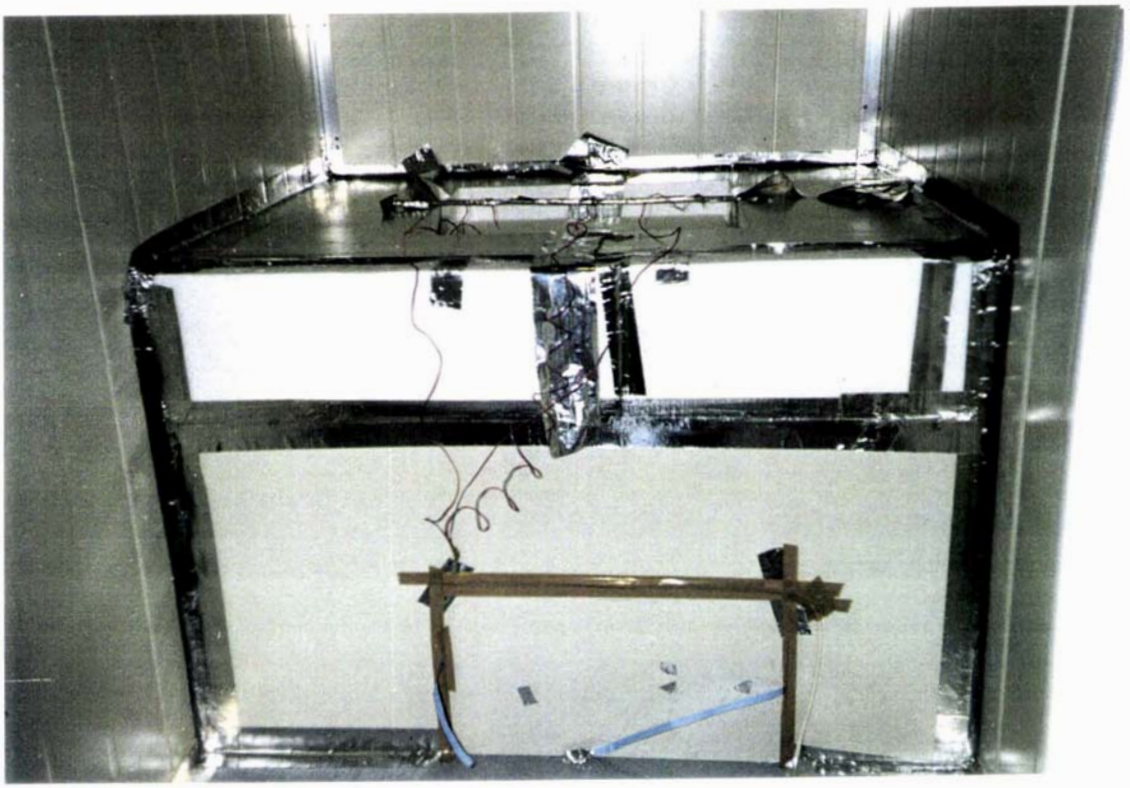

FIG. 6.3. EXPERIMENTAL APPARATUS PLACED INSIDE THE COLDSTORE.

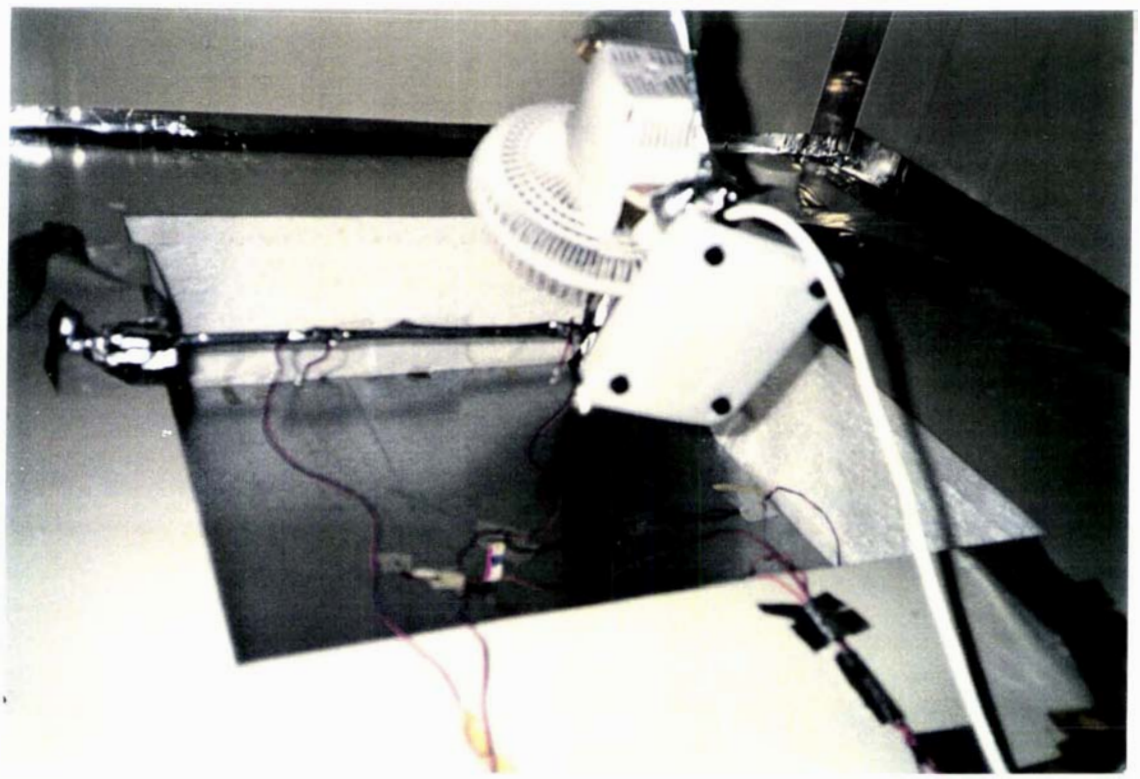

FIG. 6.4. PLACEMENT OF SLAB TESTED IN BOX.

The temperature of the coldstore environment surrounding the box varied by as much as ±2°C during a trial, due to limitations in the coldstore temperature controller and refrigeration plant. To ensure even airflow distribution with respect to the slab position, a second fan was situated facing the surface of the slab on the coldstore side. The environment surrounding the box was typically in the range -5°C to -8°C. Lower temperatures would have been preferred, but the coldstore refrigeration system capacity limited the experiments to this range.

In order to avoid confusion with previous terms describing "external" and "internal" environments, the low temperature environment external to the box will be referred to as the "coldstore environment" and the warmer environment inside the box will be called the "ambient environment".

6.2. Preparation of slabs.

Three slabs were chosen to represent sandwich panel (SPT), concrete-insulation-concrete (CIC) and concrete-insulation-metal type (CIM) walls.

Sandwich panel sections of 0.6 m x 0.6 m were constructed with slabs of rigid cellular polystyrene RC/PS class H with a density of 28 kg/m^3 (Lanwood Industries, LTD, Palmerston North) of the thicknesses specified in Table 6.1. One surface of the slab was lined with a layer of 0.42 mm mild steel. The other side of the slab was placed in contact with the steel of the bottom of the box opening that supported the slabs tested.

The CIC and CIM types ideally required concrete as one of the layers. Concrete was not used in the experimental validation since no accurate thermal data or correlations to determine the thermal properties of any locally available concrete formulation were available. Instead of concrete, Tylose MH1000, a meat analogue, was used. Measured thermal properties of Tylose are broadly similar to those of concrete and have recently been measured and reported (Lovatt, 1992; Lin, 1994 and Chuntranuluck, 1995). The expertise of the Massey University refrigeration research group in handling Tylose was also a significant factor considered in the selection of Tylose instead of concrete for investigating the behaviour of slabs with significant thermal mass. A limitation of Tylose slabs was that the slabs should be used either above 0°C or below -5°C, to ensure that the heat transfer across the Tylose slab was characterised by sensible rather than latent heat effects.

The preparation of the Tylose slabs followed the methodology outlined by Lovatt (1992). The Tylose was shaped using wooden frames to achieve the sizes required for the CIC and CIM trials. The CIC type slabs were constructed using an unfrozen Tylose layer placed at the bottom of the box opening (*i.e.* in contact with the steel of the box), a central insulation layer (rigid cellular polystyrene type H) and a frozen layer of Tylose in contact with the air of the coldstore. The latter was frozen in a coldstore at -10 °C and kept at those conditions until the CIC slab was assembled. The thicknesses of the layers are given in Table 6.2.

A 0.42 mm mild steel plate was used as the metal layer on the coldstore side in the CIM test slabs. The insulation used was also rigid cellular polystyrene type H and the thicknesses were those shown in Table 6.3. To assemble each test slab, each component was successively laid in place in such a manner that air gaps were minimised.

Some disadvantages related to the use of Tylose were noted. The recommended amount of Tylose to be processed at once is 500 g due to difficulties dispersing the Tylose powder into water. However, the heaviest Tylose slab weighted 36.9 kg so the size of the batches was increased to 1 kg. The dispersion problem was partially solved using a 3/4 HP propelled mixer which allowed the time of preparation to be decreased. The time required to process each batch led to a slight drying of the Tylose surface that had already been shaped. Secondly, during test runs, the surface of the frozen slab of Tylose in contact with the coldstore air dried slightly and some flaking of this surface was observed. In later simulations this evaporative effect was ignored; sensitivity analysis results presented in Section 6.6 showed that the system was insensitive to uncertainty in the surface heat transfer at the slab boundary in contact with the coldstore environment. Hence, no specific corrective action was taken to either quantify the evaporative effect or to suppress it experimentally.

6.3. Instrumentation.

Air velocities over the test slabs in both the coldstore and ambient environments were measured by means of a hot wire anemometer (Dantec 54N50 calibrated for the range of 0 to 5 m/s ± 0.02 m/s).

A portable data logger (Grant Squirrel 1210) with copper/copper-constantan differential and type T-thermocouples (with an accuracy of ± 0.3°C) and an electronic ambient temperature compensated reference junction were used to measure the temperatures in the system. The data logger was placed inside the box to keep it at normal room temperatures.

Differential thermocouple circuits were used for direct temperature difference measurement; the junctions were placed in contact with the relevant slab surfaces, one junction above and one below the slab to determine the temperature gradient across the slab directly.

The temperature probes were placed as illustrated in Fig. 6.2:

1) One temperature probe encased in aluminium foil in the ambient environment (inside the box)
2) One temperature probe encased with aluminium foil in the coldstore environment (outside the box)
3) In the case of the SPT slab, the following measurement points were used:
   - metal-insulation boundary (ambient environment side)
   - insulation-metal boundary (coldstore environment side)
4) In the case of the CIC type slab, the following measurement points were used:
   - metal-unfrozen Tylose boundary (ambient environment side)
   - unfrozen Tylose-insulation boundary
   - insulation-frozen Tylose boundary
   - surface of frozen Tylose layer (coldstore environment side)
5) In the case of the CIM type slab, the following measurement points were used:
   - metal-unfrozen Tylose boundary (ambient environment side)
   - unfrozen Tylose-insulation boundary
   - insulation-metal boundary (coldstore environment side)
6) Differential thermocouples were used across insulation layers in all 3 types and also across Tylose slabs in CIC and CIM.

6.4. Experimental methodology.

The slab dimensions and conditions used in the experimental trials are summarised in Tables 6.1 to 6.3. The methodology followed is outlined below:

1) The coldstore was cooled to the working temperature for each trial. This temperature was varied slightly according to the slab tested, in order to obtain the best possible stability and lowest possible value of the coldstore temperature during the trial.

2) Simultaneously, the cyclic heat generation inside the box was activated. A slab of 100 mm insulation was placed in the box opening, to ensure only slow heat exchange

between coldstore and ambient environments. This method avoided condensation on the surfaces of the box, helped to stabilize the coldstore environment and ensured that the thermal mass of the structures inside the box settled into its long term response pattern to the cycling ambient conditions.

3) The initial temperature of the test slabs were held close to the ambient environment conditions, except for the frozen Tylose slab in contact with the coldstore environment used in the CIC type test slabs which was initially held at the coldstore environment temperature. Once the working conditions in the test box were stable, the slab to be tested was loaded into the experimental box opening after the thermocouples were placed in the measurement points (Fig. 6.1) and the data logging system was switched on. These operations were carried out as fast as possible. The ambient temperature cycles were generated and data recorded for long enough to ensure that the temperatures recorded were those of a stable 7200 seconds cyclic operation. In the case of the SPT slabs, the time to achieve a stable operation was typically 8-10 hours (4-5 on-off cycles). For the CIC type slabs, this time was increased to 15-20 hours (8-10 cycles). For the CIM type slabs, about 10-12 hours were required (5-6 cycles).

4) Once the trial was completed, the data logger was recovered and the temperatures were downloaded to a computer for later analysis. The data obtained during the first 2 cycles after start-up were always discarded during the analysis of data to avoid errors due to instabilities during start-up.

6.5. Analysis of heat transfer environment.

6.5.1. Thermal properties and surface heat transfer coefficients.

The thermal properties used to characterise the layers of the slabs tested were obtained as follows:

a) *Tylose thermal properties.* The thermal conductivity and specific heat capacity of Tylose as a function of temperature are presented in Table 6.4. For all simulations presented in Section 6.6, the FEM programme used a linear interpolation of the data points. Lovatt (1992) estimated the error in the thermal properties as less than 2%, but differences in the method of preparation of the Tylose slabs between Lovatt's samples and the samples used in this work might introduce further uncertainty. The

effect of a ±5% deviation in the Tylose thermal properties on the simulated temperature profiles was investigated by means of a sensitivity analysis. This is further explained in Section 6.6.

b) *Insulation thermal properties.* The expanded polystyrene type H supplied by Lanwood Industries was manufactured according to the Australian Standard 1366, Part 3-1982, which states a maximum thermal conductivity λ of 0.034 W/m K. However, this value is dependent on the working temperature range. ASHRAE (1993) suggests that the average λ for expanded polystyrene is 0.032 W/m K for a working range of -18 °C to 24 °C. This value was used. The density of the board was obtained from the Standard (28 kg/m^3) and a specific heat capacity of 1,190 J/kg K (Perry, 1973) was used. The accuracy of these property estimates was unknown. A sensitivity analysis varying the most critical property, λ, by ±5% was carried out.

c) *Steel thermal properties.* Properties of mild steel (ρ = 7,800 kg/m^3, c = 500 J/kg K, λ = 45 W/m K) are listed in a number of reference books (*e.g.* ASHRAE, 1993). In previous simulation runs (Chapter 5), the statistically-based sensitivity analysis showed that the heat load profiles were insensitive to metal layer parameters. Hence, any error in metal thermal properties was unlikely to be important.

d) *Surface heat transfer coefficients.* In the experimental set-up, two heat transfer mechanisms at surfaces were possible: radiation and convection. Radiation shields on the light bulbs, aluminium covers for the temperature probes and aluminium foil glued to the slab surfaces were used to minimise radiation. Thus, convection contributed more significantly to the heat transfer and a Newton's law of cooling model was used. Ideally, the heat transfer coefficient would have been measured in trials independent of the transient wall experiments. In practice, the facilities were not available sufficiently long for such measurements. Alternative procedures were therefore sought. Cleland and Cleland (1992) state that approximations to heat transfer coefficients over large planar surfaces within ±10 - 20% can be obtained using the following correlation:

$$h = 7.3\ v^{0.8} \tag{6.1}$$

where:

v = air velocity (m/s)

h = surface heat transfer coefficient (W/m^2 K)

Using this correlation and measured air velocities, an estimate of 8.5 W/m^2 K was obtained for the coldstore side.

The ambient side was characterised by a much smaller enclosure with more complex air flow patterns. Measurements with the directional anemometer used were likely to underestimate the air velocity, and thus, the heat transfer coefficient derived using Eq. (6.1). The mean measured velocity was 1.5 m/s which led to predictions of 10.1 W/m^2 K. It was considered more likely that the real h for the ambient environment side would be higher rather than lower than this value.

Cross-checking was carried out as follows: Over a stable repeating cycle, the net effect of any thermal capacity is zero. In Chapter 5, the mean heat load in such circumstances was always accurately predicted by an NRN model. Therefore, this model was applied to estimate the heat transfer coefficient on both sides. The governing equation used was:

$$\frac{\lambda_{insulation}}{\Delta x_{insulation}} \Delta T_{insulation} = h \Delta T_{ambient\ air \rightarrow slab} \qquad (6.2)$$

where:

$\lambda_{insulation}$	=	thermal conductivity of insulation (W/m K)
$\Delta x_{insulation}$	=	thickness of insulation (m)
$\Delta T_{insulation}$	=	temperature difference across the insulation slab (°C)
$\Delta T_{ambient\ air \rightarrow slab}$	=	temperature difference between ambient environment and slab surface (°C)

$\Delta T_{insulation}$ and $\Delta T_{ambient\ air \rightarrow slab}$ were the mean measured values over a stable cycle. Values of h calculated through Eq. (6.2) for the SPT trials ranged from 9.3 to 11.3 W/m^2 K for the coldstore side, a little higher than the estimate obtained from Eq. (6.1). A weakness of using Eq. (6.2) is that it relies on measurement of small differences between mean ambient and surface temperature. High accuracy in the measurement of the temperatures would be required to give accurate estimates of h by this method. Considering that the accuracy of the measurement system was ± 0.3°C, significant errors were thus unavoidable. Hence, on balance, the value of 8.5 W/m^2 was considered the best estimate. Sensitivity analysis confirmed that variations in this heat transfer coefficient of ±20% did not affect the temperature profiles significantly.

On the ambient environment side, attempts to use Eq. (6.2) gave unreliable results due to the wide-ranging, cycling profile of the surface temperature, with differences of 10 °C or more between peak and minimum temperature. The limitation on the measurement accuracy mentioned above was the problem. However, it was noted that in the SPT trials, a stable lag between the ambient air temperature and the metal/insulation boundary developed during the cycle. The time between peak and minimum temperatures was about 5800 seconds in all SPT trials and the final 2000 seconds of this period was characterised by an almost constant temperature difference between the ambient air and the boundary metal layer. An approximate energy balance was applied to this part of the temperature profile:

$$h \, \Delta T_{ambient\ air-slab} = \frac{\lambda_{insulation}}{\Delta x_{insulation}} \Delta T_{insulation} + \Delta x_{metal} \, \rho_{metal} \, c_{metal} \frac{dT_{metal}}{dt} \qquad (6.3)$$

where:

Δx_{metal} = Thickness of metal sheet (m)

ρ_{metal} = Density of metal (kg/m^3)

c_{metal} = Specific heat of metal (J/kg K)

T_{metal} = Temperature of the metal layer (°C)

The term $\frac{dT_{metal}}{dt}$ was determined from the slope of the temperature-time plot in the stable 2000 second period. The temperature differences between ambient and slab surface and between both surfaces of the insulation were taken at the same time and Δx was directly measured. The estimates of h for the 4 runs were of 17, 17, 10 and 20 W/m^2 K for trial 4. These results suggested that the true h on the ambient environment side may have been as high as the mean of these values (16 W/m^2 K), rather than the 10 W/m^2 K estimated by Eq. (6.1). A sensitivity analysis was carried out testing h values of 10, 15 and 18 W/m^2 K. The latter value was selected as 3 of 4 SPT trials yielded estimates averaging this value. The value of 15 W/m K was selected rather than 16 W/m K to ensure that the values tested were reasonably distributed in the range stated; 15 W/m^2 K still closely represents the mean of all 4 h estimates via Eq.(6.3).

Cross-checking using the method outlined before were not applicable to the CIC and CIM type walls, since the effect of the thermal mass was significantly higher than in the SPT trials and no stable temperature differences were observed during the

cycles. Considering that the heat transfer coefficient models behaviour outside surfaces only, the values found for the SPT trials should also apply.

TABLE 6.1. SUMMARY OF EXPERIMENTAL TRIALS FOR THE SANDWICH PANEL TYPE SLAB.

Composite slab[3]	Trial	Thickness (m)			Ambient environment conditions		Coldstore environment conditions		Thermal properties	
		Layer								
		1	2	3	Avg $T_{a,max}$ and $T_{a,min}$ (°C)	h_1 (W/m^2 K) [1]	T_{room} avg (°C)	h_2 (W/m^2 K)	λ (W/m K)	C (kJ/m^3 K)
Layer 1: Steel Layer 2: Expanded polystyrene Layer 3: Steel	1	0.001	0.06	0.00042	$T_{a,max}$ 32 $T_{a,min}$ 22	15	-6.4	8.5	Layer 1: 45 Layer 2: 0.032[2] Layer 3: 45	Layer 1: 3,900 Layer 2: 33.3 Layer 3: 3,900
	2	0.001	0.12	0.00042	$T_{a,max}$ 32 $T_{a,min}$ 22	15	-6.4	8.5		
	3	0.001	0.18	0.00042	$T_{a,max}$ 38 $T_{a,min}$ 27	15	-6.5	8.5		
	4	0.001	0.24	0.00042	$T_{a,max}$ 36 $T_{a,min}$ 26	15	-6.5	8.5		

[1] Values selected from sensitivity analysis (Section 6.6).

[2] Factor tested in sensitivity analysis (Section 6.6).

[3] Layers are numbered sequentially according to their position respect to the ambient temperature environment. Layer 1 is the metallic skin of the box in contact with the ambient temperature environment. Layers 3 and 4 are nearest the low temperature environment.

TABLE 6.2. SUMMARY OF EXPERIMENTAL TRIALS FOR THE TYLOSE-INSULATION-TYLOSE SLAB.

Composite slab[3]	Trial	Thickness (m)[2]				Ambient environment conditions		Coldstore environment conditions		Thermal properties	
		Layer									
		1	2	3	4	Avg $T_{a,max}$ and $T_{a,min}$ (°C)	h_1 (W/m^2 K)[1]	T_{room} avg (°C)	h_2 (W/m^2 K)	λ (W/m K)	C (kJ/m^3 K)
Layer 1: Steel Layer 2:Tylose (unfrozen) Layer 3: Expanded polystyrene Layer 4: Tylose (frozen)	1	0.001	0.05	0.06	0.14	$T_{a,max}$ 34 $T_{a,min}$ 24	10	-7.5	8.5	Layer 1: 45 Layer 2[2]: Table 6.4a Layer 3: 0.032 Layer 4[2]: Table 6.4a	Layer 1: 3,900 Layer 2[2]: Table 6.4b Layer 3: 33.3 Layer 4[2]: Table 6.4b
	2	0.001	0.05	0.12	0.14	$T_{a,max}$ 36 $T_{a,min}$ 26	10	-8.0	8.5		
	3	0.001	0.07	0.12	0.14	$T_{a,max}$ 32 $T_{a,min}$ 22	10	-8.5	8.5		

[1] Values selected from sensitivity analysis (Section 6.6).

[2] Factor tested in sensitivity analysis (Section 6.6).

[3] Layers are numbered sequentially according to their position respect to the ambient temperature environment. Layer 1 is the metallic skin of the box in contact with the ambient temperature environment. Layers 3 and 4 are nearest the low temperature environment.

TABLE 6.3. SUMMARY OF EXPERIMENTAL TRIALS FOR THE TYLOSE-INSULATION-METAL SLAB.

Composite slab[3]	Trial	Thickness (m)[2]				Ambient environment conditions		Coldstore environment conditions		Thermal properties	
		Layer									
		1	2	3	4	Avg $T_{a,max}$ and $T_{a,min}$ (°C)	h_1 (W/m^2 K)[1]	T_{room} avg (°C)	h_2 (W/m^2 K)	λ (W/m K)	C (kJ/m^3 K)
Layer 1: Steel Layer 2: Tylose (unfrozen) Layer 3: Expanded polystyrene Layer 4: Steel	1	0.001	0.05	0.12	0.00042	$T_{a,max}$ 29 $T_{a,min}$ 23	10	-6.1	8.5	Layer 1: 45 Layer 2[2]: Table 6.4a Layer 3: 0.032 Layer 4: 45	Layer 1: 3,900 Layer 2[2]: Table 6.4b Layer 3: 33.3 Layer 4: 3,900
	2	0.001	0.1	0.12	0.00042	$T_{a,max}$ 35 $T_{a,min}$ 24	10	-6.6	8.5		
	3	0.001	0.05	0.18	0.00042	$T_{a,max}$ 35 $T_{a,min}$ 25	10	-6.6	8.5		

[1] Values selected from sensitivity analysis (Section 6.6).

[2] Factor tested in sensitivity analysis (Section 6.6).

[3] Layers are numbered sequentially according to their position respect to the ambient temperature environment. Layer 1 is the metallic skin of the box in contact with the ambient temperature environment. Layers 3 and 4 are nearest the low temperature environment.

TABLE 6.4. THERMAL PROPERTIES OF TYLOSE MH1000, (LOVATT, 1992; PHAM *et al.*, 1994). A) THERMAL CONDUCTIVITY

Temperature (°C)	Thermal conductivity λ, W/m K
-39.40	1.573
-38.40	1.597
-29.60	1.532
-19.70	1.437
-12.80	1.404
-8.90	1.381
-7.00	1.385
-4.40	1.296
-1.20	1.200
-0.90	0.481
3.20	0.481
14.90	0.479
27.70	0.511
37.60	0.530

B) SPECIFIC HEAT CAPACITY

Temperature (T, °C)	Specific heat capacity c, kJ/kg K
-38.93	1.890
-35.86	1.910
-28.09	2.130
-20.62	2.38
-13.56	3.36
-7.83	6.25
-4.04	13.56
-2.02	31.77
-1.09	52.88
-1.08	515.73
-0.90	515.73
-0.89	3.99
40.71	4.04

6.5.2. Characteristics of the experimental system in relation to the modelled heat transfer environment.

A number of aspects within the experimental system did not exactly match the simulated system of Chapter 5. These aspects were:

a) *Extra-layers in the experimental slab.* The metallic layer on which the test slab rested represented an extra-layer for all CIC and CIM trials. Also in these cases, a thin layered liner consisting of an aluminium foil sheet between two plastic layers was placed between the metal and the unfrozen Tylose slab to aid during the removal of the slabs at the end of the trial. Whereas both the thermal resistance and capacity of this layer were assumed negligible, the dynamics of the steel layer were considered important and thus modelled as part of the slab in FEM simulations. It was assumed that any air trapped within the layers would be expelled due to the weight of the slab and the flexible nature of the Tylose. Nevertheless, real contact may not have been perfect.

b) *Non-repeating cyclic pattern.* In some experimental trials (those presenting a significant thermal mass such as the CIC and CIM cases) a net cooling or heating of the slabs rather than perfect cycle replication occurred. In these cases, the correct statement of the initial temperatures was important to obtain a valid assessment of model performance. A linear temperature profile between both surface temperatures in the insulation layers and unfrozen Tylose layers proved to be adequate for SPT trails. For the frozen Tylose layer in the CIC case, a non-linear profile was found to be more adequate. The temperature of the outside half of the nodes were set nearly equal to the measured frozen Tylose/coldstore environment boundary temperature, whereas the inside half of the nodes were set to represent a linear profile from the measured temperature of the insulation/frozen Tylose boundary to the frozen Tylose/coldstore environment boundary temperature.

c) *Variable temperature in the coldstore environment.* Limitations in the control system of the refrigeration plant led to a coldstore temperature variation of up to ±2°C. The transients of the air temperature were modelled as accurately as possible during the simulation of the experimental trials to allow a fair comparison of the temperature profiles. However, limitations in the input data structure of the FEM programme made it impossible to exactly match the full experimental profile.

d) *Edge effects.* The design of the box limited the total heat transfer area (the area of the two flat surfaces of the slab) to 0.72 m^2 in all cases. Table 6.5 presents the ratios of the area to the slab side wall area for all the trials.

For heat transfer experiments in related but different circumstances, Cleland *et al.* (1994) suggested that the ratio of exposed slab surface area to insulated surface should be as high as possible and no less than 2 if the experiment is to closely approximate one-dimensional heat transfer. This limit was achieved in only 3 trials. Therefore, heat transfer in more than one pathway was possibly significant. To test this possibility, two thermocouples were placed in different positions in the "cold" surface of the slab of the SPT trials, one near the centre of the surface and one about 2 cm from the edge of the slab (close to the join between the test slab and the box). A statistical analysis showed no significant differences (at the 95% level) between the temperature measurements of the two positions. Hence, no evidence of significant edge heat transfer was found.

TABLE 6.5. RATIOS OF EXPOSED SURFACE AREA TO INSULATED SURFACE FOR ALL THE SLABS TESTED.

Test slab	Trial	Total thickness (m)	Area in contact with insulation (m^2)	Ratio exposed/insulated surface
SPT	1	0.0614	0.147	4.88
	2	0.1214	0.291	2.47
	3	0.1814	0.754	1.65
	4	0.2415	0.579	1.24
CIC	1	0.2510	0.602	1.19
	2	0.3510	0.842	0.86
	3	0.3710	0.890	0.81
CIM	1	0.1915	0.459	1.56
	2	0.1115	0.267	2.69
	3	0.1715	0.411	1.75

6.6. Experimental results and sensitivity analysis.

The heat load entering the coldstore environment was used as a response variable in Chapter 5. However, the experimental parameters used to compare experimental and simulated trials were the temperatures at test slab surfaces. This change was required due to the difficulty in measuring heat loads directly. Hence, the results of the sensitivity analysis are given in terms of the boundary temperatures at the ambient and coldstore environment sides.

The section of the experimental trials displaying the most stable cyclic pattern was chosen for the simulation. In all simulations, the initial boundary temperature conditions used were those measured at the start of this stable period. Simulations were continued for between 7000 and 11500 seconds only (*i.e*, more than 1 cycle of 7200 seconds), depending on the number of data points required to accurately match the measured coldstore environment temperature profile. To reduce the influence of the initial conditions in the comparison of the results, the last 7200 seconds were always chosen as the complete cycle to be analyzed. Figures 6.5 to 6.24 show experimental and simulated temperature profiles for this cycle.

6.6.1. Sensitivity analysis in the SPT trials.

Figure 6.5 shows the sensitivity analysis carried out for the SPT trial 2 to test the effect of variation in the h values at the ambient environment boundary . The temperature profiles for this boundary were not highly influenced by h and a difference of the order of ±0.5°C was observed between the peak temperatures obtained for 10 and 18 W/m^2 K. An h of 15 W/m^2 K generated the closest temperature profile to the experimental results. This value is compatible with the calculations based on Eq. (6.3), suggesting that the true h was probably close to this estimate. Furthermore, the small difference found between temperature profiles generated using low and high h values indicates that the uncertainty in this factor was not highly influential. For the coldstore environment boundary, the effect of a variation in h of ±20% proved to be even less significant than for the ambient environment side. This was expected from the results obtained in Chapter 5.

Figure 6.6 presents the results of the sensitivity analysis carried out for the thermal conductivity of the insulation. Values representing +5% (0.0336 W/m K) and -5% (0.0304 W/m K) were investigated. The first value is close to the stated maximum of 0.034 W/m K in the Australian Standard (1982) and the second is the minimum value suggested by

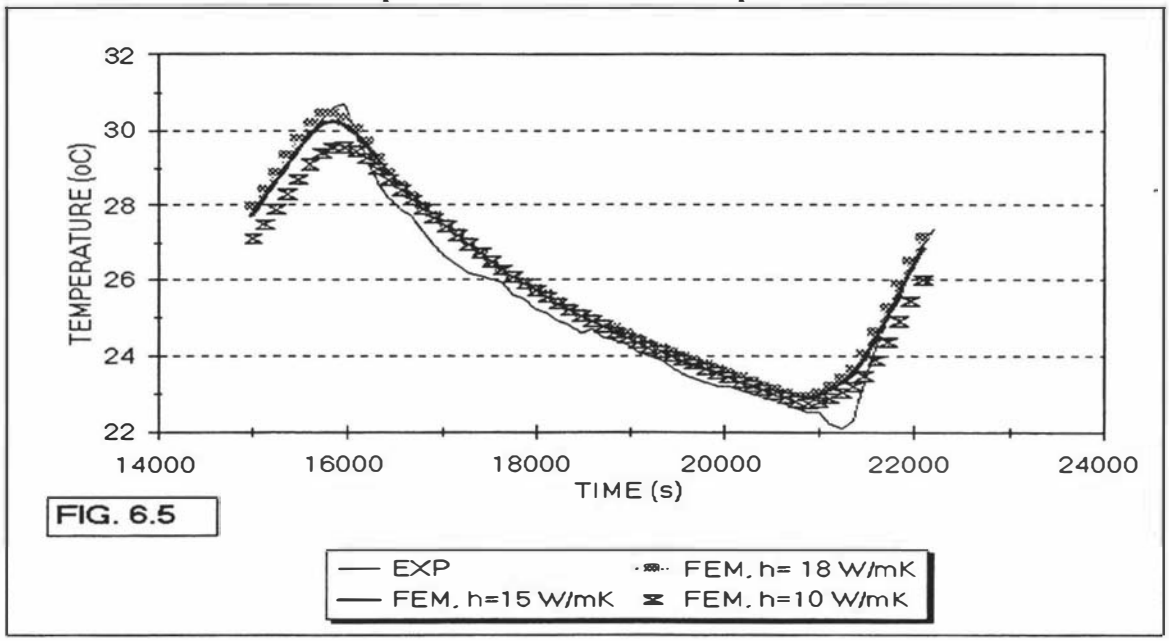

Fig. 6.5. SPT slab, trial 2. Sensitivity analysis on the $h_{\text{ambient environment-to-slab}}$ value. FEM grid: 1 element for each metal layer plus 12 elements for the insulation layer. The rest of the conditions used in the simulations are given in Table 6.1.

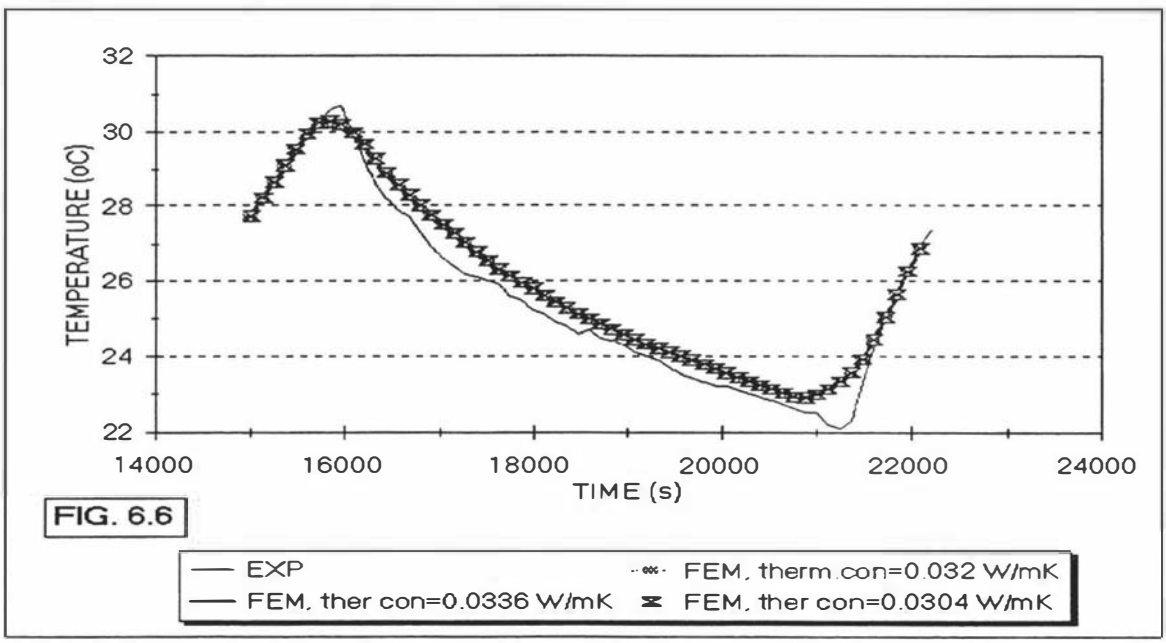

Fig. 6.6. SPT slab, trial 2. Sensitivity analysis on the value of the thermal conductivity (λ, W/m K) of the insulation. FEM grid: 1 element for each metal layer plus 12 elements for the insulation layer. The rest of the conditions used in the simulations are given in Table 6.1.

ASHRAE (1993) for this type of insulation at the experimental temperature working range. The temperature profiles generated showed an absolute difference close to 0°C, thus indicating that the SPT slab predictions were insensitive to uncertainty in this parameter.

6.6.2. Sensitivity analysis in the CIC trials.

Figure 6.7 presents the sensitivity analysis carried out on h at the ambient environment boundary for CIC trial 1. In this case, the effect of initial conditions was more noticeable. This trial was characterised by net heating throughout as the initial conditions was not equal to the mean temperature over one repeating cycle. Thus, the simulations and experimental data show a small net rise in temperature. Both rate of net rise and cycle amplitude are important and inter-twined and a simple comparison like that used for the SPT trials was not possible. The net rise appeared to be the more sensitive parameter: An h value of 10 W/m^2 K most closely matched the experimental net rise; in a second cycle, higher h values would predict temperatures rising more quickly towards stable cycling than the lower h. An h of 18 W/m K substantially over-predicted the rate of net rise. Hence, the third h value presented was between 10 and 15 W/m^2 K.

The experimental temperature profile was more damped than any of the predicted temperature profiles. Whereas an h of 15 W/m K gave the closest fit in terms of rate of temperature change with time during the cooling, the best fit during the heating was observed for a value of 10 W/m K and the latter better predicted the net rise. It was concluded that the lack of fit observed was not explainable solely by uncertainty in h. For CIC and CIM trials, an h at the ambient environment side of 10 W/m K was selected in further studies on the basis that it was important to accurately simulate the experimental temperature net rise so comparisons of cycle amplitudes were most easily made.

Figure 6.8 shows the results for the sensitivity analysis carried out to test the effect of uncertainty in thermal properties. Changes of ±5% on the thermal diffusivity ($\alpha=\lambda/\rho c$, m^2/s) were used. The effect of uncertainty in α led to an error of no more than ±0.25°C; thus this factor was unlikely to be important.

Figure 6.9 shows the effect of a +10% variation in the thickness of the Tylose slab. since it was possible that the unfrozen Tylose slab could distort in place as the material flows slightly when unfrozen. The difference with the original FEM temperature profile was only 0.01°C. It was concluded that uncertainty in this parameter was not significant.

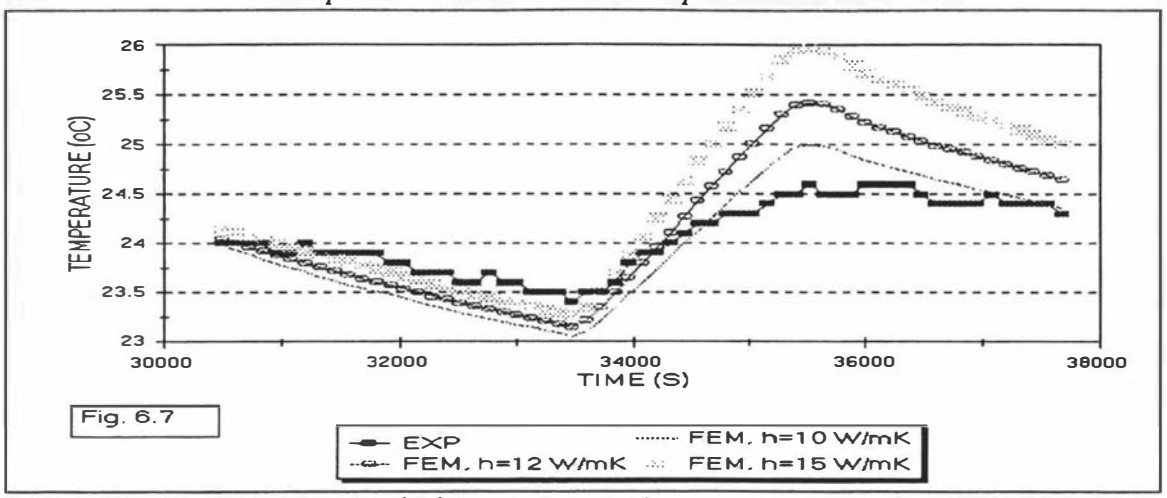

Fig. 6.7. CIC type slab, trial 1. Sensitivity analysis on the $h_{\text{ambient environment-to-slab}}$ value. FEM grid: 1 element for metal layer plus 10 elements for the unfrozen Tylose, insulation and frozen Tylose layers, respectively. The rest of the conditions used in the simulations are given in Table 6.2.

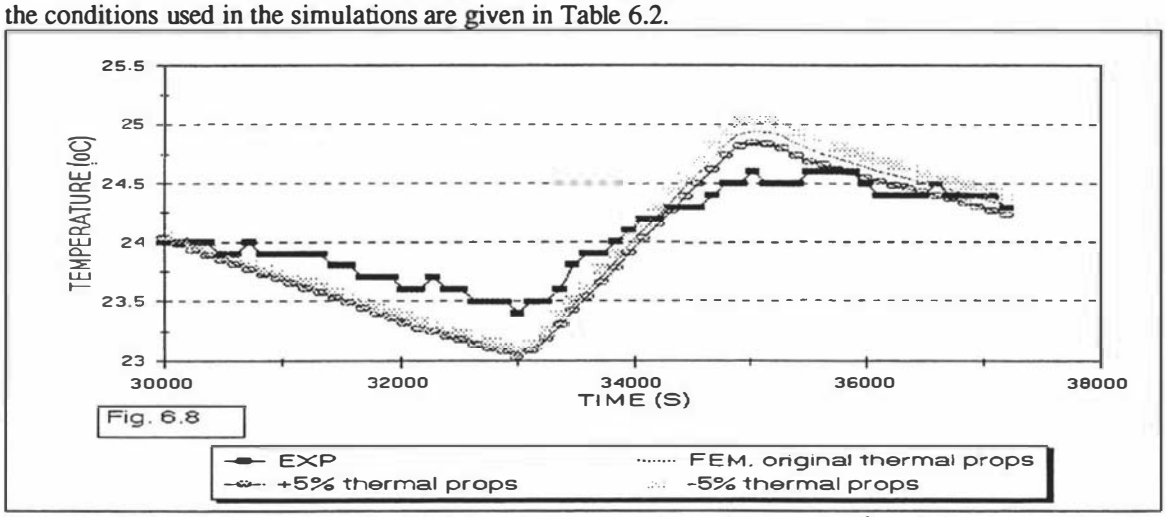

Fig. 6.8. CIC type slab, trial 1. Sensitivity analysis on the thermal properties (λ and c) values. FEM grid: 1 element for metal layer plus 10 elements for the unfrozen Tylose, insulation and frozen Tylose layers, respectively. The rest of the conditions used in the simulations are given in Table 6.2.

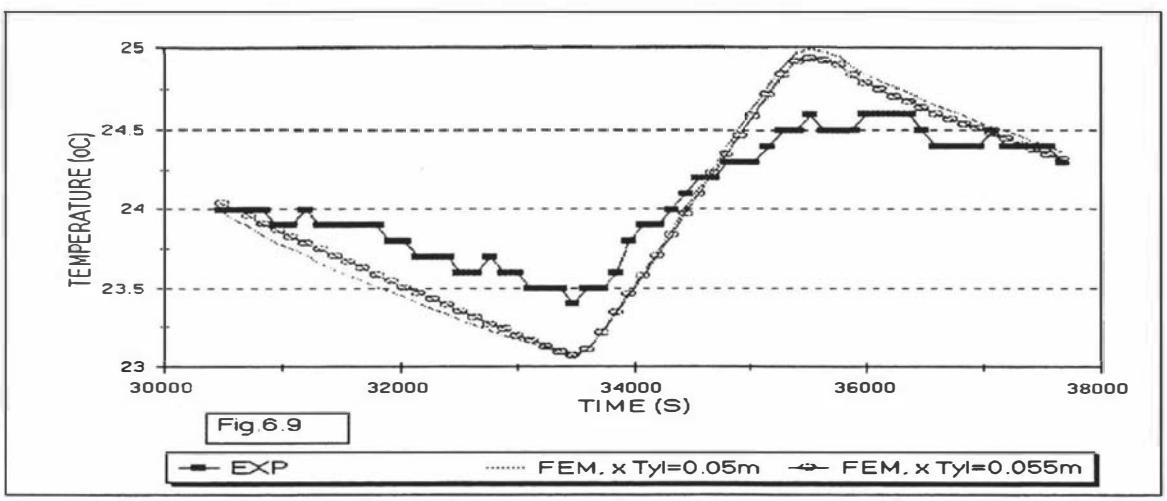

Fig. 6.9. CIC type slab, trial 1. Sensitivity analysis on the thickness (x) of the unfrozen Tylose layer. FEM grid: 1 element for metal layer plus 10 elements for the unfrozen Tylose, insulation and frozen Tylose layers, respectively. The rest of the conditions used in the simulations are given in Table 6.2.

Figure 6.10 shows the sensitivity analysis for the h value for the ambient environment boundary for CIM trial 1. This analysis was carried out in a similar manner to the CIC analysis. The temperature profiles obtained show that CIM trials were less affected than the CIC trials by a change in h. The lack of agreement between experimental and simulated trials could not be explained by likely uncertainty in h.

Figure 6.11 presents the effect of a change in ±5% in the thermal properties. Similarly to the behaviour of the CIC slabs, the predicted CIM temperature profile was only slightly affected.

A sensitivity analysis on the effect of the change of thickness was not conducted for CIM trials as the CIC type slab had shown lack of sensitivity to this parameter.

6.6.4. Comparison of experimental trials with FEM and DDD simulations.

6.6.4.1. SPT results.

Figures 6.12 to 6.15 show the comparison between the FEM and experimental profiles for all the SPT trials, using an h of 15 W/m^2 K on the ambient environment side. In the 4 trials the agreement was generally good for both boundary temperatures. Some disagreement was observed for the minimum temperature reached in the cycle of the ambient environment side. This disagreement was less than ±0.5°C in all cases. For the coldstore environment boundary, the pattern of the coldstore boundary temperatures in both experimental and simulated trials closely followed the oscillations of the coldstore air temperature, although the simulated temperature profile was more damped than the experimental. The FEM predictions generally fell within the band formed by the experimental temperatures measured with two thermocouples at different positions in the slab surface.

Overall, considering the quality of instrumentation, the difficulties in eliminating undesirable heat transfer effects (e.g. edge heat transfer) and possible uncertainties in data such as h values and initial conditions, the agreement between FEM and experiment was considered sufficiently good to validate the assumption made in Chapter 5 that the FEM method and grids selected would represent real SPT wall behaviour.

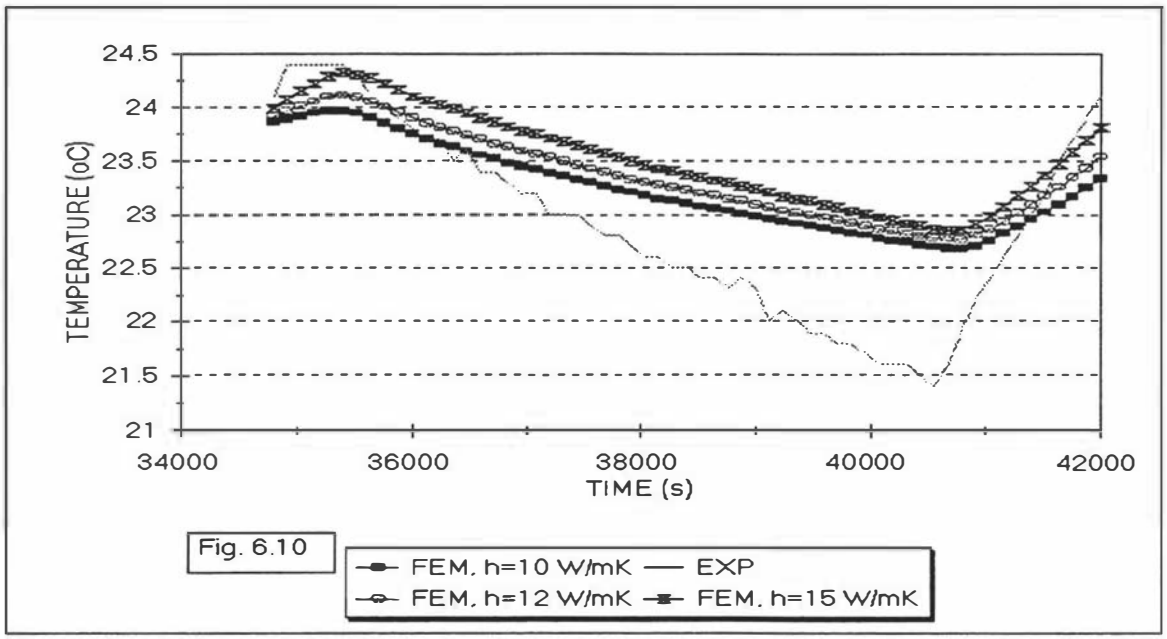

Fig. 6.10. CIM type slab, trial 1. Sensitivity analysis on the $h_{\text{ambient environment-to-slab}}$ value. FEM grid: 1 element for each metal layer plus 10 elements for the unfrozen Tylose and insulation layers, respectively. The rest of the conditions used in the simulations are given in Table 6.3.

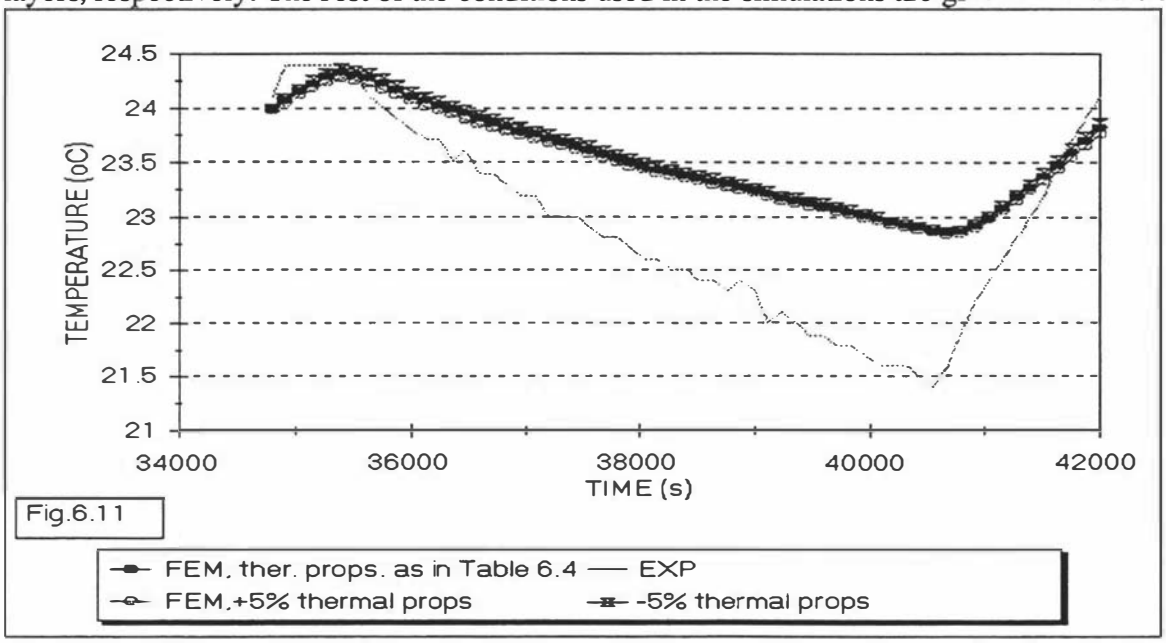

Fig. 6.11. CIM type slab, trial 1. Sensitivity analysis on the thermal properties (λ and c) values. FEM grid: 1 element for metal layer plus 10 elements for the unfrozen Tylose and insulation layers, respectively. The rest of the conditions used in the simulations are given in Table 6.3.

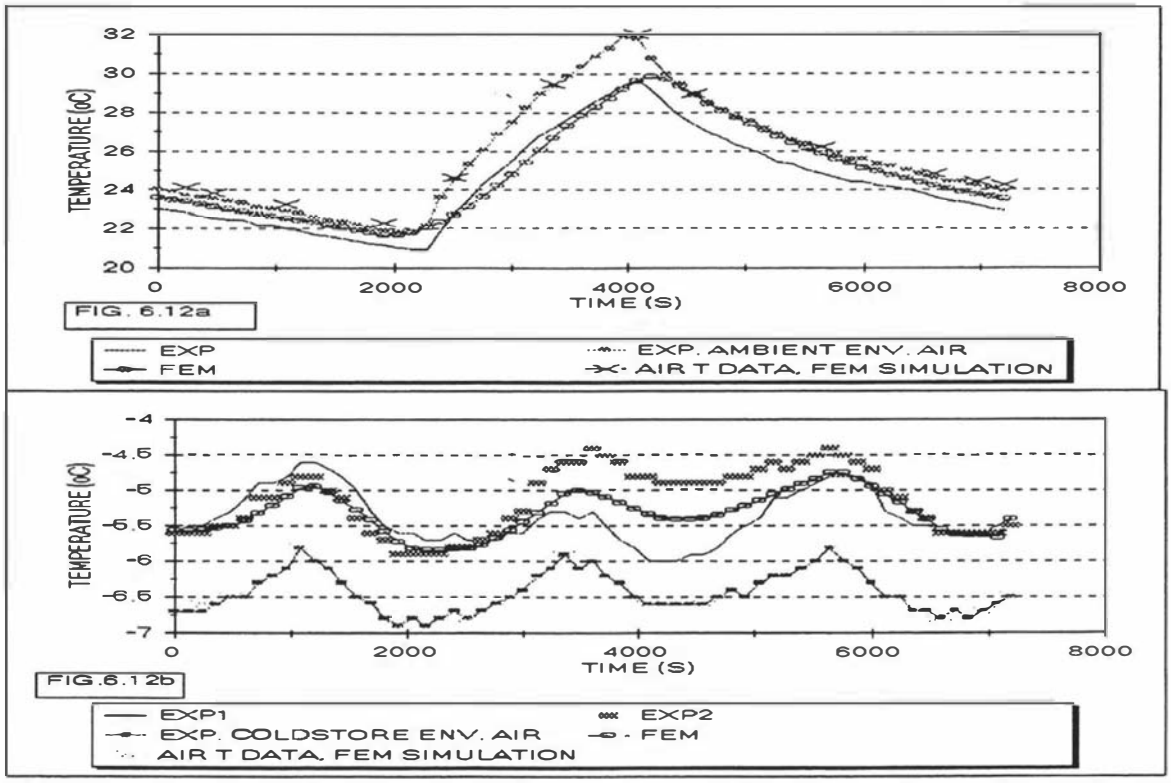

Fig.6.12. Trial 1, SPT slab: Comparison of experimental and FEM temperature profiles at **a)** metal-insulation boundary (ambient environment side) and **b)** insulation-metal boundary (coldstore environment side). FEM grid: 1 element in each metal layer and 20 linear elements in the insulation layer.

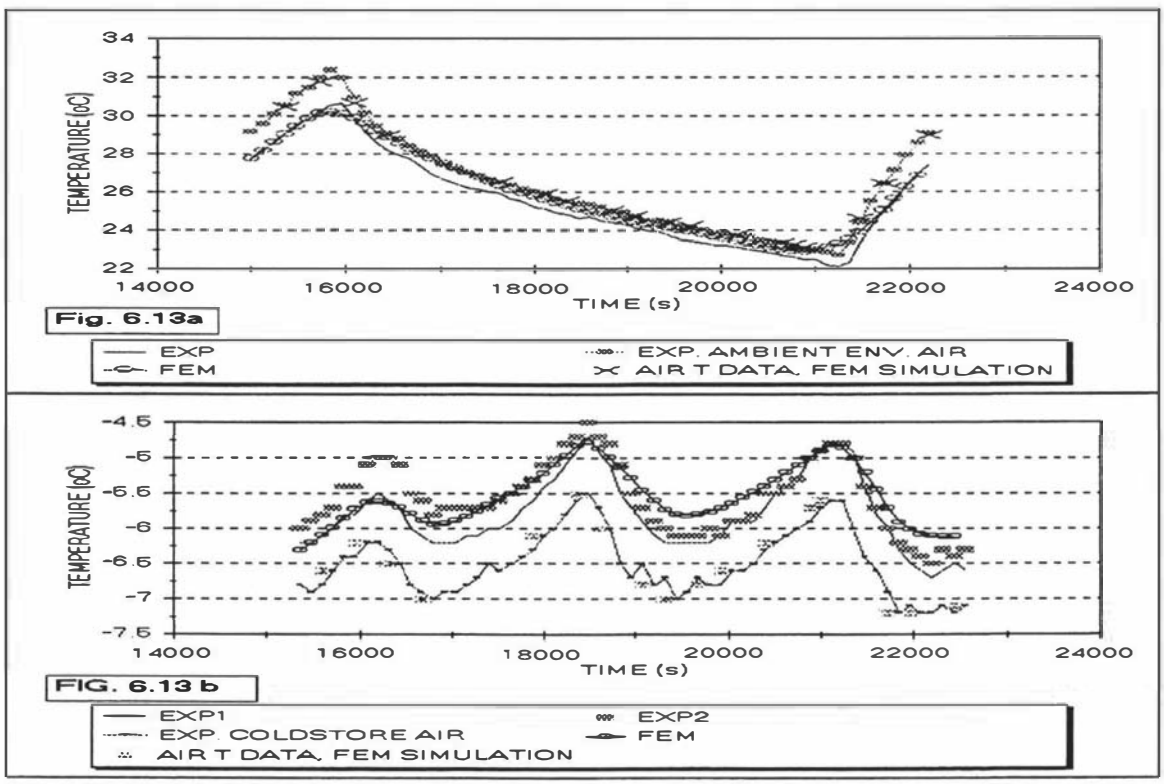

Fig. 6.13: Trial 2, SPT slab: Comparison of experimental and FEM temperature profiles at **a)** metal-insulation boundary (ambient environment side) and **b)** insulation-metal boundary (coldstore environment side). FEM grid: 1 element in each metal layer and 12 linear elements in the insulation layer. Note that $h_{ambient\ environment\text{-}to\text{-}slab}$ = 15 W/m K in both trials.

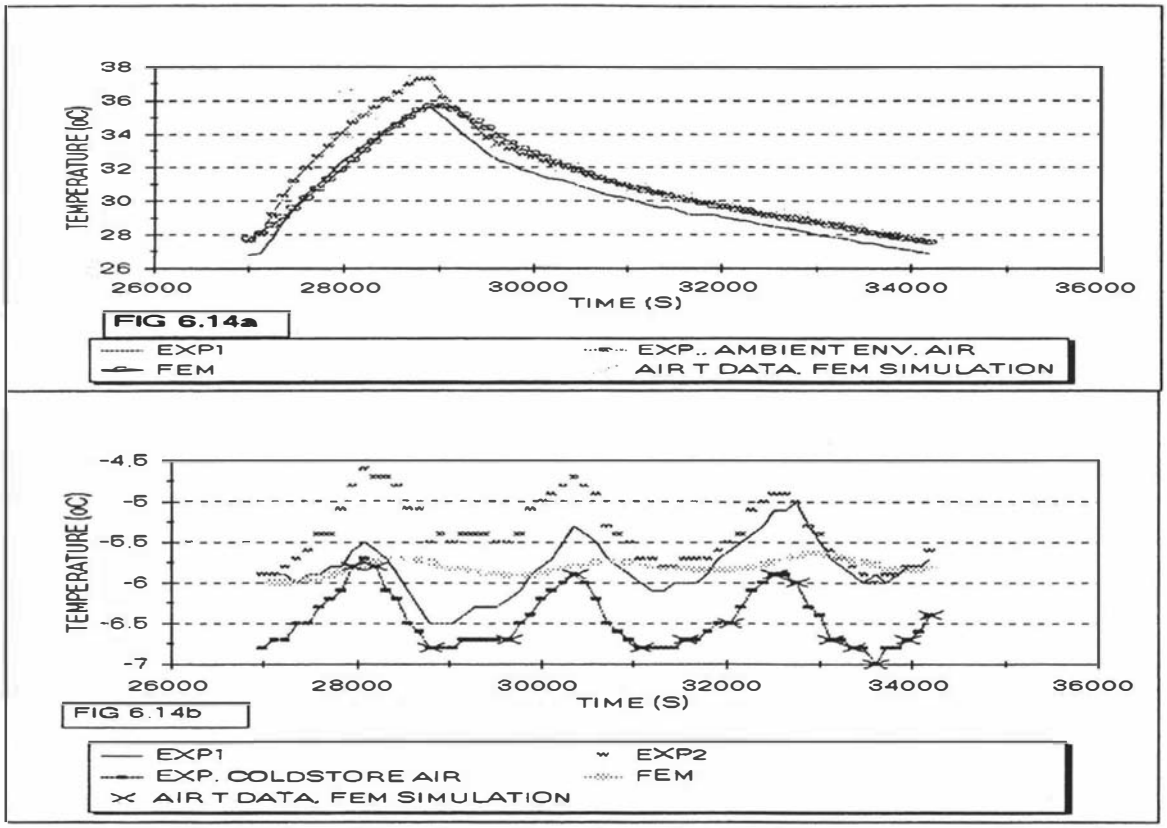

Fig.6.14. Trial 3, SPT slab: Comparison of experimental and FEM temperature profiles at **a)** metal-insulation boundary (ambient environment side) and **b)** insulation-metal boundary (coldstore environment side). FEM grid: 1 element in each metal layer and 12 linear elements in the insulation layer.

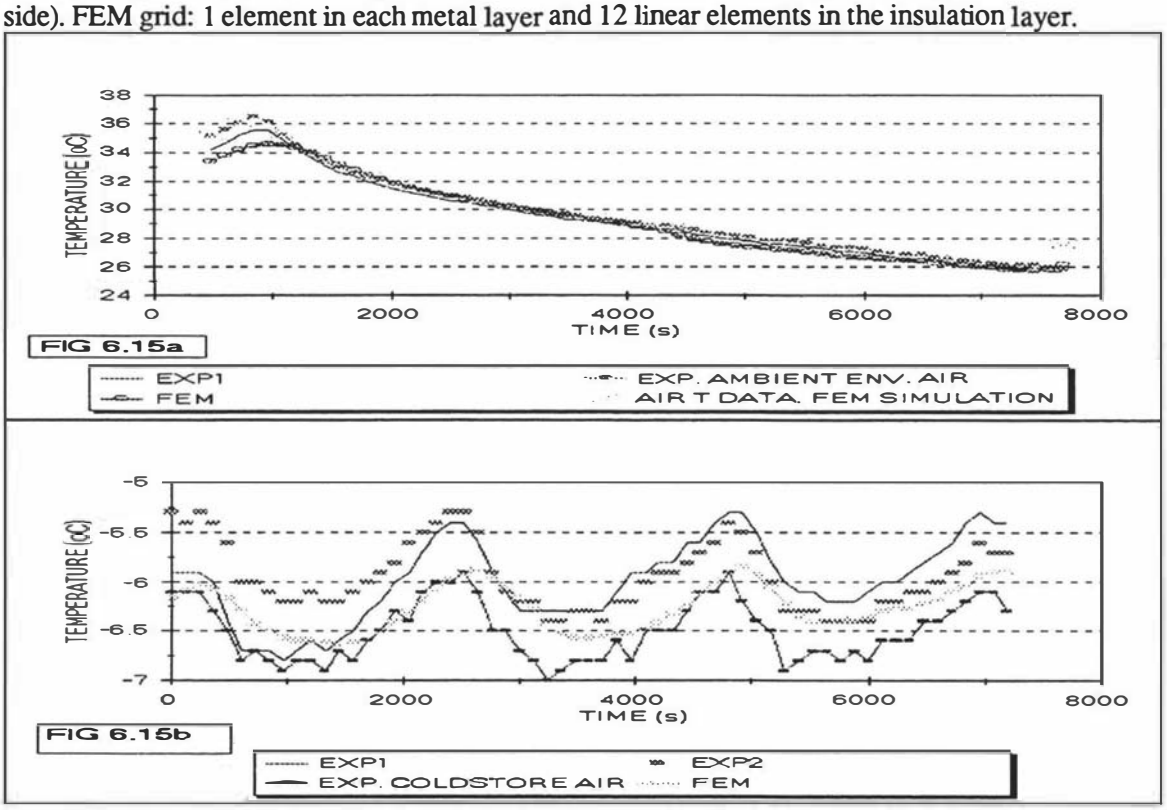

Fig. 6.15: Trial 4, SPT slab: Comparison of experimental and FEM temperature profiles at **a)** metal-insulation boundary (ambient environment side) and **b)** insulation-metal boundary (coldstore environment side). FEM grid: 1 element in each metal layer and 12 linear elements in the insulation layer. Note that $h_{\text{ambient environment-to-slab}}$ = 15 W/m K in both trials

6.6.4.2. CIC results.

Figures 6.16 to 6.21 show comparisons of model prediction with experimental data. Figures 6.16, 6.18 and 6.20 show ambient and coldstore environment temperatures as well as slab boundary temperatures.

As stated in Chapter 5, the simulations of CIC by different models were compared against the ***DDD*** model instead of the FEM predictions. The ***DDD*** computer programme did not support the use of more than 3 layers, the use of variable thermal properties or the use of time-variable coldstore environment conditions. Therefore, to allow a fair comparison between FEM and ***DDD*** predictions, the FEM simulations were re-modelled with consistent data files, excluding the metal layer in contact with the ambient environment, allowing constant thermal properties and coldstore environment temperature for each of the experimental trials.

The mean properties and temperatures used were:

- Mean thermal properties in the working temperature range of -9 to -1°C (frozen Tylose slab):

  λ = 1.3 W/m K

  c = 26.43 kJ/kg K

- Mean thermal properties in the working temperature range of 14.9 to 37.6°C (unfrozen Tylose slab):

  λ = 0.51 W/m K

  c = 4.02 kJ/kg K

- Mean coldstore air temperature:

  Trial 1: -7.3°C

  Trial 2: -7.5°C

  Trial 3: -7.5°C

For the CIC cases, the best matching of net temperature rise per cycle was obtained with h =10 W/m^2 K at the ambient environment side, thus this value was used. The rest of the data used are stated in Table 6.2.

Figures 6.17, 6.19 and 6.21 show the ***DDD*** and FEM predictions. The ***DDD*** profiles showed good agreement with the FEM trials and thus the assumption of an equivalent behaviour of FEM and ***DDD*** made in Chapter 5 was validated.

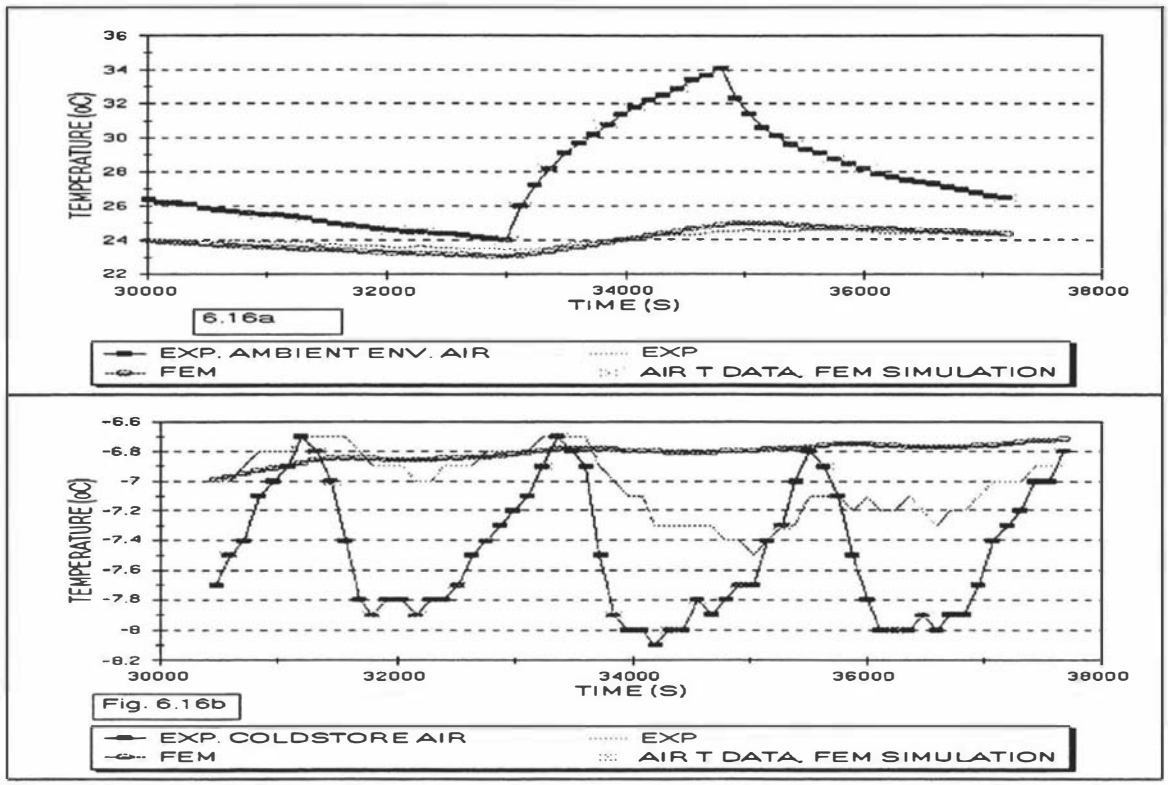

Fig. 6.16. Trial 1, CIC slab: Comparison of experimental and FEM temperature profiles at: **a)** metal-unfrozen Tylose boundary (ambient environment side) and **b)** frozen Tylose-coldstore environment boundary. FEM grid: 1 element for metal layer plus 10 elements for unfrozen Tylose, insulation and frozen Tylose, respectively.

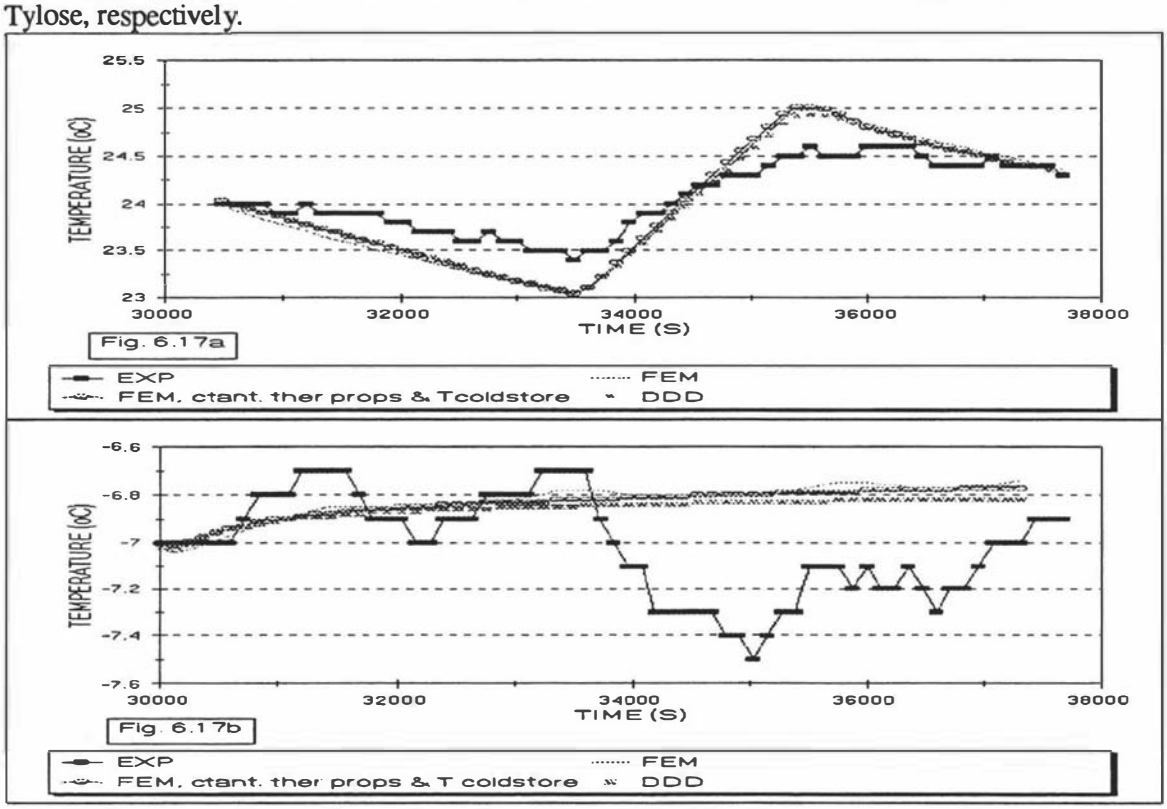

Fig. 6.17. Trial 1: Comparison of experimental, FEM and ***DDD*** temperature profiles at: **a)** metal-unfrozen Tylose boundary (ambient environment side) and **b)** frozen Tylose-coldstore environment boundary. FEM grid as mentioned before. ***DDD*** grid: 10 nodes for each layer. Note that $h_{\text{ambient environment-to-slab}}$ = 10 W/m K for all trials and comparisons between FEM and ***DDD*** were made using constant λ, c and coldstore temperature.

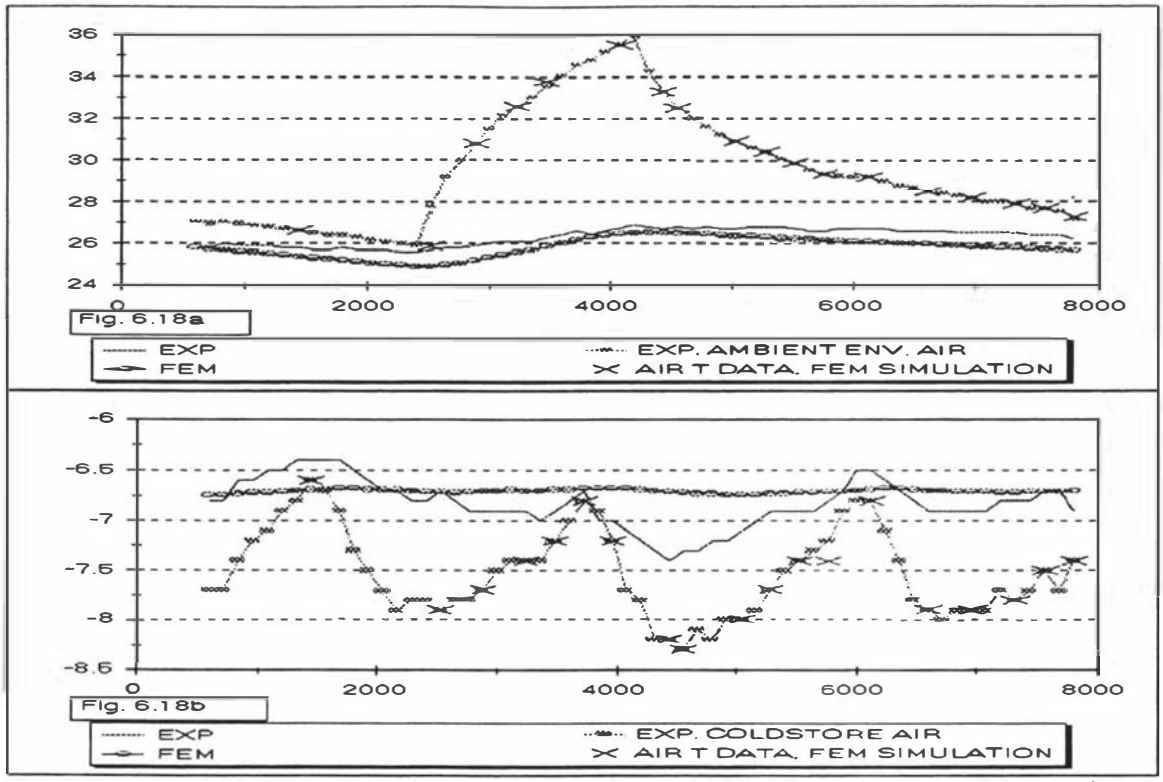

Fig. 6.18. Trial 2, CIC slab: Comparison of experimental and FEM temperature profiles at: **a)** metal-unfrozen Tylose boundary (ambient environment side) and **b)** frozen Tylose-coldstore environment boundary. FEM grid: 1 element for metal layer plus 10 elements for unfrozen Tylose, insulation and frozen Tylose, respectively.

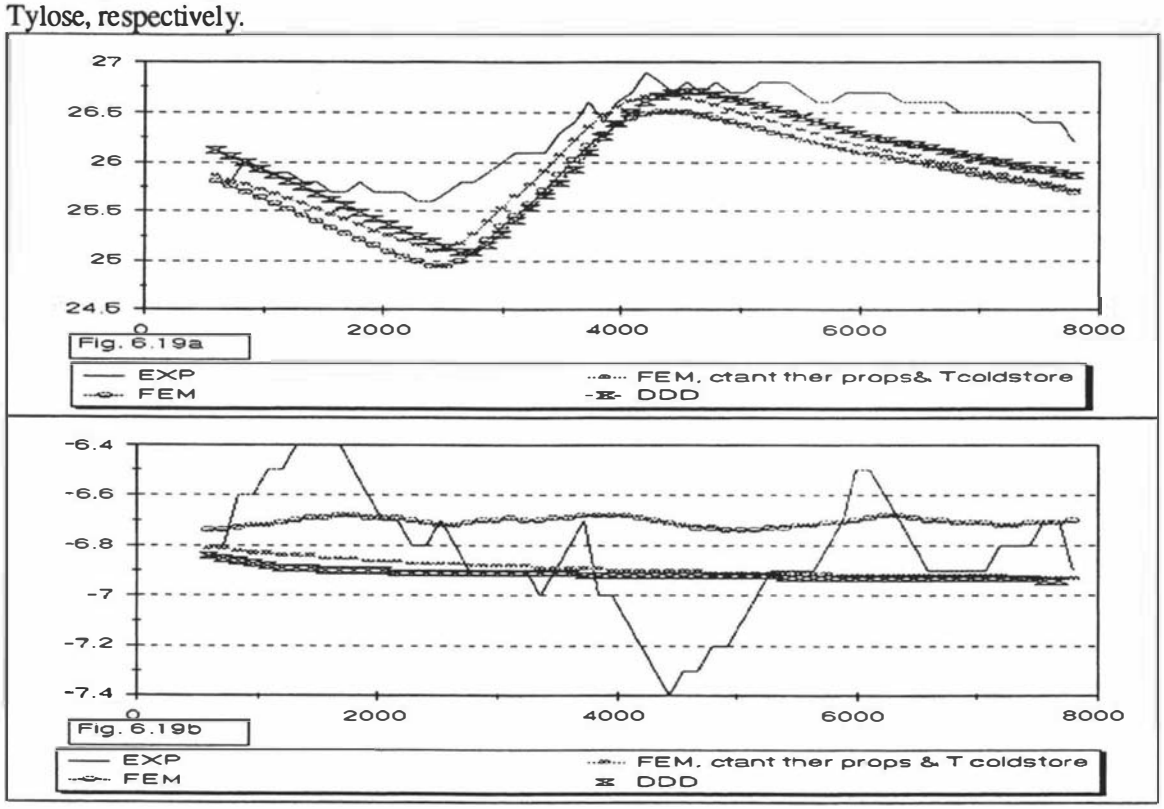

Fig. 6.19. Trial 2: Comparison of experimental, FEM and ***DDD*** temperature profiles at: **a)** metal-unfrozen Tylose boundary (ambient environment side) and **b)** frozen Tylose-coldstore environment boundary. FEM grid as mentioned before. ***DDD*** grid: 10 nodes for each layer. Note that $h_{\text{ambient environment-to-slab}}$ = 10 W/m K for all trials and comparisons between FEM and ***DDD*** were made using constant λ, c and coldstore temperature.

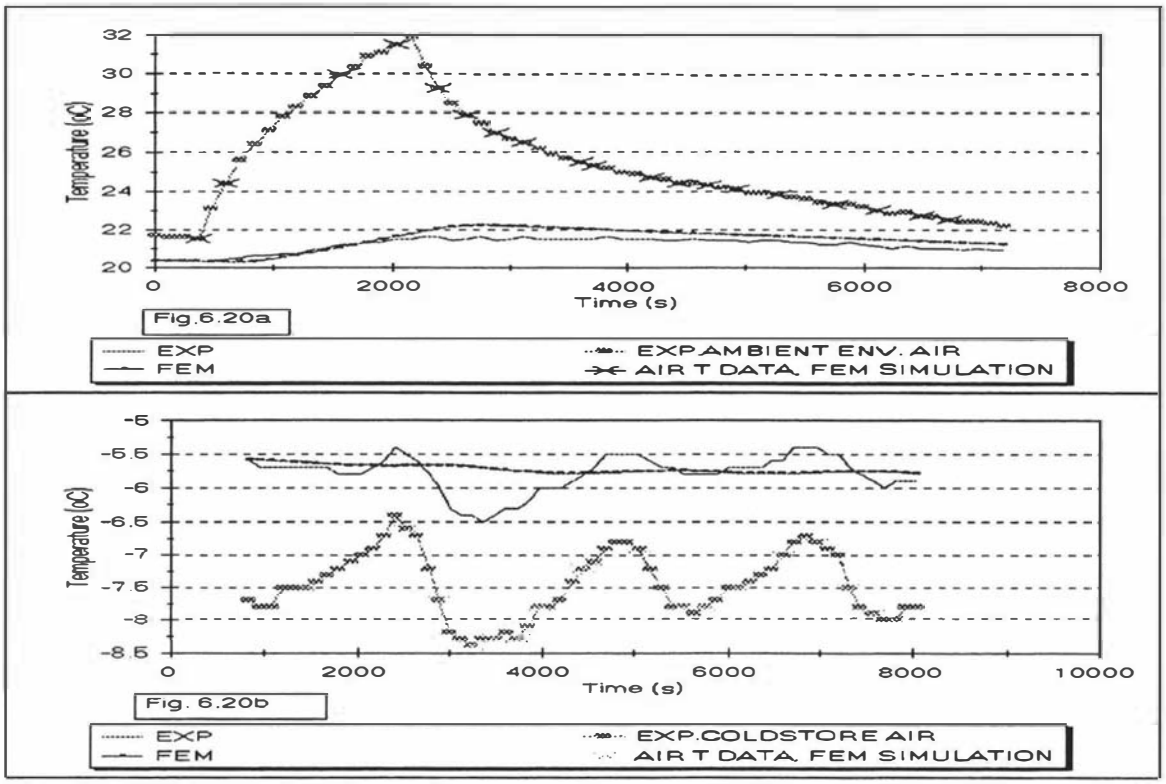

Fig. 6.20. Trial 3, CIC slab: Comparison of experimental and FEM temperature profiles at: **a)** metal-unfrozen Tylose boundary (ambient environment side) and **b)** frozen Tylose-coldstore environment boundary. FEM grid: 1 element for metal layer plus 10 elements for unfrozen Tylose, insulation and frozen Tylose, respectively.

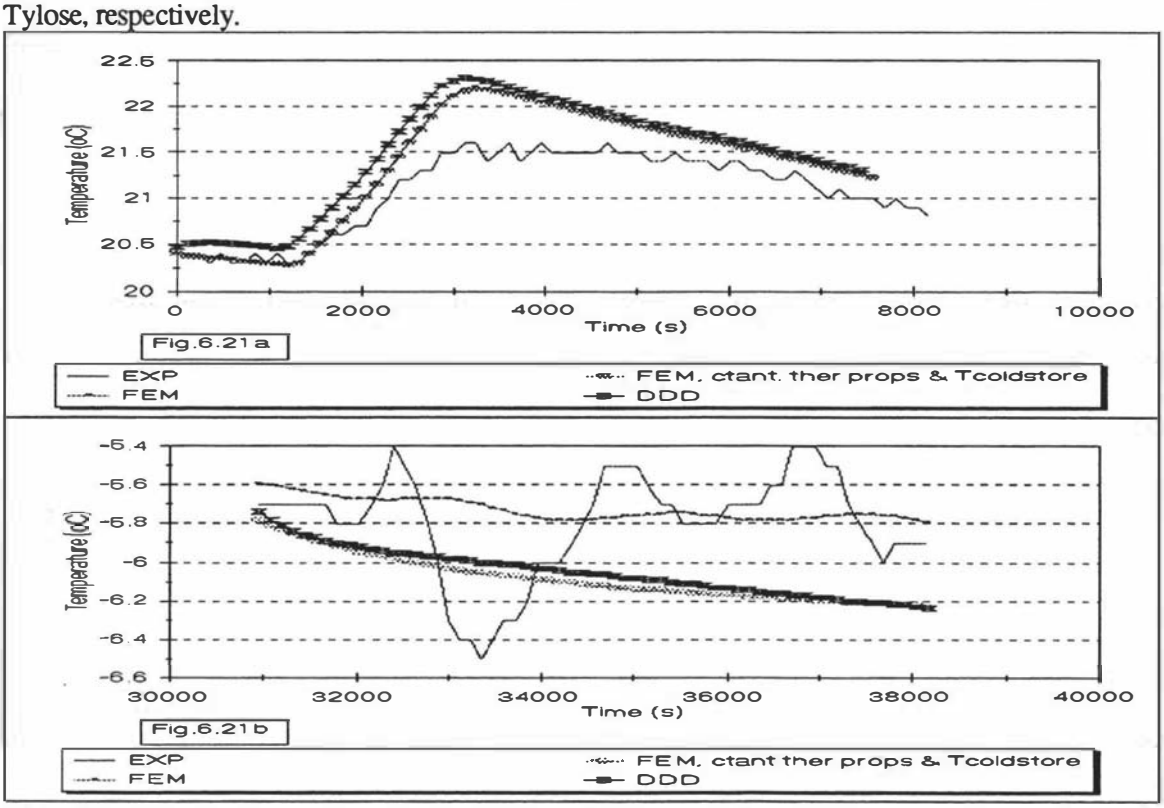

Fig. 6.21. Trial 3: Comparison of experimental, FEM and ***DDD*** temperature profiles at: **a)** metal-unfrozen Tylose boundary (ambient environment side) and **b)** frozen Tylose-coldstore environment boundary. FEM grid as mentioned before. ***DDD*** grid: 10 nodes for each layer. Note that $h_{ambient\ environment\text{-}to\text{-}slab}$ = 10 W/m K for all trials and comparisons between FEM and ***DDD*** were made using constant λ, c and coldstore temperature.

Figures 6.16, 6.18 and 6.20 present the comparison of the experimental trials and the response of FEM with full temperature-and-time-variable thermal properties and coldstore temperature. Some lack of fit between experimental and simulated profiles was observed for both boundary temperatures. For the ambient environment side, though the absolute difference between simulated and experimental profiles in the 3 trials did not exceed ±0.7°C, the shape of the FEM temperature predictions was sharper than the experimental profile, indicating less damping.

For the coldstore side, the simulated profile displayed considerably less variation in response to changes in the environment air temperature than the measured profiles, but the absolute difference with the experimental data did not exceed ±0.8°C. Note that the temperature scales chosen accentuate the apparent differences.

For both boundary temperatures, the difference between experimental and simulated profiles could potentially be explained by slight movement from the intended location of the thermocouples used for the measurements: For the ambient environment boundary temperature, the thermocouple may have been slightly embedded into the unfrozen Tylose slab rather than right at the metal/Tylose interphase. This situation was plausible due to the weight of the Tylose layer on top of the thermocouple. An embedded thermocouple would show higher damping than one at the interphase, which is consistent with the experimental and simulated results.

Similarly, for the coldstore boundary the greater variation in experimental temperatures than those predicted by FEM may indicate that the thermocouple was slightly out into the air side (or there was imperfect contact between thermocouple and the surface of the Tylose). A thermocouple more exposed to the coldstore air than at the surface could explain the more variable experimental profile.

Effects such as possible radiation and two-dimensional heat transfer phenomena may also have a significant effect, particularly for the coldstore side where the measured variability was greater than the simulated.

Taking into account all these facts, there was no evidence than FEM and ***DDD*** did not accurately predict actual CIC wall behaviour. It was therefore concluded that the use of FEM and ***DDD*** model results to represent the real wall behaviour was justified.

6.6.4.3. CIM results.

Figures 6.22 to 6.24 show the comparison of the CIM experimental and simulated profiles. For the ambient environment side, the experimental results showed less variation that the simulated responses, in a similar manner to the CIC behaviour. For the coldstore environment boundary, the simulated temperature followed the experimental profile more accurately than for the CIC slab. The thermocouple placed at the polystyrene/metal interphase for CIM could not protrude into the air, as in the previous CIC case.

For the ambient environment side, similar conclusions to the CIC results were drawn: possible misplacement of the thermocouples and other uncertainties of experimental nature are more likely to explain the lack of fit observed in the temperature profiles than inconsistencies between the FEM programme and the real wall behaviour.

6.7. Summary.

a) The sensitivity analysis conducted for the 3 slab types confirmed that uncertainty in h, λ and c was not highly influential on the simulated temperature profiles.

b) The uncertainty in the establishment of initial temperatures for the nodes between boundaries for the FEM simulations, the possible movement of thermocouples from their intended location and the need to represent the coldstore air temperature in a time-variable manner due to the variability of this parameter in the experimental system were major contributors to the observed differences between experimental and simulated profiles

c) In the SPT trials, the results were sufficiently good to validate the assumption made in Chapter 5 to use the FEM programme as a reflection of real wall behaviour.

d) In the CIC and CIM trials, the disagreement between experimental and simulated responses was larger than in the SPT trials, but still explainable in terms of the experimental resolution. The lack of fit between model and experimental results was more likely to be produced by the uncertainties mentioned in b) than by fundamental differences between the real behaviour and the FEM programme. Thus, the conclusion reached in c) also holds for CIC and CIM walls.

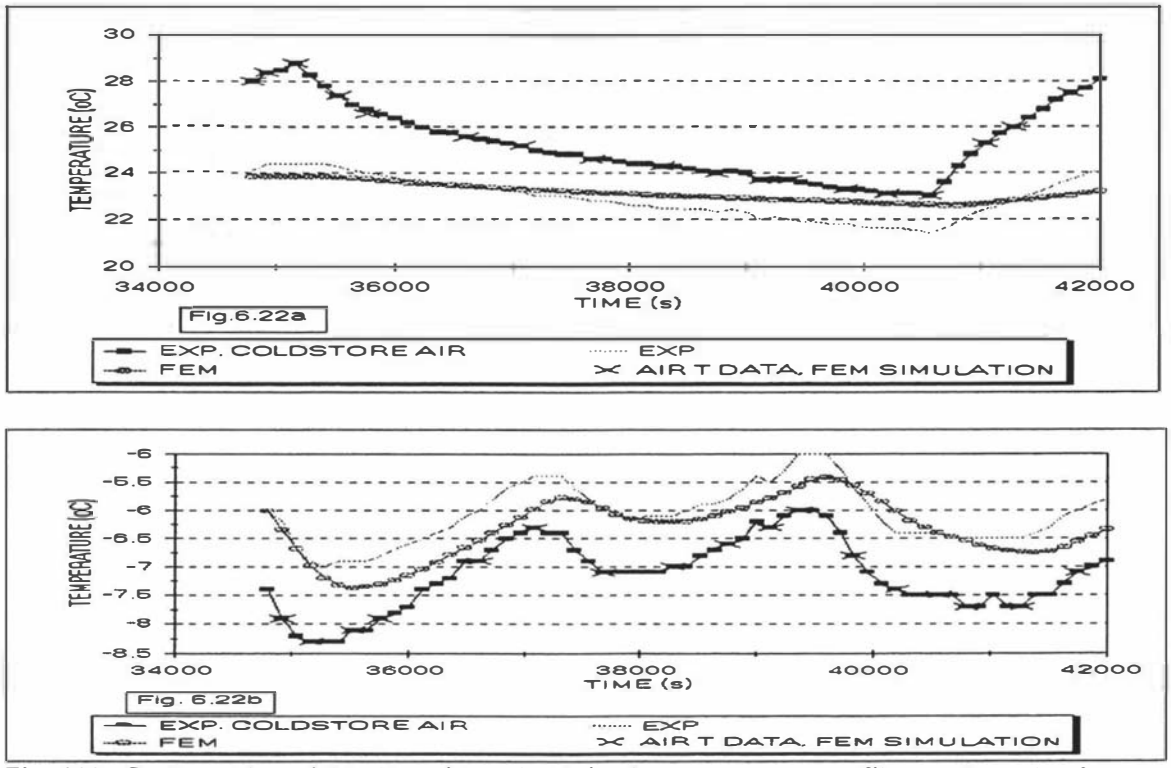

Fig. 6.22. CIM type slab, trial 1. Experimental and simulated temperature profiles at: **a)** metal-unfrozen Tylose boundary and **b)** insulation-metal boundary. FEM grid: 1 element for each metal layer plus 10 linear elements for unfrozen Tylose and insulation layers. $h_{\text{ambient environment-to-slab}} = 10\ \text{W/m}^2\,\text{K}$. the rest of the conditions are given in Table 6.3.

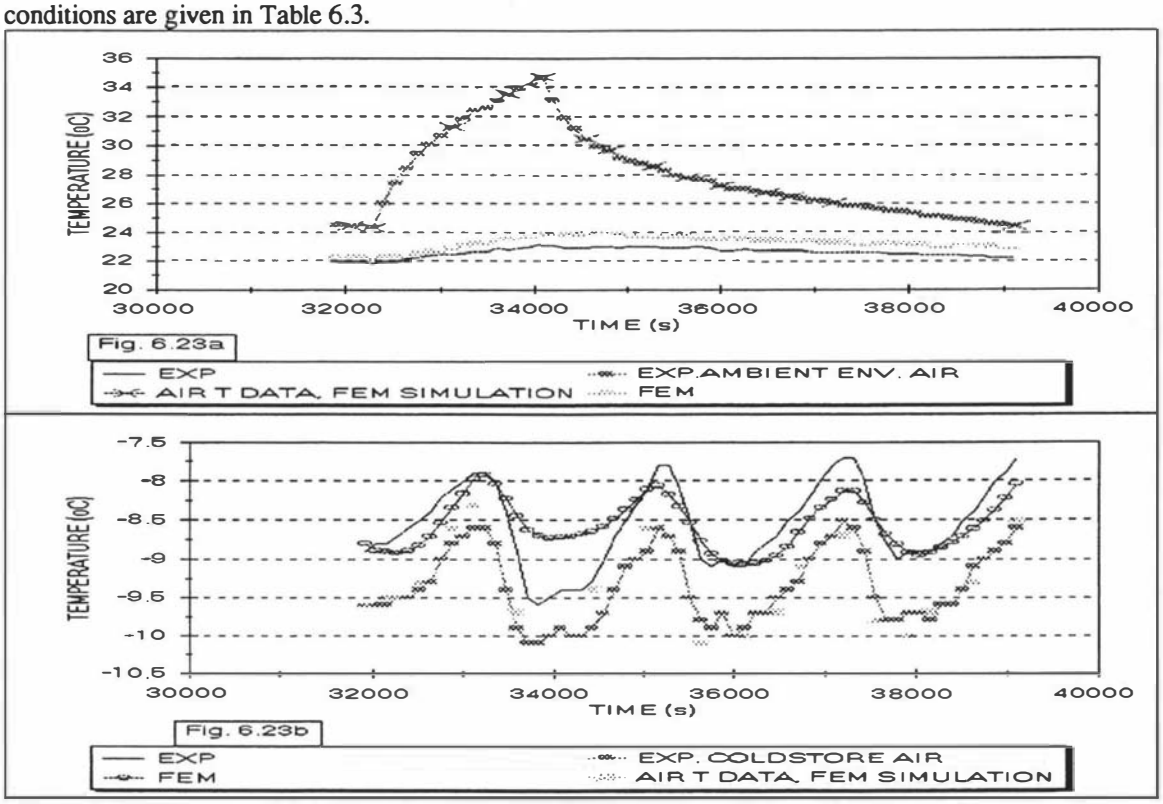

Fig. 6.23. CIM type slab, trial 2. Experimental and simulated temperature profiles at: **a)** metal-unfrozen Tylose boundary and **b)** insulation-metal boundary. FEM grid: 1 element for each metal layer plus 10 linear elements for unfrozen Tylose and insulation layers. $h_{\text{ambient environment-to-slab}} = 10\ \text{W/m}^2\,\text{K}$. the rest of the conditions are given in Table 6.3

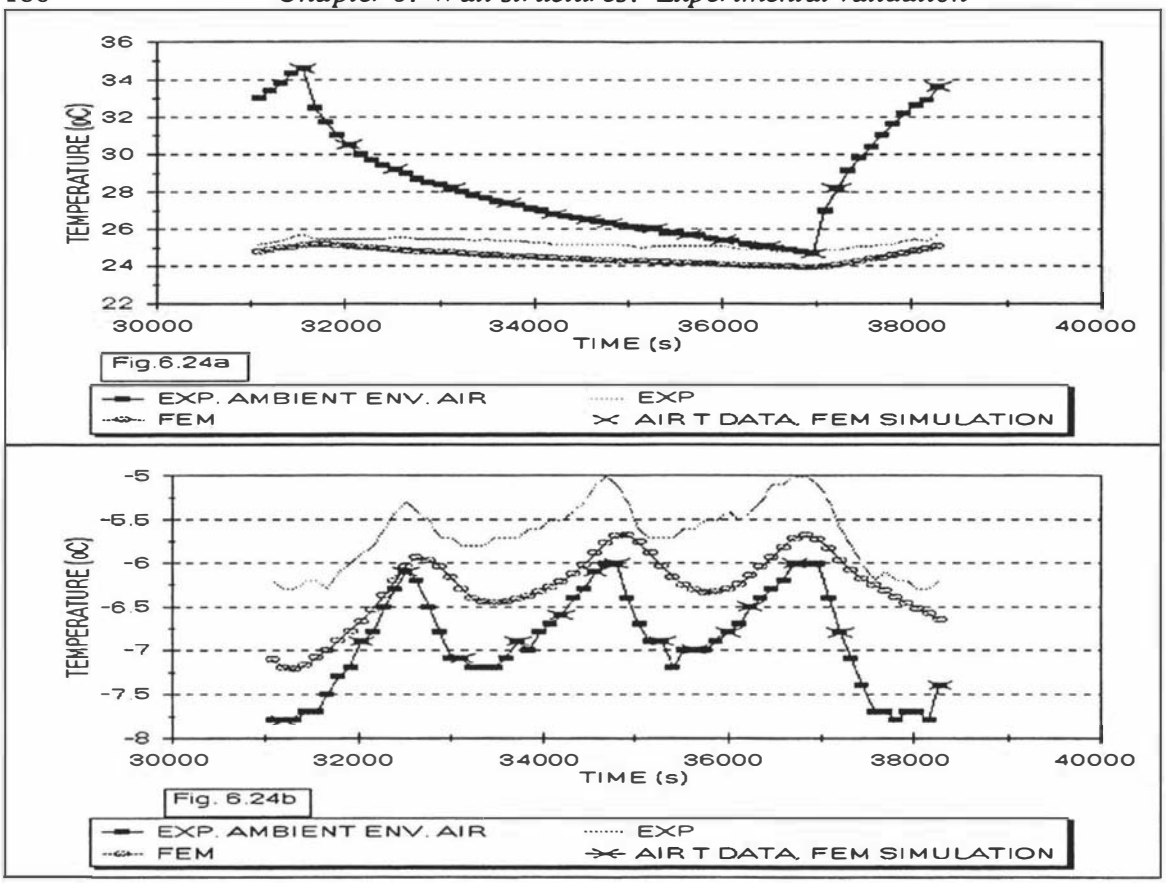

Fig. 6.24. CIM type slab, trial 3. Experimental and simulated temperature profiles at: **a**) metal-unfrozen Tylose boundary and **b**) insulation-metal boundary. FEM grid: 1 element for each metal layer plus 10 linear elements for unfrozen Tylose and insulation layers. $h_{\text{ambient environment-to-slab}} = 10$ W/m^2 K. the rest of the conditions are given in Table 6.3

CHAPTER 7: OVERALL ASSESSMENT OF WALL MODELS.

In Chapter 5, comparisons between models of different levels of complexity were made for a variety of scenarios representing typical wall types and operating conditions. Chapter 6 showed the validity of using the most complex models (FEM and ***DDD***) as accurate indicators of the real wall thermal response and hence as bases against which simpler models could be assessed. In the present chapter, practical issues affecting both the thermal behaviour of walls and the appropriate choice of models for different walls and situations are discussed.

7.1. Factors affecting the magnitude of heat infiltration across walls.

Analysis of factors affecting the magnitude of the heat flux entering a room allowed the development of principles that may give guidance to coldstore designers.

Table 7.1 summarises the contribution of changes in variables to changes in the magnitude of the incoming heat flux for an actual wall (as represented by the FEM and ***DDD*** models). According to the classification of variables stated in Section 5.1.3, the following 3 broad categories were defined:

a) Design variables: ε (external surface), $\boldsymbol{C}$ and $\boldsymbol{R}$.
b) Operational variables: T_{room} and h_2.
c) "Noise" variables: h_1 and T_a.

The measures (defined in Section 5.1.2, Chapter 5) used to characterise the incoming heat flux were also categorised into 2 groups:

a) Mean behaviour of the wall, as described by the mean heat load.
b) Time-variable (*dynamic*) behaviour of the wall as described by the start-up time and amplitude of the heat load. The offset (difference in timing of the predicted peak heat load compared to that predicted by FEM) could not be used as by definition for the FEM model it is 0.

Table 7.1 represents the main effects. Insignificant factors and interactions contributing less than 10% are not included; hence some rows do not add to 100%.

TABLE 7.1. PERCENTAGE CONTRIBUTION OF NOISE, OPERATION AND DESIGN VARIABLES ON THE PHYSICAL BEHAVIOUR OF THE WALLS TESTED (FEM AND *DDD* RESPONSE)

WALL	*TYPE OF MEASURE*	VARIABLE GROUP		
		DESIGN	OPERATION	NOISE
SPT	*mean*	53	38	0
	dynamic	81	10	9
CT	*mean*	53	38	0
	dynamic	73	0	27
CIC	*mean*	43	57	0
	dynamic	81	13	6
CIM	*mean*	49	23	0
	dynamic	78	0	22

As expected, changes in design plus operational variables accounted for between 80% and 100% of the changes in the magnitude of the mean heat load for all types of walls. This and the detailed results of Section 5.2.1 confirm the need for the wall designer to pay attention to **sizing and selection of wall materials, particularly their resistance, and the effect of room temperature.** By comparison, **use of radiation deflecting surface finishes will not significantly affect the mean incoming heat load.**

About 70% to 80% of the changes in the dynamic measures of wall behaviour were attributed to changes in the design variables. Changes in "noise" variables had an effect of less than 27% in all cases and operation variables were the least significant. For designers concerned with the dynamic nature of the heat flux infiltrated through walls, **sizing and selection of materials for walls is the most important consideration.** As discussed in Section 5.2.1, the combinations of thermal resistance and capacity is very influential for most wall types. Changes in resistance in particular have a large damping effect on the extent to which cyclic ambient conditions bring about variations in heat flux entering the room.

7.2. Measures and accuracy criteria.

Both the accuracy required of a model and the criteria used to assess the accuracy depends on the purpose of the final application of the model. The ranges of physical variables and the boundaries within which models will be useful to their final user will differ according to the ultimate goal sought. For example, a designer requiring only approximate

heat load information for preliminary sizing and selection of refrigeration system components may only need to know the mean heat load through the walls. Thus, the mean heat load is immediately defined as the appropriate response of interest and other more sophisticated measures can be ignored. The accuracy limits can then be set for this measure. However, for a refrigeration engineer interested in control strategies and controllers design, *dynamic* responses and hence measures of accuracy for how well these are modelled would be a more likely choice because size and timing of the response is important. In this case, it is still essential that the mean response is accurate.

In view of these ideas, an overall classification and ranking of measures and accuracies to assess the usefulness of models for wall thermal responses was developed.

7.2.1. Hierarchy of measures.

Possible measures were categorised as follows:

1) Primary measures: These are the initial responses sought. In the present work, the primary measure was the heat flux entering the room. In other applications, the wall external and internal temperatures might be considered (*e.g.* for evaluation of condensation risks).

2) Secondary measures: These are transformations of the primary response that characterise in a more helpful manner the system investigated. In this group, the measures of Chapter 5 can be included:

   2a) Physical measures: These were defined in Section 5.1.2, Chapter 5. Their main characteristic was that they were able to determined the performance of a wall as a heat transfer barrier.

   2b) Statistical measures: These proposed in Chapter 5 were offsets related to the actual response, standard deviations of the modelled response compared with the actual response and tolerance bands around the actual response. These gave more information about how the model response compared with the response of an accurate model (see definition of accuracy in Section 5.1, Chapter 5).

In the physical measures category, start-up times had been included because they gave information about how the effects of thermal mass and the choice of initial conditions were handled by different models. However, the interpretation of start-up results was rather difficult because few models complied with the limits established in Chapter 5. Hence, the status of start-up times as a measure was changed. The calculation of start-up times is now proposed solely as a mandatory step to characterise the time needed to nullify the effect of initial conditions on model predictions. Only those model predictions made after a period greater than the start-up time, so that a fully developed, repeatable 24 hr cycle is achieved, should be considered in comparisons between models.

7.2.2. Hierarchy of accuracy criteria.

Once meaningful measures have been defined, a stepwise method for assessment of accuracy is desirable. At any stage, once inaccurate models have been discarded, the selection between remaining models may then focus on the next most important secondary characteristic (such as which model gives the lowest computation cost). The aim is to select a model that gives optimum balance between accuracy and simplicity for the purpose.

A hierarchy for incoming heat flux was developed as follows:

0th level of accuracy: The model predicts physically realistic responses in qualitative terms, but may not be accurate quantitatively.

1st level of accuracy: The error in the mean heat load predicted by the model is less than 10%

2nd level of accuracy: The error in the amplitude of the predicted incoming heat flux is less than 10%

3rd level of accuracy: The offset from FEM of the daily cycle in heat load is less than ±4 hrs

4th level of accuracy: Peak standard deviations (SD) for several trials show that model and FEM (used as treatments) are equivalent from a statistical point of view, using an F-test at the 95% confidence level

or

Mean SD for several trials show that model and FEM (used as treatments) are equivalent from a statistic point of view, using an F-test at the 95% confidence level

5th level of accuracy: 80% or more of the total number of simulated data fall within a band of width ±10% of the peak heat flux located around the time-variable heat flux profile

6th level of accuracy: 80% or more of the total number of simulated data fall within a band of width ±10% of the mean heat flux located around the time-variable heat flux profile

7th level of accuracy: 80% or more of the total number of simulated data fall within a band of width ±10% of the energy/time rates.

With respect to the 0th level, if a model is accurate, then the predictions should be influenced by variables in the same way as in the real situation. However, inaccurate predictions of the physical measures can still occur.

The 1st level is a minimum that a model must meet if it is to have any quantitative value at all. Levels 1 to 3 combined ensure that models follow the dynamic behaviour of the wall in a realistic manner.

Only one of 4th level measures needs to be assessed. In Section 5.2.2., the mean SD proved to be more demanding than the peak SD, but they gave equivalent results in the ranking of models.

The 5th, 6th and 7th levels are even more strict. They proved useful as indicators of model weaknesses for certain scenarios and stages during the 24 hr cycle. While they give valuable information on this aspect, they can be extremely restrictive. Thus they should not be used alone to judge whether a model is sufficiently accurate or not. If models comply with levels 1 to 4, the model selected should be sufficiently accurate for many purposes such as improving process understanding. In Chapter 5 it was found that the use of energy/time rates was particularly demanding as a test of accuracy.

In all cases, tightening the criteria by reducing the percentage tolerance is possible. However, laxer criteria than the ones suggested here are considered unlikely to be sufficiently discerning between models.

7.2.3. Methodology for assessing model performance.

Using the hierarchy of measures and accuracy criteria proposed before, the overall methodology for selection of models for simulating the thermal response of walls becomes:

1) Select the primary measure to be predicted.
2) Select the accuracy bounds required for the application of the model.
3) Determine the characteristic start-up time for each model, so that later predictions are achieved in a repeatable cycle with negligible influence of initial conditions.
4) Discard obviously inaccurate models for which the 0th and 1st levels of accuracy are not achieved.
5) Evaluate the usefulness of models by testing compliance at the 2nd and 3rd levels of accuracy, discarding models that fail at each stage.
6) If a wide choice of models is still available, consider screening at higher levels 4th, 5th and 6th so that information can be gathered to make the final selection. If few models are available or the model has been selected already, these levels may help to show model performance in scenarios that may be difficult to model accurately. Failure to achieve adherence at these levels should not automatically lead to elimination of models.
7) If a second important primary measure is required, repeat step 6 changing the accuracy limit.
8) Select a model.

7.3. Assessment of models performance and choice of models for different applications.

The methodology of Section 7.2.3 was applied to each of the wall types and models considered. Table 7.2 shows the % contribution of design, noise and operating variables to changes to incoming heat flux for all models and types of walls tested. This can be compared with Table 7.1 in order to assess the 0th level of accuracy. The closeness of agreement between the percentages obtained for the mean response of models and FEM or ***DDD*** response in all cases reflected the good accuracy with which the mean heat load was modelled in all cases. For the *dynamic* response, the effect of design variables changed between models. This is a first indication that not all models were of the same accuracy. Note that, similarly to Table 7.1, Table 7.2 represents the main effects only. Insignificant factors and interactions contributing less than 10% are not included and so some rows do not add to 100%.

All the models tested accurately predicted the mean heat load (1st level of accuracy). As long as all significant thermal resistance is modelled, appropriate ambient boundary data are used and the start-up time is exceeded before predictions are selected for analysis, then any of the models tested will meet the basic criteria. The 2nd and subsequent levels are discussed for each type of wall separately below. The discussion concentrates on the modelled dynamic response, since the mean behaviour was accurate for all models.

TABLE 7.2. PERCENTAGE CONTRIBUTION OF NOISE, OPERATION AND DESIGN VARIABLES ON THE MODELLED INCOMING HEAT FLUX FOR THE WALLS TESTED (RESPONSE OF MODELS TESTED)

WALL	MODEL	*TYPE OF MEASURE*	VARIABLE		
			DESIGN	OPERATION	NOISE
S P T	***NRN***	*mean*	53	38	0
		dynamic	81	0	19
	CRC	*mean*	53	38	0
		dynamic	43	42	15
C T	***NLN***	*mean*	53	38	0
		dynamic	70	0	30
	NDN	*mean*	53	38	0
		dynamic	75	0	25
C I C	***RRR***	*mean*	43	55	0
		dynamic	87	0	13
	RRL	*mean*	40	53	0
		dynamic	87	0	13
	LRL	*mean*	39	56	0
		dynamic	76	23	1
	DRD	*mean*	40	59	0
		dynamic	52	41	7
C I M	***RRC***	*mean*	48	24	0
		dynamic	54	0	46
	LRC	*mean*	48	24	0
		dynamic	77	2	21
	LLC	*mean*	49	23	0
		dynamic	74	11	15
	RDC	*mean*	48	24	0
		dynamic	79	4	17

7.3.1. Sandwich panel type models.

Only ***NRN*** and ***CRC*** models were assessed. Both models partially fulfilled the criteria for accuracy at the 2nd and 3rd levels and both failed in the same trials for the peak and mean SDs (4th level). Although it was observed that ***CRC*** gave a closer agreement in some measures, ***NRN*** was not significantly worst at the 95% level of confidence. The only measures that showed significant differences between the models were the start-up times and the peak tolerance, which indicated a better performance of the ***CRC*** model. Overall, **no major benefit in increasing the level of model complexity to *CRC* was observed for the SPT case**, so the ***NRN*** model would be recommended in most cases on simplicity grounds. The results of Chapter 5 suggest that for both models, better accuracy should be expected for walls with low ***R*** values.

7.3.2. Concrete type wall models.

Models assessed were ***NLN*** and ***NDN***. Both models complied with the criteria for the 2nd and 3rd level of accuracy and gave equivalent results at level 4. However, the results of the ***NLN*** model were highly dependent on the grid selection. **The *NLN* model achieved its best accuracy when a capacity only (c) zone was used at the external boundary, and a grid of 8 or more zones with even distribution of thermal capacity and resistance was used.** The ***NDN*** results were equivalently accurate using grids of 5 nodes or more. With these grid strategies, **both *NDN* and *NLN* were accurate, regardless of changes in the levels of the design, operation and "noise" variables,** within the range of conditions investigated. The increasingly accurate results as the ***L*** region grid was refined indicates that **simpler models, neglecting either the thermal resistance or thermal capacity of the concrete wall, are expected to be inadequate.** Models that account for both capacity and resistance are required if the dynamic response is important.

7.3.3. Concrete-insulation-concrete type wall models.

The models assessed were ***RRR***, ***RRL***, ***LRL*** and ***DRD***; they were compared with ***DDD*** responses. The models did not fulfil the criteria for the 2nd and 3rd levels of accuracy. As for the CT wall, use of a simple ***R*** sub-model for either of both of the concrete layers was too simplistic. Also, the use of an ***R*** sub-model for the insulation layer (neglecting the insulation thermal capacity) appeared to significantly affect accuracy, as ***DRD*** and ***DDD*** differ by only

this sub-model. However, in terms of the 5th and 6th levels, the ***DRD*** and ***LRL*** models were found to be accurate.

For both ***L*** and ***D*** sub-models, a fine grid in the layer at the ambient boundary gave the best results, whereas changes in the grid representation for the layer at the internal boundary did not significantly influence the results. This suggests that **the most dynamic (ambient environment boundary) layer within the wall should be represented using a fine grid** (8 or more zones for ***L*** and 5 or more nodes for ***D***), whereas 3 zones for ***L*** (2 nodes for ***D***) was adequate for the inside wall layer. Though the magnitude of the response of CIC walls was not highly affected by the design variables, **the accuracy of all the CIC models changed significantly according to the variation of the critical design variables (ℝ and ℂ).**

7.3.4. Concrete-insulation-metal type wall models.

RRC, LRC, RDC and ***LLC*** model were assessed. Similarly to the CIC wall case, the CIM models with an ***R*** sub-model for the concrete layer failed at the 2nd level of accuracy, and for the ***L*** sub-models, at least 8 zones (with a *c* zone at the external boundary) were required. However, in terms of the 4th, 5th and 6th levels of accuracy, both ***LLC*** and ***LRC*** models performed well.

7.3.5. Summary of strategies in the use of wall models.

The suggested strategies for modelling wall layers are:

- If only average heat load is required then a ***R*** sub-model is adequate for any material. The following strategies relate to the dynamic response of layers.
- Thin metal layers: These are adequately represented by ***C*** sub-models for *dynamic* measures or ***N*** sub-models for mean measures (negligible resistance).
- Concrete layers: Both thermal capacity and resistance need to be modelled. An adequate description is given by ***L*** sub-models, with a *c* zone in the external (ambient) boundary and with an even distribution of ℂ and ℝ; the number of zones recommended is:
  - 8 or more zones for a layer adjacent to the external (ambient) environment
  - 3 or more zones for a layer adjacent to the internal (room) environment
- Insulation layers: Although an ***R*** model is recommended for mean behaviour, the conclusion for *dynamic* behaviour is less clear, especially for heavy insulated CIC and

CIM walls. In simulations, the selection of inadequate models for other layers masked the effect of using ***R*** models for insulation layers in walls with high thermal capacity. Comparisons of ***R*** and simple ***L*** models for insulation layers is needed before a definitive recommendation can be made.

Regarding grid selections for ***L*** and ***D*** regions, the following aspects should be considered:

- To achieve an accuracy similar to that of an ***L*** model with uniform distribution of **R** and **C**, the number of nodes in a ***D*** sub-model should be at least half the number of zones in an ***L*** model.
- ***D*** models offer an advantage when the model must approximate a non-uniform temperature distribution. In a ***D*** model, the number of initial temperature points stated across an object will be twice the number for an ***L*** scheme using the same number of zones.
- In comparison with ***D*** sub-models, ***L*** schemes proved to be faster in the following situations:
  - Walls with layers of very different thermal properties (*e.g.* SPT walls).
  - Walls with a heavy internal layer (concrete). In this case, an ***L*** sub-model using between 3 and 8 zones is an adequate description, if the room temperature air is not highly variable.

In some circumstances (particularly in wall models with adjacent *r* zones/***R*** regions) the iterative schemes needed may slow down the computation speed of ***L*** models. In such cases, the computation advantages of ***L*** models over ***D*** models needs careful assessment.

7.4. Specific recommendations for selection of incoming heat flux models according to the application.

Table 7.3 presents recommendations for selecting models in different applications. These were based on comparisons of the models summarised above and take account of the relative importance of mean and *dynamic* responses. In some cases, a model that was not directly investigated in Chapter 5 has been recommended, based on the results of similar models and the general guidelines established for modelling each type of layer. Such suggestions are always the minimum level of complexity that might be used as a starting point

to test further possibilities. For example, in the CIC type wall, accurate simulations of amplitudes were obtained only when using the ***DDD*** scheme. However, simpler models representing the insulation in a more detailed manner than ***R*** (*e.g.* ***LLL*** or ***DLD***) may give an acceptable accuracy. The same applies for other walls investigated.

Table 7.3 specifies ***R*** only models for mean behaviour and capacity plus resistance models when transient behaviour is required. The distribution of resistance and capacity will depend on the characteristics of the specific wall.

TABLE 7.3. GUIDELINES TO SELECT A HEAT INFILTRATION MODEL ACCORDING TO ITS FINAL USE.

MODELLING SITUATION	PRIMARY MEASURE & KEY FEATURES TO BE SOUGHT	SECONDARY MEASURES	TYPE OF WALL	MODEL RECOM MENDED	CONDITIONS OF ACCURACY[2]:	POSSIBLE ALTERNATIVES & FURTHER [1] RESEARCH SUGGESTED:
Selection & sizing of wall materials and estimates of daily heat infiltration (average conditions)	Incoming heat load: Daily mean heat flux	Mean heat flux: 1st level of accuracy	SPT	***NRN***	----	----
			CT	***NRN***	----	----
			CIC	***RRR***	----	----
			CIM	***RRN***	-----	----
Selection and sizing of wall materials and estimates of daily heat infiltration ("worst case" conditions)	Incoming heat load: Daily peak heat flux	Amplitude of cyclic heat flux and mean heat flux (Peak= 0.5 Amplitude+Mean): 1st and 2nd levels	SPT	***CRC***	Light insulation and relatively high room temperatures(**R**=2 to 4 m2 K/W and T_{room}> 0°C), *i.e.* conditions commonly found in coolstore applications.	***CLC*** or ***CDC***
			CT	***NLN***	***L4*** or ***L2***, 8 zones model, with an even distribution of **C** and **R**	----

continued...

[1] These are models suggested for further investigation in order to achieve a better complexity/accuracy trade-off. These suggestions were selected according to the weaknesses detected in the models investigated. If no indication is given, a suitable model was identified in this project

[2] A necessary condition in all cases is that "noise", design and operation variables are used within the ranges stated in Table 5.1 (Chapter 5)

Table 7.3 continued...

MODELLING SITUATION	PRIMARY MEASURES & KEY FEATURES TO BE SOUGHT	SECONDARY MEASURES	TYPE OF WALL	MODEL RECOMMENDED	CONDITIONS FOR ACCURACY[2]:	POSSIBLE ALTERNATIVES & FURTHER [1] RESEARCH SUGGESTED:
Selection & sizing of wall materials and estimates of daily heat infiltration ("worst case" conditions)	Incoming heat load: Daily peak heat flux	Amplitude of cyclic heat flux and mean heat flux (Peak= 0.5 Amplitude+Mean): 1st and 2nd levels	CIC	***DRL***	***D*** using 5 nodes or more; an ***L4***, 8 zones model, with an even distribution of **C** and **R**	Use of ***L*** or ***D*** instead of ***R*** for insulation layer
			CIM	***DRC***	***D*** sub-model uses 5 nodes or more	

continued....

[1] & [2]: See notes on previous page

Table 7.3 continued...

MODELLING SITUATION	PRIMARY MEASURES & KEY FEATURES TO BE SOUGHT	SECONDARY MEASURES	TYPE OF WALL	MODEL RECOMMENDED	CONDITIONS OF ACCURACY[2]:	POSSIBLE ALTERNATIVES & FURTHER [1] RESEARCH SUGGESTED:
Energy usage calculations, selection of controllers & design of control strategies	Incoming heat load: Daily peak heat flux and timing of peak	Amplitude and mean heat flux and heat flux offsets (with respect to external peak temperature): 1st 2nd and 3rd levels	SPT	***CRC***	See previous box	Use of ***L*** or ***D*** instead of ***R*** for insulation layer
			CT	***NLN***		
			CIC	***DRL,DRD***		
			CIM	***DRC,LLC***		

continued..

[1] & [2]: See notes on previous pages

Table 7.3 continued...

MODELLING SITUATION	PRIMARY MEASURES & KEY FEATURES TO BE SOUGHT	SECONDARY MEASURES	TYPE OF WALL	MODEL RECOMMENDED	CONDITIONS OF ACCURACY[2]:	POSSIBLE ALTERNATIVES & FURTHER [1] RESEARCH SUGGESTED:
Sub-model for heat infiltration to form part of an integrated refrigeration plant software.	Incoming heat load: Peak and offsets for daily, monthly or yearly estimations	Mean and amplitude heat fluxes, offsets, peak and mean SDs: 1st to 4th levels	SPT	***CRC***	------	Simpler models failed in some scenarios. The accuracy tolerances may need to be adjusted and the models reassessed.
			CT	***NLN***		
			CIC	***DRL,DRD***		
			CIM	***DRC,LLC***		

continued..

[1] & [2]: See notes on previous pages

Table 7.3 continued...

MODELLING SITUATION	PRIMARY MEASURES & KEY FEATURES TO BE SOUGHT	SECONDARY MEASURES	TYPE OF WALL	MODEL RECOMMENDED	CONDITIONS OF ACCURACY[2]:	POSSIBLE ALTERNATIVES & FURTHER [1] RESEARCH SUGGESTED:
Selection of most cos-effective sub-model for heat infiltration to form part of an integrated refrigeration plant software, for already accurate models simulating the incoming heat flux	Computation cost	Peak and mean SD's, tolerance bands: full hierarchy of accuracy used	SPT	4th level: ***CRC*** 5th, 6th and 7th levels:***DDD***	----	Switching strategies between two or more models to simulate different stages of a wall across the day, so that complex models are used for critically important times during the day and simpler models are used for normal situations; for example, modelling an SPT wall using an ***LLL*** model for peak times to switch later to an ***NRN*** or ***CRC*** model
			CT	4th level: ***NLN*** 5th and 6th levels: ***NLN*** 7th level:***DDD***	----	
			CIC	4th level: ***LRL,DRD*** 5th and 6th levels: ***DRD,DRL*** 7th level:***DDD***	----	
			CIM	4th level: ***LLC,DRC*** 5th and 6th levels: ***LLC, DRC*** 7th level:***DDD***	-----	

[1] & [2]: See notes on previous pages

CHAPTER 8. PRESSURE VESSELS: CONCEPTUAL AND MATHEMATICAL MODELLING

The literature review revealed a paucity of research on the dynamic behaviour of the linking elements in the refrigerant circuit such as vessels, pipes and valves, in contrast with the more numerous reports related to the simulation of condensers, compressors and evaporators. This trend was attributed to the assumed relatively low thermal mass of vessels, pipes and valves. Although some models have been developed for pressure vessels, experimental research specifically focused on the energy and mass transient parameters in vessels and pipes has not been undertaken and/or the techniques used for assessing such performance have not been clearly defined. Therefore, rigorous validation and evaluation of such models has been difficult to achieve.

The transients of the pressures and temperatures, the refrigerant distribution (vapour/liquid balance) and other associated parameters in a vessel acting as an intercooler, a receiver or a surge drum might be used as important indicators of the overall performance of a plant. The refrigerant phenomena occurring inside the tank (*i.e.* de-superheating of vapour from low stage compression, flashing to form a liquid/vapour mixture in a stream entering from the high pressure part of the plant, return/feeding of liquid from/to evaporators) are all important in the dynamics of plant operation. Practical, accurate models for pressure vessels would prove a valuable tool for the design and operation of refrigeration systems.

The first objective was to develop new models for pressure vessels, using thermal modelling approaches of various complexities. Thermal models are based on the assumption that the energy transients have the predominant effect on the system response rather than hydraulic considerations. The 4 models developed were: A) a new approach to the conceptual and mathematical representation of the vessel using more rigorous thermodynamic theory than in previous models, B) a less complex model following closely the assumptions made by Marshall and James (1979), C) the same approach as B, but neglecting transitions between saturated-superheated states in the case of the vapour phase and saturated-subcooled states in the case of the liquid phase and D) a simple model following the assumptions of Cleland (1985). The experimental research methodology used to validate and compare the pressure vessel models is described in Chapter 9.

8.1. Physical model.

Liquid separators, receivers and intercoolers are examples of the pressure vessels commonly used in refrigeration plants. The main functions of these are:

- To store the liquid refrigerant during maintenance, charging or off periods of the plant
- To act as liquid traps, separating the liquid and vapour from mixed streams and avoiding compressor damage due to liquid being recirculated to the compression chamber
- To feed flooded evaporators by pumps or natural circulation
- To act as heat exchangers, cooling the superheated vapour from the low stage compression and sometimes simultaneously sub-cooling refrigerant liquid to be fed to the evaporators

All of these functions may not be important in every pressure vessel, but there are some pressure vessels that perform all these functions and thus their operation has a key role in the overall performance of the system. One prime example is the low-pressure receiver system patented by Star Refrigeration Ltd (Koelet, 1992; Pearson, 1996), in which the manipulation of the pressure of the vessel in conjunction with the use of a four port valve replaces the use of refrigerant pumps to feed the evaporators. In this case, the receiver acts as a suction line superheater, a subcooler for the liquid refrigerant coming from the condenser, a "pump" transporting excess liquid refrigerant to the evaporator, a receiver holding the total refrigerant charge (the traditional liquid receiver placed after the condenser is not needed in the installation) and an oil rectification device, returning oil to the compressor using pressure differences.

The initial physical model proposed was a representation of a vertical closed intercooler, which allowed the investigation of some of the most interesting features of the commonly used pressure vessels. A typical intercooler as presented in Figure 8.1 is commonly used in multiple stage compression systems. In a two stage refrigeration system the vessel receives superheated gas from the low stage compression, usually bubbled into the liquid phase at the bottom of the vessel. The vapour is cooled and a flow of vapour, typically about 10°C above the saturation temperature (James, 1995), is drawn away from the head space of the intercooler by the high stage compressors. The vessel is fed via a refrigerant liquid line from the condenser. Prior to its entrance to the vessel, the liquid pressure is

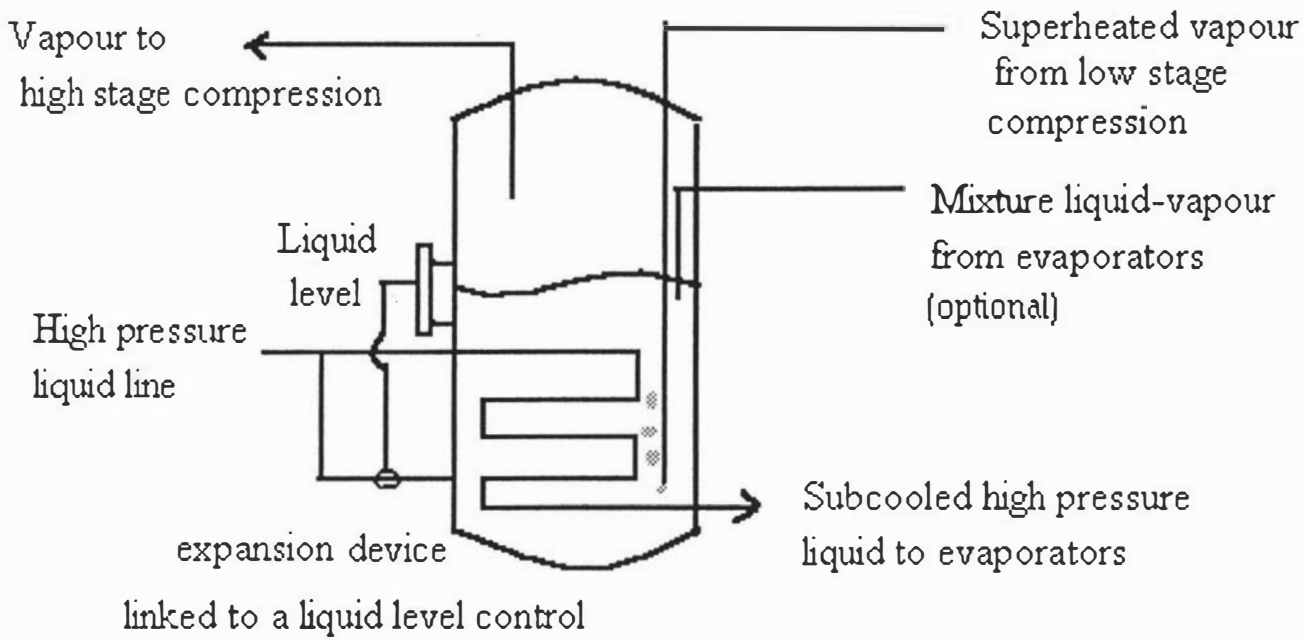

Fig. 8. 1. Typical arrangement of a vertical closed intercooler

reduced to the intercooler pressure, thus forming a mixture of saturated vapour and liquid. A second liquid line may flow through a pipe coil in the vessel so that the liquid surrounding the coil subcools the pipe contents. This usually leads to boiling of the refrigerant surrounding the coil to create vapour which joins the vapour phase. The boiling of the liquid may be so vigorous that the interphase between liquid and vapour becomes difficult to establish. In some arrangements, refrigerant from evaporators or secondary vessels might return to the intercooler. Finally, the vessel is often placed in a central plant, protected from the solar radiation but not from the influence of the ambient temperature. To minimize the effect of the ambient conditions, the vessel may be insulated and covered with a metallic vapour barrier layer, thus lowering the rate of radiative and convective heat transfer to it.

8.2. Statement of the conceptual model.

Figure 8.2 presents a conceptualization of the major phenomena occurring in such a pressure vessel. Independently of the type of vessel and its characteristic functions, the different sources of energy and mass exchange occurring with a pressure vessel can be conceptualised as one of the following:

a) Flows entering the vessel and interacting with the contents as energy and mass exchanges. The flows entering the system have a characteristic energy content, pressure and liquid/vapour mixture balance. These flows were categorised as *flow in* items, *e.g.* a mixture of liquid/vapour fed from the evaporators, a stream of liquid from the condenser.

b) Flows leaving the vessel, with the thermodynamic characteristics of either the liquid or vapour phase. These flows were described as *flow out* items, *e.g.* a stream of vapour leaving the vessel to the compressor, a stream of liquid to be fed to the evaporators.

c) *Object* items interacting with the vessel contents via heat exchange only, *e.g.* a coil with refrigerant at high pressure circulating through it in contact with the liquid phase or an external environment with which there is convective heat transfer.

Conceptually, the "history" of the flows previous to their entrance in the vessel is unimportant, provided the characteristics taken into account are the actual thermodynamic parameters present at the moment of initiation of their interaction with the vessel. From these considerations, a general conceptual model for pressure vessels was stated.

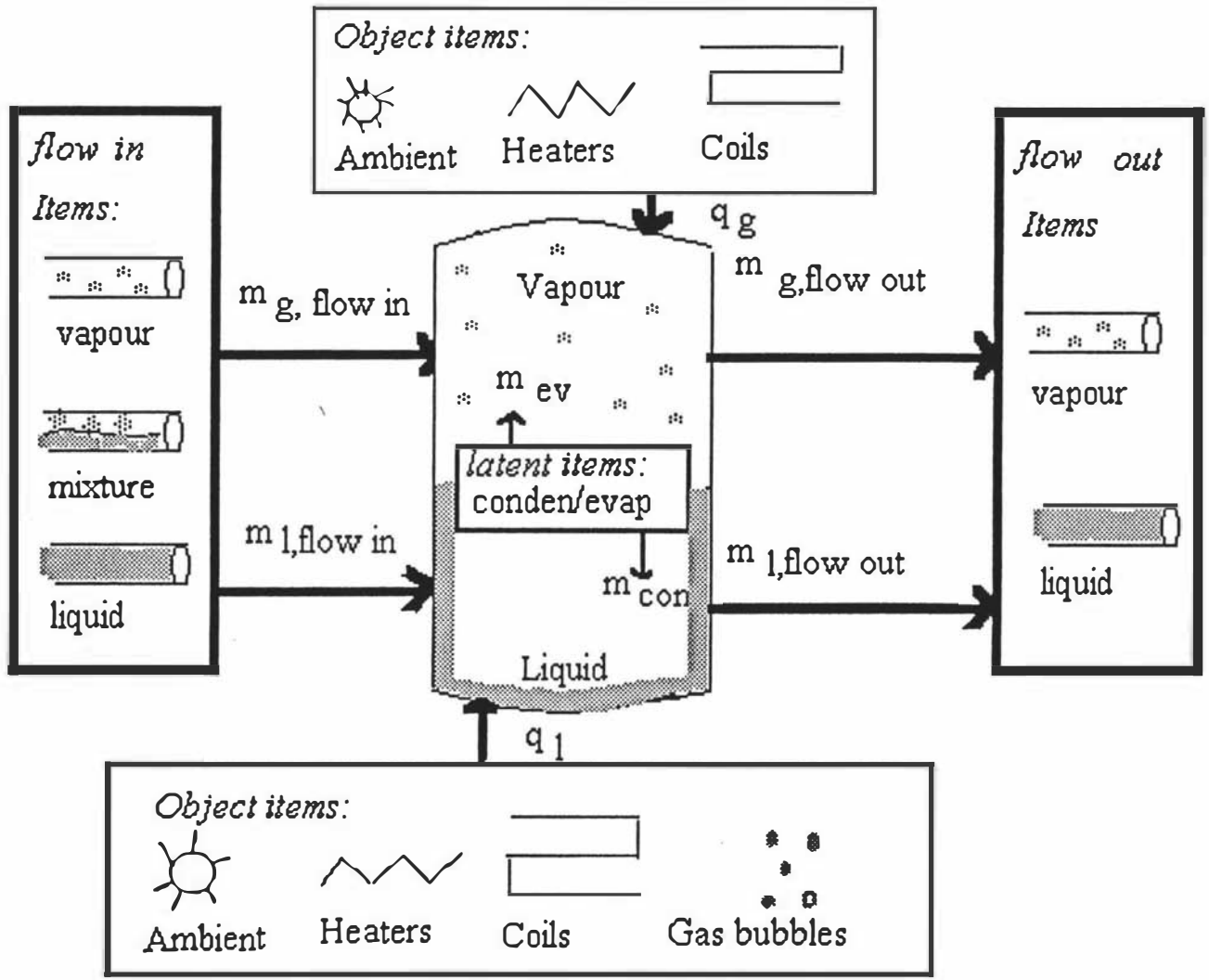

Figure 8.2. Conceptual model for pressure vessels

The basic assumptions were:

1) The vessel contents were divided into two zones: liquid and vapour. It follows that heat flow by convection between phases would be possible as well as condensation and evaporation flows crossing the internal boundary between zones.
2) The zones were assumed to be internally perfectly mixed, *i.e.* no gradients of properties (temperature, vapour quality, etc) could exist in the fluid within the boundaries of each zone.
3) All flows entering the vessel containing refrigerant mixtures were assumed to separate instantly, with liquid flows entering the liquid phase and vapour flows entering the vapour phase.
4) The liquid zone could exist in either a saturated or subcooled state, but not superheated - instantaneous boiling to re-establish a saturated state was assumed in such circumstances.
5) The vapour zone could exist in either a saturated or superheated state, but not supercooled - instantaneous condensation to re-establish a saturated state was assumed in such circumstances.
6) The objects assumed to interact with the vessel contents by heat exchange only were the external environment and direct heating/cooling structures physically located within the vessel such as heaters or liquid subcooling coils.
7) The infiltration of heat through the walls of the vessel was modelled using a two-zone lumped model, considering the insulation layer as a pure resistive material and the metallic shell as a pure capacitive layer (see Chapter 4). Also, two zones were considered in the longitudinal direction of the metallic shell: One for the metal in contact with the liquid zone and one for the metal in contact with the vapour zone. Heat transfer by conduction and convection occurred from the external environment to the shell and heat transfer by convection was assumed to occur between the shell and vessel contents. No heat transfer between the two longitudinal zones of the metallic shell was considered.
8) No thermal capacity was attributed to coil pipes or to heating elements. Though coil pipes may have significant thermal capacity, this becomes less significant when large plants are considered. This point is further discussed in Chapter 9.
10) The density of the liquid zone was assumed constant.

The existence of a stream of superheated vapour being bubbled into the liquid zone and cooled by convection is also possible. It might be assumed that the stream interacts by mass exchange with the vapour phase once it leaves the liquid boundary, but not by heat exchange. However, the conceptual model visualised this situation differently by assuming that the superheated stream joins the vapour phase conserving its superheated properties. A convective heat flow to the liquid phase then represents the cooling of the bubbles and this heat flow is subtracted from the vapour phase. As a consequence, the mass and heat exchanges in this situation are modelled independently of each other.

Evaporation or condensation flows between phases are usually a consequence of pressure changes and/or heating/cooling sources inside the vessel, thus leading to a phase change of some refrigerant to restore equilibrium in the vapour or liquid zone. These flows were categorised as *latent* items. Their main characteristic is that they are mass and energy flows created inside the system (vessel), thus differing from the *flow in* and *flow out* items described earlier.

8.3. Energy and work considerations in the energy balance.

The energy transients of a pressure vessel must be described in terms of the thermodynamic properties of the liquid and vapour present in the system rather than the "resistance only" or "capacity only" sub-models used in Chapter 4. The conceptual and mathematical models for a thermal object have to be translated to equivalent expressions using internal energies, enthalpies, temperature-pressure relationships, densities or specific volumes, and the liquid-vapour state equations.

Most of the mathematical models of plant components surveyed in Chapter 2 were stated in terms of the incoming and outgoing flows of energy and the general form of an overall energy balance was implied rather than directly stated. In the present approach the complete energy balance was developed from the basic definitions of total energy, internal energy, enthalpy and work.

The statement of the first law energy balance is as follows:

$$\begin{pmatrix} \textit{Rate of energy} \\ \textit{accumulation} \\ \textit{within the system} \end{pmatrix} = \Sigma \begin{pmatrix} \textit{Rate of energy} \\ \textit{addition by flows in} \end{pmatrix} - \Sigma \begin{pmatrix} \textit{Rate of energy} \\ \textit{removed by flows out} \end{pmatrix} + \Sigma \begin{pmatrix} \textit{Rate of heat} \\ \textit{addition by} \\ \textit{object items} \end{pmatrix} - \Sigma \begin{pmatrix} \textit{Rate of work done by} \\ \textit{the system} \end{pmatrix} \tag{8.1}$$

The total work done by the system has two components: external work and the flow work associated with movements of flows over the system boundaries. Thus, the total work is expressed as:

$$\begin{pmatrix} \textit{Total work done} \\ \textit{by the system} \end{pmatrix} = \Sigma \left(\textit{Flow work of flows out}\right) - \Sigma \left(\textit{Flow work of flows in}\right) + \Sigma \begin{pmatrix} \textit{External} \\ \textit{(shaft) work done by} \\ \textit{the system} \end{pmatrix} \tag{8.2}$$

From Eq.(8.1), the overall energy balance can be expressed as:

$$\frac{dE_T}{dt} = \Sigma m_{flows\,in}\, e_{flows\,in} - \Sigma m_{flows\,out}\, e_{flows\,out} + \Sigma q_{object} - \Sigma w_T \tag{8.3}$$

where:

E_T	=	total energy of the system (J)
$e_{flow\,in}$, $e_{flow\,out}$	=	specific total energies of *flow in* and *flow out* streams (J/kg)
$m_{flow\,in}$, $m_{flow\,out}$	=	mass flow rates of *flow in* and *flow out* streams (kg/s)
q_{object}	=	heat flow added by the object items (W)
w_T	=	work done by the system (W).

Kinetic and potential energy should be small, thus Eq.(8.3) becomes:

$$\frac{dU_T}{dt} = \Sigma m_{flows\,in}\, u_{flows\,in} - \Sigma m_{flows\,out}\, u_{flows\,out} + \Sigma q_{object} - \Sigma w_T \tag{8.4}$$

where:

U_T	=	internal energy of the system (J)
$u_{flow\,in}$, $u_{flow\,out}$	=	specific internal energies of the *flow in* and *flow out* items (J/kg).

Analyzing w_T in Eqs.(8.2) to (8.4) in relation to Fig. 8.2, it can be seen that there is no external work done by the system as a whole. However, when the system is split into the liquid and vapour zones defined in Section 8.2 there is potential for a net interchange of work between phases. Figure 8.3 presents a visualisation of the vessel system as an incompressible liquid phase acting as a piston against the compressible vapour phase. If the liquid-vapour interface is the working surface, it follows that at every change in the liquid level work is performed on the vapour zone.

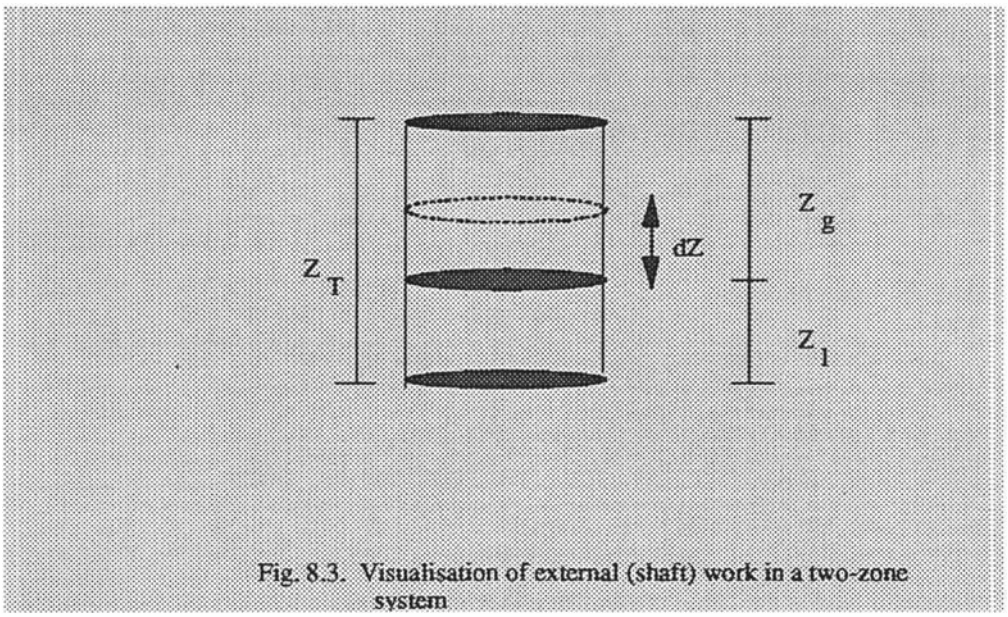

Fig. 8.3. Visualisation of external (shaft) work in a two-zone system

The work done by the liquid on the vapour by a small change in vapour height $d\,Z_g$ can be defined as:

$$dW_s = - p_g\, A\, dZ_g \tag{8.5}$$

where:

W_s	=	work performed by liquid zone (J)
A	=	area of contact liquid-vapour (m^2)
p_g	=	pressure applied at the liquid/vapour interface, also the pressure in the vapour zone (Pa).
Z_g	=	level of the vapour zone with respect to the level liquid (m)

If Eq.(8.5) is stated in terms of the rate of external work w_s (W) by the liquid:

$$w_s = \frac{dW_s}{dt} = - p_g\, A\, \frac{dZ_g}{dt} \tag{8.6}$$

Now, $Z_g = Z_T - Z_l$ and thus Eq.(8.4) can be rewritten as:

$$w_s = - p_g A \frac{d(Z_T - Z_l)}{dt} \tag{8.7}$$

where:

Z_T	=	total height of vessel (m)
Z_l	=	liquid level inside the vessel (m)

Z_T is a constant and w_s can be expressed directly in terms of the change of the liquid level and the pressure of the vapour phase:

$$w_s = p_g A \frac{dZ_l}{dt} \tag{8.8}$$

A similar expression for the vapour zone receiving the work can be developed, but a change of sign is required to show that the work is being done on the zone.

The second component of the work relates to the streams entering and leaving the system. For stream i at pressure p_i (Pa) entering a zone, the flow work for 1 kg to be forced over the boundary of the system can be expressed as:

$$w_{fi} = p_i v_i \tag{8.9}$$

where:

w_{fi}	=	specific flow work of flow i (J/kg).
p_i	=	stream pressure (Pa)
v_i	=	specific volume of flow i (m^3/kg)

Hence, substituting Eq.(8.9) into Eq.(8.2) the definition of total work becomes:

$$w_T = \Sigma (m\ p\ v)_{flows\ out} - \Sigma (m\ p\ v)_{flows\ in} + w_s \tag{8.10}$$

And the overall energy balance is expressed as:

$$\frac{dU_T}{dt} = \Sigma m_{flows\ in}\ u_{flows\ in} - \Sigma m_{flows\ out}\ u_{flows\ out} + \Sigma q_{object} + \Sigma (m\ p\ v)_{flows\ in} - \Sigma (m\ p\ v)_{flows\ out} - w_s \tag{8.11}$$

or:

$$\frac{dU_T}{dt} = \Sigma m_{flows\ in}\,(u + p\,v)_{flows\ in} - \Sigma m_{flows\ out}\,(u + p\,v)_{flows\ out} + \Sigma q_{object} - w_s \qquad (8.12)$$

The definition of the enthalpy h (J/kg) is $u + pv$ and Eq. (8.12) can be expressed as:

$$\frac{dU_T}{dt} = \Sigma m_{flows\ in}\,h_{flows\ in} - \Sigma m_{flows\ out}\,h_{flows\ out} + \Sigma q_{object} - w_s \qquad (8.13)$$

Thus the right hand side of the overall energy balance has been derived in a general fashion.

Considering now the left hand side of Eq.(8.13) for a zone containing M_T kg of homogeneous fluid it follows that:

$$\frac{dU_T}{dt} = \frac{d(M_T\,u_T)}{dt} = M_T\,\frac{du_T}{dt} + u_T\,\frac{dM_T}{dt} \qquad (8.14)$$

A mass balance allows the mass differential term $\frac{dM_T}{dt}$ to be determined by an algebraic equation as:

$$\frac{dM_T}{dt} = \Sigma\, m_{flows\,in} - \Sigma\, m_{flows\,out} \qquad (8.15)$$

Thus the left hand side of Eq.(8.13) becomes:

$$\frac{dU_T}{dt} = M_T\,\frac{du_T}{dt} + u_T\,(\Sigma\, m_{flows\ in} - \Sigma m_{flows\ out}) \qquad (8.16)$$

Eq. (8.16) can be substituted in Eq.(8.13) to give:

$$M_T\,\frac{du_T}{dt} = \Sigma m_{flows\,in}\,h_{flows\,in} - \Sigma m_{flows\,out}\,h_{flows\,out} + \Sigma q_{object} - w_s - u_T\,(\Sigma\, m_{flows\ in} - \Sigma\, m_{flows\,out}) \qquad (8.17)$$

The above equations have not required any knowledge of the nature of the streams entering and leaving the vessel: they can either be applied to a gas or a liquid. In order to work usefully with Eq.(8.17) which has both internal energy and enthalpy terms, u_T and h_T are usually reduced to a single variable. If the fluid is a liquid, the specific volume is small (*i.e.* high density) and the $p\ v$ term can be assumed to be negligibly small with little loss of

accuracy. It follows that $u_T \approx h_T$ and $\frac{du_T}{dt} \approx \frac{dh_T}{dt}$. Thus Eq.(8.17) becomes:

$$M_T \frac{dh_T}{dt} \approx \Sigma m_{flows\,in}\, h_{flows\,in} - \Sigma m_{flows\,out}\, h_{flowsout} + \Sigma q_{object} - w_s - h_T \left(\Sigma m_{flows\,in} - \Sigma m_{flows\,out}\right) \tag{8.18}$$

If the fluid is a gas, the $p\,v$ term could be significant. In this case, two arguments could be used:

1) Assuming that $\frac{du_T}{dt} \approx \frac{dh_T}{dt}$ (Marshall and James, 1973). This argument does not necessarily imply that $u_T = h_T$. The left hand side of Eq. (8.17) is the only term simplified:

$$M_T \frac{dh_T}{dt} \approx \Sigma m_{flows\,in}\, h_{flows\,in} - \Sigma m_{flows\,out}\, h_{flowsout} + \Sigma q_{object} - w_s - \left(h_T - p_T\, v_T\right) \left(\Sigma m_{flows\,in} - \Sigma m_{flows\,out}\right) \tag{8.19}$$

2) Using the correct expression for the derivative of the specific internal energy, considering the $p\,v$ term in both sides of the balance. Thus, the derivative of the specific internal energy is expressed as:

$$\frac{du_T}{dt} = \frac{d\left(h_T - p_T\, v_T\right)}{dt} \tag{8.20}$$

or:

$$\frac{du_T}{dt} = \frac{dh_T}{dt} - \left(v_T \frac{dp_T}{dt} + p_T \frac{dv_T}{dt}\right) \tag{8.21}$$

and Eq.(8.17) becomes:

$$\frac{dh_T}{dt} = \left(\frac{B_1 + \Sigma q_{object} - w_s - B_2 \left(h_T - p_T\, v_T\right)}{M_T}\right) + v_T \frac{dp_T}{dt} + p_T \frac{dv_T}{dt} \tag{8.22}$$

where:

$$B_1 = \Sigma m_{flows\,in}\, h_{flows\,in} - \Sigma m_{flows\,out}\, h_{flowsout}$$

$$B_2 = \Sigma m_{flows\,in} - \Sigma m_{flows\,out}$$

From these equations it is possible to draw the following conclusions:

a) The so-called enthalpy balances (Eqs (8.18) and (8.19)) might not be closely equivalent to the full energy balance, unless the streams involved are all liquid refrigerant or the $p\ v$ product can be proved negligibly small. Hence, whilst for liquids it might be acceptable to express the energy balance in enthalpy terms, the use of internal energies is certainly preferred for gases.

b) The approximation used in Eq.(8.19) might be valid for certain cases, but its influence on the accuracy of the predictions has not been systematically investigated in previous reports. A comparison of the derivatives of internal energies and enthalpies with respect to time might help to assess the impact of this simplification.

Bearing these considerations in mind, the mathematical descriptions of the 4 models derived from the general cases above can be summarised in the equations given below.

8.4. Model A): Two-zone model based on a full energy balance.

8.4.1. Mass balance equations.

The general model of liquid and vapour zones within the vessel presented in Fig. 8.2 comprised the following mass balance equations which follow Eq.(8.15) with the addition of explicit terms for condensation and evaporation:

$$\frac{dM_l}{dt} = \Sigma m_{l,\ flows\ in} - \Sigma m_{l,\ flows\ out} - m_{ev} + m_{con} \tag{8.23}$$

where:

M_l = mass of liquid inside the vessel (kg)

$m_{l,\ flow\ in}$ = mass flow rates of liquid flows entering the vessel (kg/s)

$m_{l,\ flow\ out}$ = mass flow rates of liquid flows leaving the vessel (kg/s)

m_{con} = mass flow rate of refrigerant condensed from the vapour to the liquid zone (kg/s)

m_{ev} = mass flow rate of refrigerant evaporated from the liquid to the vapour zone (kg/s)

$$\frac{dM_g}{dt} = \Sigma m_{g,\ flows\ in} - \Sigma m_{g,\ flows\ out} + m_{ev} - m_{con} \tag{8.24}$$

where:

M_g = mass of vapour inside the vessel (kg)

$m_{g,\,flow\ in}$ = mass flow rates of vapour flows entering the vessel (kg/s)

$m_{g,\,flow\ out}$ = mass flow rates of vapour flows leaving the vessel (kg/s)

Using the definition of mass of liquid refrigerant inside the vessel, $M_l = A\ Z_l / v_l$, Eq. (8.23) becomes:

$$\frac{dZ_l}{dt} = \left(\frac{\Sigma m_{l,\,flows\ in} - \Sigma m_{l,\,flows\ out} - m_{ev} + m_{con}}{A} \right) v_l \tag{8.25}$$

where:

A = cross-sectional area of the vessel (m^2)

v_l = specific volume of liquid phase (m^3/kg)

Similarly, the expression for the mass of vapour contained in the vessel $M_g = A\ Z_g / v_g$ is substituted in the left hand side of Eq.(8.24) which becomes:

$$\frac{d\left(\frac{A\ Z_g}{v_g}\right)}{dt} = \frac{A}{v_g}\left(\frac{d\ Z_g}{dt}\right) + A\ Z_g\left[\frac{d\left(\frac{1}{v_g}\right)}{dt}\right] \tag{8.26}$$

where:

v_g = specific volume of vapour phase (m^3/kg)

Following the same logic as used in Eq. (8.7) for the $\frac{dZ_g}{dt}$ term and using Eq.(8.25) to substitute an algebraic expression for $\frac{dZ_l}{dt}$, Eq. (8.26) becomes:

$$\frac{d\left(\frac{A\ Z_g}{v_g}\right)}{dt} = A\ Z_g\left[\frac{d\left(\frac{1}{v_g}\right)}{dt}\right] - \left(\frac{\Sigma\ m_{flows\ in} - \Sigma\ m_{flows\ out} - m_{ev} + m_{con}}{v_g}\right) v_l \tag{8.27}$$

Finally, after substitution of Eq.(8.27) into Eq.(8.24) and subsequent manipulation of the resulting expression, an equation for evaluating the change of the specific volume of the vapour with time is obtained:

$$\frac{d\left(\frac{1}{v_g}\right)}{dt} = \frac{\left(\frac{v_l}{v_g}\left(\Sigma m_{l,\,flows\,in} - \Sigma m_{l,\,flows\,out}\right) + \left(m_{ev} - m_{con}\right)\left(1 - \frac{v_l}{v_g}\right) + \Sigma m_{g,\,flows\,in} - \Sigma m_{g\,flows\,out}\right)}{A\left(Z_T - Z_l\right)} \tag{8.28}$$

8.4.2. Energy balance equations.

The energy balance equation for the liquid zone was directly expressed in the form of Eq.(8.18), with the sole exception of the addition of explicit terms accounting for condensation and evaporation phenomena:

$$\begin{aligned} M_l \frac{dh_l}{dt} \approx\ & \Sigma m_{l,flows\,in}\, h_{l,flows\,in} - \Sigma m_{l\,flows\,out}\, h_{l,flowsout} \\ & + \Sigma q_{object} - w_s - m_{ev}\, h_{g,sat} + m_{con}\, h_{l,sat} \\ & - h_l\left(\Sigma m_{l\,flows\,in} - \Sigma m_{l\,flows\,out}\right) - h_l\left(m_{con} - m_{ev}\right) \end{aligned} \tag{8.29}$$

where all the properties from the liquid zone have a subscript l and w_s is the external work (W) derived from Eqs.(8.8) and (8.25):

$$w_s = p_g\, v_l \left(\Sigma m_{l\,flows\,in} - \Sigma m_{l\,flows\,out} - m_{ev} + m_{con}\right) \tag{8.30}$$

$h_{l,\,flow\,in}$	=	enthalpy of liquid flows entering the vessel (J/kg)
$h_{l,\,flow\,out}$	=	enthalpy of liquid flows leaving the vessel = enthalpy of liquid zone h_l (J/kg)
h_l	=	enthalpy of liquid zone (J/kg)
$h_{g\,sat}$	=	enthalpy of saturated vapour at pressure p_g (J/kg)
$h_{l\,sat}$	=	enthalpy of saturated liquid at pressure p_g (J/kg)

When no mass flows are entering or leaving the vessel, Eq.(8.29) can be further simplified to:

$$M_l \frac{dh_l}{dt} \approx \Sigma q_{object} - w_s - m_{ev}\left(h_{g,sat} - h_{lsat}\right) + m_{con}\left(h_{l,sat} - h_l\right) \tag{8.31}$$

The expression for the vapour zone energy balance follows from Eq. (8.22) with the addition of explicit terms accounting for condensation and evaporation:

$$\frac{dh_g}{dt} = \left(\frac{B_1 + \Sigma q_{object} - w_s - B_2 \left(h_g - p_g v_g \right) + B_3}{M_g} \right) + v_g \frac{dp_g}{dt} + p_g \frac{dv_g}{dt} \tag{8.32}$$

where all the properties from the vapour zone are identified by the subscript g and:

$$B_1 = \Sigma m_{g\,flows\,in}\, h_{g,flows\,in} - \Sigma m_{g\,flows\,out}\, h_{g,flows\,out} \tag{8.32a}$$

$$B_2 = \Sigma m_{g\,flows\,in} - \Sigma m_{g\,flows\,out} + m_{ev} - m_{con} \tag{8.32b}$$

$$B_3 = m_{ev}\, h_{g,sat} - m_{con}\, h_{l,sat} \tag{8.32c}$$

h_g	=	enthalpy of vapour zone (J/kg)
$h_{g,flow\,in}$	=	enthalpy of vapour flows entering the vessel (kg/s)
$h_{g,flow\,out}$	=	enthalpy of vapour flows leaving the vessel (J/kg) = enthalpy of vapour zone h_g
w_s	=	external work as defined in Eq (8.30) (W)

Similarly to Eq. (8.29), when no mass flows are entering or leaving the vessel, Eq.(8.32) can be simplified to the following expression:

$$\frac{dh_g}{dt} = \left(\frac{\Sigma q_{object} + w_s + m_{ev} \left(h_{g,sat} - h_g \right) - m_{con} \left(h_{lsat} - h_g \right) + p_g v_g \frac{dM_g}{dt}}{M_g} \right) + v_g \frac{dp_g}{dt} + p_g \frac{dv_g}{dt} \tag{8.33}$$

8.4.3. Implementation of balance equations.

The mathematical model was implemented in a TurboPascal programme (Vess11.Pas). The source code, a detailed explanation of the programme and data files examples are given in Appendices A2 and A3. In general terms, this programme was structured to deal with 6 main features:

a) The numerical solution of the 4 ordinary differential Eqs. (8.25), (8.28), (8.31) and (8.33).

b) The evaluation of temperatures and pressures for the liquid and vapour zones

and the refrigerant thermodynamic routines for evaluating these.

c) The modelling of *object* items.

d) The calculation of *latent* items m_{ev} and m_{con}.

e) The transition criteria when a change of state between saturated and unsaturated conditions occurs.

A complete listing of the program is presented on Appendix 8.1. A discussion about the implementation of each of these parts is given below.

8.4.3.1. Numerical solution for the ordinary differential equations.

A numerical solution using the 4th order Runge - Kutta procedure was selected. Its implementation demands the evaluation and updating of the parameters linked to the ODE's values (such as pressures and temperatures) within each time step. The criteria used for evaluating the state of both zones and the calculation techniques used for each state and transitions are discussed below.

8.4.3.2. Modelling of temperatures and pressures for the liquid and vapour zones and refrigerant thermodynamic routines.

a) Liquid zone: The pressure of the vessel was assumed to be homogeneous in both zones (Section 8.2, assumptions 4 and 10). Hence, the pressure of the whole system was established according to the vapour zone energy and mass balances.

The liquid zone can have the thermodynamic properties of one of the following states:

- Subcooled liquid: The enthalpy of the subcooled liquid was found through Eq. (8.29). The degrees of subcooling *sc* (°C) were calculated as:

$$sc = \left(\frac{h_{l,sat} - h_l}{c_l} \right) \tag{8.34}$$

where:

c_l = specific heat capacity (J/kg K) at pressure p_g, assumed to be temperature independent.

sc = degrees of subcooling (°C)

Hence, the temperature of the liquid is defined as:

$$T_l = T_{l,\,sat} - sc \tag{8.35}$$

where:

$T_{l,sat}$ = Temperature of the liquid at p_g (°C)

- Saturated liquid: In this case, the enthalpy of the liquid must be the saturated enthalpy $h_{l\,sat}$ at the pressure p_g. Thus, the temperature of the liquid has to be the saturation temperature $T_{l\,sat}$ at p_g.

b) Vapour zone: An especially challenging issue was to derive a methodology to calculate the pressure p_g whilst knowing only the enthalpy h_g and specific volume v_g of the vapour phase. The vapour zone can have the thermodynamic properties of one of the following states:

- Saturated vapour: A direct correspondence exists between the saturated temperature of the vapour zone and the known saturated specific volume, *i.e.* $T_g = T_{g\,sat}$ at p_g and $v_g = v_{g\,sat}$ at p_g or T_g.

- Superheated vapour: The thermodynamic data equations relating the specific volume and the temperature that were used required the knowledge of the extent of superheating. Thus, an iterative routine relating the degrees of superheating s, p_g, v_g and h_g was required. This procedure is outlined below:

  1) A first estimate of the actual saturation temperature of vapour $T_{g,sat}$ (°C) was calculated from the vapour specific volume assuming that no superheating was present. An iterative solution of an empirical equation (Cleland, 1986) was used:

$$v_g = \exp\left(Y_1 + \frac{Y_2}{(T_{g,sat} + 273.15)}\right)\left(Y_3 + Y_4\,T_{g,sat} + Y_5\,T_{g,sat}^2 + Y_6\,T_{g,sat}^3\right) \tag{8.36}$$

  where Y_1 to Y_6 are constants specific to the refrigerant.

  2) An initial guess of $p_g = p_{g\,sat}$ at $T_{g\,sat}$ was set, calculating the latter through an equation of the form:

$$p_{g,sat} = \exp\left(y_1 + \frac{y_2}{(T_{g,sat} + y_3)}\right) \tag{8.37}$$

where y_1 to y_3 are constants specific to the type of refrigerant (Cleland, 1986).

3) Further specific volume and enthalpy estimates were calculated assuming 10 °C of superheating. The enthalpy at this state, $h_{g,s=10}$, was calculated using the polynomial equations of Cleland (1986):

$$h_{g,sat} = F_1 + F_2 T_{g,sat} + F_3 T_{g,sat}^2 + F_4 T_{g,sat}^3 \tag{8.38}$$

$$h_{g,s=10} = h_{g,sat}\left(1 + f_1 + f_2 s + f_3 s^2 + f_4 T_{g,sat} s + f_5 T_{g,sat} s^2 + f_6 T_{g,sat}^2 s + f_7 s^2 T_{g,sat}^2\right) \tag{8.39}$$

where:

s	=	vapour superheat (°C)
F_1 to F_4	=	constants depending on the type of refrigerant
f_1 to f_7	=	constants depending on the type of refrigerant

4) The internal energies of saturated and superheated states were calculated as follows:

$$u_{g,sat} = h_{g,sat} - p_g v_{g,sat} \tag{8.40}$$

$$u_{g,s=10} = h_{g,s=10} - p_g v_{g,s=10} \tag{8.41}$$

5) The specific heat capacity c_g was estimated using:

$$c_g \approx \left(\frac{u_{g,s=10} - u_{g,sat}}{10}\right) \tag{8.42}$$

6) The extent of superheating was estimated from:

$$s \approx \left(\frac{u_g - u_{g,sat}}{c_g}\right) \tag{8.43}$$

where u_g was calculated from h_g and v_g and the latest estimate of p_g which was changing throughout the whole iterative procedure.

7) When $s <= 0$, the internal energy u_g would have described a saturated

vapour (or a subcooled vapour, assumed to change instantly to the saturation conditions). In such cases,the following steps were used:

- $s = 0$
- determine $T_{g\,sat}$ through an iterative procedure such that $\boldsymbol{h}_{g\,sat} = \boldsymbol{h}_g$
- estimate p_g as the saturation pressure at $T_{g\,sat}$
- define $u_g = u_{g\,sat} = \boldsymbol{h}_{g\,sat} - p_g\, v_{g\,sat}$

and the calculation procedure changed to that used for the saturation state.

When $s>0$, the vapour was superheated and an apparent specific volume $v_{g,it}$ was calculated as:

$$v_{g\,sat} = \exp\left(Y_1 + \frac{Y_2}{(T_{g,sat} + 273.15)}\right)\left(Y_3 + Y_4\, T_{g,sat} + Y_5\, T_{g,sat}^2 + Y_6\, T_{g,sat}^3\right) \tag{8.44}$$

$$v_{g\,it} = v_{g,sat}\left(1 + ff_1 + ff_2\, s + ff_3\, s^2 + ff_4\, T_{g,sat}\, s + ff_5\, T_{g,sat}\, s^2 + ff_6\, T_{g,sat}^2\, s + ff_7\, s^2\, T_{g,sat}^2\right) \tag{8.45}$$

where ff_1 to ff_7 and Y_1 to Y_6 are constants specific to the refrigerant.

8) A new estimate of p_g was evaluated as:

$$p_{g,new} = p_{g,old}\left(\frac{v_{g,it}}{v_g}\right) \tag{8.46}$$

9) A value of $T_{g\,sat}$ corresponding to the new p_g was estimated through Eq. (8.35) and the calculation repeated from step 3.

10) The criteria used to stop the iteration were set according to 3 parameters: $T_{g,sat}$, s and p_g. The results were assumed to be accurate if the following criteria was fulfilled:

- When the squared difference of the new and old estimates of $T_{g,sat}$ was less than $1\text{x}10^{-8}$ °C^2
- When the squared difference of the new and old estimates of s was less than $1\text{x}10^{-8}$ °C^2
- When the ratio of the new and old estimates of p_g was $1 \pm crit$ and $crit$

was less than $1x10^{-10}$

This procedure was found to be acceptable to find the pressure and temperature for both superheated and saturated vapour regimes.

8.4.3.3. Modelling of object items.

Algebraic equations can be added to the model in order to simulate heat flow from interacting objects. Some examples are given below:

a) Energy exchange with the external environment through the vessel shell: the thermal mass of the vessel may contribute significantly to the transients of the liquid and vapour, acting as a "buffering" structure and using part of the energy entering the system. One-dimensional heat transfer to the surface of the metallic shell was assumed to occur through the insulation. As stated in Section 8.2 (assumption 7), the shell capacity model used one ODE for each zone:

$$M_{shell}\, c_{shell} \left(\frac{d T_{shell}}{d t} \right) = q_{amb \rightarrow vessel} - q_{vessel \rightarrow zone} \tag{8.47}$$

where:

$$q_{amb \rightarrow vessel} = \left[\left(\frac{\pi\, Rad_3^2}{\mathbf{R}_{11} + \mathbf{R}_{22}} \right) + \left(\frac{1}{\mathbf{R}_1 + \mathbf{R}_2} \right) \right] \left(T_{amb} - T_{shell} \right) \tag{8.47a}$$

$$\mathbf{R}_1 = \frac{1}{2\, \pi\, Rad_3\, h_{amb \rightarrow vessel}\, Z_{zone}} \tag{8.47b}$$

$$\mathbf{R}_2 = \frac{\ln \left(\frac{Rad_3}{Rad_2} \right)}{2\, \pi\, \lambda_{insul}\, Z_{zone}} \tag{8.47c}$$

$$\mathbf{R}_{11} = \frac{1}{h_{amb \rightarrow vessel}} \tag{8.47d}$$

$$\mathbf{R}_{22} = \frac{x_{insul}}{\lambda_{insul}} \tag{8.47e}$$

$$q_{vessel \rightarrow zone} = \left(2\ \pi\ Rad_1\ Z_{zone} + \pi\ Rad_1^{\,2}\right) h_{vessel \rightarrow zone} \left(T_{shell} - T_{zone}\right) \tag{8.47f}$$

Fig.8.4 illustrates the terms Rad_1, Rad_2, Rad_3, x_{insul} and x_{shell} used for the calculations and:

$q_{amb \rightarrow vessel}$	=	heat flow from the external environment to the external surface of the metallic shell (W)
$q_{vessel \rightarrow zone}$	=	heat flow from the internal surface of the metallic shell to the zone (W)
$\mathbf{R}_1$	=	external thermal resistance ambient-to shell, transversal area (m^2 K/W)
$\mathbf{R}_2$	=	thermal resistance of insulation, transversal area (m^2 K/W)
$\mathbf{R}_{11}$	=	external thermal resistance ambient-to shell, flat bottom and top (m^2 K/W)
$\mathbf{R}_{22}$	=	thermal resistance of insulation, flat bottom and top (m^2 K/W)
T_{shell}	=	temperature of metallic shell (°C)
T_{amb}	=	external ambient temperature (°C)
T_{zone}	=	liquid or vapour zone temperature (°C)
$h_{amb \rightarrow vessel}$	=	heat transfer coefficient, external environment-to-vessel (W)
$h_{vessel \rightarrow zone}$	=	heat transfer coefficient, shell-to-fluid (W)
M_{shell}	=	Mass of metallic shell (kg)
c_{shell}	=	specific heat capacity of metallic shell (J/kg K)

According to the lumped model selected, the accumulation of energy within the shell was assumed to occur in the metallic layer. The top and the bottom of the vessel were assumed to have a totally flat geometry in order to simplify the situation. The error introduced due to this assumption was expected to be small.

b) Addition/removal of energy through an object inside a zone: These items were modelled through the general equation:

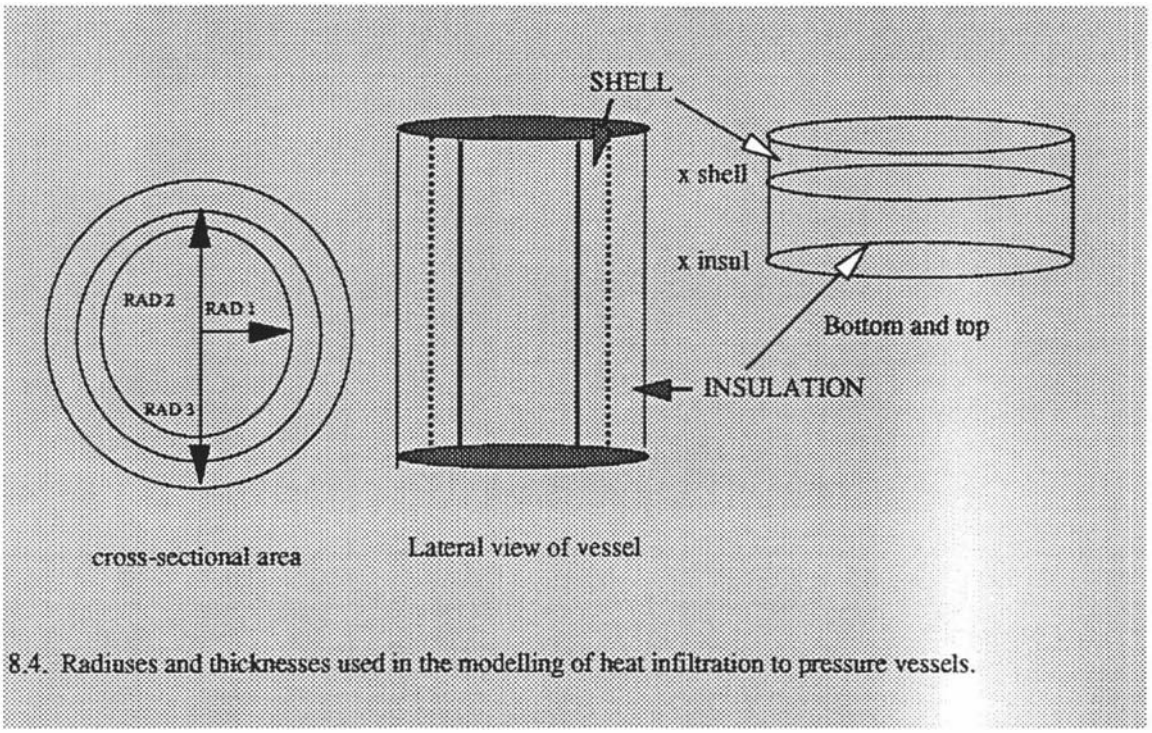

8.4. Radiuses and thicknesses used in the modelling of heat infiltration to pressure vessels.

$$q_{object} = h_{object \rightarrow zone} A_{object} \left(T_{object} - T_{zone}\right) \tag{8.48}$$

where:

q_{object}	=	heat flow from object to zone (W)
$h_{object \rightarrow zone}$	=	heat transfer coefficient object-to-zone (W/m^2 K)
T_{object}, T_{zone}	=	temperature of the object and zone, respectively (°C)
A_{object}	=	area of contact between object and zone (m^2)

The thermal capacity of the object was neglected and constant, homogeneous conditions (temperature and heat transfer coefficients) across the object's outer surface were assumed.

This simple approach was used in order to avoid complexity in secondary models such as the *object* items. However, other alternatives for modelling these, *e.g.* experimental correlations to determine the change of h respect to the temperature gradient for specific object-to-fluid situations could be used instead. Empirical correlations for h are available from Bejan (1994) for two phase flow systems such as gas bubbles dispersed in a liquid phase and heating elements provoking boiling of a substance.

If more sophisticated object sub-models are required, the structure of the program would essentially remain unchanged.

8.4.3.4. Modelling of *Latent* items: calculation of evaporation and condensation flows m_{ev} and m_{con}.

The possible states for the liquid and vapour zones and the calculation procedure are summarised in Table 8.1.

The energy and mass balances of the two zones requires the knowledge of the state of the vapour and liquid so that the interzone flows can be defined. The criteria used to define the state of the liquid and vapour were:

a) For vapour, if $u_g > u_{g\,sat}$ at p_g the vapour state was superheated and $m_{con} = 0$.

b) For liquids, if $u_l < u_{l\,sat}$ at p_g the liquid state was subcooled and $m_{ev} = 0$.

c) In any other cases, the vapour or liquid were assumed to be saturated, thus $m_{con} >= 0$ and $m_{ev} >= 0$.

The latter criterion (also specified in Section 8.2, assumptions 4 and 5) implies that in cases in which the zone (either liquid or vapour) properties define a mixture, instantaneous separation of vapour and liquid occur and the zone affected would adopt saturated properties. If the zone is saturated, then the rate of evaporation and/or condensation between zones must be such that saturation continues.

	SATURATED LIQUID	SUBCOOLED LIQUID
SAT VAPOUR	m_{ev} : *Eq*.8.50 (*algebraic*) m_{con} : *Eq*.8.51 (*algebraic*) Z_l : *Eq*.8.25 (*ODE*) v_g : *Eq*.8.28 (*ODE*) $p_g = f(\boldsymbol{h}_{g,sat}, v_g)$ $s = 0$ $\boldsymbol{h}_l = \boldsymbol{h}_{l,sat} = f(p_g)$ $\boldsymbol{h}_g = \boldsymbol{h}_{g,sat} = f(p_g)$ $sc = 0$ $u_g = u_{g,sat} = \boldsymbol{h}_{g,sat} - p_g\, v_{g,sat}$	$m_{ev} = 0$ m_{con} : *Eq*.8.51 (*algebraic*) Z_l : *Eq*.8.25 (*ODE*) p_g : $f(\boldsymbol{h}_{g,sat}, v_g)$ $\boldsymbol{h}_l$: *Eq*.8.31 (*ODE*) v_g : *Eq*.8.28 (*ODE*) $s = 0$ $\boldsymbol{h}_g = \boldsymbol{h}_{g,sat} = f(p_g)$ $sc > 0$ $u_g = u_{g,sat} = \boldsymbol{h}_{g,sat} - p_g\, v_{g,sat}$
S.HEAT VAPOUR	m_{ev} : *Eq*.8.50 (*algebraic*) $m_{con} = 0$ Z_l : *Eq*.8.25 (*ODE*) $\boldsymbol{h}_g$: *Eq*.8.33 (*ODE*) v_g : *Eq*.8.28 (*ODE*) $p_g = f(\boldsymbol{h}_g, v_g)$ $s > 0$ $\boldsymbol{h}_l = \boldsymbol{h}_{l,sat} = f(p_g)$ $sc = 0$ $u_g = (\boldsymbol{h}_g - p_g\, v_g)$	$m_{ev} = 0$ $m_{con} = 0$ Z_l : *Eq*.8.25 (*ODE*) $\boldsymbol{h}_l$: *Eq*.8.31 (*ODE*) $\boldsymbol{h}_g$: *Eq*.8.33 (*ODE*) v_g : *Eq*.8.28 (*ODE*) $p_g = f(\boldsymbol{h}_g, v_g)$ $s > 0$ $sc > 0$ $u_g = \boldsymbol{h}_g - p_g\, v_g$

TABLE 8.1. SUMMARY OF MODELS FOR LIQUID AND VAPOUR ZONES.

The algebraic expression for calculating m_{ev} was derived by rearrangement of Eq.(8.31):

$$m_{ev} = \frac{\Sigma\, q_{object} - M_l \left(\frac{d\, h_l}{d\, t} \right) - w_s + m_{con} \left(h_{l,sat} - h_l \right)}{h_{g,sat} - h_l} \tag{8.49}$$

In saturation conditions, $h_l = h_{l\,sat}$ and this equation can be further simplified to:

$$m_{ev} = \frac{\Sigma\, q_{object} - M_l \left(\frac{d\, h_l}{d\, t} \right) - w_s}{h_{g,sat} - h_{l,sat}} \tag{8.50}$$

where the term w_s was defined in Eq. (8.30).

The external work w_s is a function of m_{ev} and m_{con}, and thus explicit calculation of these terms is not possible. However, the magnitude of the specific volume of the liquid v_l is very small. Furthermore, the use of small time steps reduces the difference between the previous estimates of m_{ev} and m_{con} and the present values. Hence, an approximation to the present value of w_s was derived using the values of m_{ev} and m_{con} from the previous time step. A more sophisticated mathematical technique would have led to longer computation times with probably few advantages in terms of improving the accuracy of the calculations.

The equation for calculating the condensation flow m_{con} was derived from Eq. (8.33), considering that $h_g = h_{g\,sat}$ in saturation conditions:

$$m_{con} = \frac{\Sigma\, q_{object} + w_s - B_5 + p_g\, v_g \frac{d\, M_g}{d\, t}}{h_{l,sat} - h_{g,sat}} \tag{8.51}$$

where:

$$B_5 = M_g \left[\frac{d\, h_g}{d\, t} - v_g \left(\frac{d\, p_g}{d\, t} \right) - p_g \left(\frac{d\, v_g}{d\, t} \right) \right] \tag{8.51a}$$

The use of Eqs. (8.50) and (8.51) implies the calculation of 5 first derivative terms: $\frac{d\, h_l}{d\, t}$, $\frac{d\, h_g}{d\, t}$, $\frac{d\, p_g}{d\, t}$, $\frac{d\, M_g}{d\, t}$ and $\frac{d\, v_g}{d\, t}$ by means other than the original ODE's

(Eqs. (8.3) and (8.33)).

First estimates of these terms were made using the following backward difference approximations:

$$\frac{d h_l}{d t} \approx \frac{\left(h_{l\,sat,time=t} - h_{l,time=t-\Delta t}\right)}{\Delta t} \tag{8.52}$$

$$\frac{d p_g}{d t} \approx \frac{\left(p_{g,time=t} - p_{g,time=t-\Delta t}\right)}{\Delta t} \tag{8.53}$$

$$\frac{d h_g}{d t} \approx \frac{\left(h_{g\,sat,time=t} - h_{g,time=t-\Delta t}\right)}{\Delta t} \tag{8.54}$$

$$\frac{d M_g}{d t} \approx \frac{\left(M_{g\,sat,time=t} - M_{g,time=t-\Delta t}\right)}{\Delta t} \tag{8.55}$$

$$\frac{d v_g}{d t} \approx \frac{\left(v_{g,time=t} - v_{g,time=t-\Delta t}\right)}{\Delta t} \tag{8.56}$$

Stable integrations could only be obtained when an iterative approach to improve these first estimates was adopted. The iterative procedure used a damped improvement scheme for averaging "old" and "new" derivative estimates. The steps followed were:

1) At the start of the time step a first estimate of the derivatives was evaluated through Eqs.(8.52) to (8.56).
2) The time step was performed using these values to obtain an estimate of the system parameters at time $t+\Delta t$.
3) A second estimate of the derivatives was calculated using the following expressions:

$$\left(\frac{d h_l}{d t}\right)_{t+\frac{\Delta t}{2}} \approx \frac{\left(h_{l\,sat,time=t+\Delta t} - h_{l,time=t}\right)}{\Delta t} \tag{8.57}$$

$$\left(\frac{dp_g}{dt}\right)_{t+\frac{\Delta t}{2}} \approx \frac{\left(p_{g,\,time=t+\Delta t} - p_{g,\,time=t}\right)}{\Delta t} \tag{8.58}$$

$$\left(\frac{dh_g}{dt}\right)_{t+\frac{\Delta t}{2}} \approx \frac{\left(h_{g\,sat,\,time=t+\Delta t} - h_{g,\,time=t}\right)}{\Delta t} \tag{8.59}$$

$$\left(\frac{dM_g}{dt}\right)_{t+\frac{\Delta t}{2}} \approx \frac{\left(M_{g\,sat,\,time=t+\Delta t} - M_{g,\,time=t}\right)}{\Delta t} \tag{8.60}$$

$$\left(\frac{dv_g}{dt}\right)_{t+\frac{\Delta t}{2}} \approx \frac{\left(v_{g,\,time=t+\Delta t} - v_{g,\,time=t}\right)}{\Delta t} \tag{8.61}$$

4) The older derivative estimates and the newer derivative estimates were averaged using a weighting factor. The expressions used were the following:

$$\left(\frac{dh_l}{dt}\right)_{new} \approx \left(\frac{dh_l}{dt}\right)_{older} Wgt + \left(\frac{dh_l}{dt}\right)_{newer} \left(1 - Wgt\right) \tag{8.62}$$

$$\left(\frac{dp_g}{dt}\right)_{new} \approx \left(\frac{dp_g}{dt}\right)_{older} Wgt + \left(\frac{dp_g}{dt}\right)_{newer} \left(1 - Wgt\right) \tag{8.63}$$

$$\left(\frac{dh_g}{dt}\right)_{new} \approx \left(\frac{dh_g}{dt}\right)_{older} Wgt + \left(\frac{dh_g}{dt}\right)_{newer} \left(1 - Wgt\right) \tag{8.64}$$

$$\left(\frac{dm_g}{dt}\right)_{new} \approx \left(\frac{dm_g}{dt}\right)_{older} Wgt + \left(\frac{dm_g}{dt}\right)_{newer} \left(1 - Wgt\right) \tag{8.65}$$

$$\left(\frac{dv_g}{dt}\right)_{new} \approx \left(\frac{dv_g}{dt}\right)_{older} Wgt + \left(\frac{dv_g}{dt}\right)_{newer} \left(1 - Wgt\right) \tag{8.66}$$

Where:

Wgt = Weighting fraction

5) The time step was repeated, using the derivative values obtained in Eqs. (8.62) to (8.66).

6) New estimates using Eqs.(8.57) to (8.61) were calculated, repeating the sequence established from 3) for a predetermined number of iterations.

The iterative procedure outlined above required the establishment of an appropriate number of iterations and weighting fraction. Test trials showed that decreasing the weighting factor increased stability, but slowed convergence, and hence computation time. Figure 8.5 shows the stability of the results with a weight of 0.25 and changing from 6 to 12 iterations in a test trial and the computation time obtained using a 100 Hz Pentium computer. Use of 12 iterations and a weighting factor of 0.25 was considered adequate and gave feasible computation times.

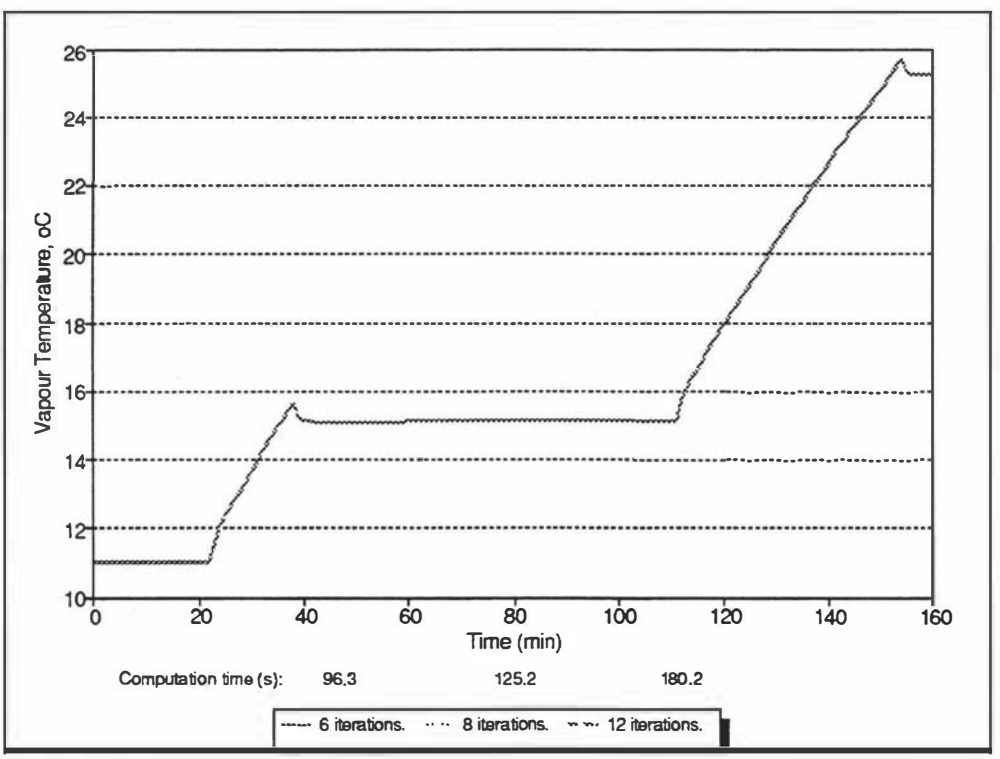

Fig. 8.5. Testing of calculation stability using a weighting factor of 0.25, changing the number of iterations. A detailed explanation of the trial conditions is given in Chapter 9 (trial 1). The computation times obtained represented an average of 3 replicates using a 100 Hz Pentium computer (16 MB RAM).

8.4.3.5. Transition criteria when a change of state between saturated and unsaturated conditions occurs.

Considering the equations for the whole system in the 4 possible scenarios (Table 8.1), two variables (Z_l and v_g) are always determined by an ODE model and two variables ($\boldsymbol{h}_l$ and $\boldsymbol{h}_g$) will vary between an algebraic model and an ODE model, depending on the thermodynamic state of the zone. During one simulation, the liquid and vapour zones might undergo a number of changes of model, according to the criteria set in Section 8.4.3.4. A scheme used to implement transition between models in the computer program was required.

Numerical errors may arise from an incorrect timing of the transition between two models: negative values of s, m_{ev}, m_{con} or sc do not have a physical meaning and thus they indicate that the wrong model is being used and the calculation must be repeated with the alternative model.

Though it would be desirable to detect the exact moment of transition and to switch immediately from one state model to the next one, the probability that a change of model coincides exactly with the end of a time step is very small. A change of model during a time step is more likely. It was decided to tolerate a small error in the timing of the response using the following scheme for transitions:

1) Continue ODE and algebraic calculations of the present model until any of the criteria for executing transition of model is activated.
2) If a change of model is detected exactly at the end of a time step, accept result and proceed to switch to new model after transition with the next time step.
3) If change of model is detected during a time step calculation, set a new time step equivalent to $\Delta t/20$ and return to the start of the ODE and algebraic calculations for the latest time step.
4) Repeat the calculations using the model before transition until change of model is detected again.
5) If change of model occurs exactly at the end of a shortened time step, accept result and proceed to switch to new model for the next shortened time step.
6) If change of model is detected during a time step, switch to the new model at the end of the shortened time step.
7) Continue ODE and algebraic calculations. After the first calculation using new model has been completed, reset time step to the original value.

The initial conditions used to restart calculations after transitions are the last values obtained from a complete but shortened time step. The error involved in this method was expected to be tolerably small due to the time step reduction method.

The specific cases that can arise are:

a) Liquid zone:

- Saturated liquid zone changing to subcooled liquid zone. This transition changes the calculation from an algebraic equation to a differential equation. A negative value in m_{ev} (which implies that h_l is less than $h_{l\,sat}$) is the indicator that initiates the transition.

- Subcooled liquid zone changing to saturated liquid zone. This transition is the reverse of the previous case, passing from an ODE to an algebraic equation. It has been previously pointed out that a zone containing a liquid-vapour mixture is treated as a saturated case. If the calculated h_l value exceeds $h_{l\,sat}$ at p_g then a transition occurs. The transition from the ODE scheme to the algebraic scheme implies that the liquid enthalpy lies on the saturation line at time t, and then moves along the saturation line during the next time step.

b) Vapour zone:

- Saturated vapour zone changing to superheated vapour zone. This transition changes the calculation from an algebraic model to an ODE model. The criterion for transition is the calculation of a negative m_{con}, since this is the first value calculated in the saturated vapour model.

- Superheated vapour zone changing to saturated vapour zone. This transition is the reverse of the previous case, passing from an ODE equation to an algebraic equation. Comparison of u_g and u_{sat} establishes whether the system has become saturated so that a transition is required.

Because some small oscillations were observed during the change between steady-and unsteady-state conditions, a tolerance band of 10 J/kg around the saturation line was established to avoid switching between models solely due to "noise" in the calculation. Thus,

if a difference greater than 10 J/kg between the ODE-predicted and saturated internal energies of liquid or vapour was observed, transition would occur.

8.5. Models B) and C): Two-zone models based on enthalpy balances

These models were derived by applying a number of simplifications to model A, thus decreasing the level of complexity of the original model. The underpinning assumption of the existence of separate liquid phase and vapour phases was applied in both models B and C.

Model B used the following simplifying assumption:

1) No work was considered to occur between phases in the system (w_s=0). Furthermore, the model followed the work of Marshall and James (1979) by introducing the following simplifications:

$$\frac{du_g}{dt} \approx \frac{dh_g}{dt} \tag{8.67}$$

$$\frac{dE_g}{dt} \approx \frac{d(M_g h_g)}{dt} \tag{8.68}$$

Thus the energy balances described in Eqs.(8.31) and (8.32) were simplified, obtaining the following expression for the liquid enthalpy:

$$M_l \frac{dh_l}{dt} \approx \Sigma q_{object} - m_{ev}\left(h_{g,sat} - h_{lsat}\right) + m_{con}\left(h_{l,sat} - h_l\right) \tag{8.69}$$

The vapour zone energy balance in Eq. (8.33) was simplified to:

$$\frac{dh_g}{dt} = \left(\frac{\Sigma q_{object} + w_s + m_{ev}\left(h_{g,sat} - h_g\right) - m_{con}\left(h_{lsat} - h_g\right) + p_g v_g \frac{dM_g}{dt}}{M_g} \right) \tag{8.70}$$

The equations used for calculating the mass flow rates of evaporated and condensed refrigerant become:

$$m_{ev} = \frac{\Sigma q_{object} - M_l \left(\frac{dh_l}{dt} \right)}{h_{g,sat} - h_{l,sat}} \tag{8.71}$$

$$m_{con} = \frac{\Sigma\, q_{object} - M_g \left(\frac{dh_g}{dt} \right) + p_g\, v_g\, \frac{dM_g}{dt}}{h_{l,sat} - h_{g,sat}} \qquad (8.72)$$

The mathematical expressions for the calculation of the liquid level and density of vapour were the same as those presented in Eqs.(8.23) to (8.26). The transition criteria and the models presented in Table 8.1 still applied.

Model C introduced a second simplification:

2) The enthalpy of the liquid zone was always calculated through Eq.(8.69) and no reconciliation with the state of the vapour was included in the mathematical model. Hence, no transition models and criteria were required. This assumption was first proposed by Marshall and James (1979).

The 4 ODE's for liquid and vapour enthalpy, specific volume and liquid level (Eqs.(8.25), (8.28), (8.69) and (8.70)) were used during the whole simulation process.

Models B and C were implemented in the programmes Vess22.Pas and Vess33.Pas, respectively, in TurboPascal language. The complete source code, a detailed explanation of the code and data files examples are given in Appendices A2 and A3.

8.6. Model D): One-zone model based on the liquid zone

This model adopted by Cleland (1986) is the least complex mathematical scheme, having the following characteristics:

1) The vessel was characterised by the dynamics of the liquid zone only. The mass of the vapour was included in the liquid mass.
2) The assumption of thermodynamic equilibrium between zones was used, the vapour phase existing at the saturation pressure corresponding to the liquid temperature. The vapour temperature was assumed to be the same as the liquid temperature.
3) The mass flow rates of liquid and vapour entering and leaving the vessel all interacted with the liquid zone.

4) Any source of heating/cooling to the vapour zone was assumed to affect the liquid zone.
5) The level of liquid was constant, *i.e.* liquid and vapour masses were also assumed to remain constant.
6) No explicit terms for evaporation or condensation were used.

A steady - state mass balance equation was derived from assumption 5:

$$\Sigma\, m_{flows\,in} = \Sigma\, m_{flows\,out,l} + \Sigma\, m_{flows\,out,g} \tag{8.73}$$

The energy balance equation was derived from Eq. (8.13):

$$M_l \frac{du_l}{dt} = M_l\, c_l \frac{dT_l}{dt} = \Sigma\, m_{flows\,in}\, h_{flows\,in} - \Sigma\, m_{flows\,out}\, h_{flows\,out} + \Sigma\, q_{object} \tag{8.74}$$

Model D assumed that the liquid zone was saturated, thus the pressure p_g was calculated directly from the temperature, according to Eq.(8.37). Hence, this model avoided the iterative routine described in Section 8.4.3.2.

Model D was implemented in a TurboPascal programme (Rads_vess.Pas). The complete source code, a detailed explanation of the code and data files examples are given in Appendices A2 and A3.

CHAPTER 9. PRESSURE VESSELS: EXPERIMENTAL VALIDATION.

Experimental validation of the dynamic models for pressure vessels required the measurement of vessel temperatures and pressures under a variety of operating conditions. Two calorimeters commonly used to assess the steady-state performance of refrigerants were used and an experimental plan to adapt the operation of a calorimeter to the dynamic purposes of the present investigation was developed.

In a broad sense, the calorimeter can be described as a refrigerant flow meter measuring the mass flow of refrigerant by calculating the enthalpy change produced by the heat input, which is known and controlled (Pearson, 1995).

A calorimeter installation typically consists of a small refrigeration plant with a compressor, a condenser, an expansion valve and an evaporator coil. The later is enclosed in an insulated cylindrical vessel containing a secondary refrigerant that might be present as both vapour and liquid, according to the vessel pressure and type of refrigerant. An electrical heater is placed in the bottom of the vessel below the liquid refrigerant level. When the heater is activated, boiling of the liquid leads to the formation of vapour which accumulates in the head space of the vessel around the evaporator coil.

9.1. Principles of the calorimeter technique to assess temperature and pressure transients.

The energy sources affecting the contents of the calorimeter vessel can be described in an energy balance:

$$\begin{pmatrix} \textit{Rate of energy} \\ \textit{accumulation} \\ \textit{in vessel} \end{pmatrix} = \begin{pmatrix} \textit{Rate of energy} \\ \textit{addition by heater} \end{pmatrix} - \begin{pmatrix} \textit{Rate of energy removal by} \\ \textit{evaporator coil} \end{pmatrix} + \begin{pmatrix} \textit{Rate of energy} \\ \textit{addition by} \\ \textit{infiltration through shell} \end{pmatrix} \tag{9.1}$$

Under steady-state, the accumulation term in the left hand side of Eq. (9.1) disappears and the balance of the system depends on the 3 energy flows.

Ideally, the thermodynamic performance of the refrigerant in the primary circuit is evaluated under steady-state conditions and so the aim of an experimental run is to maintain steady-state during the measurement of the system parameters. However, for the purposes of

this project, the main aim was to record the transient behaviour of the vessel during unsteady-state conditions. Measurements of the primary circuit parameters during steady-state conditions gave supplementary information about the system, but the focus was the transient behaviour of the secondary refrigerant after a sudden change of conditions away from steady-state.

The equipment items used were a calorimeter installed at South Bank University (London) and a calorimeter installed at Star Refrigeration Ltd (Glasgow). In both calorimeters, few or no changes from the original design were made, but the experimental methodologies differed significantly from the commonly used techniques for calorimetric measurements.

9.2. Description of experimental facilities.

The calorimeters used are presented in Figures 9.1 to 9.5 and general descriptions of their components is given in Table 9.1.

9.2.1. South Bank Calorimeter.

The South Bank calorimeter consisted of an R-22 plant with a hermetic compressor of 750 W motor capacity, a water cooled condenser, a TEV and an evaporator coil placed inside an insulated vessel containing R-134a as secondary refrigerant. When the electric heaters were energised the liquid was evaporated until a low liquid level cut-off was activated. High pressure safety cut-outs were also placed in the vessel and compressor to break the whole electrical circuit if this was necessary.

The vessel was insulated with layers of glass fibre and polystyrene. In order to minimise radiation losses and to act as a vapour barrier, the calorimeter was also covered with aluminium foil.

The instrumentation of this plant included bourden tube gauges to measure the condenser, evaporator and calorimeter pressures. Because the accuracy of bourden tube gauges is typically of ±0.1 bar (plus the error in the measurement of the ambient pressure), data from these were used for cross-checking and only measured temperatures were used during the analysis of data.

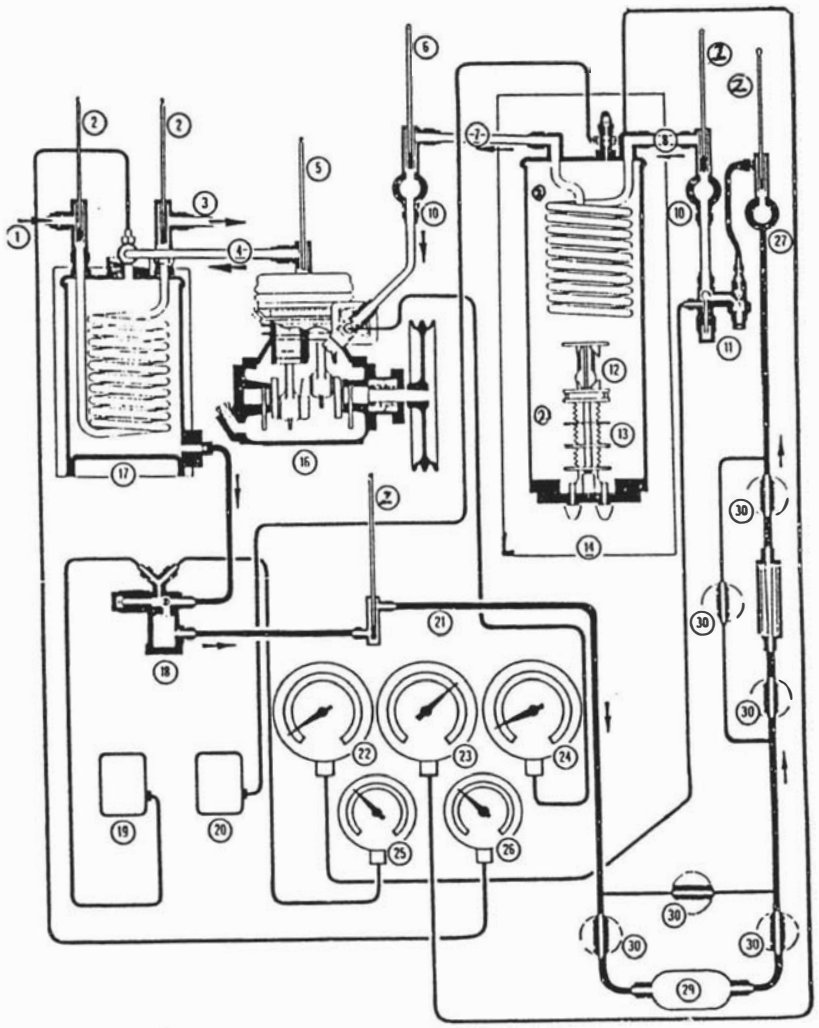

Fig. 9.1. Schematic diagram of the South Bank calorimeter.

1: Water inlet
2, 5, 6, 9, 15: Thermocouples
3: Water outlet
4: Delivery line
7: Suction line
8: Expansion line
10: Sight glass
11: Constant pressure regulator
12: Float switch
13: Heaters
14: External shell, aluminium
16: Compressor
17: Water cooled condenser
18: Liquid stop valve and strainer
19: H.P. Cut-out (condenser)
20: H.P. Cut-out (calorimeter)
21: Liquid line
22: Low pressure gauge, expansion line
23: Low pressure gauge, calorimeter
24: Low pressure gauge, suction line
25: High pressure gauge, liquid line
26: High pressure gauge, delivery line
27: Sight glass
29: Liquid line drier
30: Stop valve

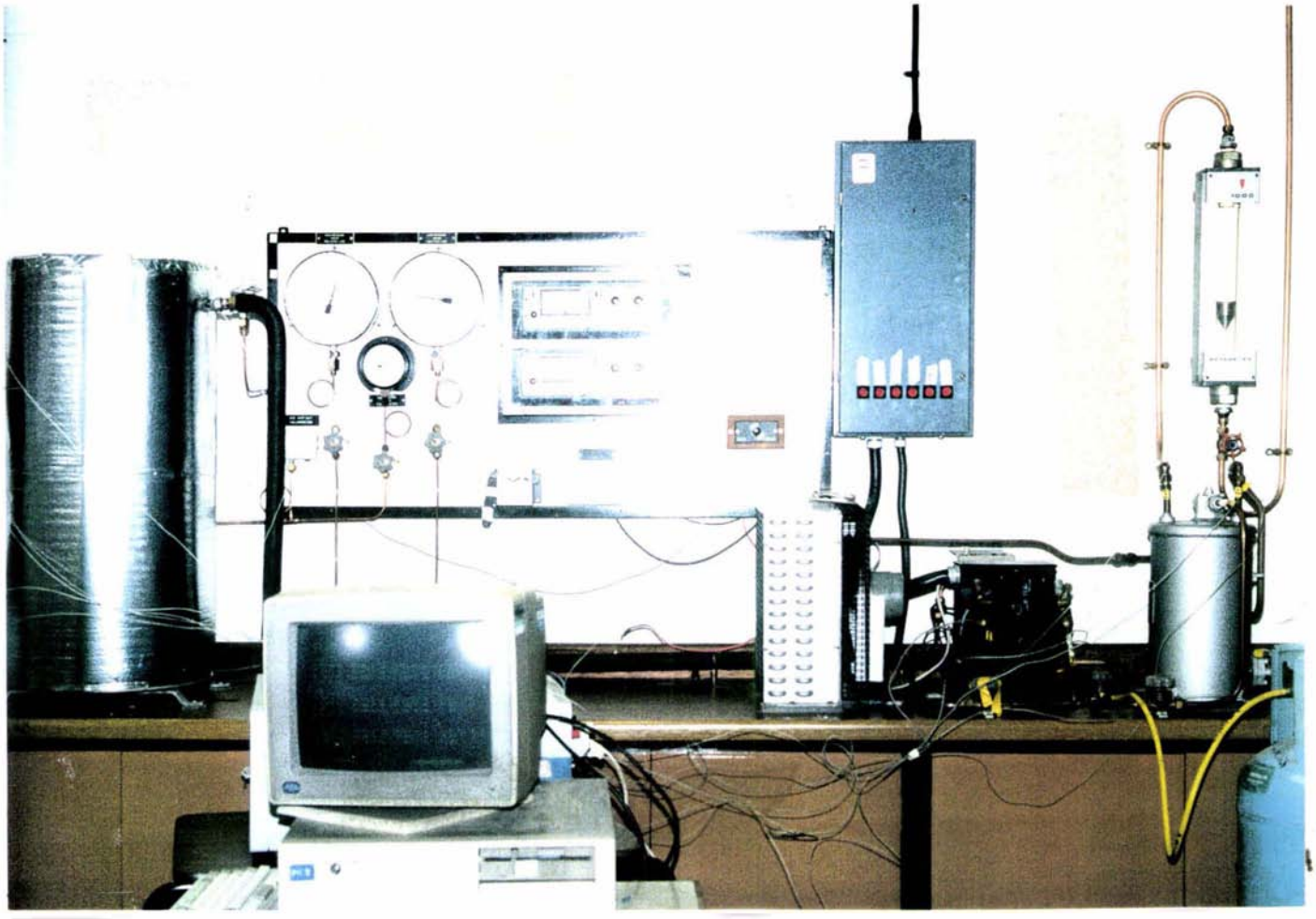

Fig. 9.2. The South Bank calorimeter

Fig.9.3. The pressure vessel of the South Bank calorimeter used for the trials

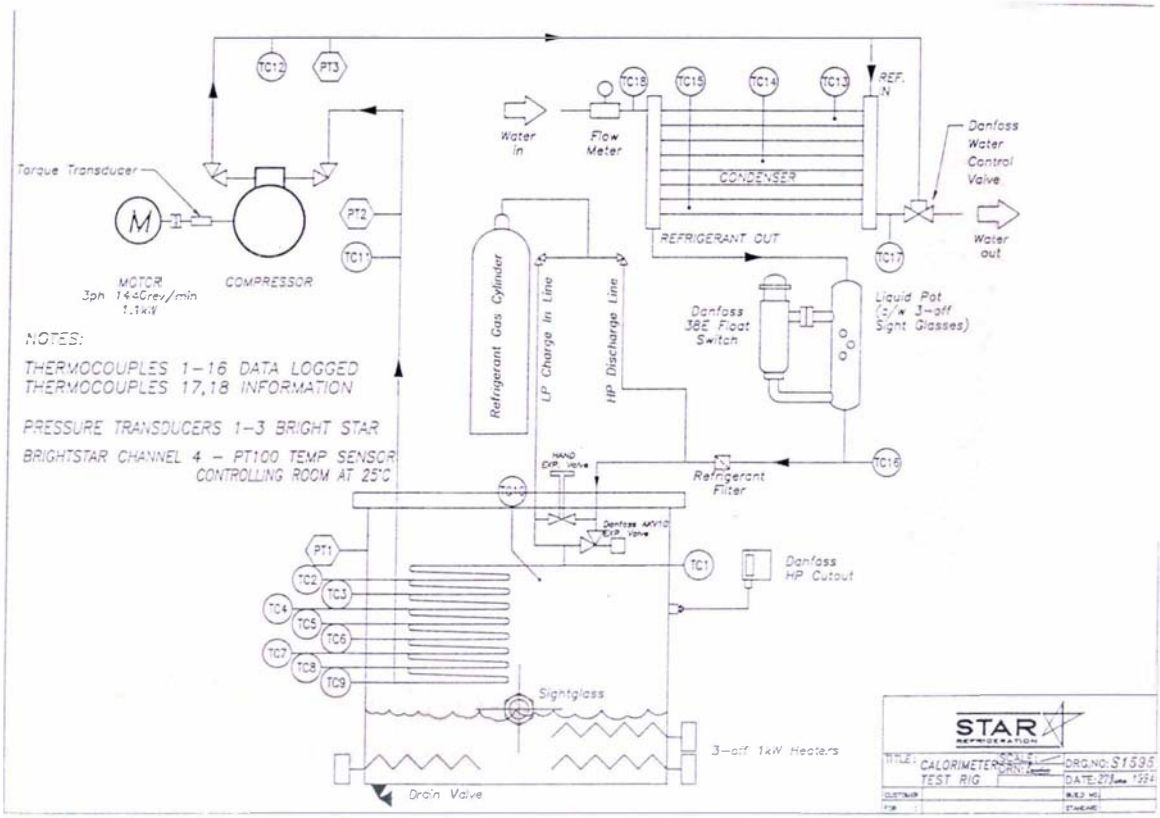

Fig. 9.4. Schematic diagram of the Star calorimeter.

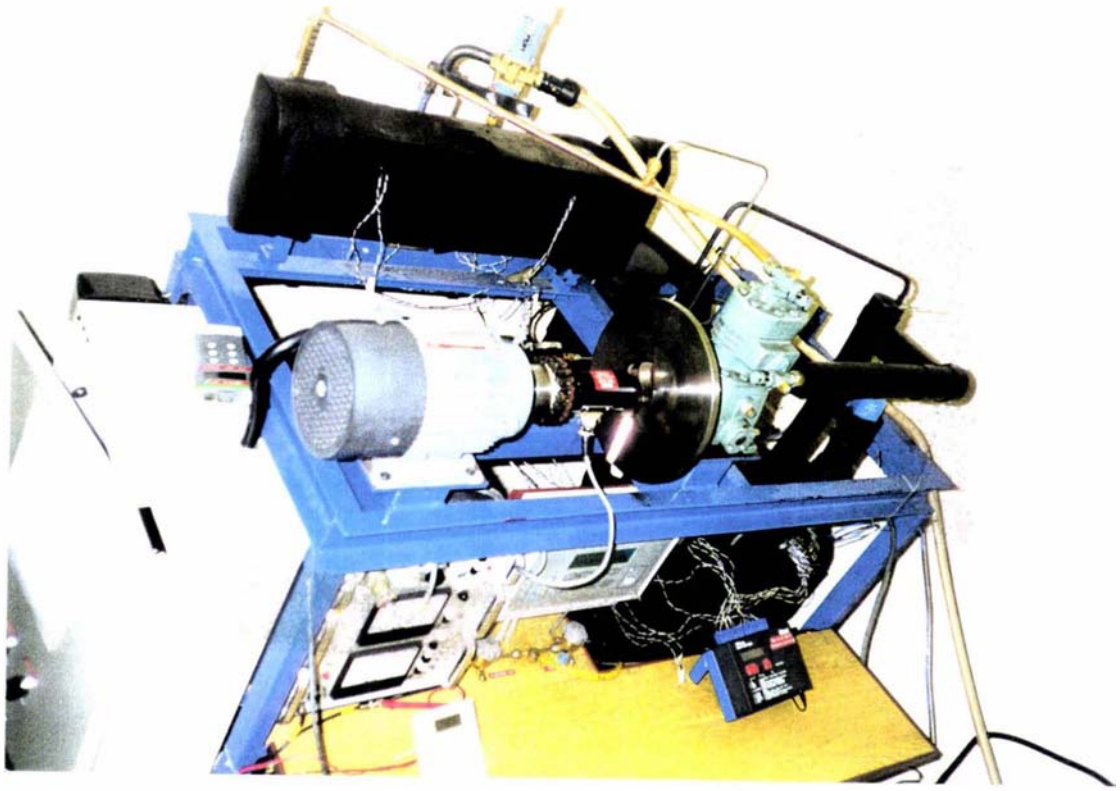

Fig. 9.5. The Star calorimeter.

TABLE 9.1. DESCRIPTION OF THE STAR AND SOUTH BANK CALORIMETER EXPERIMENTAL RIGS.

Equipment	South Bank	Star
Compressor	Prestcold K75/0010 (hermetic compressor). Swept volume=0.01 m^3 s^{-1}. Motor: 0.75 kW.	Bitzer Type 2 (open type). Motor: 1.1 kW
Condenser	Water cooled unit (shell and coil type)	Water cooled unit (shell and tube)
Type of expansion valve	Thermostatic (Danfoss)	Automatic (Danfoss AKV-10)
Evaporator coil	3.8 m of 15.875 mm o.d. copper tubing (circular coil; internal volume of 0.0011 m^3) Weight = 3.6 kg	6.3 m of 15.875 mm o.d. copper tubing (ellipsoidal coil; internal volume of 0.00122 m^3) Weight = 10 kg
Calorimeter metallic shell	Material: Steel, BS1501 161 430A Internal height: 580 mm Internal diameter: 180 mm Shell thickness: 7.5 mm Volume: 0.0148 m^3 Weight =42 kg	Material: Steel, BS1501 161 430A Internal height = 675 mm Internal diameter = 335 mm Shell thickness = 10 mm Volume = 0.0595 m^3 Weight: 152.3 kg
Insulation and external covers	2 mm polystyrene layer glued to the vessel surface plus 200 mm glass fibre plus 1 mm steel cover plus aluminium foil External diameter=595 mm External area of insulated vessel = 0.985 m^2	100 mm of Armaflex class "O", black surface External diameter= 230mm External area of insulated vessel = 1.695 m^2
Heaters	1 variable (0 to 1.5 kW) and 1 fixed (1.5 kW)	Interchangeable heaters (0.4, 1 and 1.5 kW)

The measurement of temperatures was carried out using copper/copper-nickel type T thermocouples (British Standard 4937). These thermocouples were standarised by the manufacturer for operation in the temperature range from -200°C to 400°C, with a typical response time of 2 seconds. Two thermocouples were placed in contact with the liquid and vapour phase, respectively. At a similar height but in the external surface of the metallic shell, two thermocouples were placed to observe the effect of the thermal capacity of the

vessel wall. The temperatures of the primary circuit were measured at nine key positions shown in Fig. 9.1 using the type T thermocouples previously described. In all cases, good contact between the temperature probe and the surface of the equipment was assured by using aluminium tape to fix the thermocouples into place. The tape also reduced measurement errors due to radiative effects. A rotameter was used to measure the condenser water flow rate and wattmeters measured the power consumption of the compressor and the variable heater input.

The room space in which the calorimeter rig was placed was heated by radiators, which maintained the temperature of the room within ±2.5°C. Temperature data were collected every 30 s using a 3531 Orion data logger. The thermocouple leads were taken directly to the input terminals, which operated as the "cold" junction. The system had an internal ambient temperature "cold" junction compensation. The operating conditions of the Orion data logger were:

- Range of operating conditions: -130 to 390°C
- Total measurement error, (includes analogue/digital conversion, multiplexer and reference junction compensation: less than ±1.0°C

The initial level of liquid was calculated from the known cut-off liquid level control of the heater element. The liquid level was monitored to ensure it remains within ± 0.02 m of the original level (0.119 m). In the event of low or high liquid level, both the heater and primary rig were switched off. In all trials carried out in this calorimeter this controller was never activated. The total quantity of liquid was also measured by direct weighting of the empty and full vessel. The mass of refrigerant using both techniques was found to be 6.52 kg. This value was considered accurate to better than ±0.1 kg.

9.2.2. Star Calorimeter.

The Star calorimeter was designed to work with refrigerants tested as possible replacements for R-22. The size of the vessel was larger than the South Bank installation. The compressor was equipped with a torque transducer and a six-pole, three phase, 1.1 kW motor. The water cooled condenser operation was controlled using a pressure operated water flow constricting valve at the condenser outlet. The refrigerant circulation rate was controlled by a level controller sending an on/off signal to the expansion valve. To smooth the control

action, a hand expansion valve was used in parallel to the Danfoss AKV-10 automatic valve to ensure that there was always some refrigerant flow. The refrigerant exiting the evaporator coil returned to the compressor at a temperature close to the ambient temperature. The secondary refrigerant (fluid in the vessel) was R-134a. The ambient temperature was controlled to ±1°C by an on-off controller using a PT-100 sensor.

The pressure transducer placed inside the vessel used to record the pressures of the system (suction, discharge and vessel) was rated with an accuracy of ±0.1 bar by its manufacturer. During normal operation the pressure of the vessel was controlled by the on/off action of the heaters, inducing a steady-state condition. Mean energy consumption was estimated from periodic readings of a wattmeter. All these items of equipment were regularly recalibrated by Star personnel so only limited calibration checks were undertaken. Published correlations of the refrigerating effect versus the evaporation temperature inside the coil (Pearson, 1995) were used to ensure that the readings of the wattmeters were accurate.

Temperatures were measured at 14 locations within the refrigerant circuit and two further thermocouples were placed inside the tank to measure the R-134a liquid and vapour temperatures. The measurement and logging of the temperatures were carried out with type T thermocouples and a Squirrel 1205 portable data logging system. The accuracy expected from the recording of temperatures was ±0.3°C.

The quantity of refrigerant inside the vessel was evaluated from the known initial level of liquid, observed through a sight-glass and by considering the vapour occupying the head space. The total initial mass of refrigerant was estimated as 13.54 kg. Again, uncertainties were such that the actual mass may have been different - perhaps as by much as ±0.1 kg.

9.3. Experimental methodology for dynamic data collection.

The experimental methodology followed for all trials with both calorimeters comprised the following steps:

1) The experimental rig was switched on, selecting the desired initial operating conditions for the following parameters:
   - condenser water flow rate and temperature
   - evaporation temperature
   - suction and discharge pressures

- heater input

2) The temperatures of the R-134a liquid and vapour phases were monitored until steady-state conditions were obtained. Usually, it was considered that if the measured system changes were less than 0.5 °C in 20 minutes, steady-state conditions had been achieved.

3) Once the initial conditions were steady, the first step change in the operating conditions was carried out. This was achieved changing the energy input of the heater, leaving the rest of the operating conditions at the same levels. The system then underwent a period of transient behaviour before stabilising at the new steady-state conditions.

4) Once the new steady-state was achieved, any further step change would be undertaken by repeating steps 2 and 3.

Thus, several step changes could be carried out in a sequence. The time to reach the new steady-state conditions depended on the magnitude of the step change.

9.4. System energy balance on experimental trials.

9.4.1. Thermodynamic analysis of the experimental system.

A variety of trials using different conditions and different step change strategies were carried out. In order to select the trials to be used in comparisons to model predictions, a global energy balance was adopted as an indicator of the quality of the experimental data.

Eqs. (8.31) and (8.33) which are themselves simplified by removal of all terms for mass flows over the calorimeter boundary the energy balances for the refrigerant in the experimental system during transient conditions are brought forward:

$$\frac{dE_l}{dt} = \Sigma q_{object} - w_s - m_{ev}\left[\left(u_{g,sat} + p_g\, v_{g\,sat}\right) - \left(u_g + p_g\, v_g\right)\right] + m_{con}\left[\left(u_{l\,sat} + p_g\, v_l\right) - \left(u_g + p_g\, v_g\right)\right] \tag{9.2}$$

where all the terms apply as stated in Section 8.4.2.

$$\frac{dE_g}{dt} = \Sigma q_{object} + w_s + m_{ev}\left[\left(u_{g,sat} + p_g v_{gsat}\right) - \left(u_g + p_g v_g\right)\right] - m_{con}\left[\left(u_{lsat} + p_g v_l\right) - \left(u_g + p_g v_g\right)\right] \quad (9.3)$$

The term q_{object} grouped several models defined in Chapter 8. In the experimental set-up, the following objects were considered as contributors:

- Heaters: Contribute by adding energy to the system
- Coil: Contributes by removing energy from the system

Both the coil and the vessel shell contributed also as objects possessing thermal mass.

To simplify the overall situation, those terms adding or removing energy to/from the system were lumped in a term q_{net} (W).

The total change in the energy of the system can thus be defined as:

$$\frac{dE_T}{dt} = \frac{dE_g}{dt} + \frac{dE_l}{dt} + \frac{dE_{shell}}{dt} + \frac{dE_{coil}}{dt} = q_{net} \quad (9.4)$$

where :

E_T = Total energy in the experimental vessel (J)
E_l = Energy of the liquid zone (J)
E_g = Energy of the vapour (J)
E_{shell} = Energy of the shell (J)
E_{coil} = Energy of the metallic coil (J)
q_{net} = Net energy input and removal from object items (W)

When Eq. (9.2) and Eq. (9.3) are added together, all work terms cancel.

If Eq. (9.4) is expressed in an integrated manner between states 1 (immediately before transient period) and 2 (immediately after transient period), the resulting expression describes the conservation of energy in the experimental system:

$$E_{T,2} - E_{T,1} = \int_{t_1}^{t_2} q_{net}\, dt \quad (9.5)$$

where:

$E_{T,1}$ = Total energy of the system at the start of the transient period (J)

$E_{T,2}$ = Total energy of the system at the end of the transient period (J)

t_1 = Time at the start of transient period (s)

t_2 = Time at the end of transient period (s)

The right hand side of Eq. (9.5) was directly obtained from a time-weighted sum of energy inputs from the objects to the system during the unsteady-state period. However, the left hand side of Eq. (9.5) required additional analysis.

As stated earlier, the total energy of the vessel was composed of the energy within the liquid, vapour and metallic structures contacting the liquid and vapour phases (metallic shell and coil):

$$E_T = E_l + E_g + E_{coil} + E_{shell} \tag{9.6}$$

The left hand side of Eq. (9.5) was evaluated using the following expressions:

$$E_{T,1} = \left(M_{shell}\, u_{shell} + M_{coil}\, u_{coil} + M_l\, u_l + M_g\, u_g\right)_1 \tag{9.7}$$

$$E_{T,2} = \left(M_{shell}\, u_{shell} + M_{coil}\, u_{coil} + M_l\, u_l + M_g\, u_g\right)_2 \tag{9.8}$$

$$\begin{aligned} E_{T,2} - E_{T,1} = {} & M_{shell,2}\, u_{shell,2} + M_{coil,2}\, u_{coil,2} + M_{l,2}\, u_{l,2} + M_{g,2}\, u_{g,2} \\ & - M_{shell,1}\, u_{shell,1} - M_{coil,1}\, u_{coil,1} - M_{l,1}\, u_{l,1} - M_{g,1}\, u_{g,1} \end{aligned} \tag{9.9}$$

where the subscripts 1 and 2 refer to states 1 and 2 and:

M_l = Mass of liquid inside vessel (kg)

M_g = Mass of vapour inside vessel (kg)

M_{shell} = Mass of shell structure (kg)

M_{coil} = Mass of coil structure (kg)

u_l = Specific internal energy of liquid inside vessel (J/kg)

u_g = Specific internal energy of vapour inside vessel (J/kg)

u_{shell} = Specific internal energy of shell structure (J/kg)

u_{coil} = Specific internal energy of coil structure (J/kg)

During the transient period the metallic masses remained constant, but the liquid and vapour masses changed due to evaporation and/or condensation. If the net amount of refrigerant mass evaporated (*i.e.* evaporated mass minus condensed mass) is defined as M_{net} (kg), the following equations can be established:

$$M_{net} = M_{l,1} - M_{l,2} = M_{g,2} - M_{g,1} \tag{9.10}$$

$$M_{l,2} = M_{l,1} - M_{net} \tag{9.11}$$

$$M_{g,2} = M_{g,1} + M_{net} \tag{9.12}$$

Substituting the latter expressions in Eq.(9.9) and grouping terms, the resulting equation is:

$$\begin{aligned} E_{T,2} - E_{T,1} = {} & M_{shell}\left(u_{shell,2} - u_{shell,1}\right) + M_{coil}\left(u_{coil,2} - u_{coil,1}\right) \\ & + M_{l,1}\left(u_{l,2} - u_{l,1}\right) + M_{g,1}\left(u_{g,2} - u_{g,1}\right) + M_{net}\left(u_{g,2} - u_{l,1}\right) \end{aligned} \tag{9.13}$$

This expression was used to define the total energy difference between the initial and final states of the vessel. The equations used for the liquid, shell, coil and vapour components are summarised below.

9.4.2. Calculation of the total energy difference between the initial and final states of the vessel.

For solids and liquids (shell, coil and liquid zone), it may be assumed that:

$$u_{source,2} - u_{source,1} \approx h_{source,2} - h_{source,1} \tag{9.14}$$

and:

$$h_{source,2} - h_{source,1} \approx c_{source}\left(T_{source,2} - T_{source,1}\right) \tag{9.15}$$

where the subscript *source* indicates shell, coil or liquid components and:

c_{source}	=	Mean specific heat capacity of component (J/kg K) considered constant throughout the trial
$T_{source,1}$	=	Temperature of component at the start of the trial (°C)
$T_{source,2}$	=	Temperature of component at the end of the trial (°C)

The specific expressions used to determine the energy balance of the experimental system are given below:

1. **Sensible heat taken up by shell.** This source accounted for the effect of the thermal capacity of the metallic shell of the vessel and it was estimated using the following equation:

$$M_{shell}\left(u_{shell,2} - u_{shell,1}\right) = M_{shell}\, c_{shell}\left(T_{shell,2} - T_{shell,1}\right) \tag{9.16}$$

where:

c_{shell}	=	Specific heat capacity of metallic shell (J/kg K)
$T_{shell,\,1}$	=	Temperature of metallic shell at the start of the trial (°C)
$T_{shell,\,2}$	=	Temperature of metallic shell at the end of the trial (°C)

2. **Sensible heat taken up by coil.** This source accounted for the effect of the thermal capacity of the metallic coil. The thermal mass was calculated using the following equation:

$$M_{coil}\left(u_{coil,2} - u_{coil,1}\right) = M_{coil}\, c_{coil}\left(T_{coil,2} - T_{coil,1}\right) \tag{9.17}$$

where:

c_{coil}	=	Specific heat capacity of metallic coil (J/kg K)
$T_{coil,\,1}$	=	Temperature of coil at the start of the trial (°C)
$T_{coil,\,2}$	=	Temperature of coil at the end of the trial (°C)

3. **Sensible heat taken up by liquid phase.** This source accounted for the thermal capacity of the liquid phase inside the vessel. Using the simplification of Eq. (9.15) it was calculated as follows:

$$M_{l,1}\left(u_{l,2} - u_{l,1}\right) \approx M_{l,1}\, c_l\left(T_{l,2} - T_{l,1}\right) \tag{9.18}$$

where:

c_l	=	Mean specific heat capacity of liquid (J/kg K)
$T_{l,\,1}$	=	Temperature of liquid at the start of the trial (°C)
$T_{l,\,2}$	=	Temperature of liquid at the end of the trial (°C)

4. **Sensible heat taken up by vapour phase.** This source accounted for the thermal capacity of the vapour phase inside the vessel. The equation used was stated as in Eq. (9.13):

$$E_{g,1} = M_{g,1} \left(u_{g,2} - u_{g,1} \right) \tag{9.19}$$

The internal energies were calculated assuming saturation in the vapour phase and using the routines of Cleland (1986, 1994) to find the enthalpies and pressures. The definition of internal energy ($u_g = h_g - p_g v_g$) was applied directly.

5. **Latent heat from evaporation/condensation.** This source accounted for the energy involved in the change of phase of the refrigerant, according to an overall balance of the mass of vapour at the start and at the end of the trial. The mass of vapour created was determined from the differences between the final and initial values of the total volume of vapour V_g (m^3) and the vapour specific volume v_g (m^3/kg). Saturated conditions in both states were assumed, thus:

$$M_{net} \left(u_{g,2} - u_{l,1} \right) = \left(M_{g,2} - M_{g,1} \right) \left(u_{g,2} - u_{l,1} \right) \tag{9.20}$$

where $u_{g,2}$ and $u_{l,1}$ were evaluated as stated in Eqs. (9.18) and (9.19).

Details of the calculation of these terms for the experimental trials are given in Appendix V.

9.4.3. Calculation of the net energy input q_{net} to the system.

This term was calculated by lumping all the sources directly adding or removing energy to/from the system. The left hand side of Eq. (9.5) was evaluated by numerical integration:

$$\int_{t_1}^{t_2} q_{net} \, dt \approx \Sigma \, q_{net} \, \Delta t \tag{9.21}$$

where values of Δt where chosen sufficiently small to ensure that numerical integration error was small.

The sources considered in q_{net} were the following:

6. **Sensible heat infiltrated through the insulation to the metal shell** ($q_{amb \rightarrow vessel}$, W). This heat flow was dependent on the thermal resistance of the insulation and air surrounding the shell.

7. Energy added by heater (q_{heater}, W).

8. Energy removed by coil (q_{coil}, W).

The term $q_{amb \rightarrow vessel}$ was calculated using Eqs.(8.47a) to (8.47e). The term q_{heater} was calculated assuming that the energy input by the heater increased or decreased instantaneously once the heating power was changed, thus neglecting any possible effect of the thermal mass of the heating element on the response.

During steady-state periods, by definition $q_{coil} = q_{amb \rightarrow vessel} + q_{heater}$. Between steady-states, q_{coil} changes. Figs. 9.6a to 9.6c show measured coil temperature data, which was used to obtain some insight into how the coil heat removal might be modelled. Figure 9.6a shows an approximately linear change in coil temperatures in the Star calorimeter, which implies approximately linear change in coil temperature difference and hence q_{coil}. Figure 9.6b and 9.6c present equivalent data for the South Bank calorimeter in which the coil inlet and outlet temperatures change more. These are less linear, but the assumption of linear change between steady-states was made to avoid the use of more complex schemes to model the coil temperature change. The linear change of the coil energy removal is illustrated in Fig. 9.7.

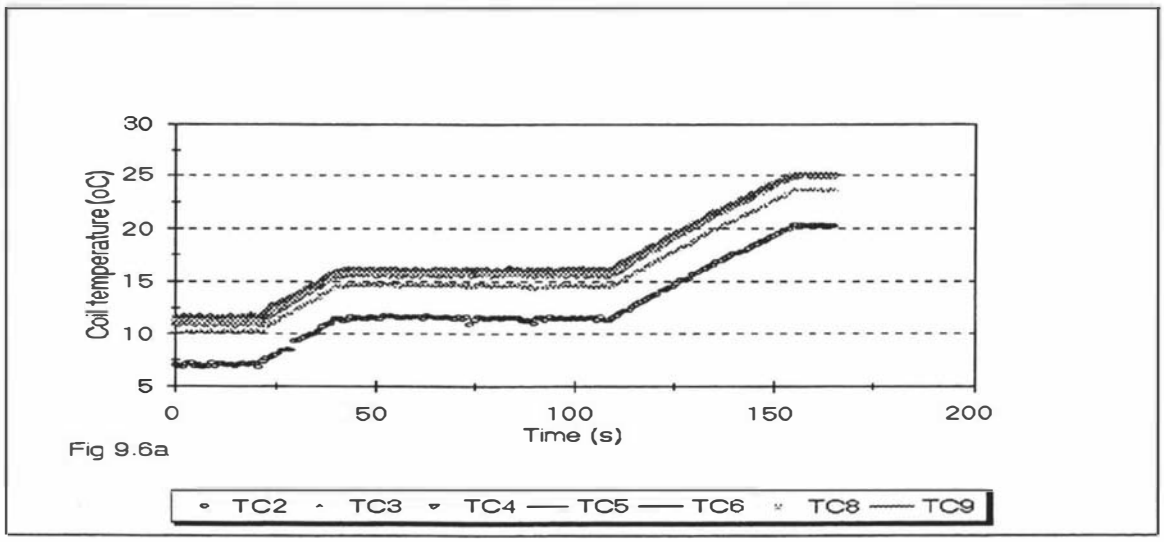

Fig. 9.6a. Coil temperature profile measured in Trial 1, Star calorimeter. Experimental conditions are given in Table 9.2. The temperatures were measured in 7 positions along the length of the coil, as shown in Fig. 9.2. The thermocouples were distanced as follows:
TC2: 0.08 m from coil entrance to vessel (closer thermocouple to expansion valve)
TC3: 1.34 m from coil entrance to vessel
TC4: 2.58 m from coil entrance to vessel
TC5: 3.84 m from coil entrance to vessel
TC6: 5.07 m from coil entrance to vessel
TC8: 7.56 m from coil entrance to vessel
TC9: 8.79 m from coil entrance to vessel (thermocouple placed at the end of coil)Total length of coil, including return to the top of the vessel: 10.53 m

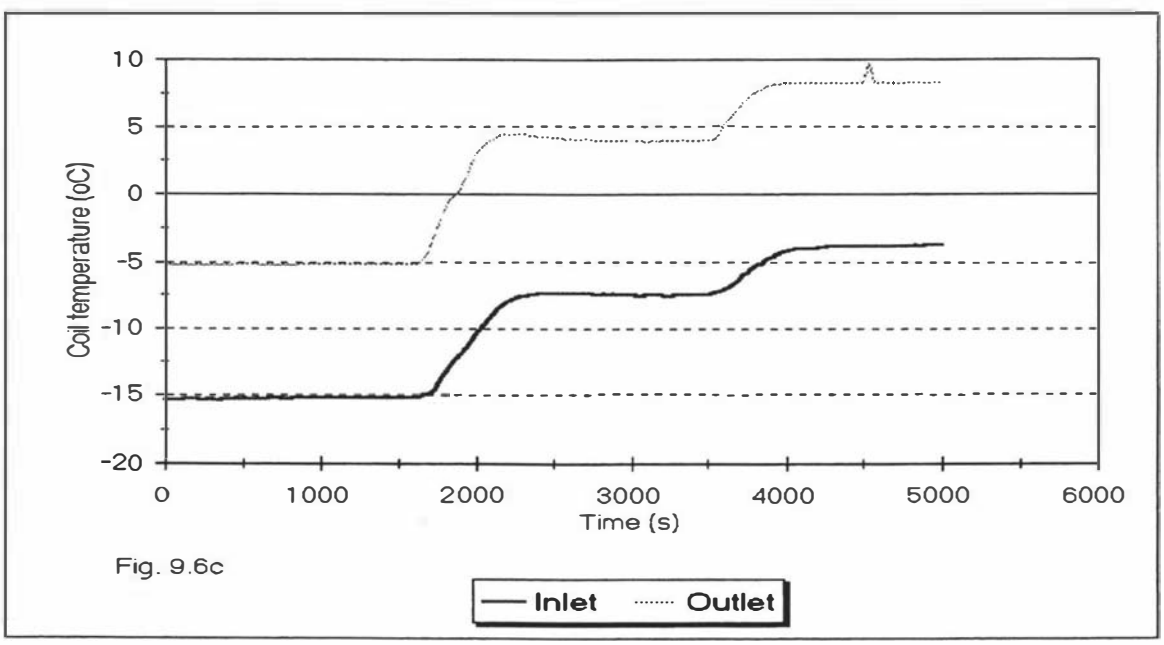

Fig. 9.6b. Coil temperature profile measured in Trial 3, South Bank calorimeter. Experimental conditions are given in Table 9.2. The temperatures were measured in the inlet and outlet of the coil. The thermocouples were placed as follows: **Inlet**: immediately after the TEV (0.05 m from TEV outlet) **Outlet**: immediately at the exit from the vessel (0.05 m from vessel shell)

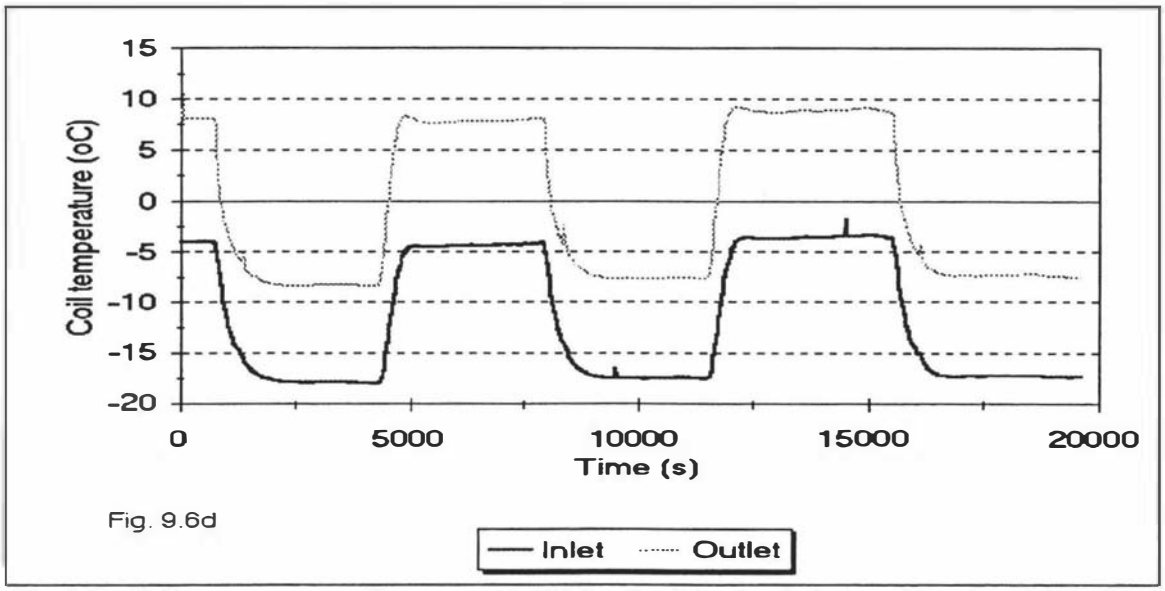

Fig. 9.6c. Coil temperature profile measured in Trial 4, South Bank calorimeter. Experimental conditions are given in Table 9.2. The temperatures were measured in the inlet and outlet of the coil. The thermocouples were placed as follows: **Inlet**: immediately after the TEV (0.05 m from TEV outlet)
Outlet: immediately at the exit from the vessel (0.05 m from vessel shell)

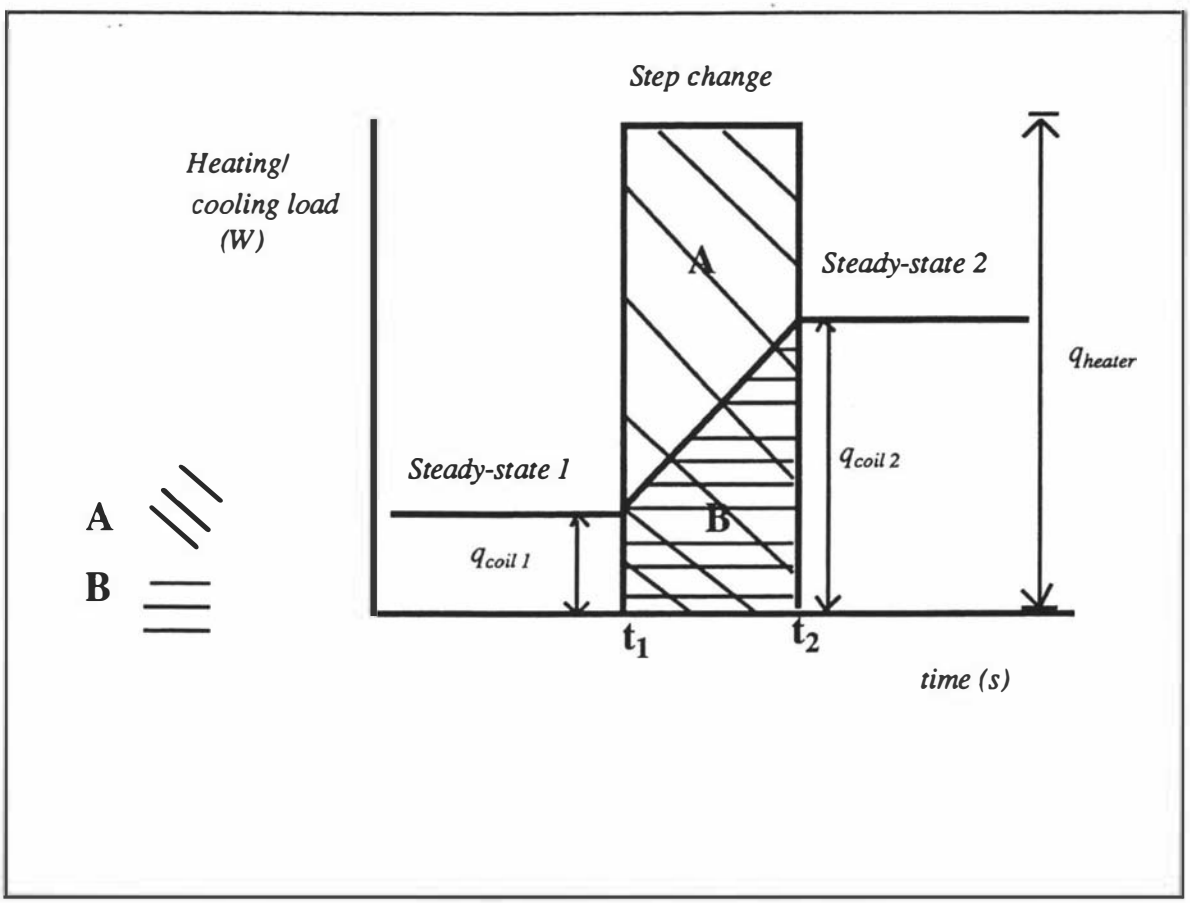

Figure 9.7. Visualisation of q_{heater} and q_{coil} during a step change.

$t_2 - t_1$	=	Duration of transient period (s)
q_{heater}	=	Heating power (W)
q_{coil1}	=	Coil cooling load, steady-state 1 (W) = $q_{heater,\ steady\text{-}state\ 1}$ (W)
q_{coil2}	=	Coil cooling load, steady-state 2 (W) = $q_{heater,\ steady\text{-}state\ 2}$ (W)
A	=	Heater input during transient period (J), $q_{heater}\ (t_1 - t_2)$
B	=	Energy removed by coil during transient period (J), $0.5\ (q_{coil1} + q_{coil2})\ (t_2 - t_1)$

During the transient period, the term q_{net} was calculated as follows:

$$q_{net} = q_{heater} + q_{amb \rightarrow vessel} - \left[q_{coil\,1} + \left(\frac{t - t_1}{t_2 - t_1} \right) \left(q_{coil\,2} - q_{coil\,1} \right) \right] \qquad (9.22)$$

9.4.4. *Acceptable error in energy balances.*

The relative error between the net energy input and the total energy difference between the initial and final states of the vessel was:

$$\% \ error = 100 \left(\frac{\Sigma \ q_{net} \ \Delta \ t \ - \ (E_{T,2} \ - \ E_{T,1})}{\Sigma \ q_{net} \ \Delta \ t} \right) \tag{9.23}$$

Those trials that presented a relative difference of more than 15% between the net energy input and the total energy difference were regarded as unacceptable.

9.4.5. Thermal properties and heat transfer parameters of the system.

Table 9.2 summarises the thermal properties used in the calculation of the energy balances and during the simulation of the trials. The calculation of enthalpies, temperatures and pressures for both liquid and vapour used the equations developed by Cleland (1994) for R-134a. The calculation of the vapour specific volumes also used these routines. The liquid density and specific heat capacity were calculated as the mean of the values at the initial and final temperatures for each trial, according to data published by ASHRAE (1995). The specific heat capacity of the metallic shell was also taken from ASHRAE (1995). The thermal conductivity of the insulation was given by the manufacturer (Armaflex II by Amstrong Industry Products Division, according to standard ASTM C 534, Type II). The density and specific heat capacity of copper were evaluated at the temperature working range of -100°C to 27 °C from data of Whitaker (1977).

The heat transfer coefficient to the external cylindrical surface of the calorimeter combined natural convection and radiation. A typical value would be about 5 to 10 W/m^2 K. The heat transfer resistance of the insulation was much more important, so there was no value in seeking an accurate estimate and so 10 W/m^2 K was used. For the heat transfer coefficient inside the vessel, guidelines stated by Bejan (1993) regarding the boiling of a liquid refrigerant inside a cylindrical vessel suggested a much higher value of 500 W/m^2 K be used. It was later observed that results were very insensitive to both the external and internal heat transfer coefficient values.

TABLE 9.2. THERMAL PROPERTIES OF SYSTEM COMPONENTS USED IN THE CALCULATION OF THE EXPERIMENTAL ENERGY BALANCES.

Thermal property	Copper tube, coil	Metallic shell	Insulation layers
λ (W/m K)	---[1]	--[1]	0.037
c (J/kg K)	375	500	---[2]
ρ (kg/m^3)	8,954	7,800	---[1]
v (m^3/kg)	---[1]	---[1]	---[1]

[1] These values were not required for calculations. Note that the thermal properties of liquid and vapour phases were calculated separately for each trial. The properties of these zones are presented in Appendix V.

[2] The thermal mass of the insulation was neglected in all calculations.

Of the 20 trials carried out in both experimental calorimeters, about 40% did not fulfil the selection criterion of less than 15% relative error. The reasons for disagreement may include the following:

Experimental set-up:

a) A significant effect of "thermal bridging" through pipes and other structures in contact with the vessel shell and/or vessel contents.

b) Unexpected variations in the current voltage used by the heating element or errors in the calibration of the wattmeters used to measure the energy consumption.

c) Uncontrolled changes in the conditions of the primary refrigeration circuit, leading to unknown changes in the energy removed by the coil.

d) Slow response of the measurement system (thermocouples and transducers).

Energy balance calculations:

e) Approximations in the calculation of the energy balance, *e.g.* the assumption of constant thermal capacities of system components during a trial.

f) Inadequacies in the assumptions of instantaneous step change of energy input (heater) and linear time-dependency of energy removal (coil). Non-linear time-dependency and fluctuating rates of input and removal may have been possible.

From the 12 successful trials, 6 were selected to investigate the behaviour of the pressure vessel in detail and to illustrate the general performance of the models in response to a variety of step change strategies. The conditions of these trials are summarised in Table 9.3 and Figs. 9.8a to 9.8f. Appendix V presents details of these trials.

TABLE 9.3. SUMMARY OF SELECTED EXPERIMENTAL TRIALS FOR MODEL VALIDATION.

TRIAL	HEATING POWER (W)[1]	DURATION (s)	TEMPERATURES IN REFRIGERATION PLANT		VESSEL PRESSURE (R-134a, Bar.a)	T_{room} (°C)
			Evaporation, R-22 (°C)	Condensing,R-22 (°C)		
1, Star. Fig. 9.8a	1. 564 I. 1000 2. 577 II. 1000 3. 630	1. 1320 I. 960 2. 4380 II. 2580 3. 1760	1. -27 2. -27 3. -27	55	1. 4.30 2. 5.69 3. 6.58	25
2, Star Fig. 9.8b	1. 2400 I. 0 [2] 2. 0 [2]	1. 0.01 I. 11500 2. 50	1. 0 2. --[3]	1. 55 2. --[4]	1. 7.64 2. 5.58	18
3, South Bank Fig. 9.8c	1. 1700 I. 2500 2. 2500 II. 3000 3. 3000	1. 1620 I. 630 2. 1320 II. 460 3. 980	1. -15 2. -8 3. -4	10.5	1. 2.43 2. 3.10 3. 3.98	18
4, South Bank [5] Fig. 9.8d	1. 1500 [6] I. 1500 [7] 2. 3000 [6] II. 3000 [8]	1. 2600 I. 580 2. 2600 II. 3030	1. -4.0 2. -17.5	10.5	1. 3.95 2. 2.18	16
5, South Bank [5] Fig. 9.8e	1. 2300 [6] I. 2300 [7] 2. 3000 [6] II. 3000 [8]	1. 3090 I. 490 2. 3090 II. 490	1. -4.5 2. -10.0	11.6	1. 3.93 2. 3.11	15
6, South Bank [5] Fig. 9.8f	1. 2300 [6] I. 2300 [7] 2. 3000 [6] II. 3000 [8]	1. 8350 I. 1020 2. 2580 II. 1020	1. -37.4 2. -14.0	6.8	1. 7.60 2. 2.27	12

[1] I and II represent the unsteady-state period. [2] Ambient heat load only. [3] Instantaneous change in heating power [4] Switch off condition [5] Periodic signal. [6] 1 and 2 represent steady-state conditions at lowest and highest levels of heating power, respectively [7] I represents the unsteady-state conditions at the lowest heating power level. [8] II represents unsteady-state conditions at the highest power level.

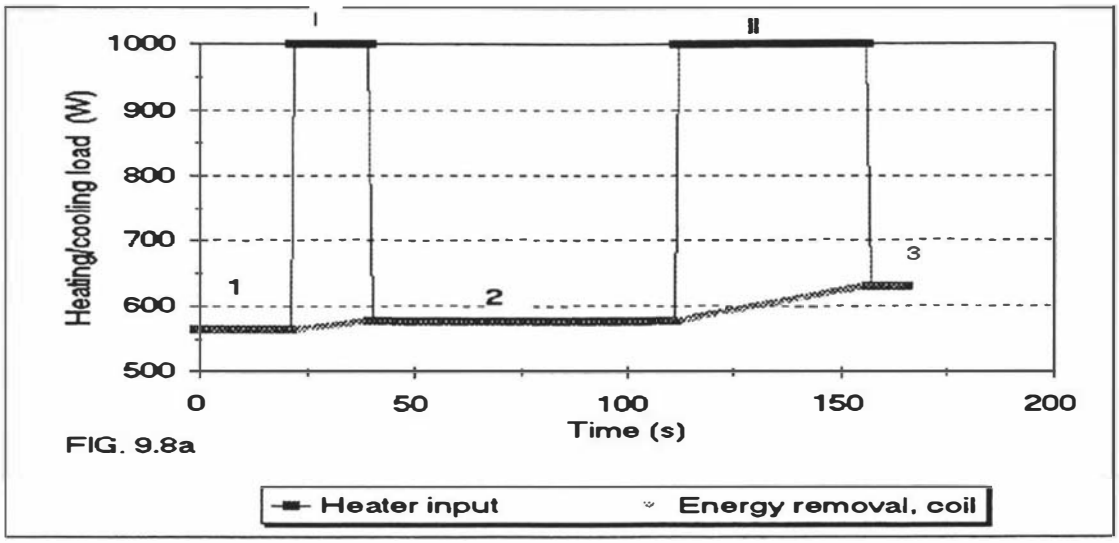

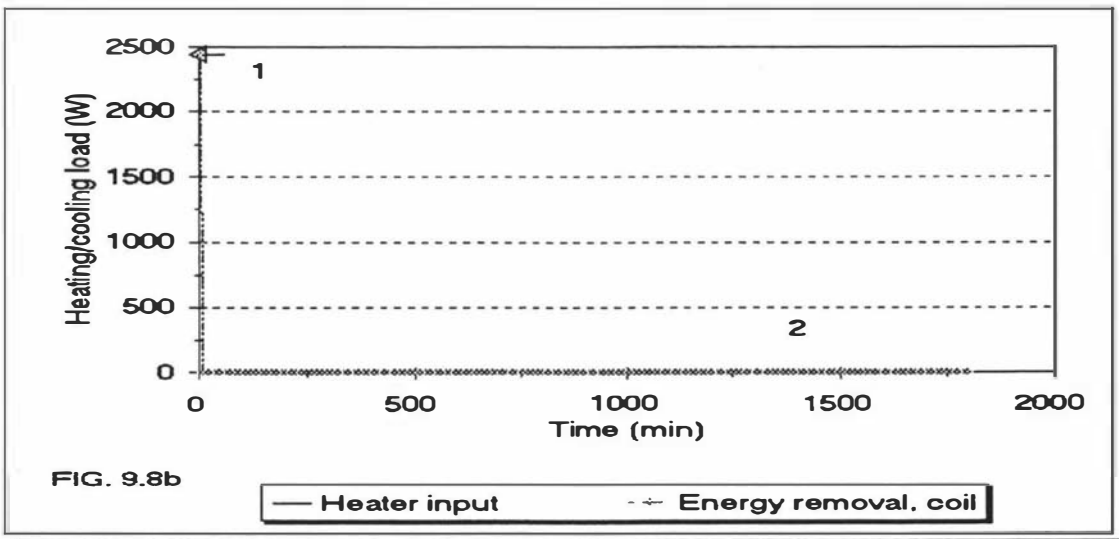

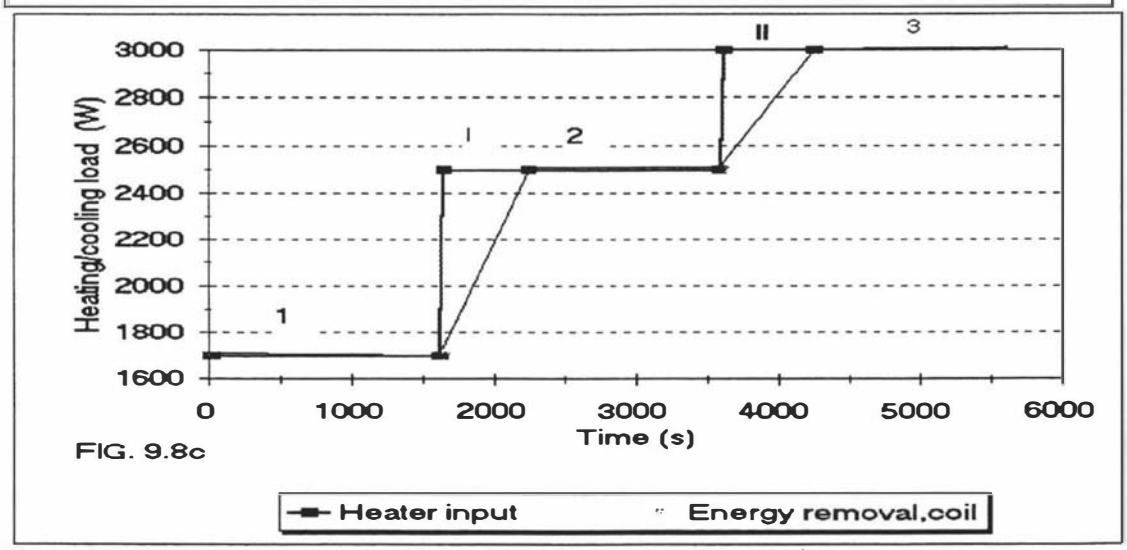

Figure 9.8. Assumed heating and cooling profiles for the experimental trials. The changes shown in the coil correspond to the assumption of linear behaviour between steady-states. **a) Trial 1**: An on/off controller was used to switch the variable heaters; **b) Trial 2**: Heaters and R-22 primary system were switched off. The only path for heat exchange was through the vessel shell; **c) Trial 3**: A sudden increase of the heating power was used. The conditions of the trials are given in Table 9.2.

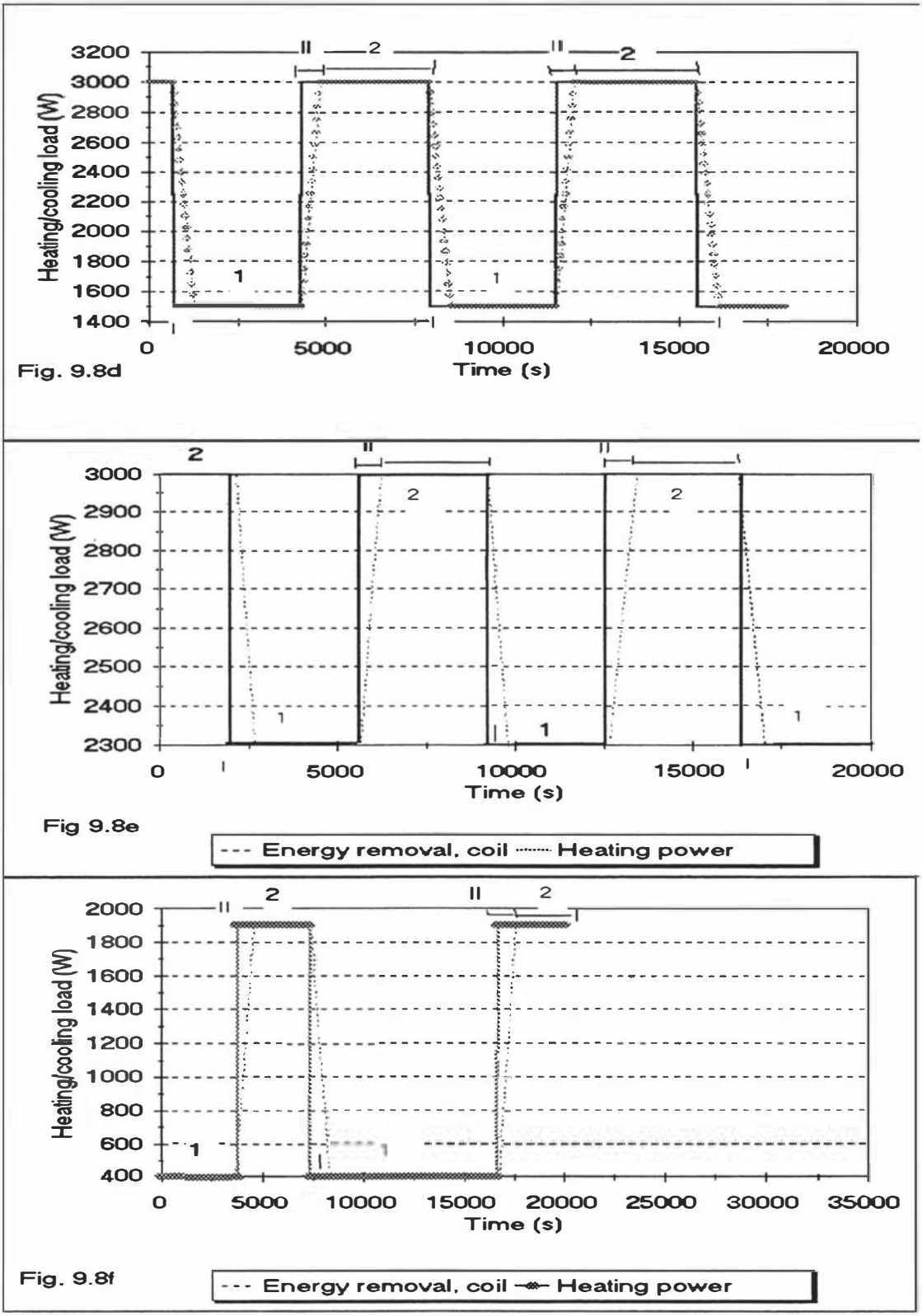

Figure 9.8 (cont). Heating and cooling strategies for the experimental trials. The changes shown in the coil correspond to the assumption of linear behaviour between steady-states. In these 3 trials, cyclic variations of the heating power were achieved, increasing and decreasing the heating power alternatively during constant periods. The conditions of the trials are given in Table 9.2. **d) Trial 4; e) Trial 5; f) Trial 6.**

9.5. Interpretation of general models in relation to the experimental systems.

In Chapter 8, a detailed explanation of models A, B, C and D was presented. Tables 9.4 indicates which of the eight energy sources described in Sections 9.4.1 and 9.4.2 are included in each model. The main thermodynamic characteristics of the models were:

MODEL A: Two-zone model based on a full energy balance.

1) Work between phases included
2) Strict definition of internal energy used:

$$\frac{d u_g}{d t} = \frac{d(h_g - p_g v_g)}{d t}$$

3) Model allows transition between:
   a) saturated liquid-saturated vapour
   b) saturated liquid-superheated vapour
   c) subcooled liquid-saturated vapour
   d) subcooled liquid-superheated vapour
4) Thermal capacities of liquid, shell and vapour considered.

MODEL B: Two-zone model based on the enthalpy balance

1) Work between phases not included
2) Approximation of $\frac{d u_g}{d t} \approx \frac{d h_g}{d t}$
3) Model allows transition between:
   a) saturated liquid-saturated vapour
   b) saturated liquid-superheated vapour
   c) subcooled liquid-saturated vapour
   d) subcooled liquid-superheated vapour
4) Thermal capacities of liquid, shell and vapour considered.

MODEL C: Two-zone model based on an enthalpy balance

1) Work between phases not included
2) $\frac{d u_g}{d t} \approx \frac{d h_g}{d t}$

3) Transitions between phases are not recognised.

4) Thermal capacities of liquid, shell and vapour considered.

MODEL D: One-zone model based on enthalpy balance.

1) Work between phases not included

2) Vapour zone not modelled

3) Transitions between phases are not recognised.

4) Only thermal capacities of liquid and metal shell considered.

TABLE 9.4. SOURCES OF ENERGY APPLICABLE TO MODELS TESTED, ACCORDING TO CLASSIFICATION OF SECTIONS 9.4.1 AND 9.4.2. The energy sources considered in the model are marked with a cross

SOURCE	MODEL A	MODEL B	MODEL C	MODEL D
1. Sensible heat, shell	X	X	X	X
2. Sensible heat, coil				
3. Sensible heat, liquid	X	X	X	X
4. Sensible heat, vapour	X	X	X	
5. Latent heat (liquid↔vapour)	X	X	X	
6. Sensible heat infiltrated	X	X	X	X
7. Energy added by heater	X	X	X	X
8. Energy removed by coil	X	X	X	X

9.6. Results and discussion: comparison of experimental and simulated responses.

Tables 9.5 to 9.10 present the net energy input and total energy difference for the 6 selected trials used in the comparison of models. Figures 9.10 to 9.15 show the experimental and simulated liquid and vapour temperature profiles for the 6 selected trials. A typical simulation for models A, B and C used a time step of 0.01 seconds; time steps greater than this did not lead to instability, but the accuracy of the internal energy balance decreased. For the simulations of model D, a time step of 1 second was adequate.

Figure 9.9 illustrates the contribution of each component to the thermal mass of the two experimental systems used, considering only their sensible heat buffering effects. The thermal mass of the vessels and liquid represented about 95% of the total thermal mass of both systems. All the models neglected the thermal capacity of the coil, which contributed less than 5%.

FIG.9.9. APPROXIMATE THERMAL MASSES (Mc VALUES) IN EXPERIMENTAL SYSTEMS

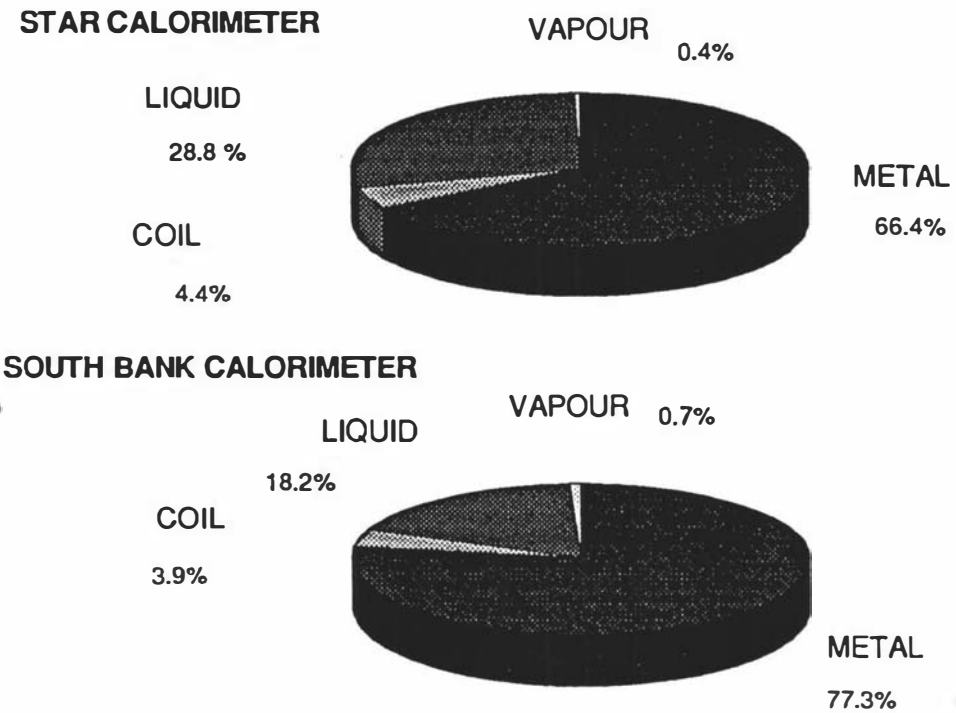

TABLE 9.5. ENERGY BALANCE IN STAR EXPERIMENTAL CALORIMETER AND MODELS A, B, C AND D. TRIAL 1.

ENERGY COMPONENTS	SYSTEM				
	EXPERIM	SIMULATIONS			
		MOD A	MOD B	MOD C	MOD D
Initial temperature (liq,vap),°C[1]	11.1,13.3	11.1,11.1			
Final temperature (liq,vap),°C[1]	24.6,24.9	25.9,25.9	25.9,25.9	25.9,25.9	26.6
Sensible heat taken up by shell, kJ	1003.3 [2]	1124.1	1123.9	1123.9	1186.7
Sensible heat taken up by coil, kJ	47.4	0	0	0	0
Sensible heat taken up by liquid phase, kJ	236.2	259.6	259.6	259.5	296.2
Sensible heat taken up by vapour phase, kJ	9.8	8.0	8.0	8.0	0
Latent heat from evap/condens, kJ	82.7	106.7	106.7	106.6	0
TOTAL (sources 1 to 5), kJ	**1379.5**	**1498.4**	**1498.2**	**1498.2**	**1483.0**
Total energy input by heater (full time of trial), kJ	7770.1	7770.1	7770.1	7770.1	7770.1
Total energy removal by coil (full time of trial), kJ	-6357.3	-6357.3	-6357.3	-6357.3	-6357.3
Energy infiltrated through shell, kJ	-71.6	73.6	73.6	73.6	70.2
TOTAL (sources 6 to 8), kJ	**1484.4**	**1486.4**	**1486.4**	**1486.4**	**1483.0**
% ERROR (internal energy balance)	7.6	0.8	0.8	0.8	0.002

[1] A detailed explanation of the conditions and calculation procedure is given in Appendix V.

[2] A weighting technique was applied to account for the mass of metal in contact with the vapour and the mass of metal in contact with the liquid. The complete calculation in given in Appendix V.

TABLE 9.6. ENERGY BALANCE IN STAR EXPERIMENTAL CALORIMETER AND MODELS A, B, C AND D. TRIAL 2.

ENERGY COMPONENTS	SYSTEM				
	EXPERIM	SIMULATIONS			
		MOD A	MOD B	MOD C	MOD D
Initial temperature (liq,vap),°C[1]	28.0,28.1	28.0,28.0			
Final temperature (liq,vap),°C[1]	18.5,19.2	20.8,20.8	20.8,20.8	20.8,20.8	20.6
Sensible heat taken up by shell, kJ	-670.1 [2]	-554.7	-555.5	-555.4	-567.6
Sensible heat taken up by coil, kJ	-35.6	0	0	0	0
Sensible heat taken up by liquid phase, kJ	-147.8	-121.5	-121.7	-121.9	-143.9
Sensible heat taken up by vapour phase, kJ	-7.8	-7.3	-6.5	-6.4	0
Latent heat from evap/condens, kJ	-60.1	-51.4	-51.6	-51.9	0
TOTAL (sources 1 to 5), kJ	**-921.4**	**-735.0**	**-735.3**	**-735.6**	**-711.3**
Total energy input by heater (full time of trial), kJ	0	0	0	0	0
Total energy removal by coil (full time of trial), kJ	0	0	0	0	0
Energy infiltrated through shell, kJ	-874.0	-739.5	-739.4	-739.3	-711.4
TOTAL (sources 6 to 8), kJ	**-874.0**	**-739.5**	**-739.4**	**-739.3**	**-711.4**
% ERROR (internal energy balance)	5.1	0.6	0.6	0.5	0.012

[1] A detailed explanation of the conditions and calculation procedure is given in Appendix V.

[2] A weighting technique was applied to account for the mass of metal in contact with the vapour and the mass of metal in contact with the liquid. The complete calculation in given in Appendix V.

TABLE 9.7. ENERGY BALANCE IN SOUTH BANK EXPERIMENTAL CALORIMETER AND MODELS A, B, C AND D. TRIAL 3.

ENERGY COMPONENTS	SYSTEM				
	EXPERIM	SIMULATIONS			
		MOD A	MOD B	MOD C	MOD D
Initial temperature (liq,vap), °C[1]	-5.4,-5.1	-5.4,-5.4			
Final temperature (liq,vap),°C[1]	8.7,8.8	8.3,8.3	8.3,8.3	8.3,8.3	8.6
Sensible heat taken up by shell, kJ	296.1 [2]	287.1	287.1	287.1	293.7
Sensible heat taken up by coil, kJ	11.1	0	0	0	0
Sensible heat taken up by liquid phase, kJ	120.5	117.6	117.6	117.6	122.3
Sensible heat taken up by vapour phase, kJ	0.5	0.8	0.8	0.8	0
Latent heat from evap/condens, kJ	11.9	12.0	12.0	12.0	0
TOTAL (sources 1 to 5), kJ	**440.1**	**417.5**	**417.5**	**417.5**	**416.0**
Total energy input by heater (full time of trial), kJ	13134.5	13134.5	13134.5	13134.5	13134.5
Total energy removal by coil (full time of trial), kJ	-12740.0	-12740.0	-12740.0	-12740.0	-12740.0
Energy infiltrated through shell, kJ	22.5	21.8	21.8	21.8	21.6
TOTAL (sources 6 to 8), kJ	**417.1**	**416.3**	**416.3**	**416.3**	**416.0**
% ERROR (internal energy balance)	5.2	0.3	0.3	0.3	0.0001

[1] A detailed explanation of the conditions and calculation procedure is given in Appendix V.

[2] A weighting technique was applied to account for the mass of metal in contact with the vapour and the mass of metal in contact with the liquid. The complete calculation in given in Appendix V.

TABLE 9.8. ENERGY BALANCE IN SOUTH BANK EXPERIMENTAL CALORIMETER AND MODELS A, B, C AND D. TRIAL 4.

ENERGY COMPONENTS	SYSTEM				
	EXPERIM	SIMULATIONS			
		MOD A	MOD B	MOD C	MOD D
Initial temperature (liq,vap), °C[1]	8.5,8.8	8.8,8.8			
Final temperature (liq,vap),°C[1]	-8.2,-7.6	-7.3,-7.3	-7.3,-7.3	-7.3,-7.2	-7.6
Sensible heat taken up by shell, kJ	-350.7 [2]	-330.5	-330.5	-330.5	-337.6
Sensible heat taken up by coil, kJ	-18.6	0	0	0	0
Sensible heat taken up by liquid phase, kJ	-141.8	-133.7	-133.7	-133.7	-140.15
Sensible heat taken up by vapour phase, kJ	-0.7	-1.5	-1.5	-1.5	0
Latent heat from evap/condens, kJ	-11.7	-11.6	-11.6	-11.6	0
TOTAL (sources 1 to 5), kJ	**-523.5**	**-477.4**	**-477.3**	**-477.3**	**-477.7**
Total energy input by heater (full time of trial), kJ	39384.8	39384.8	39384.8	39384.8	39384.8
Total energy removal by coil (full time of trial), kJ	-39935.6	-39935.6	-39935.6	-39935.6	-39935.6
Energy infiltrated through shell, kJ	-72.7	-72.3	-72.3	-72.3	-73.1
TOTAL (sources 6 to 8), kJ[3]	**-479.0**	**-478.9**	**-478.9**	**-478.9**	**-477.7**
% ERROR (internal energy balance)	8.5	0.3	0.3	0.3	0.004

[1] A detailed explanation of the conditions and calculation procedure is given in Appendix V.

[2] A weighting technique was applied to account for the mass of metal in contact with the vapour and the mass of metal in contact with the liquid. The complete calculation in given in Appendix V.

[3] Note that (-) and (+) signs indicate whether the energy is being taken out (-) or added (+) to the system.

TABLE 9.9. ENERGY BALANCE IN SOUTH BANK EXPERIMENTAL CALORIMETER AND MODELS A, B, C AND D. TRIAL 5.

ENERGY COMPONENTS	SYSTEM				
	EXPERIM	SIMULATIONS			
		MOD A	MOD B	MOD C	MOD D
Initial temperature (liq,vap),°C[1]	8.2,8.5	8.2,8.2			
Final temperature (liq,vap),°C[1]	1.6,1.8	3.4,3.4	3.4,3.4	3.4,3.4	3.3
Sensible heat taken up by shell, kJ	-140.7 [2]	-101.1	-101.1	-101.1	-103.4
Sensible heat taken up by coil, kJ	-8.2	0	0	0	0
Sensible heat taken up by liquid phase, kJ	-56.7	-41.5	-41.5	-41.5	-43.47
Sensible heat taken up by vapour phase, kJ	-0.7	-0.5	-0.5	-0.5	0
Latent heat from evap/condens, kJ	-5.6	-4.2	-4.2	-4.2	0
TOTAL (sources 1 to 5), kJ	**-211.9**	**-147.3**	**-147.3**	**-147.3**	**-146.9**
Total energy input by heater (full time of trial), kJ	52452.3	52452.3	52452.3	52452.3	52452.3
Total energy removal by coil (full time of trial), kJ	-52648.0	-52648.0	-52648.0	-52648.0	-52648.0
Energy infiltrated through shell, kJ	51.9	48.5	48.5	48.5	48.8
TOTAL (sources 6 to 8), kJ	**-184.8**	**-147.5**	**-147.5**	**-147.5**	**-146.9**
% ERROR (internal energy balance)	12.8	0.1	0.1	0.1	0.002

[1] A detailed explanation of the conditions and calculation procedure is given in Appendix V.

[2] A weighting technique was applied to account for the mass of metal in contact with the vapour and the mass of metal in contact with the liquid. The complete calculation in given in Appendix V.

TABLE 9.10. ENERGY BALANCE IN SOUTH BANK EXPERIMENTAL CALORIMETER AND MODELS A, B, C AND D. TRIAL 6.

ENERGY COMPONENTS	SYSTEM				
	EXPERIM	SIMULATIONS			
		MOD A	MOD B	MOD C	MOD D
Initial temperature (liq,vap),°C[1]	-32.8,-32.0	-32.8,-32.8			
Final temperature (liq,vap),°C[1]	-3.7,-3.5	-3.4,-3.4	-3.4,-3.4	-3.4,-3.4	-3.8
Sensible heat taken up by shell, kJ	612.0 [2]	615.0	614.9	615.4	624.3
Sensible heat taken up by coil, kJ	33.4	0	0	0	0
Sensible heat taken up by liquid phase, kJ	242.0	243.4	243.4	243.6	248.5
Sensible heat taken up by vapour phase, kJ	0.6	0.6	0.6	0.6	0
Latent heat from evap/condens, kJ	16.3	17.4	17.4	17.4	0
TOTAL (sources 1 to 5), kJ	**904.3**	**876.4**	**876.3**	**877.0**	**872.9**
Total energy input by heater (full time of trial), kJ	6271.0	6271.0	6271.0	6271.0	6271.0
Total energy removal by coil (full time of trial), kJ	-5476.5	-5476.5	-5476.5	-5476.5	-5476.5
Energy infiltrated through shell, kJ	179.4	169.3	169.3	169.3	168.6
TOTAL (sources 6 to 8), kJ	**973.9**	**874.3**	**874.3**	**874.3**	**873.6**
% ERROR (internal energy balance)	8.0	0.2	0.2	0.3	0.08

[1] A detailed explanation of the conditions and calculation procedure is given in Appendix V.

[2] A weighting technique was applied to account for the mass of metal in contact with the vapour and the mass of metal in contact with the liquid. The complete calculation in given in Appendix V.

Fig. 9.10. Comparison of temperature profiles.Exp. and simulated data

Trial 1

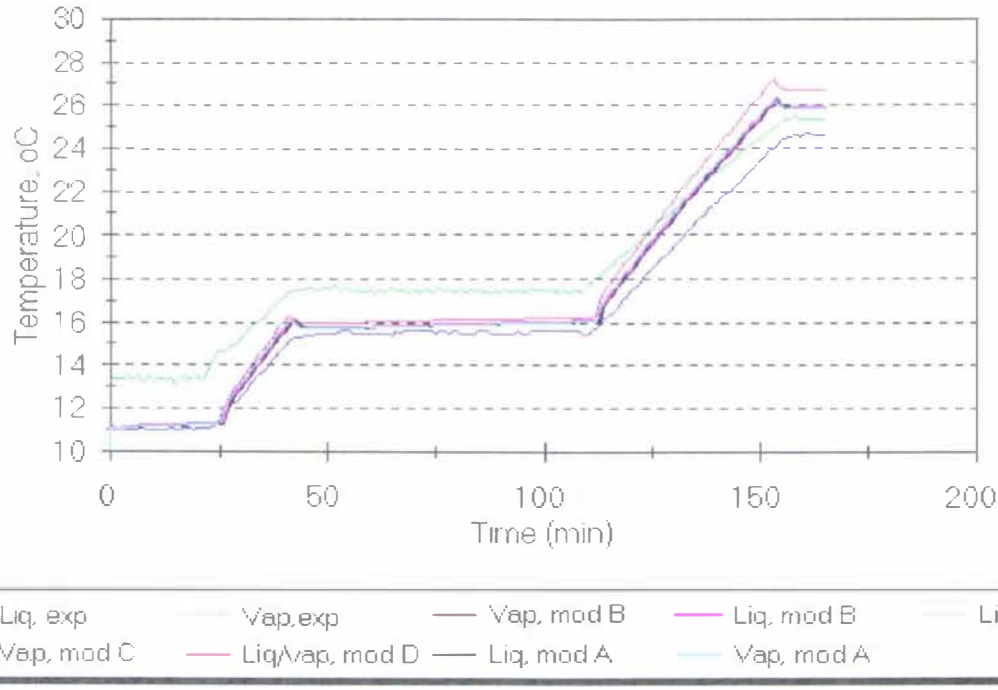

Fig. 9.11. Comparison of temperature profiles. Exp. and simulated data. **Trial 2**

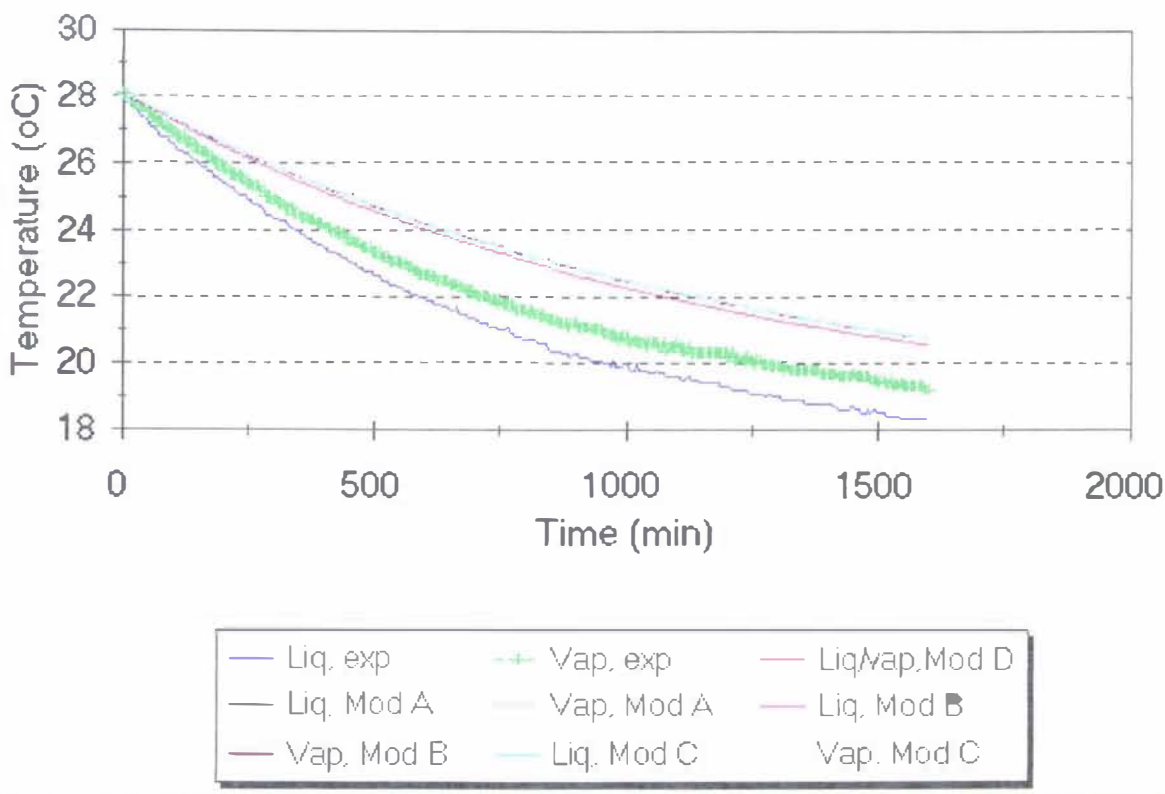

Fig. 9.12. Comparison of temperature profiles. Exp. and simulated data. Trial 3

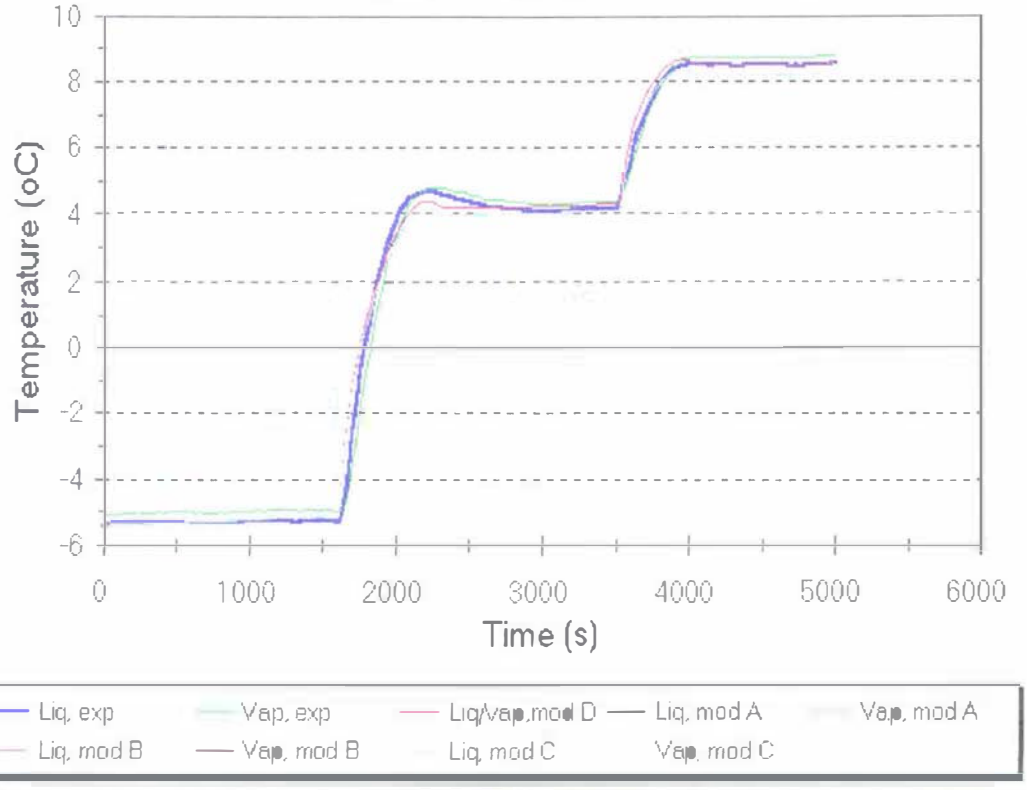

Fig. 9.13. Comparison of temperature profiles. Exp and simulated data **Trial 4**

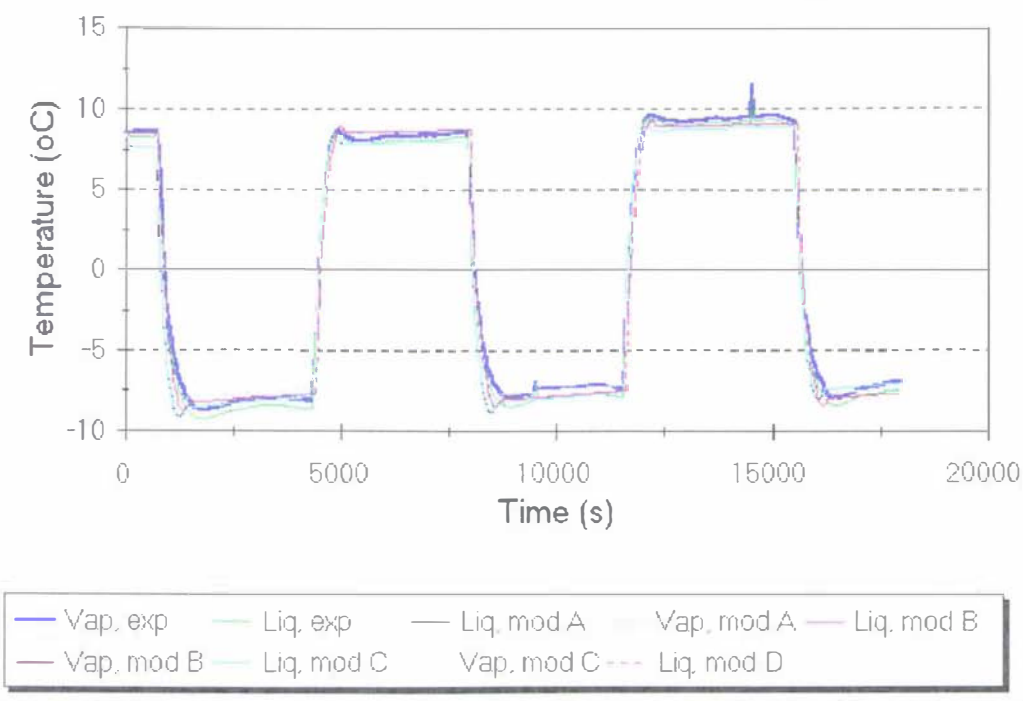

Fig. 9.14. Comparison of temperature profiles. Exp. and simulated data. **Trial 5**

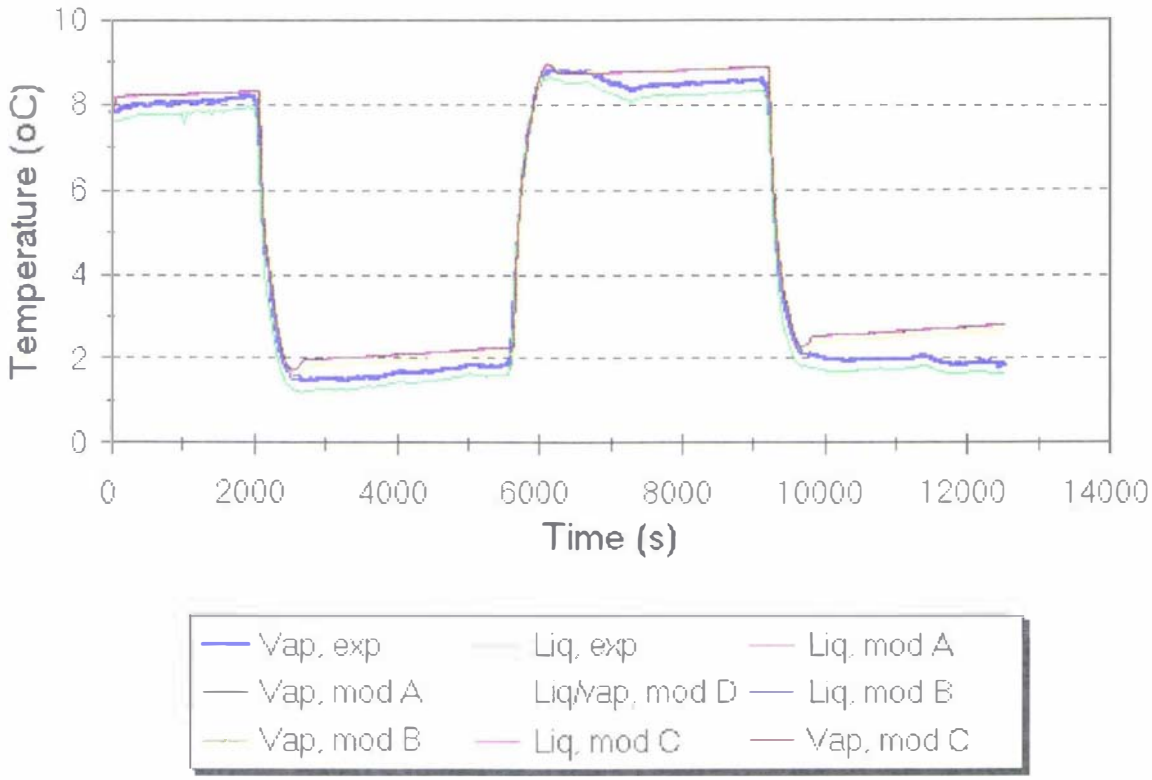

Fig.9.15. Comparison of temperature profiles. Exp. and simulated data. **Trial 6**

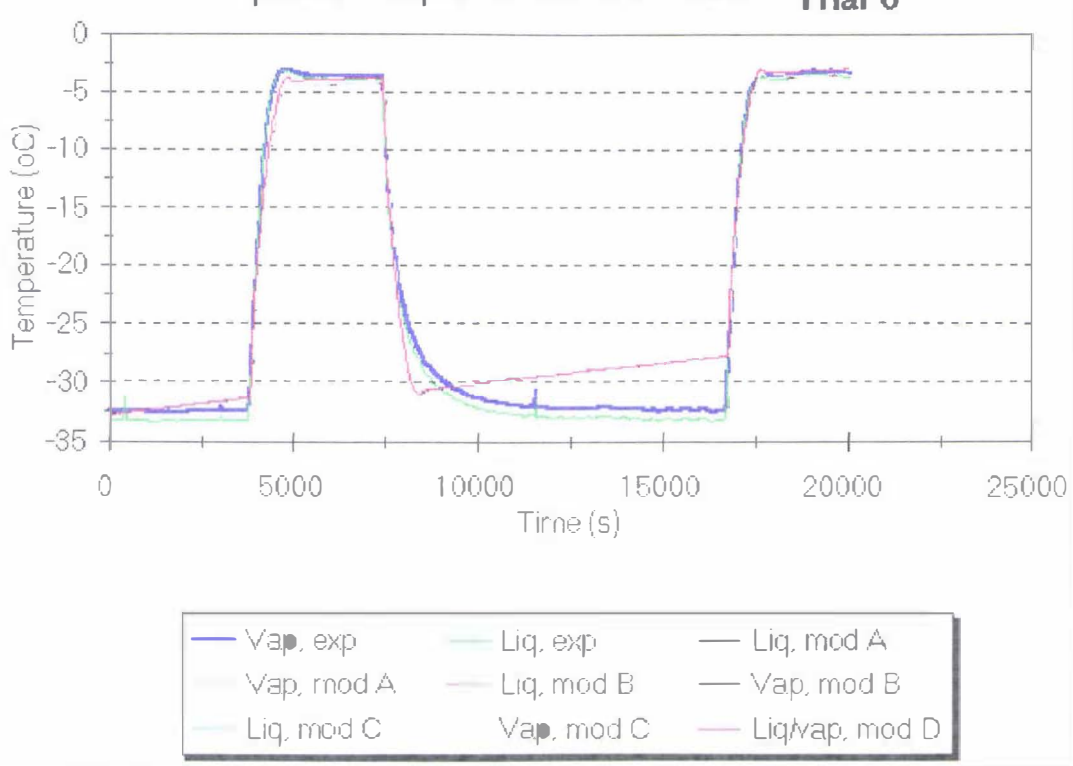

Models A, B and C had similar internal energy balances, which indicates that the use of the simplifications related to enthalpy and work terms did not significantly affect the predictions obtained. The internal energy balances of model D showed more congruence than those of models A, B and C, even with the use of significantly larger time steps in the simulation. The poorer internal balances for models A, B and C (which were still less than 1% in all cases) were probably due to the use of iterative procedures to find the saturated and superheated vapour properties and the estimates of the first derivatives with respect to time of vapour and liquid enthalpies, vapour mass, pressure and vapour specific volume. Model D avoided iterative procedures by assuming that all the refrigerant existed as saturated liquid. Model D only required the use of one ODE for the metal shell.

Model D tended to overpredict the rate of the change of temperatures of the shell and liquid, due to the lack of terms to account for energy used in the latent heat of evaporation. In models A, B and C, the heat taken up by the vapour phase was less than 1% of the total energy. However, the contribution of latent heat effects was about 2% for South Bank calorimeter trials and about 6% for the Star calorimeter trials.

Uncertainty in the estimates of the thermal capacity of the liquid refrigerant and the metallic shell and temperature measurement and the sources of error described in Section 9.4.3 all contributed to differences between measured and simulated temperature profiles. In the South Bank calorimeter (trials 3 to 6), the measured difference between vapour and liquid was always less than 0.2°C, and thus, within the precision of the instrumentation. Hence, the data were not suitable for testing whether the model adequately simulated any superheating or subcooling processes occurring. In the Star calorimeter (trials 1 and 2) the measured temperature difference between liquid and vapour phases was up to 2°C. In trial 1, there are 3 quasi-steady-state periods during which both condensation on the coil in the vapour and evaporation induced by the heater in the liquid were occurring simultaneously, and equally. This suggests that the vapour phase (if fully mixed) will be close to saturated, yet the measured data suggest superheat. The two most likely explanations are incomplete mixing in the vapour zone, with the thermocouple being located in an area away from the coil where there may be significant superheat, or measurement error. One possibility for the latter was that the thermocouple was influenced by the shell (*e.g.* by thermal bridging to it). Without dissembling the plant (which was not possible), this potential explanation could not be checked.

The differences between measured and experimental data must be interpreted in

relation to the experimental energy balances of Tables 9.5 to 9.11. For example, in trial 1, the measured temperature data suggested that $E_{T,1}$-$E_{T,2}$ was 7.6% less than Σq_{net} (*i.e.* the observed temperature change was consistent with a value of Σq_{net} 7.6% less than that measured). All models overpredicted the measured temperature change by about 10% when using essentially the same Σq_{net} as measured. The 6 experimental energy balances were all in error by 5 to 12% and considering this the agreement between experimental and simulated trials was satisfactory. Even the known major weaknesses in model D (neglect of latent heat effects between phases) was not particularly important. Trial 2 was worst predicted. This reflects a greater influence of inaccurate evaluation of $q_{amb \rightarrow vessel}$ for this run in which q_{heater} and q_{coil} were 0. The R of the insulation was not as accurately known as q_{heater} and q_{coil}.

Overall, because all the models accounted for the effect of the dominant thermal masses (liquid and metallic shell) in the systems studied (Fig.9.9), the good performance of all models was not surprising. The most complex models A, B and C did not display a noticeably higher level of accuracy than the simpler model D.

9.7. Practical example: scale-up of pressure vessels and simulated response using new models.

The two experimental systems used for the collection of experimental data were characterised by a high thermal mass in the metal shell of the vessel. In an industrial system, this might not necessarily be so.

Figure 9.16 shows predicted masses of metal, liquid and vapour for several sizes of vertical intercoolers and Fig. 9.17 presents the thermal mass (on a sensible heat only basis) of each component. The experimental calorimeters are at the lower end of the range where the metal shell is the largest thermal mass component. As the size of the vessel increases, the contribution of the liquid becomes more important than the effect of the metal shell. The vapour is never particularly important in itself. Although not shown, the latent heat would also be expected to remain important as vessel size increases.

In order to test the behaviour of the models when the liquid thermal mass is predominant, an example using a vessel of 1524 mm outer diameter was tested. A two-stage increase of energy input and energy removal by the coil was simulated, using a similar heating and cooling strategy to that in trial 3. The characteristics of the system investigated and the parameters of simulation are give in Table 9.11.

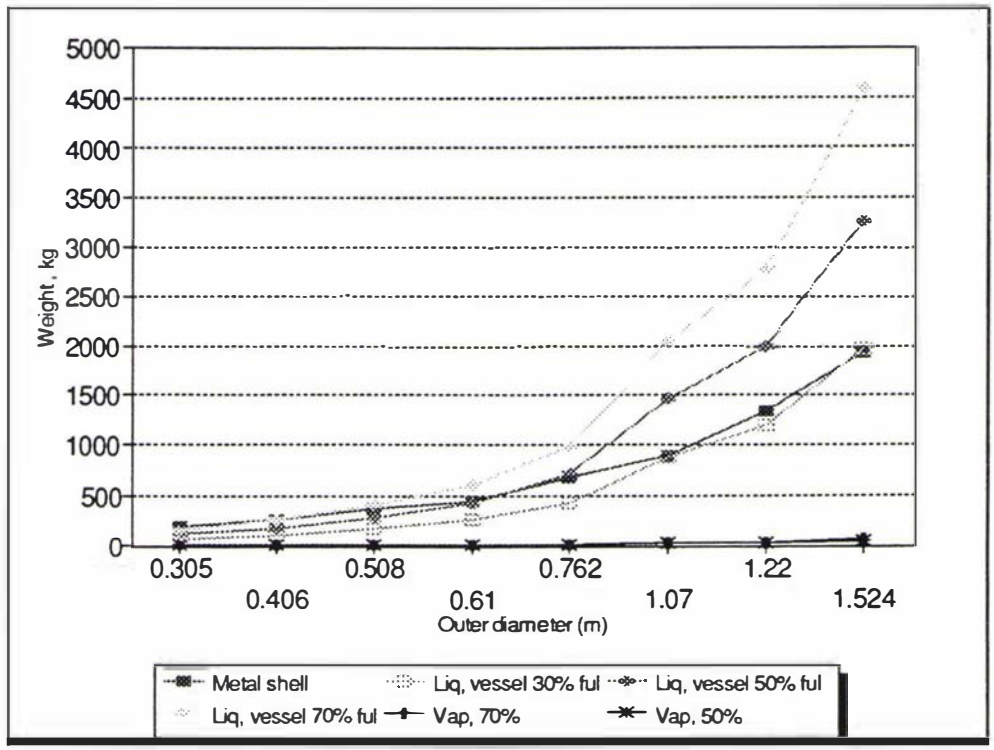

Figure 9.16. Total mass of components of a typical intercooler containing R134a

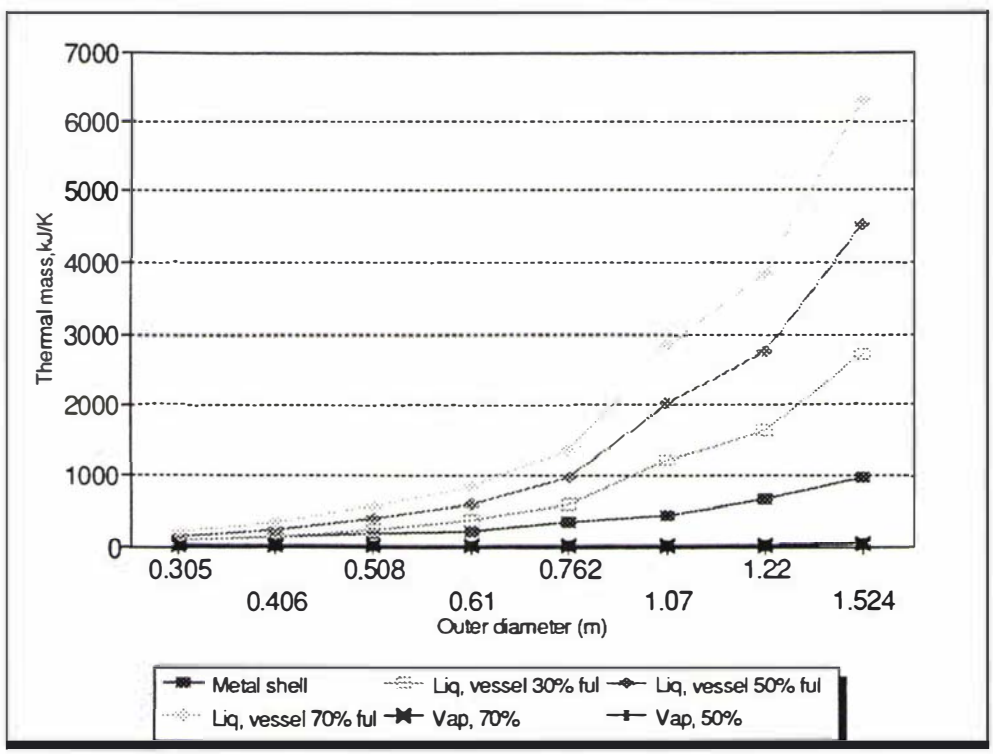

Figure 9.17. Components of sensible heat thermal mass for R134a in a typical vertical intercooler

TABLE 9.11. DATA USED IN THE PRACTICAL CASE OF SCALE-UP OF PRESSURE VESSELS.

TYPE OF DATA	SPECIFIC DATA REQUIREMENT	VALUES USED					
Computational factors	Time step (s)	0.1					
	Total simulation time (s)	8500					
	Iteration parameters	Number of iterations =12,Weighting = 0.25					
Time vs energy data	Timing of step changes (s)	0	1000	3000	4000	6000	8500
	Heat removal (kW), coil	-1	-1	-10	-10	-20	-20
	Heat input (kW), heater	1	10	10	20	20	20
Physical characteristics of vessel	Total height (m)	2.72					
	Internal diameter (m)	1.51					
	Thickness (m), metal shell, cylindrical part	0.007					
	Thickness (m), metal shell,	0.007					
	Thickness (m), metal shell, top	0.007					
	Thickness (m), insulation	0.2					
	Weight of empty vessel (kg)	1000					
Thermal properties	λ (W/m K), insulation	0.04					
	c (J/kg K), metal shell	500					
Refrigerant conditions	Refrigerant	R134a					
	Mass of refrigerant (kg)	2000					
	Flows in and out the vessel	None					
	$h_{vessel \rightarrow fluid}$ (W/ m^2 K)	500					
	Initial transition sub-model	liq saturated, vap saturated					
	Initial temperature, liquid (°C)	-5.4					
	Initial temperature, vapour (°C)	-5.4					
External environment	T_{room} (°C)	25					
	$h_{amb \rightarrow vessel}$ (W/ m^2 K)	10					

Only models A, C and D were tested, since the previous simulations did not show any significant difference between the predictions of models A and B. Table 9.12 presents the energy balances obtained for the 3 models and Figs. 9.18 to 9.20. show the response of the models in terms of:

a) The temperature of the liquid zone in the vessel (Fig. 9.18).
b) The evaporation and condensation mass flow rates between liquid and vapour zones (Fig.9.19).
c) The liquid level (Fig. 9.20)

Table 9.12 shows that models A, C and D retained their internal energy balances. The sensible heat taken up by the liquid contributed 80% to the net thermal storage, compared to a less than 30% contribution for the smaller experimental systems. Latent heat effects contributed about 4% to the energy storage and the vapour thermal mass accounted for only 0.3%.

The predictions from models A and C were virtually identical. Figure 9.18 shows that the differences of the final refrigerant temperature between model D and the most complex A and C models was only 0.2 °C out of a total temperature change of 6°C. This can be almost totally attributed to the omission of latent heat effect in model D.

An advantage of models A and C is their ability to predict the change of liquid level and the latent heat phenomena. Fig. 9.19 shows that for short times after the transition between steady-and unsteady-states some erratic behaviour of predicted evaporation and condensation rates occurs. Simulations carried out using smaller time steps showed the same behaviour. These oscillations were attributed to weaknesses in the approximations used to calculate the mass, enthalpies, pressures and specific volume time derivatives. The predicted changes in liquid level were consistent with the difference between evaporation and condensation mass flow rates. The oscillations illustrate that implementation of models A, B and C requires solution of a difficult set of equations. The improvement in accuracy over model D may not justify the extra effort involved.

TABLE 9.12. ENERGY BALANCE OBTAINED FOR MODELS A, B, C AND D. PRACTICAL CASE OF SYSTEM SCALE-UP.

ENERGY COMPONENT	MOD A	MOD C	MOD D
Initial temperature (liq,vap),°C[1]	-5.4,-5.4		
Final temperature (liq,vap),°C[1]	0.6,0.6	0.6,0.6	0.8
Sensible heat taken up by shell, kJ	3010.3	3009.6	3126.5
Sensible heat taken up by coil, kJ	0	0	0
Sensible heat taken up by liquid phase, kJ	15768.9	15769.8	16560.8
Sensible heat taken up by vapour phase, kJ	67.9	67.5	0
Latent heat from evap/condens, kJ	864.5	864.7	0
TOTAL (sources 1 to 5), kJ	**19711.7**	**19711.6**	**19687.3**
Total energy input by heater, kJ	121000	121000	121000
Total energy removal by coil, kJ	-102000	-102000	-102000
Energy infiltrated through shell, kJ	691.7	691.7	688.3
TOTAL (sources 6 to 8), kJ	**19690.8**	**19690.8**	**19687.3**
% ERROR (internal energy balance)	0.1	0.1	0.001

The systems studied experimentally did not include mass flows entering and/or leaving the system, so these parts of the models remain untested. However, it is expected that the thermal storage of the liquid will remain dominant over other buffering mechanisms in the system and that fluctuations in the liquid level created by flows will probably be more important than the condensation and evaporation mass flow rates in terms of liquid level prediction.

Fig.9.18 SCALE-UP COMPARISON OF TEMPERATURES FOR MODELS A, C AND D

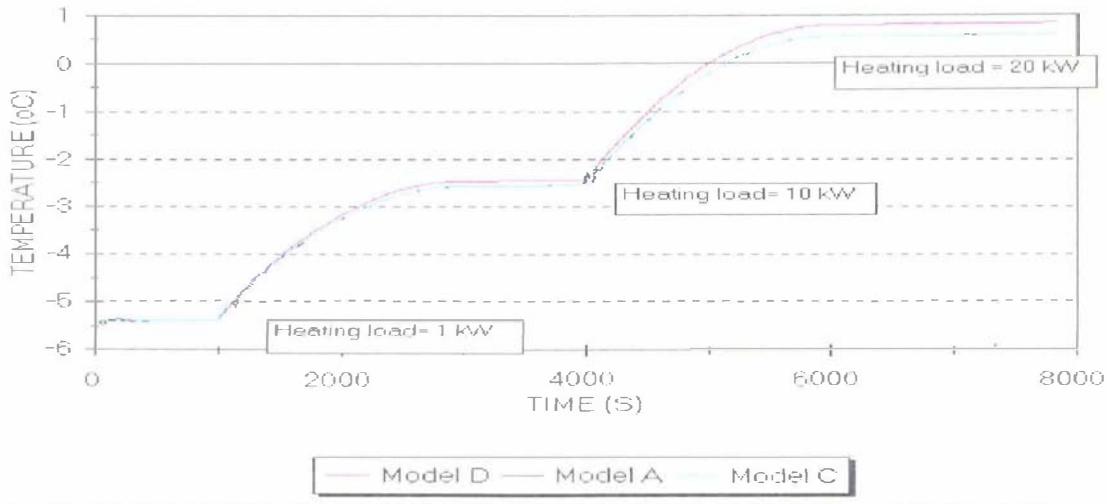

Fig.9.19 EVAP AND CONDEN MASS FLOW RATES FOR MODELS A, C AND D

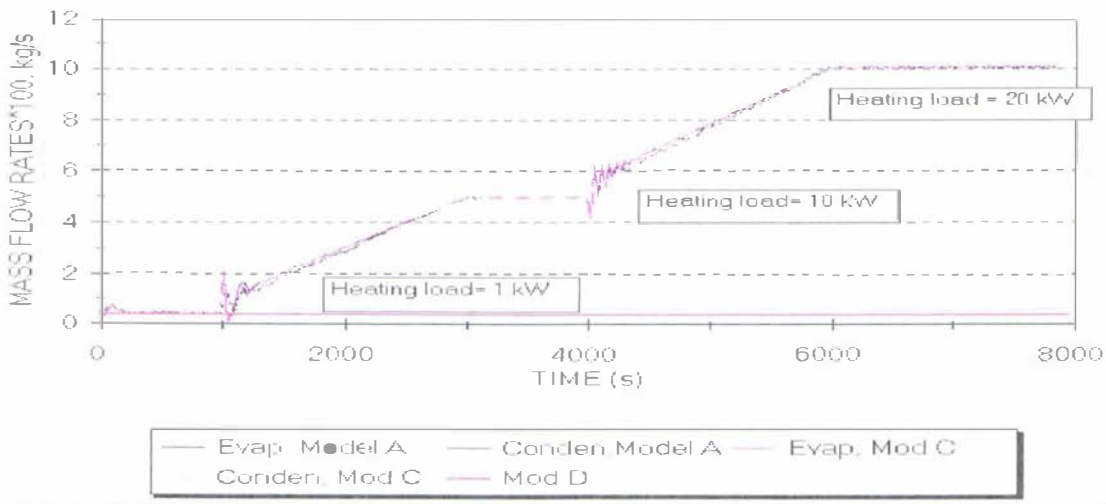

Fig.9.20 LIQUID LEVEL SIMULATION FOR MODELS A, C AND D

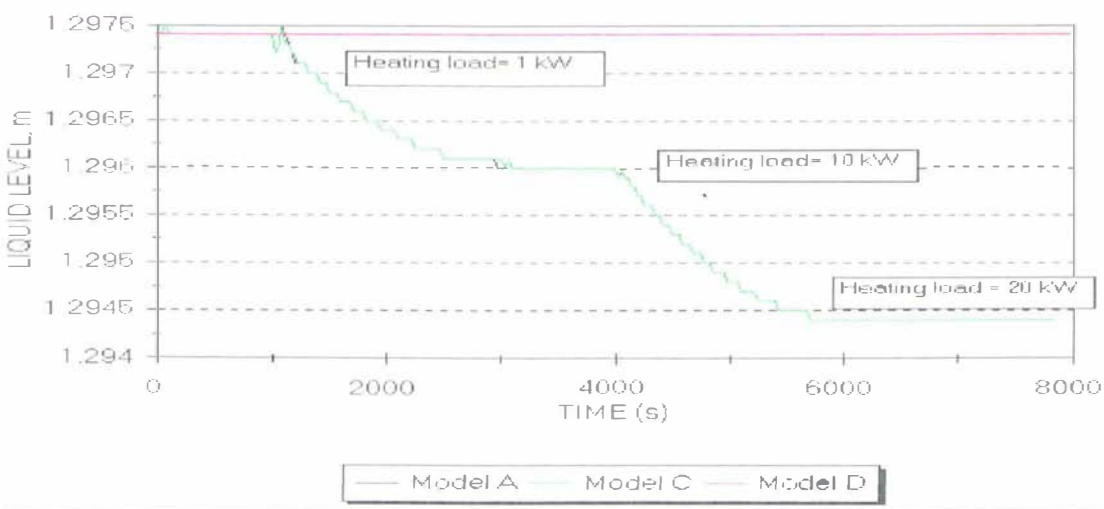

9.8 *Overall evaluation of pressure vessels models*

The experimental validation of the models was performed in systems characterised by small variations in the liquid level and conditions very close to saturation.

- In the experimental systems the thermal masses of the metallic shell and liquid phase were the most significant energy holding components. Other components, such as latent heat, thermal capacity of coil and vapour phase, contributed less than 7% to the energy storage.

- The effect of work between phases (caused by change of volume of liquid and vapour zones) and the effect of the approximation $\frac{du_g}{dt} \approx \frac{dh_g}{dt}$ were both negligibly small, meaning that Models A and B were essentially equivalent in performance.

- The almost saturated conditions of the refrigerant in the trials made it difficult to evaluate the accuracy of the modelling of transitions between phases. Model C (which lacked transition sub-models) predicted almost exactly the same temperature profiles as models A and B (which considered transitions)

- The simple one refrigerant-zone (liquid only) thermal model D, which did not consider latent phenomena, predicted rates of temperature change that were less than 10% different from those predicted by other models. Model D also offered considerable advantages in terms of ease of computer implementation and computational cost.

- The ranges covered by the experimental work do not encompass all conditions that may be encountered industrially, particularly in respect to liquid level, deviation from saturation and extent of vessel pressure variation. However, the industrial case study suggested that the conclusions from the small scale work may be valid for wider ranges than investigated experimentally.

- This research verified that for models operating with good liquid level control and close to saturation, the earlier assumptions of James (1972) and Cleland (1986) used in development of models B, C and D are valid and hence these models are expected to perform satisfactorily in many situations commonly found in industrial pressure

vessels.

- Future development of thermal-only modelling strategies for pressure vessels might be most effective if based on simple models such as the one refrigerant-zone model D tested in this project. The addition of an extra empirical term to account for the latent heat effect in this model may be worthwhile.

- A potential advantage of more complex models that account for mass transients is their possible application for selection of liquid level controllers and the evaluation of the real state of the refrigerant mass flows leaving vessels (rather than assuming saturation). More analysis of models A, B and C and further experimental data collection following the mass transients of vessels would be needed to evaluate Models A, B and C for these applications.

- Some of the mathematical models developed here for pressure vessels might be applicable elsewhere, *e.g.* in evaporator models, where transition sub-models for detecting refrigerant phase changes are necessary. Further investigation of iterative solution methods to solve the resulting equation sets more efficiently is recommended.

CHAPTER 10: CONCLUSIONS

10.1. Wall structures

All physically realistic models for regions within solid heat conducting walls in low temperature applications can be constructed from 5 basic concepts: null (***N***), resistance (***R***), capacity (***C***), lumped (***L***) and distributed (***D***). These concepts underpin the classification of mathematical models according to the selection of thermal characteristics to be modelled, decisions made about the distribution of resistance and capacity within the wall and the degree of model complexity.

Experimental testing confirmed that predictions by a finite element method (FEM) with grids selected according to good engineering practice were accurate simulations of real wall behaviour. The observed lack of fit was explainable by uncertainties associated with the experimental set-up and model input data. A fully distributed finite difference model (***DDD***) yielded predictions in good agreement with the FEM responses. Simpler models could therefore be validly evaluated by comparison to FEM or ***DDD*** predictions.

Mean heat flux, amplitude of the cyclic heat flux and offset between FEM and models were valuable measures for characterising the thermal behaviour of low temperature room walls and identifying physically inadequate models. They were unsuitable for ranking of physically sensible models in terms of accuracy. Peak and mean standard deviations of differences between predicted and actual heat flux were more useful to assess accuracy. Tolerance-related measures were most useful for indicating weaknesses of models at certain times during the daily cycle of thermal behaviour.

All models, regardless of the type of wall represented and the level of model complexity, simulated the mean behaviour of the wall (represented by the mean heat flux) in an accurate manner. The simplest algebraic approach ***RRR*** is thus the most complex model required.

The recommended models for dynamic behaviour of wall layers are:

- Insulation: ***R*** model for thin layers or ***L*** or ***D*** models for thick layers
- Metal: ***C*** model

- Concrete: ***L*** or ***D*** models, (but for external wall layers more zones are required than for internal wall layers)

Overall, for walls of low resistance and capacity an ***RRR*** model can be adequate. As the thermal resistance and/or capacity rise, retention of accuracy in dynamic modelling requires use of increasingly complex models and grid selection strategies, leading eventually to ***LLL*** or ***DDD*** models. The following grid selection strategies are then recommended:

- ***L*** models: 8 zones or more to represent an external layer; 5 zones or more to represent an internal layer; even distribution of resistance and capacity within a layer; setting of a capacitive zone at the environment boundaries.

- ***D*** models: 5 nodes or more to represent an external layer; 3 nodes or more to represent an internal layer.

The choice of model complexity must ultimately reflect the final application of the model, so the proposed methodology cannot be applied arbitrarily without sound engineering judgement.

10.2. Pressure vessels.

The measured rate of temperature change of the experimental refrigerant vessel systems in response to changes in heat input was most strongly influenced by sensible heat storage in the metal shell and liquid refrigerant.

The models that ignored work exchange caused by volume change in the liquid and vapour phases and substituted the rate of vapour internal energy change with time by the rate of enthalpy change with time, performed no differently to the model that did not make these simplifying assumptions. Inclusion of transition criteria to allow models to move between saturated, subcooled and superheated states did not improve predictions for the experimental systems, but all trials were conducted near saturation conditions. A model considering thermal capacity in only the vessel shell and liquid refrigerant predicted rates of temperature change within 10% of predictions by all other models.

In situations with good liquid control and close to saturation conditions, the simplest thermal capacity only model would be expected to perform satisfactorily. An industrial case

study suggested that this finding could well apply to wider ranges than studied experimentally.

Areas justifying further study include empirical adjustment of the simple shell and liquid refrigerant model to include compensation for evaporation/condensation effects between phases, fuller evaluation of mass flow and liquid level effects, and application of pressure vessel model principles to other refrigeration system component models.

NOMENCLATURE

A	area (m^2)
a	constant = 1.86
b	constant = 2.2
B_1, B_2, B_3, B_4	algebraic variables in Eqs. (8.33) and (8.51)
c	specific heat capacity (J/kg K)
C	volumetric spec. heat capacity (J/m^3 K)
CIC	concrete-insulation-concrete type wall
CIM	concrete-insulation-metal type wall
CT	concrete type wall
$\mathbf{C}$	thermal capacity within a region (J/m^2 K)
$\boldsymbol{C}$	thermal capacity model
c	pure capacitive zone
$crit$	iteration criteria, Section 8.4.3.2
$\boldsymbol{D}$	distributed model
D_a	astronomical day length (hrs)
E	energy (J)
e	specific energy (J/kg)
FD	finite differences
ff	constants of vapour specific volume, polynomial Eq (8.45)
FEM	finite element method
g	gravitational acceleration (9.81 m/s^2)
h	heat transfer coefficient (W/m^2 K)
H	heat generation rate (W/m^3)
Hg	heat generation (W/m^2)
$\boldsymbol{h}$	enthalpy (J/kg)
hr	radiative heat transfer coefficient (W/m^2 °C)
$\boldsymbol{L}$	lumped model
$\boldsymbol{L1}$	$\boldsymbol{L}$ model with a r zone in both boundaries
$\boldsymbol{L2}$	$\boldsymbol{L}$ model with a c zone in both boundaries
$\boldsymbol{L3}$	$\boldsymbol{L}$ model with an r zone in external boundary and a c zone in internal boundary
$\boldsymbol{L4}$	$\boldsymbol{L}$ model with an r zone in internal boundary and a c zone in external boundary
L_8	orthogonal array, experimental design
M	mass (kg)
m	mass flow rate (kg/s)
$\boldsymbol{N}$	null model
$\boldsymbol{n}$	number of measurements in Eq (5.4)

ODE	ordinary differential equation
p	pressure (Pa)
PDE	partial differential equation
Q	heat flux (W/m^2)
QE	quality engineering
q	heat flow (W)
$\mathbf{R}$	thermal resistance within a region (m^2 K/W)
$\boldsymbol{R}$	pure resistive region
r	pure resistive zone
s	superheating (°C)
sc	subcooling (°C)
SD	standard deviation
SPT	sandwich panel type wall
T	temperature (°C)
$\boldsymbol{T}$	temperature (K)
t	time (s)
t_d	solar time in a 24 hr daily cycle (hrs)
t_{min}	time of minimum ambient temperature in a daily cycle (hrs)
T_{max}	maximum ambient temperature in a daily cycle (°C)
T_{min}	minimum ambient temperature in a daily cycle (°C)
t_{set}	solar time at start of ambient temperature decay (hrs)
U	internal energy (J)
u	specific internal energy (J/kg)
V	volume (m^3)
v	specific volume (m^3/kg)
$\boldsymbol{v}$	velocity (m/s)
$\boldsymbol{W}$	solar constant= 1390 W/m^2
Wgt	weighting fraction, Section 8.4.3.4
W_{fl}	flow work (J)
w_{fl}	specific flow work (J/kg)
W_s	external work (kJ)
w_s	specific external work (kJ/kg)
w_T	total work (W)
x	distance (m)
$\boldsymbol{x}$	magnitude of measurement in Eq. (5.4)
$\bar{\boldsymbol{x}}$	arithmetic mean of measurement in Eq. (5.4)
X	total dimension (m)
Y	constants of vapour specific volume, polynomial Eq (8.45)

z	constant =-0.17
Z	length (m)
Z_T	total length (m)
Z_g	vapour level (m)
Z_l	liquid level (m)

Greek letters

α	absorptivity (dimensionless)
Δ	increment
σ	Stefan-Boltzmann constant = 5.66 x 10^{-8} W/m^2 K^4
ρ	density (kg/m^3)
λ	thermal conductivity (W/m K)
∂	partial differential
ε	emissivity (dimensionless)
Θ	Incidence angle of solar rays (radians)
ϕ_1,ϕ_2	Heat flux term used in algebraic systems (W/m^2)
γ	Spatial weight for thermal capacity within a zone in lumped sub-models
ζ	Spatial weight for thermal conduction within a zone in lumped sub-models
ψ	Spatial weight for thermal capacity and thermal resistance within a zone in distributed models

Subscripts

1,2,3	in thermal properties: layer number; in thermodynamic properties: stream number
a	instantaneous external ambient condition
acc	accumulated
amb	mean external environment condition
a→w	transfer from external environment to wall
c	convection
coil	property of cooling coil, pressure vessels
cond	conduction only heat transfer
con	condensation flow property
em	emitted
ev	evaporation flow property
fl	property of vapour entering the vessel
flows in	flows entering system boundaries
flows out	flows leaving system boundaries
g	vapour property
heater	property of heater, pressure vessels
i	index for streams and thermodynamic properties

i	counter in Eq. (5.4)
in	flow entering a layer from left to right
inc	incident
insul	insulation
it	iterated property, Section 8.4.3.2
j	space index, finite difference equations
l	liquid property
latent	latent heat property
max	maximum
mean	to mean heat load
min	minimum
n	number of zone
nr	number of region
NR	total number of regions
nz	total number of zones
out	flow leaving a layer from left to right
object	property of object in contact with system
old	property value of previous time step, Section 8.4.3.2
peak	peak heat load
room	mean internal environment condition
rad	radiation
sat	saturated properties
shell	metal shell
sky	related to sky temperature
source	energy component in Eqs.(9.14) and (9.15)
T	total
w→room	transfer from wall to room

Superscripts

i	time index, finite difference equations

Special Symbols

→	Used to indicate the precedence (from left to right) of one region/zone over another region/zone.

REFERENCES

Amos, N. (1995). *Mathematical modelling of heat transfer and water vapour transport in apple coolstores*. PhD Thesis. Massey University, New Zealand. 269 pp.

Amraie, M., Missenden, J. F. and James, R. W. (1988). A critical survey of chilling carcass meat within the refrigerated enclosures. *Research Memorandum 110 , Inst. of Env. Eng.* South Bank Polytechnic. London.

Amraie, M, Missenden, J. F. and James, R. W. (1989). Air velocity performance on pig carcasses in pre-chill room. *Research Memorandum 117 , Inst. of Env. Eng.* South Bank Polytechnic. London.

Amraie, M. (1993). *An investigation into improved room air movement and velocity distribution within meat chilling rooms*. PhD thesis. CNAA, South Bank University.

Ansari, F.A., Charan, V. and Varma, H.K. (1984). Heat and mass transfer analysis in air-cooling of sperical food products. *Int. J. Refrig.* 7: 194-197.

Athienitis, K. A., Stylianou, M. and Shou, J. (1990). A methodology for building thermal dynamics studies and control applications. ASHRAE Tech Data Bull. *Building Thermal Dynamics: Techniques and Applications*. 6(3): 23-32.

ASHRAE (1995). *ASHRAE Handbook of Fundamentals*. Amer. Soc. of Heat., Refrig. and Air Cond. Eng. Atlanta, GA.

Bartolini, C. M. and Caressana, F. (1991). Mathematical model for the prediction of screw compressor performance. *Proc. 18th Int. Cong. Refrig*. Montreal, Can. 3: 1239-1242.

Bejan, A. (1993). *Heat transfer*. John Wiley & Sons, Inc. New York. 675 pp.

Bonte, A and Vedhoven, V. B. (1983). Dynamic behaviour of a refrigeration plant. *Proc. 16th. Int. Cong. Refrig.* 2: 845-851.

Chan, C. K. and Scott, R. D. (1988). A critical survey of mathematical models for predicting room air movement. *Research Memorandum 109 , Inst. of Env. Eng.* South Bank University, London.

Chen, Z. J and Ling, W. H. (1991). Dynamic simulation and optimal matching of a small-scale refrigeration system. *Int. J. Refrig.* 14: 26-34.

Chen, Z. J., Ding, G. L., Wang, X. F. and Que, X. C. (1995) Dynamic simulation and optimal matching of a small-scale refrigeration system with multi-refrigerant. *Proc. 19th Int. Congr. Refrig.* 3a: 262-269.

Chi, J and Didion, D. (1982). A simulation model of the transient performance of a heat pump. *Int. J. Refrig.* 5: 176-184.

Cleland, A. C. (1983). Simulation of industrial refrigeration plants under variable load conditions. *Int. J. Refrig.* 6: 11-19.

Cleland, A. C. (1985). Experimental verification of a mathematical model for simulation of industrial refrigeration plants. *Int. J. Refrig.* 8: 275-282.

Cleland, A. C. (1986). Computer subroutines for rapid evaluation of refrigerant thermodynamic properties. *Int. J. Refrig.* 9: 346-351.

Cleland, A. C. (1990). *Food Refrigeration Processes.* Analysis, Design and Simulation. Elsevier Applied Science Ed. London. 284 pp.

Cleland, A. C. (1994). Polynomial curve-fits for refrigerant thermodynamic properties: extension to include R134a. *Int. J. Refrig.* 17: 245-249.

Cleland, D. J. (1985). *Prediction of freezing and thawing times for foods.* PhD thesis. Massey University, New Zealand. 281 pp.

Cleland, D. J, Boyd, N. S. and Cleland, A. C. (1982). A model for fish freezing and storage on board small New Zealand fishing vessels. *Refrig. Sci. and Tech.* (1982-1): 81-88.

Cleland, D. J. and Cleland, A. C. (1995). *Cost-effective refrigeration.* Massey University. New Zealand. 400 pp.

Cleland, D.J., Cleland, A.C. and Jones, R.S. (1994). Collection of accurate experimental data for testing the performance of simple methods for food freezing time prediction. *J. Food Proc. Eng.* 17 (1994): 93-119.

Clements, D. (1989). *Mathematical modelling: A case-study approach.* Cambridge University Press, New York. 166 pp.

Colding, L. (1987). Energy consumption in the refrigeration plant of a cold store. *Refrig. Sci. and Tech.* (1987-1): 119-125.

Colding, L., Danig, P. O. and Thuesen, S. E. (1991). Dynamic model of refrigerating systems using air cooled condensers. *Proc. 18th Int. Cong. Refrig.* Montreal, Can. 3:1208-1212.

Cornelius, M. (1991). *Refrigeration Analysis, Design and Simulation Package: "RADS". Notes for users. Release 3.1.* Food Tech. Research Centre. Massey University, New Zealand.

Crosbie, E. R. (1984). Continuous and discontinuous-change models: concepts for simulation languages. In: Oren,T.I, Zeigler, B.P. and Elzas, M.S. (eds). *Simulation and Model-based Methodologies: an integrative View.* NATO-ASI Series V. F10. 337-356.

Cunniffe, M. James, R. W., Dunn, A. (1985). An analysis of fault occurrence in refrigeration plant and the effect on current practice. *Proc. Inst. of. Refrig. (UK).* 8pp.

Darrow, J.B., Lovatt, S.J. and Cleland, A.C. (1991). Assessment of a simple mathematical model for predicting the transient behaviour of a refrigeration system. *Proc. 18th Congr. Refrig.* 3: 74-80.

Delsante, A. E., Stokes, A. N. and Walsh, P. J. (1983). Application of Fourier transforms to periodic heat flow into the ground under a building. *Int J. Heat Mass Transfer.* 26: 121-132.

Deng, S. M. (1990). A mathematical model of a direct expansion air cooling plant. *Research Memorandum 24 , Inst. Env. Eng.* South Bank Polytech. 42 pp.

Deng, S. M. and Missenden, J. (1990). Validation and simplification of a direct expansion air cooler model. *Research memorandum 128, Inst.Env. Eng.* South Bank Polytech. 23 pp.

Ding, G. L., Zhang, C. L., Wang, X. F. and Chen Z. J. (1995). Calculating the wall z-transfer function with state space method for unsteady heat transfer through thermal insulation layer. *Proc. 19th. Int. Cong. Refrig.* 2: 65-72.

Finer, S. I, Cleland, A. C and Lovatt, S. J. (1993). Simple mathematical model for predicting the transient behaviour of an ice-bank system. *Int. J. Refrig.*, 16: 312-320.

Gaffney, J. J, Baird, D. C. and Chau, V. K. (1985). Influence of airflow rate, respiration, evaporative cooling and other factors affecting weight loss calculations for fruits and vegetables. *ASHRAE Trans.* 91: 690-707.

Glockner, G. and Findeisen, F. (1984). The computing program LF74. A software solution for typical simulation problems of air and refrigeration engineering. *Refrig. Sci. and Tech.* (1984-1): 231-236.

Gloeckner, J. Hoffer, B, Kluge, Ch, Schroth, H. and Wobs, E. (1990). Simulation of refrigerating plants for cold stores. *Refrig. Sci. and Tech.* (1990-1): 487-493.

Gosney, W. B. and Olama H. A. L. (1975). Heat and enthalpy gains through cold room doorways. *Research Memorandum 25 , Inst. of Env. Eng.* South Bank Polytech. London.

Grey, W. A. and Muller, R. (1974). *Engineering calculations in radiative heat transfer.* Pergamon Press, Oxford, N.Y. 161 pp.

Grossmann, W., Konig, P. and Scheunemann, K.H. (1967). System for the calculation of transient thermal responses of rooms. *Refrig. Sci. and Tech.* (1969-1): 163-168.

Hargreaves, M. R. O. and James, R. W. (1979). A model of a marine chilled water plant for microprocessor control development. *Proc. Inst. of Refrig.* (UK). 76: 28-38.

Higuchi, K. and Hayano, M. (1982). Dynamic characteristics of thermostatic expansion valves. *Int. J. Refrig.* 5: 216- 220.

ISO reference: see p.290

James, K. A. (1988). *Dynamic mathematical modelling of refrigeration systems and heat pumps.* PhD thesis. South Bank Polytechnic, London. 277 pp.

James, K. A. and James, R. W. (1986a). Dynamic analysis of a heat pump using established modelling techniques. *Research Memorandum 98 , Inst. of Env. Eng.* South Bank Polytechnic. London. 16 pp.

James, K. A. and James, R. W. (1986b). Transient analysis of thermostatic expansion valves. *Research Memorandum 99 , Inst. of Env. Eng.* South Bank Polytechnic. London. 28 pp

James, K. A, James, R. W and Dunn, A. (1986). A critical survey of dynamic mathematical models of refrigeration systems and heat pumps and their components. *Research*

Memorandum 97, Inst. of Env. Eng. Polytechnic of the South Bank, London.

James, R. W. and Marshall, S. A. (1973). Dynamic analysis of a refrigeration system. *Proc. Inst. Refrig* (UK). 70: 13-24.

James, R. W. and Marshall, S. A. (1976). The heat pump as a means of utilising low grade heat energy. Building Society of England, 13:202-207.

James, R. W. and Eftekhari, M. (1990). A flow regulation system for dry expansion evaporators. *Proc. Inst. Refrig. (UK).* 1990-91: 6-1 to 6-7.

Kelijnen, J. (1974). *Statistical techniques in simulation.* M. Dekker, New York. 776 pp.

Kusuda, T. (1985). Heat transfer in buildings. In: Rohsenow, W.M, Hartnett, J.P. and Ganic, E.N. (Eds). *Handbook of heat transfer applications.* 2nd Ed. Mc Graw Hill, Inc. 964 pp.

Kimball, B. A. and Bellamy, L. A. (1986). Generation of diurnal solar radiation, temperature and humidity patterns. *Energy in Agriculture.* 5: 185-197

Koelet, P. C. (1992). *Industrial Refrigeration. Principles, design and applications.* The MacMillan Press Ltd. Houndmills, U. K. 429 pp.

Kosgaard, V. (1967). Thermal and electrical models for solving problems of non-stationery heat transfer through walls. *Refrig. Sci. and Tech.* (1969-1): 87-90.

Lopez, A., Lacarra, G. and Grenier, Pp. (1995). Dynamic analysis of centralised refrigeration systems in food plants. *Proc. 19th Int. Congr. Refrig.* 3a: 538-545.

Lovatt, S. T. (1992). *Development of a dynamic modelling methodology for the simulation of industrial refrigeration systems.* PhD Thesis. Massey University, New Zealand. 254 pp.

Lovatt, S. T. (1995). A unified strategy for modelling meat refrigeration process indicators. *Proc. 19th Int. Congr. Refrig.* 3a: 653-659.

MacArthur, J. W. (1984). Transient heat pump behaviour: a theoretical investigation. *Int. J. Refrig.* 7(2): 123-132.

MacArthur, W. J and Grald, W. E. (1989). Unsteady compressible two phase flow model for predicting cyclic heat pump performance and a comparison with experimental data. *Int. J. Refrig.* 12: 29-41.

MacArthur, W. J., Mathur, A. and Zhao, J. (1990). On-Line recursive estimation for load profile prediction. ASHRAE Technical Data Bulletin. *Building Thermal Dynamics: Techniques and Applications.* 6: 66-73.

Marshall, S. A. and James, W. R. (1975). Dynamic analysis of an industrial refrigeration system to investigate capacity control. *Proc. Inst. Mech. Eng.* 189: 437-444.

Meer, van der J. S., Machielsen, C. H. M. and Touber, S. (1984). Simulation of a dry evaporator fed by a liquid sensing expansion valve. *Refrig. Sci. and Tech.* (1984-2): 205-212.

Meffert, H. F. (1988). Basic elements of a physical model for refrigerated vehicles. II: temperature distribution. *Refrig. Sci. and Technol.*, (1988-1): 221-231.

Meffert, H. F and Van Beek, G. (1983). Basic elements of a physical model for refrigerated vehicles: I-Air circulation and distribution. *Proc. 16th Int. Congr. Refrig.* 4: 465-476.

Missenden, J. F., Lovatt, S. J. and Amraie, M. (1995). Improved air mixing inside meat chillers. *Proc. Inst. of Refrig. (UK).* 2-1 : 2-10.

Moreno, J. (1987). Air interchange rate through a cold store open door. *Proc 17th Int. Cong. Refrig.* 138-143.

Murphy, W. E. and Goldschmidt, V. W. (1984). Measurement of transient temperatures downstream of the evaporator in an insulated duct. *ASHRAE Trans.* 90, 1: 245-61.

Myers, G. (1971). *Analytical methods in conduction heat transfer.* Mc Graw Hill, New York. 508 pp.

Neelemkavil, F. (1987). *Computer Simulation and Modelling.* Wiley & Sons Co. 307 pp.

Nowotny, S. (1983). Long-term experiences with the application of mathematical models to analyze the steady state and dynamic behaviour of refrigerating systems and components - General aspects to establish a catalogue of computer programs. *Proc. 16th. Int. Cong. Refrig.* 1:51-59.

Pala, M. and Devres, Y.D. (1988). Computer simulated model for power consumption and weight loss in a cold store. *Refrig. Sci. and Tech.* (1988-1):233-241.

Patankar, S.V. (1980). *Numerical heat transfer and fluid flow.* Mc Graw Hill, N.Y. 370 pp.

Pearson, S.F. (1995). Automatic calorimeter for refrigerant mixtures. *Refrig. Sci. and Tech.* (1995-4b): 481-485.

Pearson, S. F. (1996). Ammonia Low Pressure receivers. *Proc. Inst. Refrig. (UK).* London, (4-1): 4-8.

Perry, E. J. (1987). Refrigeration system optimization. *Int. J. of Refrig.* 10(7): 217-223.

Pham, Q. T. (1991). Computer calculation of meat plant refrigeration requirements. *Technical Report MIRINZ-ISSN* 0465-4390. 14 pp.

Pham, Q. T., Wee, H. K., Kemp, R. M and Lindsay, D. (1994). Determination of the enthalpy of foods by an adiabatic calorimetric. *J. Food Eng.* 21: 137-156.

Radford, D, R., Herbert, S. L. and Lovett, A. D. (1976). Chilling of meat -A mathematical model for heat and mass transfer. *Refrig. Sci. and Tech.* (1976-1): 323-330.

Ree, van der H., Basting, J. W. and Nievergeld, M. G. P. (1974). Prediction of temperature distributions in cargoes with the aid of a computer program using the method of finite elements. *Refrig. Sci. and Tech.* 1974-1: 195-219.

Reynoso, R. O. and De Michelis, A. (1988). Simulation of cryogenic batch freezers. *Int. J. Refrig.* 11(1): 6-10.

Ross, P. J. (1989). *Taguchi techniques for quality engineering: Loss function, orthogonal experiments, parameter and tolerance design.* McGraw Hill, New York. 279 pp.

Ruud, D. M, Mitchell, W. J. and Klein, A. S. (1990). Use of building thermal mass to offset cooling loads. ASHRAE Technical Data Bulletin. *Building Thermal Dynamics: Techniques and Applications.* 6(3): 4-13.

Sluis, van der, S.M. (1993). Cooling and freezing simulation of bakery products. *Refrig. Sci. and Tech.* (1993-3): 249-258.

Sluis, van der, S.M. (1995). Prediction of chilling of turkey carcasses using a finite element method. *Proc. 19th Congr. Refrig.* 3a: 692-699.

Shen, X., Ji, S., Wang, L., Xi, J. and Zao, G. (1995). Experimental verification of a mathematical model for simulation of a compressor refrigeration capacity test system. *Proc. 19th Int. Congr. Refrig.* 3a: 530-537.

Stephenson, D. G. and Mitalas, G. P. (1967). *Room thermal response factors.* Paper presented in ASHRAE Meeting, Detroit, Mich .1-10.

Stera, A. (1996). Marine refrigerated transport: Recent achievements and outlook for the future. *Bull. Int. Inst. Refrig.* (96-2):4-17.

Sunden, B. (1987). Numerical prediction of transient heat conduction in a multilayered solid with time-varying surface conditions. In: Lewis, R.W, Morgan, C. and Habashi, W. G. (eds). *Numerical Methods in Thermal Problems.* 4: 651-659.

Taguchi, G. (1986). *System of experimental design.* Quality Resources, Amer. Supp. Inst. Vol. II. 440 pp.

Tamm, W. (1963). Airflow within air curtains to protect cold rooms. *Proc. 11th Int. Cong. Refrig.* I: 1025-1033.

Touber, S. (1984). Principles and methods for mathematical modelling steady-state and dynamic behaviour of refrigeration components and installations. *Refrig. Sci. and Tech.* (1984-2): 163-175.

Tree, R. D and Weiss, W. B. (1986). Two time constant modelling approach for residential heat pumps. *Refrig. Sci. and Tech.* (1986-1): 231-234.

Vidmar, V. (1987). Dynamic behaviour of draft condensers. *Proc. of the 17th. Int. Cong. Refrig.* 534-535.

Wade, N. L. (1984). Estimation of the refrigeration capacity required to cool horticultural produce. *Int. J. Refrig.* 7(6): 358-366.

Wang, H. (1991). *Modelling of a refrigerated system coupled with a refrigerated room.* PhD Thesis. University of Delft. The Netherlands. 217 pp.

Wang, H. and Touber, S. (1987). Prediction of air flow patterns in cold stores based on temperature measurements. *Proc. of the 17th Int. Cong. Refrig.* 4: 52-60.

Wang, H. and Touber, S. (1988). Simple non-steady state modelling of a refrigerated room accounting for air flow and temperature distributions. *Refrig. Sci. and Tech.* (1988-1):1-8.

Wang, H. and Touber, S. (1990). Distributed dynamic modelling of a refrigerated room. *Int. J. Refrig.* 13: 214-222.

Wang, H. and Touber, S. (1991). Distributed and non-steady state modelling of an air cooler. *Int. J. Refrig.* 14: 98-109.

Wang, H. and Touber, S. (1991). Saving energy with better capacity control systems. *Proc. 18th Int. Cong. Refrig.* 3: 1218-1224.

Wee, H. K., Loeffen, M. P. F. and Pham, Q. T. (1991). Fan speed control in a blast freezer using model reference control. *Proc. 18th. Int. Cong. Refrig.* 3: 997-1000.

Wenxue, H. and Kraft, H. (1991). A mathematical model of an evaporator based on the step exciting method. *Proc. 18th. Int. Cong. Refrig.* 3: 182-186.

Whitaker, S.(1977). *Fundamental principles of heat transfer*. Pergamon Press, Inc. 556 pp.

Wong, A. K. H. and James, R. W. (1986). A critical survey of control in refrigeration systems and heat pumps. *Research Memorandum 96 , Inst. Env. Eng.* South Bank Polytech. 27 p.

Wong, A. K. H. and James R. W. (1987). Control strategies of an intelligent controller for a liquid chilling plant. *Research Memorandum 105 , Inst. Env. Eng.* South Bank Pol. 21 pp.

Wong, H. K. A and James, R. W. (1988). A simple dynamic fluid liquid chilling plant model. *Research Memorandum 108 , Inst. of Env. Eng.* South Bank Polytechnic, London. 9 pp.

Yasuda, H, Touber, S and Machielsen, C. H. M. (1983). Simulation model of a vapour compression refrigeration system. *ASHRAE Trans.* 89(2A): 408-425.

Yasuda, H, Nakayama, S, Mori, T and Taneka, H. (1995). Modelling of a vapour compression refrigeration cycle with a scroll compressor and its design application. *Proc. 19th Int. Cong. Refrig.* 3a: 538-545.

Yu, B. F., Wang, Z. G., Yue, X., Han, B. Q., Wang, H. S. and Chen, F. X. (1995). Simulation, computation and experimental investigation for on-off procedures of refrigerators. *Proc. 19th Int. Congr. Refrig.* 3a: 546-553.

Zalewski, W. (1993). Mathematical model of heat and mass transfer processes in evaporative condensers. *Int. J. Refrig.* 16: 23-30.

Zhijiu, C and Weihan, L. (1990). Dynamic simulation and matching research of a small scale refrigeration system. *Refrig. Sci. and Tech.* (1990-3): 501-509.

ISO Metrology Group (1994). *Standard 5725-2: 1994. TC69/SC6.* Accuracy (trueness and precision) of measurement methods and results. Part 1: General principles and definitions. 17p.

19th INTERNATIONAL CONGRESS OF REFRIGERATION
THE HAGUE, THE NETHERLANDS, AUGUST 20-25, 1995

Proceedings II

THEME 2

Storage, Transport and Distribution

(Including workshop Large Coldstores and workshop Sales Cabinets)

For A Better Quality Of Life

INTERNATIONAL INSTITUTE OF REFRIGERATION
INSTITUT INTERNATIONAL DU FROID (IIR/IIF)

MODELLING OF THERMAL BEHAVIOUR OF WALLS FOR LOW TEMPERATURE APPLICATIONS: SANDWICH PANEL TYPE

S. ESTRADA-FLORES[1], A.C. CLELAND[2] and D.J. CLELAND[1]
Departments of Process & Environmental Technology[1] and Food Technology[2]
Massey University, Palmerston North, New Zealand

INTRODUCTION

A number of steady-state and dynamic mathematical models for refrigeration system components have been published /Ref. 1,2/. Detailed models simulating the real dynamics of the systems are often constrained by long computation times, detailed input data requirements and high development costs. Less detailed models are expected to produce simulations of lower accuracy than more complex models, but have possible advantages in development times and costs. Hence, a balance between simplicity and accuracy is required.

A literature review revealed a lack of systematic procedures for evaluating the validity of refrigeration systems models. Even though the nature of such models differ to some extent, there is a need for establishing unified methodologies for comparison purposes between models. James *et al.* /Ref. 2/ stated that "some component models are integrated into experimentally validated system models but there is no record of a comparison between models for a particular component being undertaken". Advantages and disadvantages of most published models have been discussed by the proposers, but a systematic, objective methodology for comparisons has not been adopted.

Several factors contributing to the transient behaviour of a refrigeration system, such as product heat loads, changes in equipment operation levels and others, have been investigated /Ref. 1,3,4/. Less well known is the thermal behaviour of room structures, such as walls, ceiling and floor. Whilst considerable effort has gone into studying walls dynamics in air conditioned buildings, low temperature refrigerated room walls may exhibit quite different thermal behaviour. Such walls usually include significant quantities of low thermal mass and high heat transfer resistance insulation, often with only thin layers of external sheeting. There are rarely windows. Thus the methodologies used for calculating heat load due to infiltration through air conditioned building walls may be inappropriate for low temperature room walls.

Whatever modelling methodology is used it must link the dynamic behaviour of the wall structures to the dynamics of the whole refrigerated room. The present work was focused on the so-called sandwich panel wall type (insulation enclosed between two metal sheets), and had the following objectives: a) to evaluate the accuracy of models of different levels of complexity when simulating the energy transients in low temperature room walls, and b) to investigate the use of peak heat load (maximum heat load in a 24 hour cycle) and the timing of the heat load response as measures for evaluating model response and accuracy.

MODELLING PHILOSOPHY

The thermal performance of a wall can be defined by 3 concepts:

1) thermal resistance (R), which includes the dimension in direction of the heat flow and the thermal conductivity,
2) thermal capacity (C), which is the energy stored in the object per unit temperature per unit surface area, and
3) a null thermal effect (N) which arises when the transient behaviour is ignored so instantaneous response to changes in adjacent conditions can be assumed.

Using these concepts a number of mathematical sub-models are possible. The modelled temperature profiles are shown in Figure 1(a). Overall models for any wall could use one or more of the sub-models for regions defined by different materials within the wall. A sub-model is required to describe the boundary conditions for boundary regions of the wall.

a) **Resistance only.** This sub-model assumes that the region possesses thermal resistance only and neglects its thermal capacity. The general heat flux equation for a wall modelled as an infinite slab is an algebraic equation:

$$\lambda\left(\frac{\Delta T}{\Delta x}\right) = \frac{q}{A} = Q_{conduction} \tag{1}$$

b) **Capacity only.** This sub-model assumes that the region possesses only thermal capacity and neglects its thermal resistance. The defining equation is an ordinary differential equation (ODE):

$$\Sigma\, Q_{incoming} - \Sigma\, Q_{outgoing} = \left(\frac{V \varrho c}{A}\right)\frac{dT}{dt} \tag{2}$$

c) **Resistance plus capacity.** In this sub-model capacity and resistance are both considered important. There are two strategies that can be followed:

Lumped sub-model (L). This strategy assumes a number of zones within the region, defining zones as alternately purely capacitive or purely resistant elements, as shown in Figure 1(a). The defining equation for a C element with two R elements either side is:

$$\Delta x_n \varrho\, c\left(\frac{dT}{dt}\right)_n = \lambda\left(\frac{\Delta T}{\Delta x}\right)_{n-1} - \lambda\left(\frac{\Delta T}{\Delta x}\right)_{n-1} \tag{3}$$

where n= the number of the capacity region.

Distributed sub-model (D). This strategy assumes continuous distribution of the thermal resistance and thermal capacity in a physically correct manner. The defining equation is a partial differential equation:

$$\varrho\, c\,\frac{\partial \theta}{\partial t} = \frac{\partial}{\partial x}\left(\lambda\,\frac{\partial \theta}{\partial x}\right) \tag{4}$$

d) **"Null" region.** The component does not contribute to the exchange of heat between regions, but acts as a perfect conduit.

e) **Boundary conditions.** Radiation and convection were considered to occur in the external environment to which the wall is exposed:

$$Q_{ambient-wall} = h_{bound}(T_e - T_{bound}) + Q_{r,incident} - Q_{r,emitted} \tag{5}$$

whereas convection only was assumed in the internal environment:

$$Q_{wall-room} = h_{bound}(T_{bound} - T_{room}) \tag{6}$$

Models that describe New Zealand weather conditions were sought for use in defining the terms of Eq. (5). The ambient temperature and solar radiation were modelled using equations published by Kimball and Bellamy /Ref. 5/, whereas the radiative terms were calculated using the well-known expressions of emitted and incident loads /Ref. 6/. In practice it was found that the inclusion of sinusoidal signals (solar radiation and ambient temperature) amplified differences in model responses.

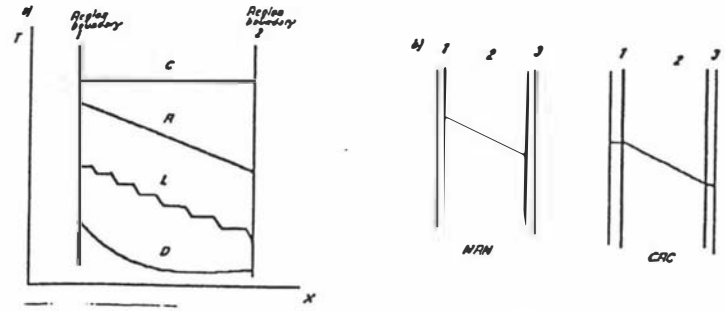

Figure 1. Modelled temperature profiles in wall structures: a) Conceptual sub-models C,R,L and D regions. b) NRN and CRC models for sandwich panel wall.

MATHEMATICAL MODELS

The level of complexity of the models selected for study of sandwich panel type walls was set by the conceptualization of resistance and capacity and by the number of zones. The main characteristic of a sandwich panel wall is the low thermal mass of the thick insulation layer situated between the two metal sheets (often aluminium). Two models of different level of complexity were selected. The modelled temperature profiles are shown in Figure 1(b):

a) An NRN model was constructed by assuming that the insulation layer possesses thermal resistance only, since it combines low thermal conductivity and low density. The resistance and the heat capacity of the metal layers were assumed negligible in this model, resulting in a model combining a null region + a pure resistance region + a null resistance region. The model demands the simultaneous solution of Eq. (1), (5) and (6):

$$Q_{ambient-wall} = Q_{conduction,2} = Q_{wall-room} \tag{7}$$

The algebraic equation system was solved using an iterative procedure.

b) A CRC model was constructed by assuming a negligible resistance but significant thermal capacity in the metal layers. The insulation was represented as a "resistance only" layer as for NRN. Hence, the model combined a pure capacitive region + a pure resistance region + a pure capacitive region. The model comprised two ODEs based on Eq. (2) for each of the metal layers:

$$\frac{V_1 \varrho_1 c_1}{A}\left(\frac{dT_1}{dt}\right) = Q_{ambient-wall} - Q_{conduction,2} \tag{8}$$

$$\frac{V_3 \varrho_3 c_3}{A}\left(\frac{dT_3}{dt}\right) = Q_{conduction,2} - Q_{wall-room} \tag{9}$$

The NRN model which assumes instantaneous transfer of heat is commonly used in design. The use of a more complex model than CRC was difficult to justify on grounds of complexity. Hence, models such as CLC or LLL were not tested, though they are theoretically possible.

VERIFICATION AND VALIDATION OF MODELS

In order to test the NRN and CRC models, it was necessary to know the "real" behaviour of a wall. It was decided to use predictions from an accurate finite element (FEM) computer programme /Ref. 7/ as the representation of reality. This programme implemented a fully distributed scheme (DDD), modelling each region by Eq. (4). A grid comprising one linear element in each metal layer plus 15 linear elements in the insulation gave reliable results with small numerical errors.

A trial simulated the behaviour of the wall, starting from a uniform initial condition, exposed to a cyclic 24 hour weather pattern in terms of ambient and sky temperatures and incident radiation (Figures 2 and 3). The simulation was carried out until a repeating 24 hour cycle was achieved. The predicted heat load entering the internal environment from the wall was used as the key response variable. Analyses of the variations in the heat load were carried out with two distinct focuses:

a) Factors influencing the heat load response (magnitude and timing of the cycle).
b) Factors influencing the accuracy of the models (i.e. how closely CRC and NRN models matched the FEM response).

A fractional factorial design (FFD) was set, according to the Quality Engineering methodology of Taguchi /Ref. 8/, to compare model performance and identify factors with greatest influence. Levels were chosen to cover the full range of likely values in industrial practice. Tables 1 and 2 summarise the conditions used as input data for the CRC, NRN and FEM models.

A number of measures derived from the rate at which heat transferred from the wall to the room were used to enable numerical comparisons to be made. Ten measures were established, but only those that had an obvious physical meaning are presented here. Figure 2 illustrates their physical interpretation:

a) Start-up time. This was calculated as the time to achieve a repeating 24 hour cycle pattern (within a predetermined tolerance) in the heat load in response to the 24 hr cycle of the external boundary conditions.
b) Amplitude of the heat load cycle. The amplitude was calculated as the algebraic difference of the maximum (peak) and the minimum heat load simulated in a 24 hr cycle.
c) Offset in time of the model compared to FEM for reaching peak heat load in a 24 hr cycle.
d) Mean heat load. The average heat load entering the room in a 24 hr cycle.

RESULTS AND ANALYSIS

Table 3 summarises the contribution of factors affecting model heat load response and accuracy.

Factors affecting heat load response.

1) *Start-up time.* Insulation resistance most affected the time to establish a repeating cycle for FEM models. The relatively high importance of thermal capacity in the internal layer for CRC but lower importance of this factor for FEM indicates a fundamental difference in models. NRN predicted a zero start-up time, due to the absence of a thermal capacity term thus leading to an immediate response to the external environment signal.
2) *Amplitude.* The insulation resistance was the predominant factor affecting the amplitude. The FFD statistical analysis attributed 60% to 70% of the differences between the 8 trials to this parameter for the 3 models. Figure 4(a) shows that there is an approximately exponential relationship between amplitude of the heat load cycle and insulation resistance, amplitude decreasing as resistance increases. In physical terms, the extent of

FACTOR	LEVEL 1	LEVEL 2
A. h_{fixed} (W/m² K)	3	10
B. h_{fixed} (W/m² K)	3.5	26.5
C. T_{ext} (°C)	15	28
D. Emissivity, external layer	0.12	0.92
E. T_{room} (°C)	-25	10
F. $R_{insulation}$ (m² K/W)	2	8
G. $C_{layer\ 3}$ (kJ/m²K)	4.8	23.8

Table 1. Factors and levels tested in models.

	FACTORS AND LEVELS						
TRIAL	A	B	C	D	E	F	G
1	1	1	1	1	1	1	1
2	1	1	1	2	2	2	2
3	1	2	2	1	1	2	2
4	1	2	2	2	2	1	1
5	2	1	2	1	2	1	2
6	2	1	2	2	1	2	1
7	2	2	1	1	2	2	1
8	2	2	1	2	1	1	2

Table 2. Experimental design showing levels and factors.

MEASURE	MODEL	ACCURACY	MAGNITUDE
START-UP TIME	CRC	F(26%),B(15%),A(14%)	B(52%),G(40%),E(8%)
	NRN	NONE	NONE
	FEM	——-	F(60%),B(18%),G(11%)
AMPLITUDE	CRC	F(42%),A(18%),C(15%)	F(58%),A(21%),G(12%)
	NRN	F (77%)	F(66%),A(15%)
	FEM	----	F(70%),A(16%),G(8%)
OFFSET[1]	CRC	F (77%)	---
	NRN	F (76%)	---
MEAN HEAT LOAD	CRC	NONE	F (53%), E (38%)
	NRN	NONE	F (53%), E (38%)
	FEM	NONE	F (53%), E (38%)

[1] Offset is a measure of accuracy by definition.

Table 3. Percentage contribution of factors affecting the accuracy and magnitude of parameters used for comparison of models.

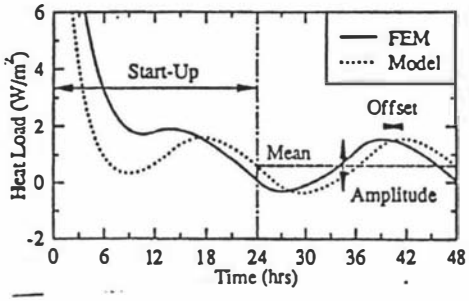

Figure 2. Definition of measures used in the comparison of models.

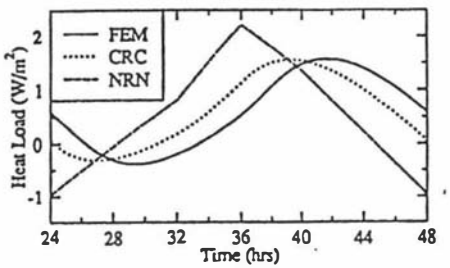

Figure 3. Typical heat load profiles for NRN, CRC and FEM models.

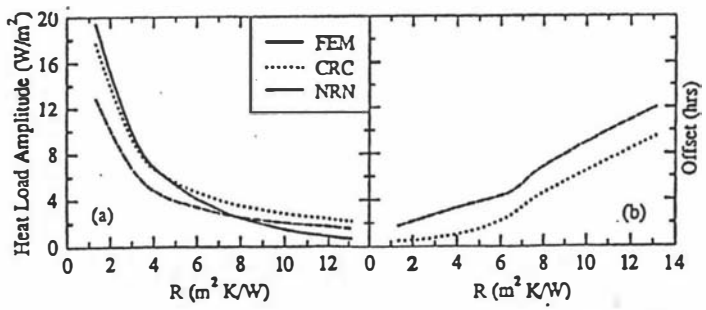

Figure 4. Variation of amplitudes and offsets with respect to insulation resistance changes.
(a) Effect of insulation resistance on amplitude for CRC, NRN and FEM models.
(b) Effect of insulation resistance on offset from FEM for CRC and NRN models.

damping of the incoming cyclical wave in the heat load increases in an approximately exponential manner as the insulation thickness (x) increases and/or thermal conductivity (λ) decreases. Large differences between resistances of 2 m² K/W to 5 m² K/W are observed, but at higher resistances little change is observed in amplitude and increasing in x and/or decreasing λ has a much smaller effect on the amplitude of the heat load cycle.

3) *Mean heat load.* As expected, for all 3 models insulation resistance and room temperature explained most of the differences between FFD trials. The mean heat load of runs set for high room temperature/high resistance levels were 20 times lower than those at low room temperature/low resistance levels. Mean heat load was relatively unaffected by changes in variables such as emitted and incident radiation levels over the wall.

Factors affecting model accuracy.

1) *Start-up time.* Both the NRN and CRC models failed to accurately predict the start-up times. For CRC, the effects discussed above led to over-prediction of start-up times at low levels of resistance and an under-prediction of start-up when using high levels of resistance. NRN maximises error by failing to predict start-up at all.
2) *Amplitude.* Insulation resistance determined the accuracy of NRN; as resistance increased, NRN was progressively less accurate. Similar behaviour was observed for CRC, though the accuracy of this model was also affected by the external heat transfer coefficient and the mean external ambient temperature.
3) *Offset.* NRN and CRC progressively predicted the timing of the peak heat load less accurately as resistance rose. Figure 4(b) shows the approximately exponential relationship between offset and insulation resistance. In the best case, a time offset for the peak heat load of 1.7 hours occurred for NRN and 0.7 hours for CRC at the same resistance level. In the worst case, the offset was of 12 hours for NRN and 9.7 hours for CRC. Linking this behaviour to that of the amplitude (Figure 4(a)), higher accuracy is expected for low resistances.

DISCUSSION AND CONCLUSIONS

The applicability of simple models such as NRN or CRC for simulating the heat transfer across a sandwich panel wall depends on the use of the model. If mean heat loads are required (as is often the case in sizing of insulation layers), both NRN and CRC give accurate results. When the purpose of the simulation is designing for "worst case" conditions, the CRC model is more accurate than the NRN model in the calculation of the peak heat load through walls and its timing. Nevetheless, because variations in the thermal capacity of the metal layers had little influence on heat load, the benefit achieved in moving from an NRN to a CRC model was not large.

There are practical situations where the dynamic behaviour of the wall is a significant part of the total heat load or in which inaccurate representation of the wall-related transients (magnitude plus timing) might lead to build-up of errors due to coupled phenomena (e.g. evaluation of condensation risks, calculation of start-up power, etc). In these cases, the shortcomings of both models are significant and these limit the ability to achieve acceptably accurate predictions. In such cases, a more accurate representation of the insulation layer (e.g. considering the insulation thermal capacity) would be required to achieve better predictions.

NOMENCLATURE

A	surface area (m^2)	Greek letters	
c	specific heat capacity (J/kg K)	Δ	difference
C	thermal capacity (J/m^2 K)	ϱ	density (kg/m^3)
h	heat transfer coefficient (W/m^2 K)	λ	thermal conductivity (W/m K)
n	region number	Subscripts	
Q	heat flux (W/m^2)	1,2,3	layer 1, 2 or 3.
q	heat flow (W)	a	instant external ambient condition
R	thermal resistance (m^2 K/W)	amb	mean external environment condition
T	temperature (°C)	$room$	mean internal environment condition
t	time (s)	$boun1$	external environment/wall boundary
V	volume (m^3)	$boun2$	wall/internal environment boundary
x	dimension (m)	r	radiation

REFERENCES

/1/ A. C. Cleland. *Food Refrigeration Processes. Analysis, Design and Simulation.* Elsevier Applied Science, London (1990), 284 p.

/2/ K.A. James, R.W. James and A. Dunn. A critical survey of dynamic mathematical models of refrigeration systems and heat pumps and their components. *Inst. Env. Eng. Tech. Memo.* (1986), No. 97, 28 p.

/3/ K.A. James and R.W. James. Transient analysis of thermostatic expansion valves. *Inst. Env. Eng. Tech.* Memo (1986), No. 99, 28 p.

/4/ S.J. Lovatt. Development of a dynamic modelling methodology for the simulation of industrial refrigeration systems. PhD Thesis. Massey University, N.Z. (1992), 254 p.

/5/ B.A. Kimball and L.A. Bellamy. Generation of diurnal solar radiation, temperature and humidity patterns. *Energy in Agriculture*, (1986), vol 5, p. 185-197.

/6/ W.A. Gray and R. Mueller *Engineering Calculations in Radiative Heat Transfer.* Pergamon Press. Oxford, N.Y. (1974), 161 p.

/7/ D.J. Cleland. Prediction of freezing and thawing times for foods. PhD Thesis. Massey University, N.Z. (1985), 281p.

/8/ G. Taguchi. *System of Experimental Design.* Quality Resources, Amer Supp Inst, (1986), Vol II, 440p.

SUMMARY

A sandwich panel type wall was modelled using two models of different conceptual complexity. The models were validated against a well-tested finite element method across a range of external and internal heat transfer conditions. The degree of accuracy was measured using a number of responses derived from the cyclic heat load transferred from the wall to the internal room environment. A model using two ordinary differential equations which included the thermal capacity of the external metal layers as well as considering the insulation resistance was more accurate than an algebraic model considering only insulation resistance, but the benefits of increasing the level of complexity were not large. Both models were significantly less accurate as insulation resistance rose. It is probable that insulation thermal capacity must be included if better accuracy is to be achieved.